1-1-2004

Solid and melt state processing of polymers and their composites in supercritical carbon dioxide.

Manuel A. Garcia-Leiner
University of Massachusetts Amherst

SOLID AND MELT STATE PROCESSING OF POLYMERS AND THEIR COMPOSITES IN SUPERCRITICAL CARBON DIOXIDE

A Dissertation Presented

by

MANUEL A. GARCIA-LEINER

Submitted to the Graduate School of the
University of Massachusetts Amherst in partial fulfillment
of the requirements for the degree of

DOCTOR OF PHILOSOPHY

September 2004

Polymer Science and Engineering

SOLID AND MELT STATE PROCESSING OF POLYMERS AND THEIR COMPOSITES IN SUPERCRITICAL CARBON DIOXIDE

A Dissertation Presented

by

MANUEL A. GARCIA-LEINER

Approved as to style and content by:

Alan J. Lesser, Chair

Richard J. Farris, Member

H. Henning Winter, Member

Shaw L. Hsu, Department Head
Polymer Science and Engineering

DEDICATION

I would like to share and dedicate this work to a very special group of people without whom this and every achievement in my life would be meaningless:

To my parents, Abelardo and Guadalupe,

For their immense love and unconditional support.

To my two best friends and brothers: Lobsang and Luis Antonio.

For all the memories and the wonderful times to come.

To the Herrera-Alonso family.

For all their kind support throughout these years.

To Margarita.

Because my world revolves around her.

For being there all the time,

bringing light to every moment.

For walking through each day by my hand,

being my eyes, my life and my sunshine.

ACKNOWLEDGMENTS

It is difficult to express in words the enormous appreciation and profound rcspect that I have for my advisor Professor Alan J. Lesser. Working for him has becn a great, rewarding and enjoyable experience. He has made my stay here, and in his group very pleasant and I will always be grateful for his help throughout my Ph.D.

I would also like to thank my committee members, Professor Richard J. Farris and Professor Henning Winter. Both have made significant contributions and suggestions to my thesis that have helped me to improve the quality of my work. Having these three exceptional scientists in my committee has been a great opportunity to improve my knowledge and natural interest in Polymer Science and Engineering evcn further.

I would like to acknowledge the Polymer Science and Engineering Department, all the faculty, students and staff involved in making this an exceptional doctoral program. Eileen Besse, Joan Chauvin, Ann Brainerd, Louis Raboin and Alan Waddon have made my life and research efforts in the department much easier. Also, I want to thank the Lesser Group, both current and former members. This group has been a wonderful place to work, learn, play and make good friends.

My life in Amherst would not have been the same without the company of a very special group of friends: Angelo, Bhavini, Kishore and Margarita, who have made this an unforgettable experience, filling my mind with good memories that I will take with me forever.

ABSTRACT

SOLID AND MELT STATE PROCESSING OF POLYMERS AND THEIR COMPOSITES IN SUPERCRITICAL CARBON DIOXIDE

SEPTEMBER 2004

MANUEL A. GARCIA-LEINER, B.S., UNIVERSIDAD NACIONAL AUTONOMA DE MEXICO

M.S., UNIVERSIDAD NACIONAL AUTONOMA DE MEXICO

M.S., UNIVERSITY OF MASSACHUSETTS AMHERST

Ph.D., UNIVERSITY OF MASSACHUSETTS AMHERST

Directed by: Professor Alan J. Lesser

Supercritical carbon dioxide ($scCO_2$) has been widely studied as an environmentally friendly alternative to organic solvents in many applications. This thesis will describe specific routes for both melt and solid-state processing of polymers in $scCO_2$-mediated environments. The primary goal is to analyze the influence of $scCO_2$ on the final properties of polymers as well as to design novel processing routes using $scCO_2$ that could allow access to well-defined structures and novel materials, and processing of "intractable" polymers.

Most of the fiber-drawing studies of polymers in $scCO_2$ have focused on permeable conditions, where the plasticization process of $scCO_2$ dominates the interaction and the effect of the imposed hydrostatic pressure is negligible.[1-3] In this thesis, the interactions of $scCO_2$ with solid state polymers under non-permeable conditions are investigated through the drawing behavior of highly crystalline, highly oriented, polymorphic fibers (UHMWPE) within this environment. The high-pressure environment appears to

stabilize the crystal structure of the fiber, which in this case is the major component. As a consequence, $scCO_2$-treated samples display a constant mechanical and thermal response compared to air-drawn samples that show significant temperature dependence in their behavior.

In addition, the interactions of $scCO_2$ with polymers in the melt are analyzed by designing a modified processing system that allows to process polymers in $scCO_2$. Using this system, the foaming process of polyethylene in $scCO_2$ is studied, and $scCO_2$-assisted polymer processing is then applied to high molecular weight polymers, including fluoropolymers and high molecular weight polyolefins, as a novel processing-route. The success of this method is based on the effect of $scCO_2$ on the melting behavior of semicrystalline polymers, along with its large plasticizing properties observed primarily in fluoropolymers.

Finally, the feasibility of preparing polymer-clay nanocomposites by this route using a variety of approaches is also studied. The use of polymers with controlled hydrophilicity, as well as the introduction of chemically designed hydrophilic polymers or compatibilizers that enhance the interaction between the polymer and the clay have been used to understand the effect of $scCO_2$ on the melt intercalation process as well as on the final structure and morphology of these systems.

TABLE OF CONTENTS

LIST OF TABLES

LIST OF FIGURES

CHAPTER 1

INTRODUCTION

Supercritical carbon dioxide ($scCO_2$) has proven to be an environmentally friendly alternative for a wide range of applications. At these conditions, CO_2 has a unique combination of properties from both liquid and gas states, exhibiting liquid-like densities combined with low viscosities and high diffusion rates characteristic of a gas phase.[4-11] Due to its high compressibility, its solvent properties can be tuned and controlled by small changes in temperature and pressure, acting as a "reversible plasticizer" that can be easily removed from the system during depressurization, leaving the final product solvent-free, reducing the costs of solvent removal.[12] With some particular exceptions, $scCO_2$ is a non-solvent for conventional polymers, however, it can plasticize most of them very efficiently. Recently, several strategies have been used to design $scCO_2$-philic materials to overcome the poor solubility of most materials in $scCO_2$.[5,6,11]

There are several ways in which $scCO_2$ has been introduced into conventional processing techniques. This project will analyze a variety of routes, involving solid and melt state polymer processing, in which $scCO_2$ could be used both as a plasticizers and as a processing aid. The goal of this research is to understand the specific effect of $scCO_2$ on the final properties of the polymer as well as to design novel processing routes using $scCO_2$ that could allow access to well-defined structures and novel materials, and processing of "intractable" polymers.

1.1 Fiber Drawing in Supercritical Carbon Dioxide

Over the years, improving the physical and mechanical properties of high performance fibers by various synthetic and processing techniques has been a major concern. Certainly, this interest has been driven by new technological and engineering applications along with more stringent design requirements and the development of advanced materials.

1.1.1 Fiber Drawing under Permeable Conditions

The interaction of $scCO_2$ with semicrystalline polymers under permeable conditions during fiber drawing is such that it acts both as a pressurizing media and plasticizer, which can significantly increase the chain mobility. In general, it is widely accepted that permeation of $scCO_2$ is selective to the amorphous phase, since the difference between the solubility parameters of CO_2 and most polymers is greater than two, impeding its permeation into the crystalline phase.

Drawing fibers in the presence of $scCO_2$ can impart a significant amount of molecular orientation and under certain conditions can induce crystallization.[13] Hobbs and Lesser[1,2] have investigated the drawing of flexible chain polymers in a high pressure CO_2 environment with the purpose of improving the physical and mechanical properties of conventional organic fibers. They have shown that the final properties of PET fibers drawn by a two-stage process are considerably affected by the presence of $scCO_2$, reporting significant increases in both elastic modulus and strength for $scCO_2$-treated samples. Also, considerable effects have been observed in a variety of systems where samples drawn in $scCO_2$ show significantly higher crystallinity and orientation along with

improved mechanical properties.[3] Since this behavior is expected to be valid in other semicrystalline polymers as well, significant improvements in the ultimate properties of a polymer when drawn in $scCO_2$ under permeable conditions are expected to occur.

1.1.2 Fiber Drawing under non-Permeable Conditions; Drawing of Ultrahigh Molecular Weight Polyethylene Fibers (UHMWPE)

Under certain conditions, as in the case of highly crystalline polymers or highly oriented materials, the plasticization of CO_2 is restricted, and as a consequence, hydrostatic effects start to dominate the interactions of polymers with CO_2, and so the final properties of the polymer. In fact, the imposed hydrostatic pressure has been related to some experimentally observed changes, and crystal-crystal transitions have been detected in the case of polymorphic materials when extreme conditions are imposed.[14-18] Under non-permeable conditions, the presence of $scCO_2$ may promote changes in the state of stress of drawing, imposing hydrostatic contributions to the principal stresses that in some cases might be able to modify the physical and mechanical properties of the deformed material. This effect has not been studied and the overall hydrostatic contribution of $scCO_2$ in the drawing process has not been quantified and understood yet.

In this regard, based on their commercial and practical relevance, polyolefins are probably the most important type of polymers, and particular efforts have been concentrated in introducing polyethylene materials to a variety of applications. Currently, polyethylene materials are designed with particular properties particularly suited for specific applications, and several strategies have been proposed to obtain high modulus polyethylene fibers.[19] In this regard, UHMWPE fibers, commercially known as Spectra

or Dyneema, represent the first case of a successful conversion of a flexible polymer into an ultra-strong fiber and they have rapidly gained acceptance in many applications in which high strength and modulus are required.[20] Many investigations suggest that the ultimate properties of UHMWPE materials are remarkably influenced by their specific drawing conditions, including drawing temperature and rate.[21,22] In this project, UHMWPE fibers are used as a model to highly crystalline, highly oriented, polymorphic materials that could be used to understand the drawing behavior of these systems in $scCO_2$ and learn about the specific contribution of hydrostatic pressure into the final properties of a fiber during deformation.

1.2 Foaming of Polymers with Supercritical Carbon Dioxide

The technological and scientific importance of polymeric foams continues to grow at a rapid pace in our modern world. This area is continuously enriched with new ideas and the introduction of these materials to applications never imagined before is challenged every day by the advent of new polymers and alternative foaming technologies.

Polymeric foams in general are comprised of a cellular structure created by the expansion of a blowing agent, which is usually a volatile gas or a liquid.[2] The intrinsic properties of the blowing agent and its specific interaction with the polymer melt have a direct effect on the final properties of the foam. In particular, the interest in using $scCO_2$ as an alternative blowing agent to produce polymer foams is related to the fact that its inherent properties resemble those required in a successful blowing agent. At supercritical conditions, CO_2 combines in a unique way a variety of properties observed in pure liquid and gas states, which along with its reduced cost make it a real and

environmentally friendly alternative for conventional processing techniques. During extrusion, CO_2 dissolves into a polymer melt under high pressures, and diffuse away from the polymer substrate at ambient conditions.[12]

A vast amount of research, particularly in the area of microcellular polymer foams has been focused in understanding the relation between the processing conditions, particularly in extrusion and injection molding, and the final polymer morphology when CO_2 is introduced.[25-36] In general, a reduced cell size and an increase in the cell density promote improved properties. High impact strength (five-fold increase over unfoamed material), high toughness, high stiffness to weight ratio (three to five times larger than unfoamed material), high fatigue life, high thermal stability, low dielectric constant and low thermal conductivity are among the unique properties of these materials.[30]

A variety of research groups have studied the production of microcellular foams in extrusion, using conventional foaming techniques that promote the dissolution of the gas in the melt and enhance cell nucleation.[25-36] Park et al.[28,31] have developed a continuous process to manufacture low-density microcellular polymers, using a strategy both to control cell growth after nucleation and to prevent cell coalescence. In addition, the plasticization effect of CO_2 during extrusion has been quantified by analyzing the viscosity drop of a system after CO_2 is dissolved into the melt, decreasing the shear thinning behavior resulting in an increase of the power law index.[30]

Regarding the nucleation process, it is expected that without a foaming agent, homogeneous nucleation dominates and nucleation is promoted by a thermodynamic instability in the process, which is typically a pressure drop along the extrusion line.[28] The homogeneous process is characterized by a typical thermodynamic barrier related to

the energy required to create a nucleus. However, in the presence of small impurities, a thermodynamically more favorable heterogeneous nucleation mechanism occurs. Both heterogeneous and homogeneous nucleation processes have been studied in the production of microcellular polymers. Heterogeneous nucleation studies, conducted by Han et al.[34] have shown that direct processing parameters play an important role in the final morphology of the polymer. In addition, Lee et al. have suggested that the size and distribution of the cells are controlled by the melting temperature, chemical structure and molecular weight of the resin.[36]

In this project, a modified processing system will be used to produce polymer foams with controlled morphology using $scCO_2$ as the blowing agent. A detailed study of the foaming process of polyethylene systems during extrusion will be conducted, mainly to understand the relation between the final extrudate morphology and the processing conditions in the system.

1.3 Processing of Intractable Polymers

1.3.1 Plasticization of Polymers in Supercritical Carbon Dioxide

The use of CO_2 particularly at supercritical conditions as an alternative processing aid in polymer extrusion has been analyzed extensively for the past two decades.[35-36] Polymeric foams down to the microcellular range can be obtained in some cases and a good understanding of the relation between processing conditions and the final morphology can be achieved. It is easy to imagine that the processability of a given material could be dramatically increased in $scCO_2$, mainly through a plasticization

process of the polymer by CO_2, that in some cases could be large enough to provide an alternative processing-route for high melt viscosity polymers.

A variety of models have been proposed to describe the plasticization process of a polymer by a small molecule diluent such as CO_2. Couchman and Karasz[79] analyzed the effect of composition on the glass transition temperature of multicomponent systems based on classic thermodynamics, where the glass transition temperature of the mixture is described in terms of the individual glass transition temperatures of the pure components. This approach could be successfully applied to describe the plasticization of a polymer by CO_2, however it requires for a specific value of the glass transition temperature of CO_2, a parameter difficult to define or measure in an accurate manner.

In 1980, Chow[37] proposed an expression to describe the plasticization phenomenon through molecular interpretation of the glass transition in polymer-diluent systems. Plasticization is described in terms of the Tg depression that occurs in a system due to the presence of a small molecule diluent at low concentrations. The model provides an explicit expression for the glass transition depression (Tg/Tg_0) as the ratio of the glass transition temperature of a polymer-diluent system (Tg) to that of the pure polymer (Tg_0), using an equilibrium approach in terms of the change in configurational entropy (S_c) of a system during the glass formation.

$$S_c = S_{liquid} - S_{glass} \qquad (1)$$

It suggests that in a polymer-diluent system, S_c is not only a function of the temperature as in the case of a pure polymer, but it is also dictated by the number of diluent molecules (N) in the system.

$$S_c(N,T) = \int_{T_g}^{T} \Delta C_p(N,T')d\ln T \qquad (2)$$

where ΔC_p is the difference in heat capacity at constant pressure between the supercooled liquid and glass. On the basis of both classical and statistical thermodynamics, Chow proposed the following expression to describe the glass transition depression.

$$\ln\left(\frac{T_g}{T_{g0}}\right) = -\frac{1}{\Delta C_p}\left[\ln\left(\frac{Q^N_{liquid}}{Q^0_{liquid}}\right) + T\frac{\partial}{\partial T}\ln\left(\frac{Q^N_{liquid}}{Q^0_{liquid}}\right)\right] \qquad (3)$$

where Q is the configurational partition function of the system. Any of the polymer-lattice theories can be used to evaluate the ratio of partition functions and obtain an expression for the glass transition depression based on this equation. Chow model uses the Bragg-Williams approximation of an order-disorder transition to determine the configurational partition function. It suggests that in the plasticization of a polymer by a small molecule diluent such as CO_2, the main contribution to the partition function (and so to the ratio Tg/Tg_0) comes from the mixing of diluent molecules among lattice sites, and so the main interest relies on the configuration of small molecules on the lattice rather than on the arrangement of the polymer itself (since Tg_0 is known). Using this approximation, the partition function of the pure polymer is always equal to unity and that of a polymer-diluent system is given in terms of the energetic interactions of the diluent molecules.

$$Q^0_{liquid} = 1 \qquad (4)$$

and

$$Q^N_{liquid} = \frac{(N+L)!}{N!L!}\exp\left(\frac{NL}{N+L}\frac{z\varepsilon}{2kT}\right) \qquad (5)$$

where N is the number of diluent molecules randomly distributed in a lattice of N+L sites, assuming that each diluent molecule occupies a singe lattice site and L is the number of vacant sites. The lattice coordination number z can be roughly estimated by the nearest whole number to the ratio of the molecular weights of the monomer and diluent.[38] Also, $\varepsilon=\varepsilon_{NN}+\varepsilon_{LL}-2\varepsilon_{NL}$, with ε_{NN}, ε_{LL}, ε_{NL} describing the energies of each NN, LL, NL pair respectively. Substituting, the final expression for the Chow model can be obtained

$$\ln\left(\frac{T_g}{T_{g0}}\right)=\beta\left[(1-\theta)\ln(1-\theta)+\theta\ln\theta\right] \tag{6}$$

where β, α are non dimensional parameters given by

$$\beta=\frac{zR}{M_p\Delta C_{pp}} \tag{7}$$

$$\theta=\frac{N}{N+L}=\frac{M_p}{2M_d}\frac{\omega}{1-\omega}=\frac{V_p}{2V_d}\frac{\phi}{1-\phi} \tag{8}$$

where M_p and M_d are the molecular weights of the polymer repeating unit and diluent, respectively. ΔC_{pp} is the excess transition isobaric specific heat of the polymer, ω and ϕ represent the weight and volume fraction of diluent in the system, and V_p and V_d correspond to the molar volumes of the polymer repeating unit and diluent, respectively.

Equation (6) provides an explicit expression to quantify the plasticization of a polymer-diluent system in terms of intrinsic properties of the pure polymer and diluent. In our particular case, this expression will be used to quantify the amount of plasticization in our system, using only two parameters that are either available in the literature or that can be easily estimated or prescribed by the processing conditions. In this regard, the parameter β is only dependent on the magnitude of ΔC_{pp}, a

thermodynamic property of the polymer. On the other hand, θ depends on the weight fraction of CO_2 that can be prescribed for each polymer system at equilibrium as the equilibrium mass uptake of CO_2, determined by conventional diffusion experiments.

1.3.2 Melting Behavior of Polymers in Supercritical Carbon Dioxide

As suggested, the Chow model appears to be appropriate to describe the plasticization process of a polymer in the presence of CO_2. While the plasticization effect of CO_2 in a variety of polymers has been reported extensively in the literature, the effects of CO_2 on the crystallization and melting temperatures have only been analyzed for a few systems.[40-41] Zhang and Handa[41] have done extensive work with syndiotactic polystyrene (s-PS) systems, suggesting that CO_2 promotes crystallization of glassy s-PS into its various crystalline forms (α and β). Also in these systems, $scCO_2$ induces crystal-crystal transformations between them at temperatures below the melting temperature of the α form that could only be understood if the α crystals undergo melting at a depressed temperature before transforming into the β form. They have shown in fact that CO_2 has a direct effect on the melting behavior of semicrystalline polymers. A significant depression in the melting point is observed in $scCO_2$, due to its high solubility in s-PS, showing no change in Tm when CO_2 was replaced with N_2. This behavior has been observed in other polymers as well, showing that the depression in melting temperature is dictated by both the polymer-gas interactions and the intrinsic crystal characteristics. The decrease in Tm is related to an increase in the specific surface free energy δe caused by the dissolved CO_2. Using the Thomson-Gibbs equation, the change in melting temperature is given by

$$Tm = Tm^0\left(1 - \frac{2\delta e}{l\Delta h}\right) \qquad (9)$$

where Tm^0 is the melting point of an infinitely large crystal, l is the lamellar thickness and Δh is the heat of fusion per unit volume. Since Tm, l and Δh are generally constant, the change in Tm is attributed to δe. This behavior is expected to occur in other polymer-gas systems whenever the gas sorption and the plasticization effects are pronounced.

1.3.3 Conventional Processing Methods for the Selected Materials

In this study, the processability of three different commercially available polymers will be analyzed to assess the feasibility of $scCO_2$-assited polymer processing as a processing route for high molecular weight, high melt viscosity or "intractable" polymers.

The first material is polytetrafluoroethylene (PTFE), a widely used and intractable commercially available fluoropolymer. In general PTFE shows an extremely high molecular weight resulting in a melt viscosity, which is about six orders of magnitude higher than that of most common thermoplastic polymers (10^{10}-10^{12} Pa s). The chemical inertness and stability as well as the low surface energy of PTFE is related to its physical conformation, which creates an almost perfect cylindrical structure comprised of an outer layer of fluorine atoms surrounding a carbon based core.[42] Typically the virgin powders display a melting point around 345 °C with a corresponding degree of crystallinity of 60-90%, depending on the crystallization conditions. After melting, the re-crystallization process is restricted due to the extremely high melt viscosity, and as a consequence, the crystallinity is significantly reduced. The restricted re-crystallization process significantly reduces the crystal size, thus the lower melting point. As a consequence, the processing

alternatives for PTFE are reduced to RAM extrusion and compression molding, and the possibility of an alternative and easy processing route for PTFE is of major relevance.

In addition to PTFE, another fluoropolymer, fluorinated ethylene propylene copolymer (FEP) is selected in this study. FEP is a random copolymer of tetrafluoroethylene (TFE) and hexafluoropropylene (HFP), with a structure very similar to that of PTFE except for the HFP units that are responsible for significant changes in the physical properties, acting as defects in crystallites that reduce the overall melting point to 260°C.[42] Typically FEP is found in lower molecular weights than PTFE, and as a consequence, FEP has a reduced melt viscosity in comparison to PTFE that enhances its processability. FEP can be melt processed using twin-screw extruders with additional mixing devices. The crystallinity of the virgin polymer is lower than that of PTFE, and in this case the thermal behavior is not affected by the high molecular weight, and the re-crystallization process is not restricted, so that most of the crystallinity in the sample can be recovered after melting.

In addition to fluoropolymers, polyolefins of high molecular weight will be considered in this study. An example of these is s-PS, which is a relatively new partially crystalline commodity plastic with a high melting point (>250°C), suggesting higher service temperatures than common plastics. Recently, several studies have shown that the amount of crystallinity, the type of crystal structure and morphology in s-PS systems can be controlled by the process conditions. Thus, a consistent strategy to melt-process s-PS is of great relevance, since the properties that make s-PS an attractive material are strongly affected by the amount and distribution of the crystalline phase. As in the case of FEP, the re-crystallization of s-PS is not restricted despite the high molecular weight, so

that after melting most of the crystallinity can be recovered. Even though s-PS is considered a melt processable polymer, as in the case of FEP specific requirements and processing techniques are required, including the use of twin screw extruders and additional mixing devices.

1.4 Polymer-clay Nanocomposites

Nanotechnology has recently gained a lot of attention leading the way to better and unique materials for almost any type of application. Recent developments in this area have shown the possibility of incorporating diverse inorganic materials into engineering polymer systems producing polymer nanocomposites that in many cases provide an alternative for better mechanical and physical properties. Polymer nanocomposites contain fillers with at least one dimension in the nanometer scale. Aluminosilicate clay systems have been commonly used as the nanoscale fillers in these systems. Within this group, a naturally occurring aluminosilicate, montmorillonite, with the general structure $Na^{+}_{0.86}[Mg_{0.86}Al_{3.14}Si_{8.0}O_{20}H_4]^{-}$ has been widely used to produce polymer-clay nanocomposites. These clays form platelets with individual sheets measuring approximately 250 nm in length and 10 Å in thickness. Defects in their crystal structure during their natural formation, create a net anionic surface charge, which is countered through the presence of surface cations such as sodium and calcium.

Unmodified clays are highly hydrophilic and typically, surface modification involving cation interchange reactions with alkyl ammonium surfactants is required to facilitate their interaction with organic polymers. This reduces the enthalpic barrier related to polymer diffusion into the individual platelets to form intercalated or exfoliated

structures. At the same time, the use of long alkyl chains modifies the d-spacing of the clay, reducing the entropic barrier required to introduce polymer into confined geometries.

1.4.1 Intercalated and Exfoliated Nanocomposites

Exfoliated nanocomposite materials require careful synthetic or processing routes to achieve high degrees of dispersion, which is typically required for efficient improvements in the final properties. Here the silicates are homogenously dispersed throughout the polymer matrix with little or no interaction between individual platelets. Using modified silicates, organic-inorganic clay composites have been produced using a wide range of engineering polymers, including epoxy thermosets,[52,53] polyamide,[54,55] polyimide,[56] polystyrene,[57] polyurethane[58,59] and polypropylene.[60,61] Current developments in polymer-clay nanocomposites are focused in obtaining exfoliated morphologies, which have been related to improvements in the thermal, mechanical and barrier properties at low filler concentrations.

The intercalated morphology is characterized by a distinct peak in the X-ray diffraction pattern, signifying the presence of a lamellar structure and retention of order within the silicate domains. It is thought that the intercalated morphology is created after one or two polymer chains have entered into the gallery spacing, increasing the d-spacing. In general the intercalated morphology requires less rigorous production techniques and is therefore more easily manufactured. More importantly, it is believed that intercalated silicate nanocomposites have the potential of providing much improved mechanical properties unattainable by the exfoliated structure. Recent investigations[62]

suggest that since most of the material improvements in nanocomposites come from interactions on the molecular scale and since toughening occurs over a specific length scale, effective toughening mechanisms require a specific filler size (> 0.1 μm[63]) that may not be achieved by individual nanoscale particles.[52] As a consequence, it is suggested that the extremely reduced scale of a fully exfoliated structure may not be favorable for toughening, while an intercalated system, where polymer has entered into the galleries between silicates but has not fully delaminated them, may promote considerable interaction between silicate layers at a length scale large enough to promote toughening. Individual clay platelets are often too small to provide toughening through a crack bridging mechanism and cannot effectively enhance crack trajectory tortuosity, resulting simply invisible to the propagating crack.

1.4.2 Melt Intercalation Process

A variety of synthetic approaches as well as processing techniques have been developed to produce novel structures of polymer-clay nanocomposites. One technique that has attracted enormous industrial interest is the polymer melt intercalation method.[65] This simple method represents a promising new approach to fabricating polymer nanocomposites using conventional polymer processing techniques.

The general approach involves a mixture of polymer and clay that is heated up above the polymer melting temperature, conferring enough mobility to the polymer chain to diffuse into the clay galleries. This technique has been typically restricted to surface modified clays and chemically altered polymers, displaying enough enthalpic interactions between each other to overcome the overall energetic barrier associated with the exfoliation/intercalation process. In addition, compatibilizers that can enhance the

interaction between the polymer and clay systems have been also proposed as a feasible way to produce nanocomposites by melt intercalation. In this case, the miscibility of the small molecule compatibilizer with the polymer is extremely important to produce good clay dispersions, which are again related to enhanced properties of the composite.

CHAPTER 2

DRAWING OF ULTRAHIGH MOLECULAR WEIGHT POLYETHYLENE (UHMWPE) FIBERS IN SUPERCRITICAL CARBON DIOXIDE

The drawing behavior of ultra-high molecular weight polyethylene (UHMWPE) fibers in supercritical carbon dioxide ($scCO_2$) is compared to that in air at different temperatures. Temperature substantially influences the drawing properties in air, while in $scCO_2$ a constant draw stress and tensile strength are observed. Differential scanning calorimetry (DSC) shows an apparent development of a hexagonal phase along with a significant increase in crystallinity of air-drawn samples with increasing temperature. The existence of this phase is not confirmed by wide-angle x-ray scattering (WAXS) showing rather that air-drawn samples crystallize in an internally constrained manner. In contrast, $scCO_2$ allows crystals to grow without constraints through a possible crystal-crystal transformation, increasing the processing temperature to 110°C.

2.1 Introduction

The commercial and practical relevance of polyethylene has grown in a significant manner since it was introduced into our everyday life. Currently, polyethylene materials are synthesized and processed to attain properties particularly suited for specific applications. In this sense, several strategies have been proposed to obtain high modulus polyethylene fibers.[19] As mentioned in Chapter 1, UHMWPE fibers have rapidly gained acceptance in many applications in which high strength and modulus are required.[20] Since many investigations suggest that the final properties of UHMWPE materials are

remarkably influenced by their specific drawing conditions,[21,22] there is a considerable interest in understanding the effect of different processing variables, including drawing temperature and rate, on the final response of these fibers.

In general, it is widely accepted that under permeable conditions the interaction of $scCO_2$ with a semi-crystalline polymer is dominated by plasticization imposed by the presence of $scCO_2$. As mentioned before, under these conditions $scCO_2$ selectively permeates the amorphous phase and under certain conditions can induce secondary crystallization processes.[13] As presented in figure 2.1 this plasticization process can be observed in a stress-strain curve where systems processed in $scCO_2$ show decreases in the draw stress and significant enhancements in their overall drawability.[1,2] Also, as shown in figure 2.2 samples drawn in $scCO_2$ show significantly higher crystallinity and orientation along with improved mechanical properties.[3] This behavior has been observed in a variety of semicrystalline polymers.

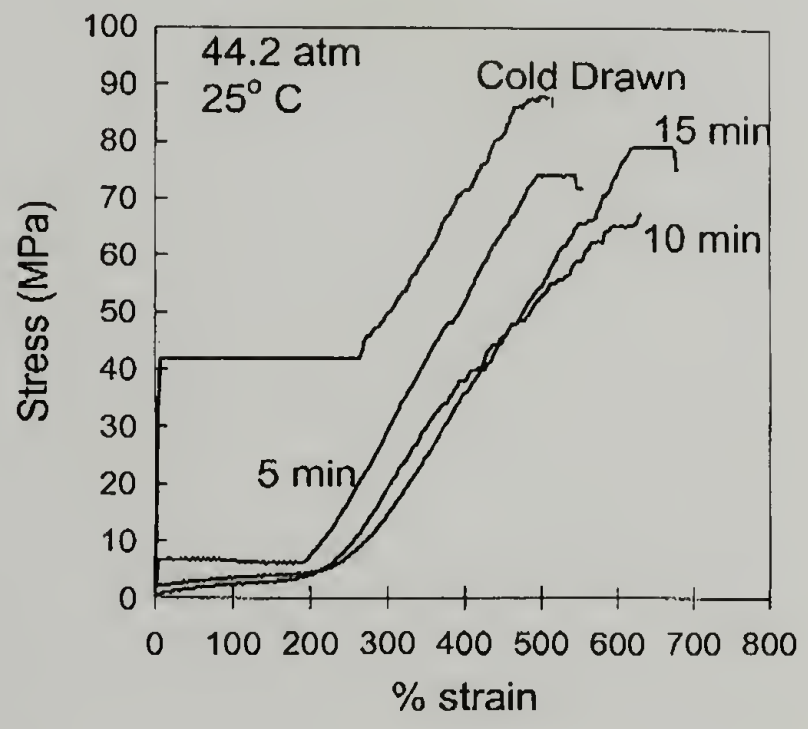

Figure 2.1. Stress-strain behavior of PET fibers plasticized in CO_2 at different conditions.[1,2,3]

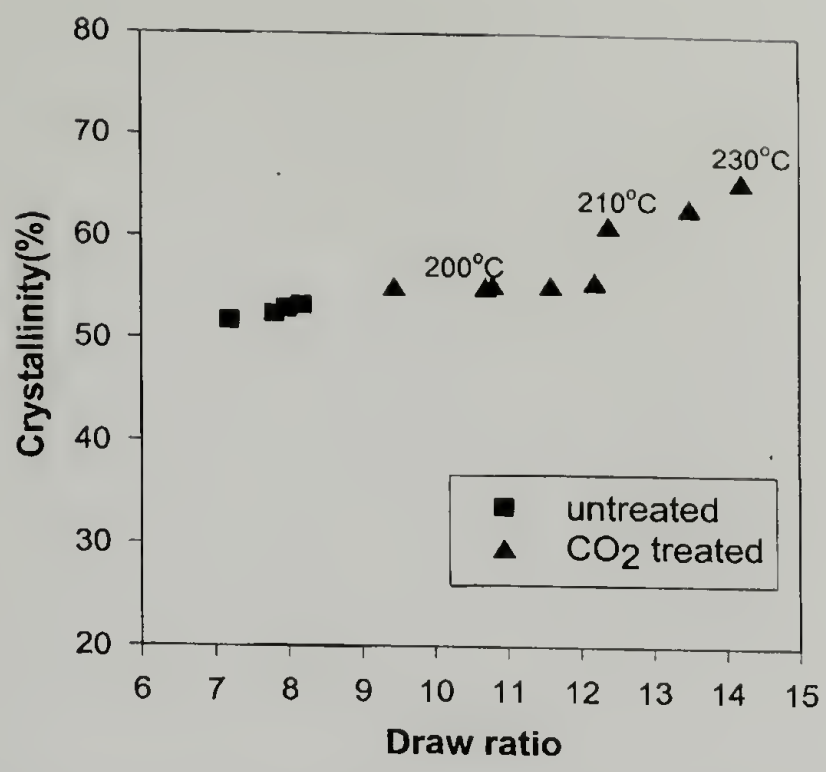

Figure 2.2. Crystallinity percent of PET fibers at different conditions.[1,2,3]

Under non-permeable conditions, the interaction of $scCO_2$ with a semicrystalline polymer is no longer dominated by plasticization, and the imposed hydrostatic pressure becomes the dominating effect. These conditions will apply to highly crystalline materials where the amorphous phase is restricted, thus reducing the possibility of a plasticizing effect by CO_2. As shown in figure 2.3, at these conditions, $scCO_2$ will promote changes in the state of stress of drawing, imposing hydrostatic contributions to the principal stresses that in some cases might be able to modify the physical and mechanical properties of the deformed material.

$$\begin{bmatrix} \sigma_{11} & \sigma_{12} & \sigma_{13} \\ \sigma_{21} & \sigma_{22} & \sigma_{23} \\ \sigma_{31} & \sigma_{32} & \sigma_{33} \end{bmatrix} = \begin{bmatrix} \sigma_t + p & 0 & 0 \\ 0 & p & 0 \\ 0 & 0 & p \end{bmatrix}$$

Figure 2.3. State of stress for uniaxial deformation under hydrostatic pressure (Non-permeable condition).

In polymorphic systems, crystal-crystal transformations can be triggered as a consequence of the high-pressure environment. In general, this effect has not been studied and the overall hydrostatic contribution of $scCO_2$ in the drawing process has not been quantified and understood yet.

Crystalline Phase Characteristics	Graphical Representation
Orthorhombic • Most common crystalline phase in PE. • Cuboid, all axes have different length, and all internal angles are 90°. • Contains 2 complete ethylene units. • Density of 1.00 g/cm3. • Branching not allowed. Branches larger than a methyl group are excluded from the crystalline lattice.	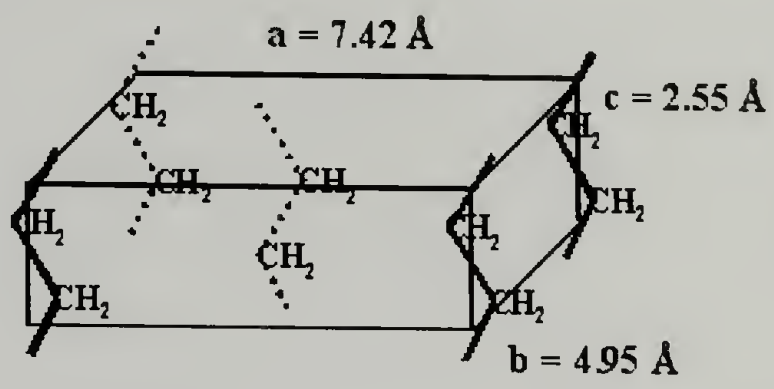
Monoclinic • Metastable crystalline phase. • Formed under conditions of significant elongation. • Temperatures above 60-70 °C revert it to the orthorhombic form.	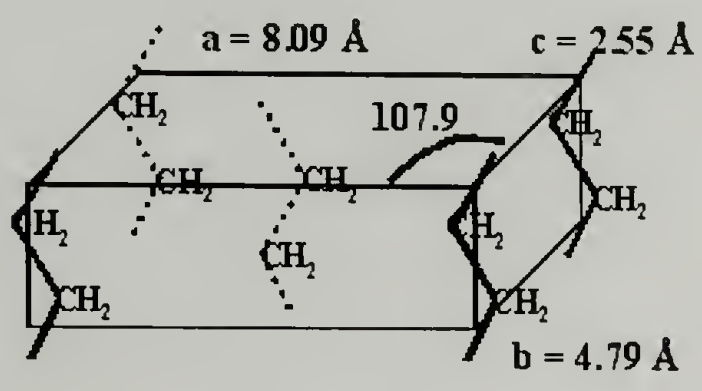
Hexagonal • Very rare. • Produced by crystallization at high pressures. • High mobility phase. Sometimes referred as the "rotator phase", due to the possibility of free rotation of individual chain stems in this phase at random angles with respect to their neighbors.	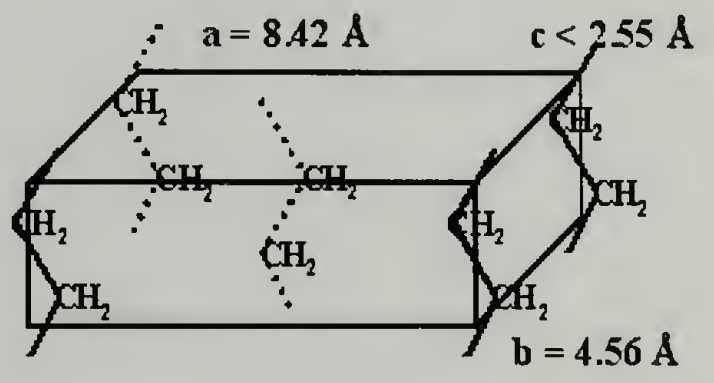

Table 2.1. Crystalline phases in polyethylene.

In polyethylene, the polymorphic behavior has been well-characterized and crystal transitions to the hexagonal phase have been detected when extreme conditions are

imposed.[14-18] The typical crystalline phases observed in polyethylene as well as the main characteristics of each phase are summarized in table 2.1.

In this work, the in-situ drawing behavior along with the physical and mechanical properties of UHMWPE fibers drawn uniaxially in $scCO_2$ have been compared to those observed when the deformation is done in air. Significant differences are observed both in the thermal and mechanical properties of $scCO_2$-drawn fibers with respect to the air-drawn fibers at the same processing conditions. Because of the high crystallinity of these materials (>90%), a typical plasticization effect of $scCO_2$ into the amorphous phase is not expected. In contrast, the effect of the hydrostatic pressure brought about by the presence of $scCO_2$ is related to the observed changes in the properties of the $scCO_2$-drawn fibers. Experimental data support the idea of a possible crystal-crystal transformation to the more mobile hexagonal phase, due to a synergistic effect of the drawing temperature and the higher pressures imposed when the deformation is done in $scCO_2$.

2.2 Experimental

UHMWPE fibers (Spectra® 900) obtained from Honeywell have been used in this study. The drawing experiments are conducted using an originally designed apparatus shown in figure 2.4. The apparatus is mounted on a universal tensile testing machine (Instron model 1333) and it is constructed primarily of standard high-pressure fittings. The apparatus is able to make *in-situ* force measurements using a calibrated stainless steel cantilever beam and a linear variable displacement transducer (LVDT). As depicted in figure 2.4, the mechanical grips are located inside a high-pressure vessel and directly attached to the movable piston of the Instron.

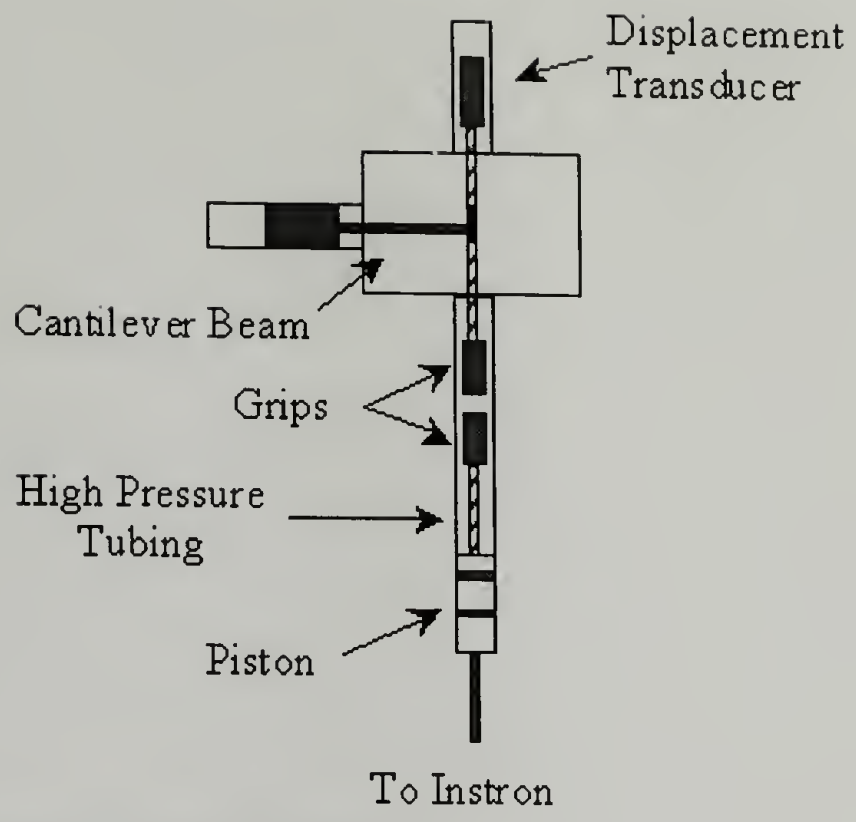

Figure 2.4. High pressure drawing apparatus.

A high-pressure CO_2 pump (Hydro-Pac, Inc.) with a maximum discharge pressure of 286.84 MPa is used to introduce ultra-high purity CO_2 to the system. Specific control over the pressure is maintained during the experiment. The signals and crosshead displacements are monitored using a PC with MTS Teststar II software. The initial cross sectional area is determined both with SEM images of the specimens and by the ratio of the linear density of the fibers and the density of the undrawn UHMWPE fiber (0.97 kg/m^3). Strain is calculated from the relative displacement between the crosshead and the beam divided by the original specimen gauge length. All the drawing experiments are conducted at a deformation rate of 0.01 m/60 s and the sample gauge length is maintained at 0.060 m ± 0.005 m.

Single filament tests are performed on an Instron 1123 universal testing machine. Specimens of 0.020 m ± 0.002 m are cut and tested at a deformation rate of 10%/60 s. The fiber diameter is estimated either by using a high magnification optical microscope calibrated with a micrometer scale or by the ratio of their linear density and 0.97 kg/m^3

and the corresponding SEM images of the tested specimen. Due to the negligible adhesion of UHMWPE fibers to commercially available epoxy adhesives, a special mechanical grip was designed for these measurements. In this grip, both ends of the fiber are wrapped around two small stainless steel cylinders (1.27 cm long and 0.32 cm in diameter), which were previously polished to prevent friction. Both cylinders are then placed on the base of the grip and are tightened using two independent screws on each side. The original design of this grip prevents any slippage of the fiber during the deformation.

Differential Scanning Calorimetry (DSC) experiments are conducted using a TA Instruments thermal analyst model 2100 DSC at a heating rate of 1 °C/min, to analyze the thermal behavior of the samples. The overall morphology of these samples is investigated using a Scanning Electron Microscope (SEM) model JEOL-CS-35 with a filament voltage of 20 KV. In addition, analysis of the crystal structure is done by Wide-Angle X-ray Scattering (WAXS) in a Statton camera device on a Rigaku RU-200 rotating-anode diffractometer with Fuji As-Va image plates, using an operating voltage of 40 KV and a total current of 30 mA under vacuum conditions. The geometry of the measurements is such that the fibers are placed perpendicular to the direction of the beam.

2.3 Experimental Results

2.3.1 *In-situ* drawing behavior

The drawing behavior of bundles of UHMWPE fibers (120 filaments per bundle) is analyzed and compared at different conditions. A representative behavior is depicted in figure 2.5. A typical elastic region is observed in which all the filaments in the bundle

deform uniformly. The upper limit of this region is depicted by a strain (ε_1) and a level of stress (σ_1), which describes the conditions at which the first filament of the bundle fails. Beyond this point, subsequent failure of a few additional filaments in the bundle is observed at varying stress levels, up to a certain value σ_f, defined as the draw stress. σ_f represents the stress at which the remaining filaments in the bundle are homogeneously deformed up to a maximum strain (ε_f) prior to a catastrophic failure of the sample. The value of (ε_f) is used to estimate the maximum draw ratio obtained in the sample.

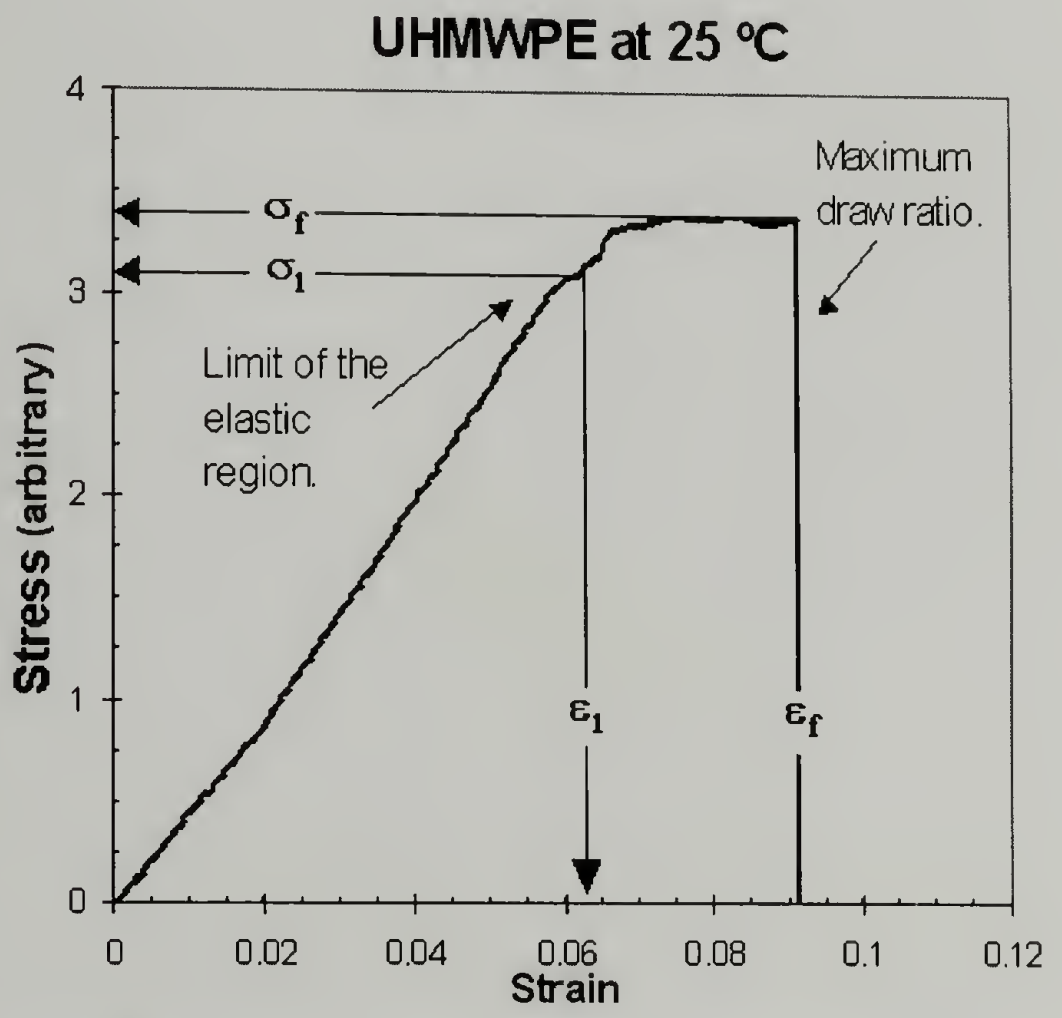

Figure 2.5. Typical drawing behavior of an UHMWPE fiber bundle.

Since the drawing behavior of bundles is analyzed in this section, load-strain curves are used to describe the behavior at different conditions. Stress-strain curves are going to be used in later sections to describe the properties of individual fibers processed at various conditions.

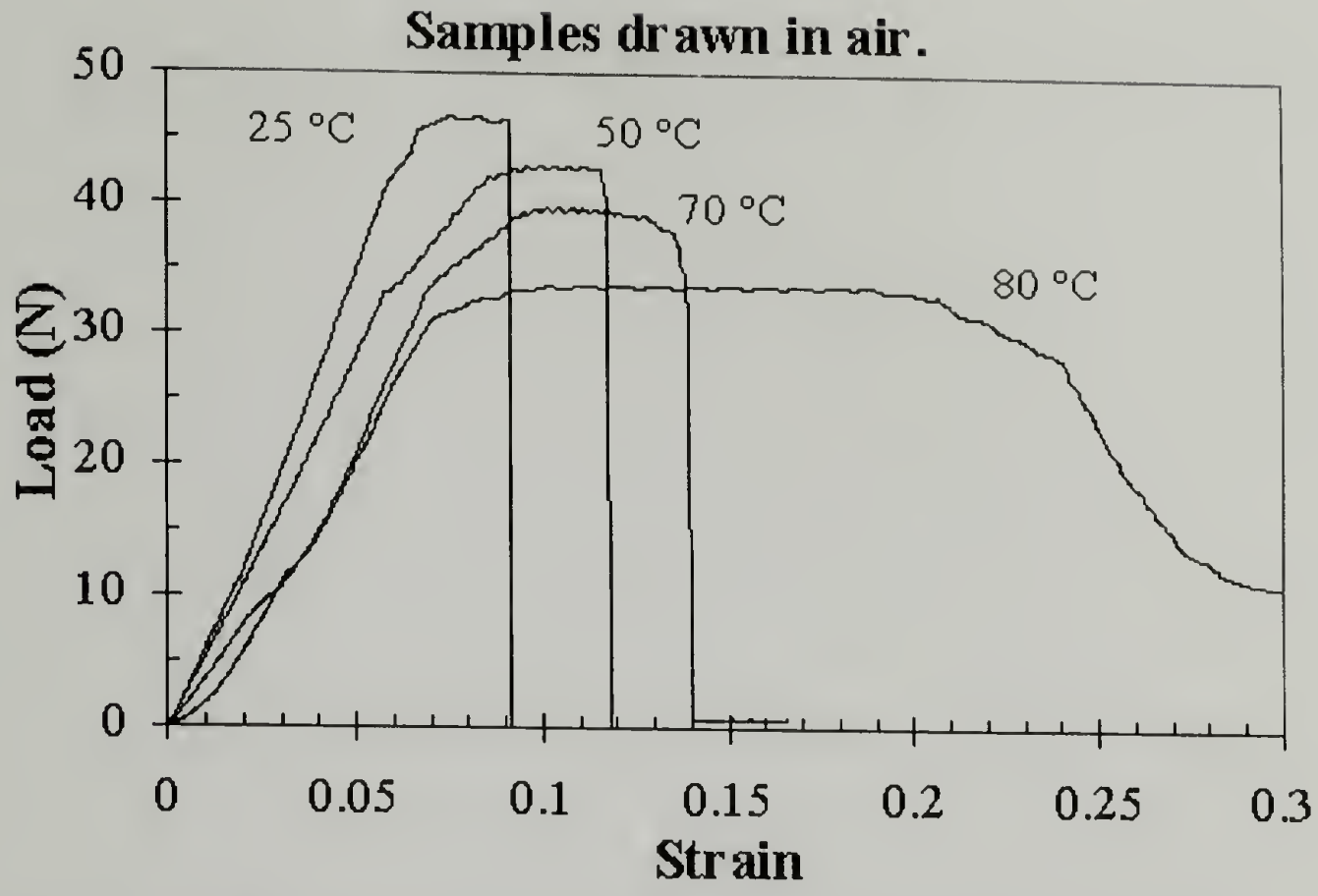

Figure 2.6. Drawing behavior of UHMWPE fibers deformed in air at different temperatures.

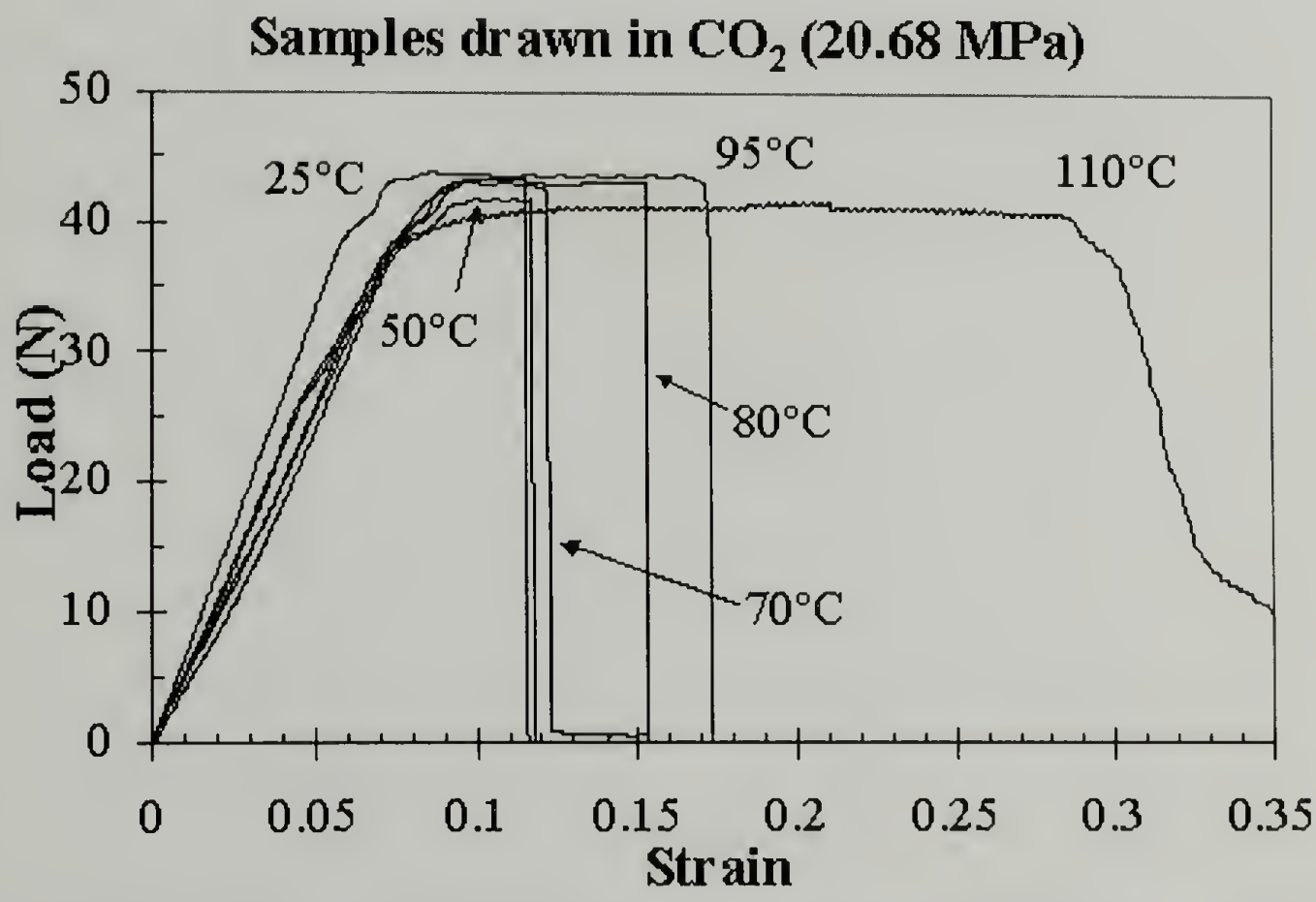

Figure 2.7. Drawing behavior of UHMWPE fibers deformed in the presence of CO_2 at different temperatures.

In this regard, the drawing behavior of UHMWPE fibers treated in $scCO_2$ (20.68 MPa) is compared to that observed at ambient pressures within a certain temperature range. The *in-situ* drawing results indicate that the behavior is completely modified by the presence of $scCO_2$. From figure 2.6, it is evident that the drawing behavior in air is highly temperature dependent. An increase in the drawing temperature substantially reduces both the apparent modulus and the draw stress (σ_f). The value of σ_f decreases from 308 MPa at 25 °C to 224 MPa at 80 °C (figure 2.9). It is convenient to point out that in this case a maximum processing temperature of 80 °C is observed. This limiting temperature corresponds to the α-transition of polyethylene, as shown in figure 2.8, which in this case is located in a rather small temperature range (80-83 °C) due to the high orientation and crystallinity.[14] This transition is generally related to movements of the polymer chains within the crystals, something that substantially reduces the mechanical integrity of a fiber.

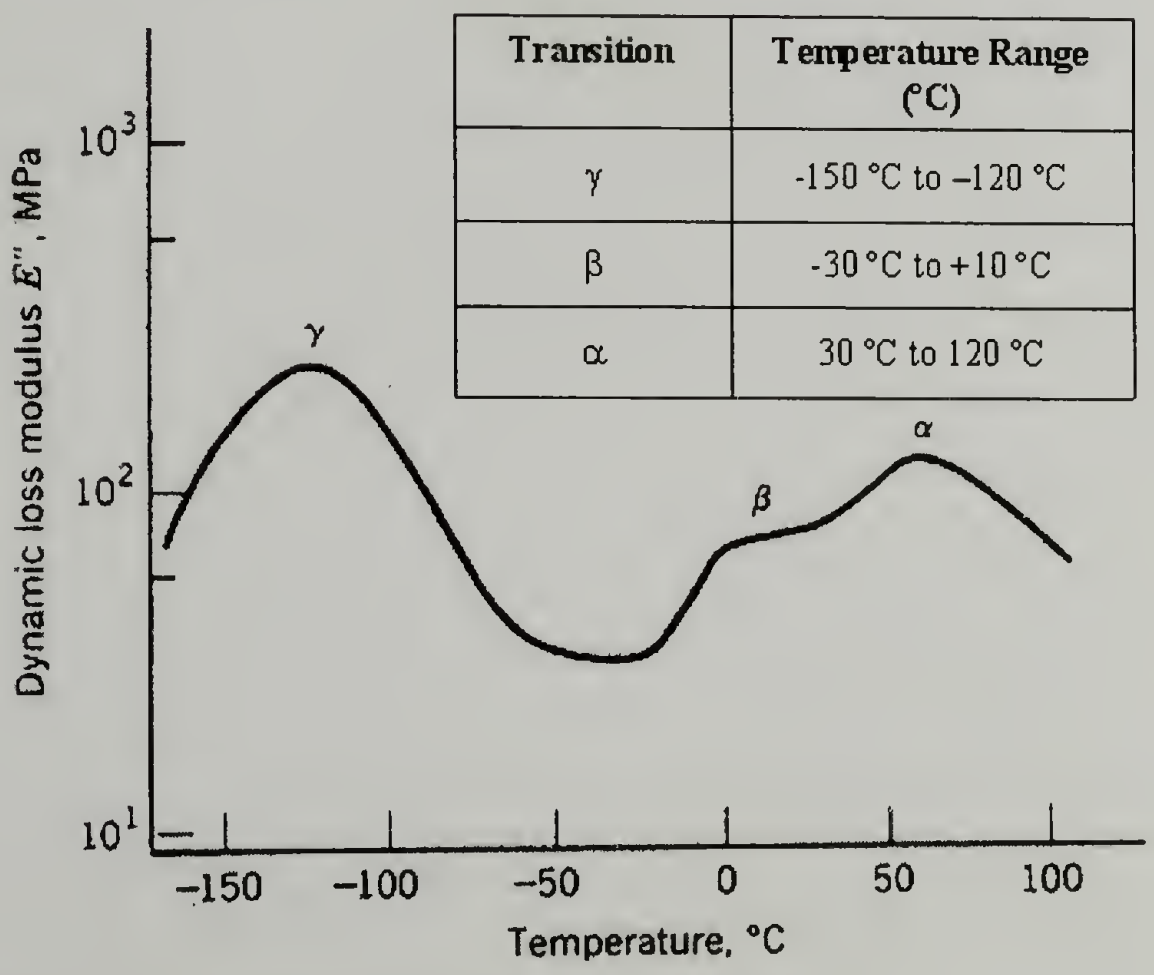

Figure 2.8. Thermal transitions/relaxations in polyethylene.[69]

This behavior differs from that observed in the presence of $scCO_2$. As depicted in figure 2.7, both the apparent modulus and the draw stress (σ_f) are not affected by an increase in temperature. Clearly, the temperature dependence observed in air-drawn samples is completely suppressed by conducting the deformation in $scCO_2$. In contrast from what it is observed for the air-drawn samples, the value of σ_f remains constant at a 286 MPa over the entire range (figure 2.9). In addition, the processing range of these fibers is increased up to a temperature of 110 °C, i.e. a 30 °C increase in the processing range is obtained when the deformation is done in $scCO_2$.

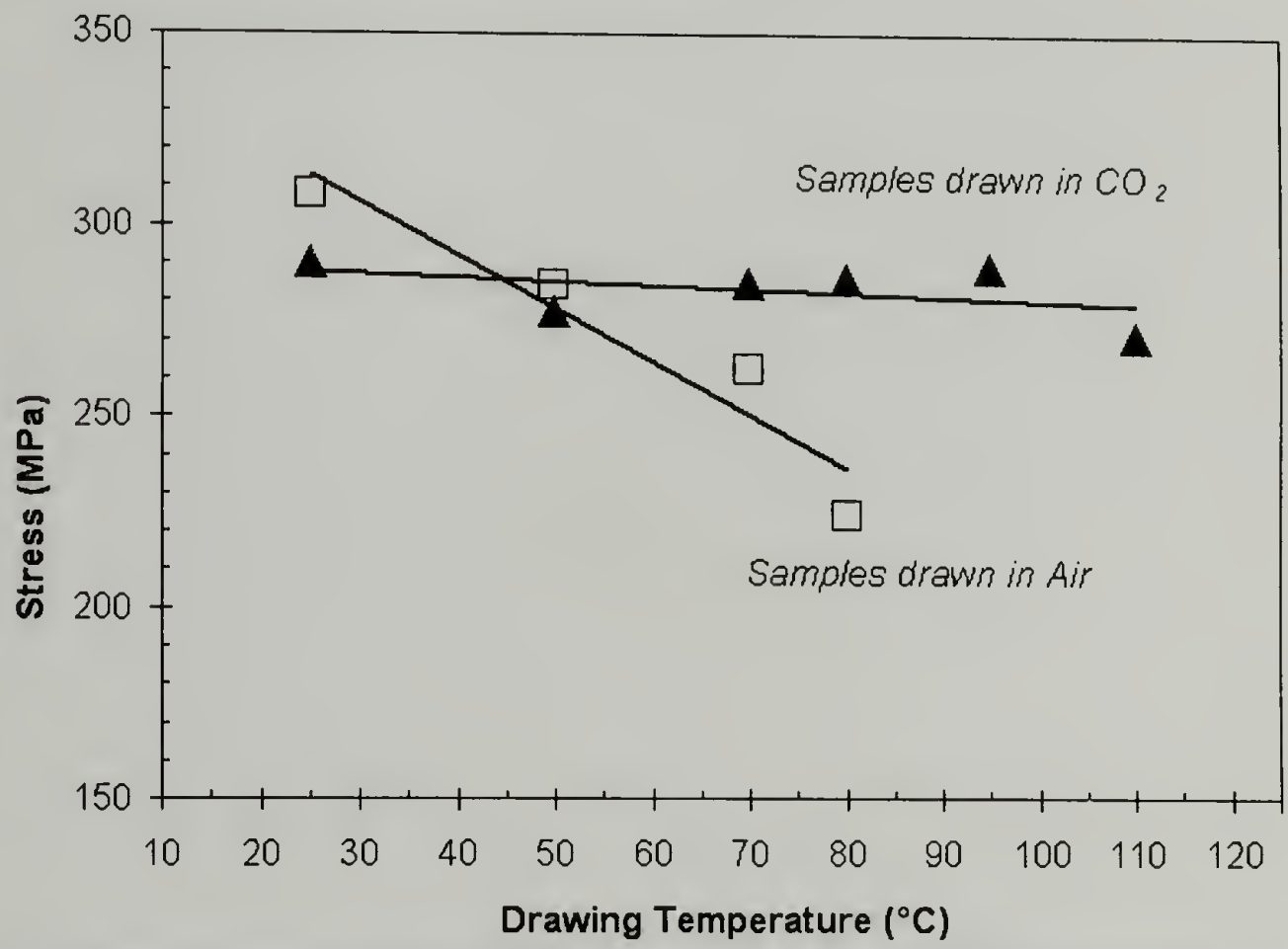

Figure 2.9. Draw stresses of UHMWPE fibers deformed at different processing conditions.

The maximum draw ratios estimated from ε_f are summarized in table 2.2. These results show that the maximum draw ratio increases in a significant way with temperature. In general, for a given temperature, higher deformations are obtained without $scCO_2$. These results suggest that the mechanical properties of these fibers are maintained when processing the sample in $scCO_2$.

Drawing Temperature (°C)	Air-drawn samples Draw ratio	$ScCO_2$-drawn samples Draw ratio
25	1.06	1.08
50	1.08	1.08
70	1.16	1.12
80	1.24	1.13
95	-	1.16
110	-	1.35

Table 2.2. Maximum draw ratios of UHMWPE fibers deformed at different processing conditions.

The initial elastic region is quantitatively described in table 2.3 and figure 2.10. A constant value of σ_1 (255 MPa aprox.) is observed along the entire range when processing in $scCO_2$, as shown in table 2.3. In contrast, , clear temperature dependence is observed in air-drawn samples, decreasing the value of σ_1 from 280 MPa to 206 MPa when the drawing temperature is increased to 80 °C.

Sample	Drawing Temperature (°C)	σ_1 (MPa)
Air-drawn	25	280
Air-drawn	50	219
Air-drawn	70	222
Air-drawn	80	206
CO_2-drawn	25	259
CO_2-drawn	50	251
CO_2-drawn	70	263
CO_2-drawn	80	252
CO_2-drawn	95	256
CO_2-drawn	110	255

Table 2.3. σ_1 values for UHMWPE fibers drawn at different conditions.

On the other hand, figure 2.10 shows that the limiting strain of the elastic region (ε_1) seems to be independent of the presence of $scCO_2$, suggesting that the drawing temperature is the predominant factor upon the value of ε_1.

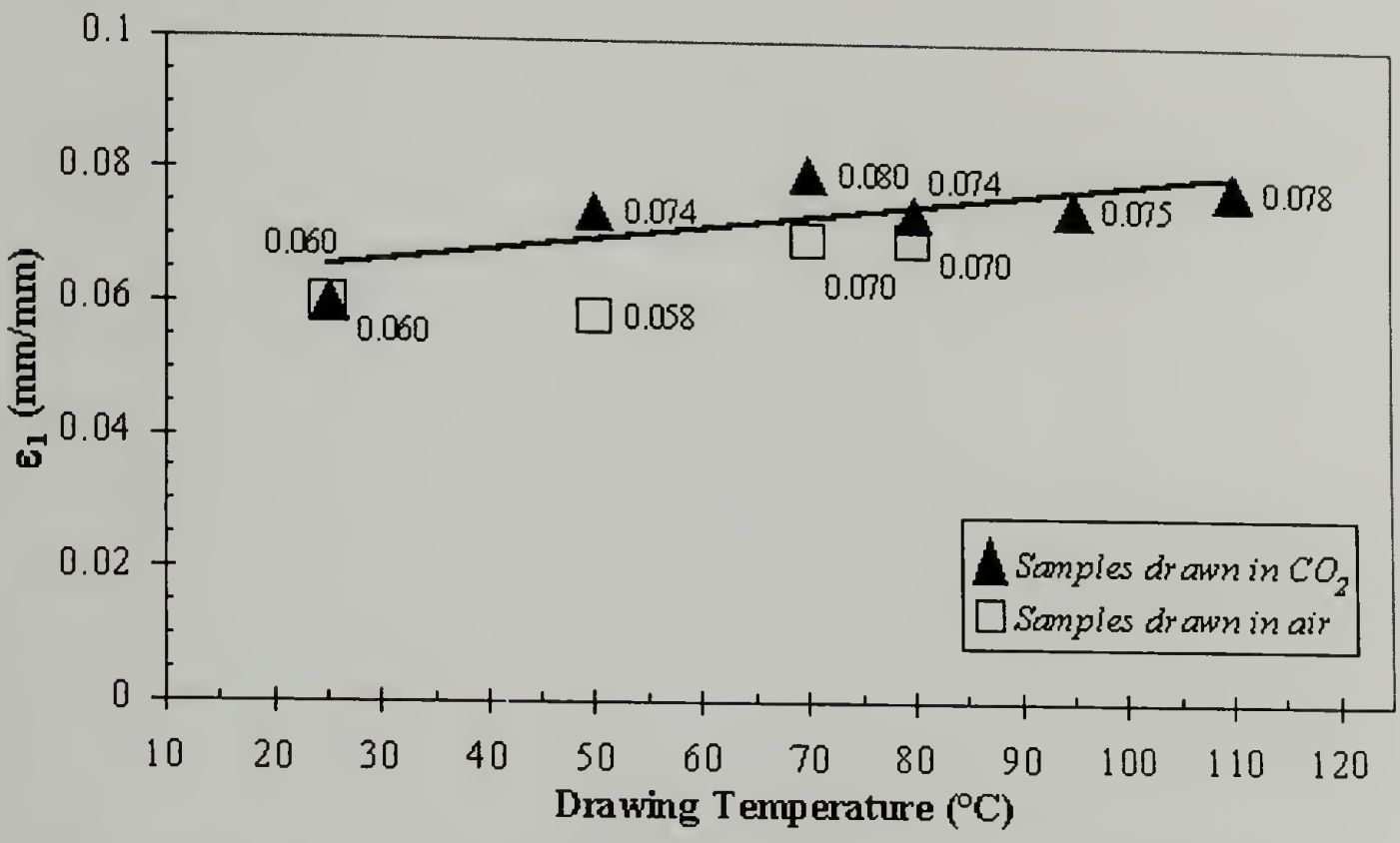

Figure 2.10. ε_1 of UHMWPE fibers deformed at different processing conditions.

2.3.2 Thermal Behavior-Differential Scanning Calorimetry (DSC)

DSC experiments are conducted over a temperature range of 25-210 °C using a slow heating rate (1 °C/min) to increase precision on the detection of the thermal transitions of UHMWPE. As depicted in figures 2.11 and 2.12, two melting endotherms are detected in all samples. At approximately 142 °C, a large endotherm corresponding to the typical transition involving the melting of crystals in an orthorhombic unit cell is observed. In addition, another endotherm is observed at 150 °C that corresponds to the transition of crystals in a hexagonal unit cell to the melt phase. The presence of this hexagonal phase as described in the literature[15,16,23] is mainly associated with the presence of a highly oriented structure and is typically observed in samples processed under high pressure.

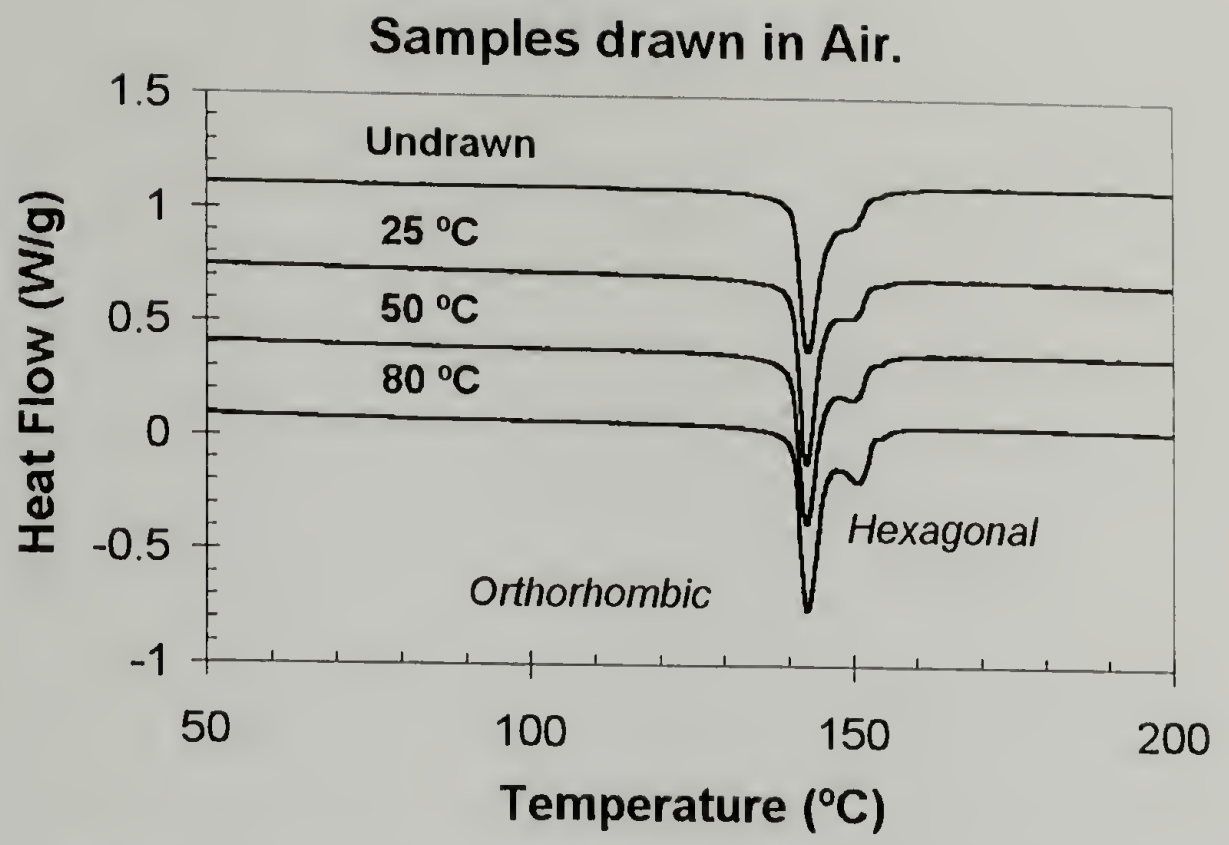

Figure 2.11. Thermal behavior of samples drawn in air at different temperatures.

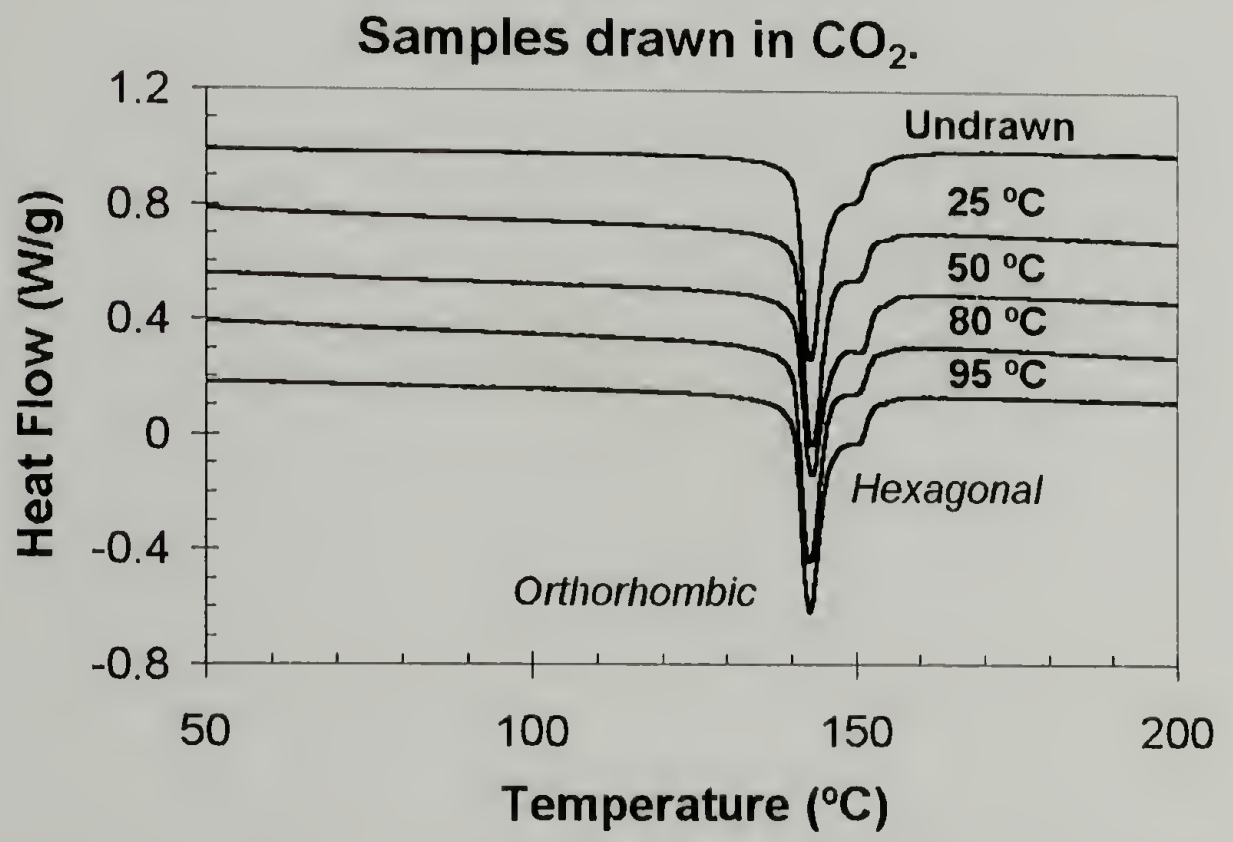

Figure 2.12. Thermal behavior of samples drawn in $scCO_2$ at different temperatures.

As depicted in figure 2.11, a considerable growth of the melting endotherm at 150 °C with increasing temperature is observed in air-drawn samples. This result suggests an apparent development of the hexagonal phase for these samples with increasing drawing temperature. In contrast, figure 2.12 shows that samples treated in $scCO_2$ maintain their

crystalline composition, showing no difference in their thermal behavior over the entire range of processing temperatures.

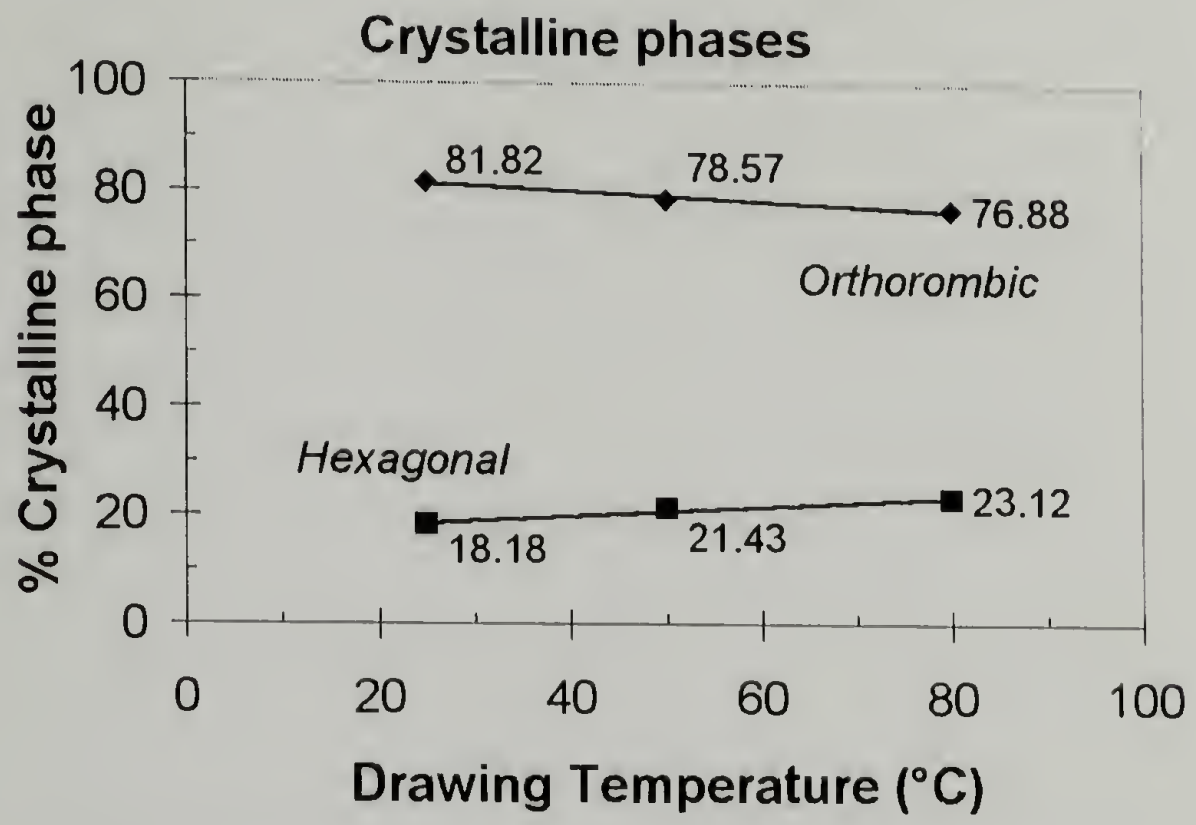

Figure 2.13. Crystalline compositions as calculated by DSC for samples drawn in air at different temperatures.

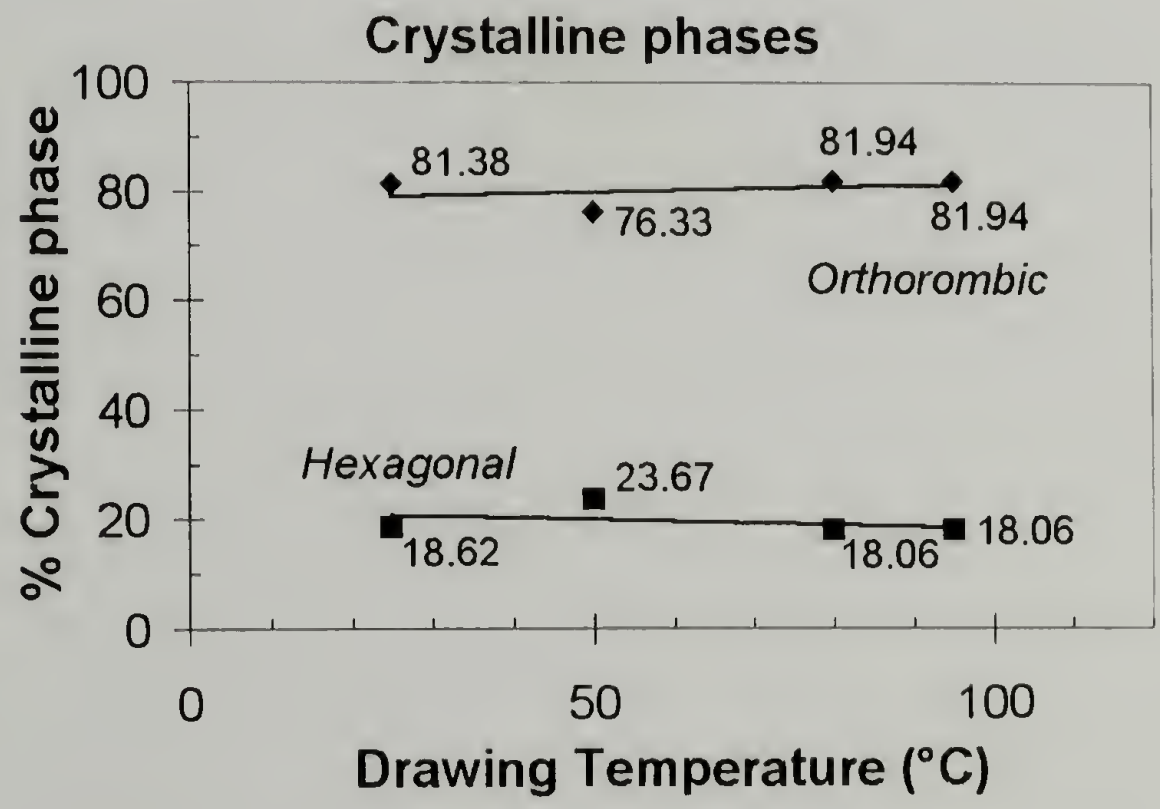

Figure 2.14. Crystalline compositions as calculated by DSC for samples drawn in CO_2 at different temperatures.

These observations are corroborated by estimating the crystalline composition based on the melting peaks observed in DSC. Deconvolution of the signals renders the amount of hexagonal crystals created during the heating process. These results are shown in figures 2.13 and 2.14, suggesting that the amount of hexagonal crystals is maintained constant for $scCO_2$ treated samples but it increases with drawing temperature for the case of samples drawn in air.

The total crystallinity of the samples is estimated by the ratio of the melting enthalpy of both endotherms and the heat of fusion for polyethylene (288.89×10^3 J/Kg). As presented in table 2.4, the crystallinity of air-drawn samples increases considerably up to a value of 98% at higher drawing temperatures. In contrast, no significant changes are observed in the crystallinity of $scCO_2$-treated samples. These results suggest that $scCO_2$ helps to maintain the integrity of the crystalline phase besides the fact that it does not interact with it.

Sample	**Drawing Temperature (°C)**	**Crystallinity (%)**
Undrawn UHMWPE	-	90.1
Air-drawn	25	91.2
Air-drawn	50	95.2
Air-drawn	70	96.1
Air-drawn	80	98.7
CO_2-drawn	25	91.0
CO_2-drawn	50	92.6
CO_2-drawn	80	93.7
CO_2-drawn	95	93.3

Table 2.4. Crystallinity changes for UHMWPE fibers drawn at different conditions.

No changes in the apparent melting points are observed regardless of the processing conditions, suggesting that the imposed deformation does not promote changes or alterations to the crystalline phase. In all cases, a second scan in the DSC shows a broad melting peak around 139 °C, showing that the high orientation of the sample is destroyed during the melting process.

2.3.3 General Morphology-Scanning Electron Microscopy (SEM)

SEM analysis is employed to analyze the macroscopic morphology of the deformed materials. SEM images are used to estimate and compare the amount of macroscopic damage created by the deformation and its relation with the processing conditions. As shown in figure 2.15, the general morphology of these fibers is characterized by a considerably smooth surface, with no evident flaws even at higher magnifications. These factors arise as a consequence of the highly oriented structure of the fibers. Fibers of 20-30 μm in diameter with no significant size polydispersity characterize this material. Also from this figure, it is evident that regardless of the processing conditions, no significant changes in the general morphology are observed. The imposed deformation and in some cases the hydrostatic pressure have no significant effect in the smoothness and orientation of the material. These observations suggest that the differences between materials processed at different conditions become apparent at a smaller length scale, without promoting significant changes in the macroscopic morphology of the fiber.

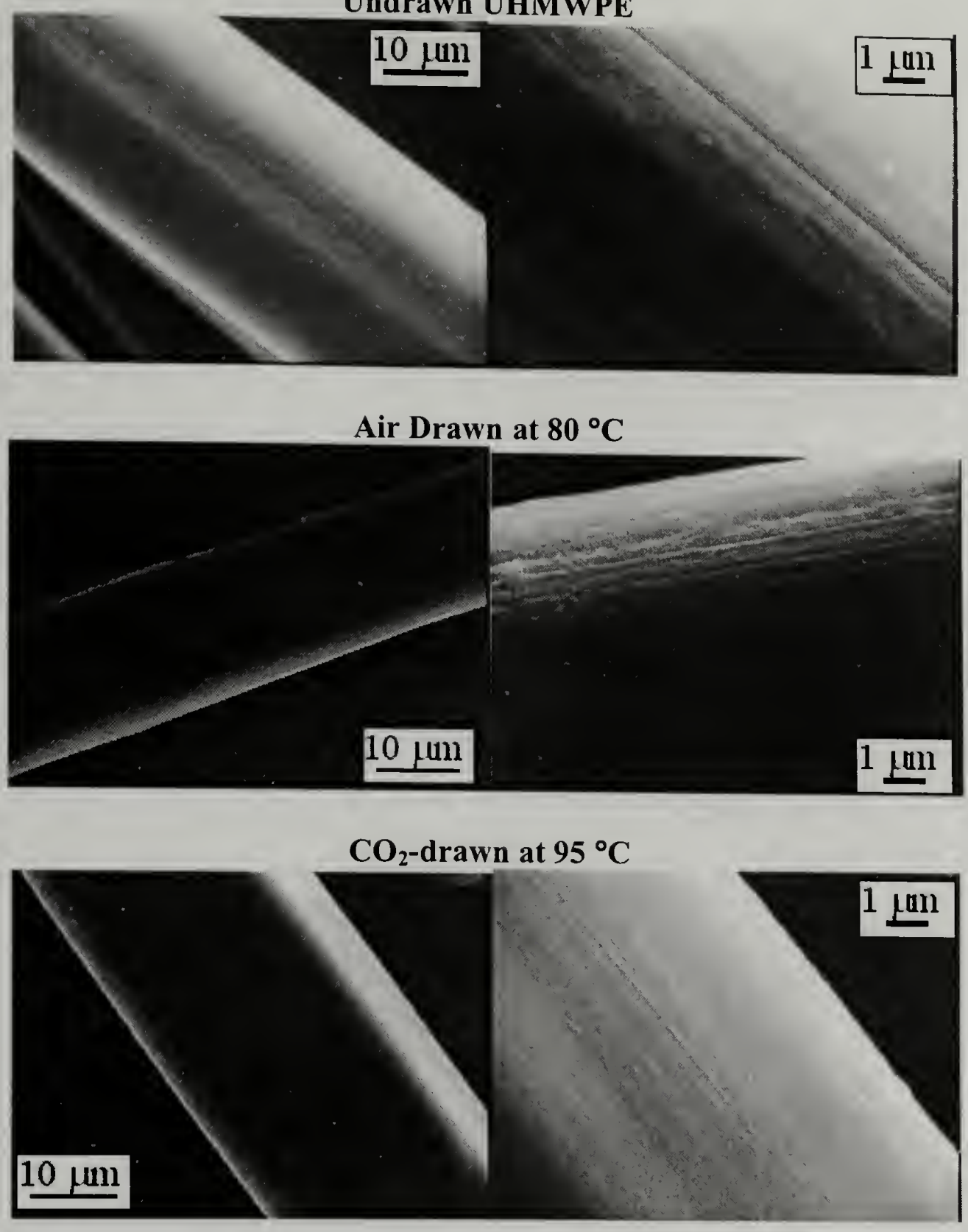

Figure 2.15. SEM images of UHMWPE fibers processed at different conditions.

2.3.4 Crystal Structure-Wide Angle X-ray Scattering (WAXS)

WAXS experiments are employed both to quantify the crystalline composition of the samples and to estimate the effects of the deformation on the crystal integrity of the samples. The geometry of the measurements is such that the fibers are placed perpendicular to the direction of the beam.

The scattering pattern of the undrawn fiber is compared to that of fibers drawn at different conditions. The results are presented in figure 2.16. Well-defined reflections are obtained for all samples, evidence of their highly oriented structure and their highly crystalline nature. The high orientation remains unchanged regardless of the processing conditions. The strong reflections dominate completely the scattering pattern with almost no sign of an amorphous halo, corroborating the high values of crystallinity, as suggested by DSC.

Two principal reflections are observed in all cases. As shown in table 2.5, the d-spacings of these reflections match with an orthorhombic type of unit cell (4.10 and 3.70 Å, respectively). The first reflection corresponds to the 110 plane in an orthorhombic unit cell, a reflection typically observed in polyethylene.[16,23] The second reflection is assigned to the 200 plane, also from an orthorhombic unit cell.

Sample	**d-spacing (Å)**	**d-spacing (Å)**
Theoretical orthorhombic	4.10 **(110_o)**	3.70 **(200_o)**
Theoretical monoclinic	4.55 **(100_m)**	-
Theoretical hexagonal	4.33 **(100_h)**	-
Undrawn UHMWPE	4.101	3.703
Air-drawn at 80°C	4.136	3.740
CO_2-drawn at 95°C	4.128	3.720

Table 2.5. Typical d-spacings in polyethylene and their comparison with the observed reflections.

Undrawn UHMWPE

Air-drawn 80 °C

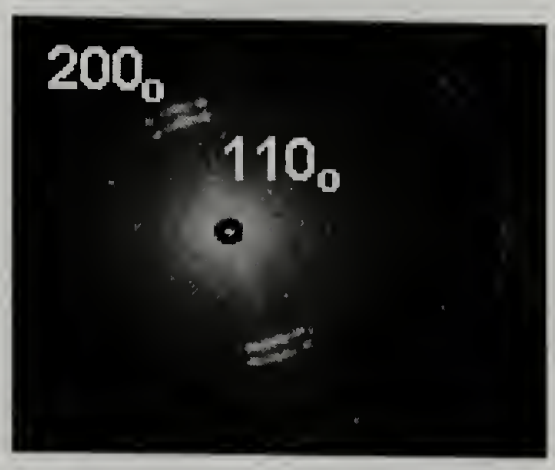

CO_2-drawn 95 °C

Figure 2.16. WAXS analysis of UHMWPE fibers drawn at different conditions.

In contrast of what is observed by DSC, the presence of the hexagonal phase in the air-drawn samples deformed at higher temperatures is not confirmed by WAXS. No reflections are assigned to a hexagonal type of unit cell showing that the hexagonal phase is not present in any of these samples at ambient conditions. This observation suggests that the high-temperature melting peak observed in the air-drawn samples correspond to hexagonal crystals created during the heating process. The transition from orthorhombic

to hexagonal phases in polyethylene fibers has been reported in the literature.[15,16,18] This transition is generally related to the presence of constraints into the sample due to their highly oriented structure.

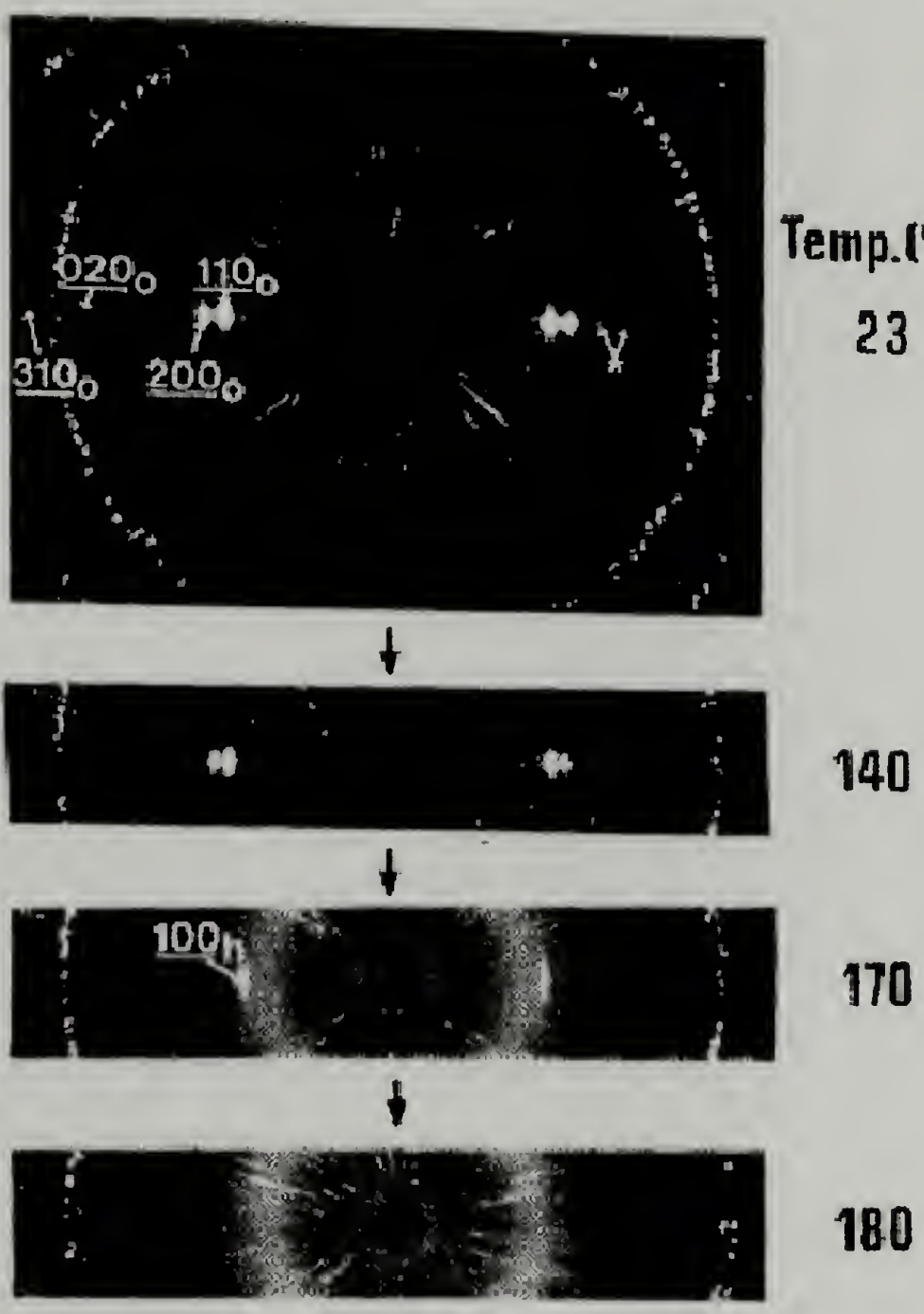

Figure 2.17. WAXS analysis showing the transition from orthorhombic to hexagonal in epoxy embedded UHMWPE fibers.[15,16,18]

In fact, as presented in figure 2.17, polyethylene fibers embedded into a rigid epoxy substrate will shift to the more mobile hexagonal phase when approaching the melting temperature. As shown, the two peaks from the orthorhombic phase will coalesce into one that corresponds to the 100 plane of the hexagonal phase. In addition, highly oriented polyethylene samples will present a completely different thermal behavior when heated

under constrained conditions, as shown in figure 2.18. In addition to the melting of orthorhombic crystals, some will shift to the hexagonal phase, which appears to be thermodynamically more stable, before the melting process takes place.

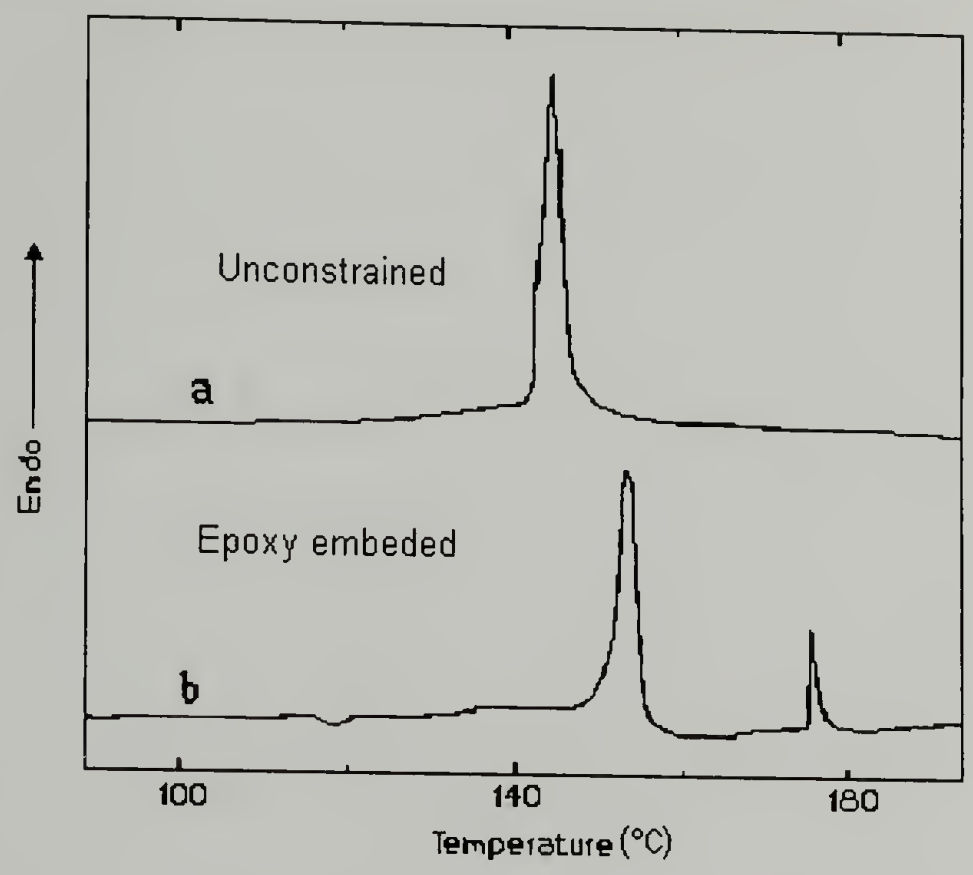

Figure 2.18. DSC analysis of highly oriented polyethylene samples under constrained and unconstrained conditions.[15,16,18]

2.3.5 Mechanical Properties

The final properties of fibers drawn at different conditions are determined by single fiber mechanical tests. Some of the typical responses observed at different conditions are shown in figure 2.19. Elastic modulus, strain at break and break stress or tensile strength are calculated from the response of at least 10 identical specimens tested at the same conditions. The results are presented in figures 2.20 and 2.21 and summarized in table 2.6.

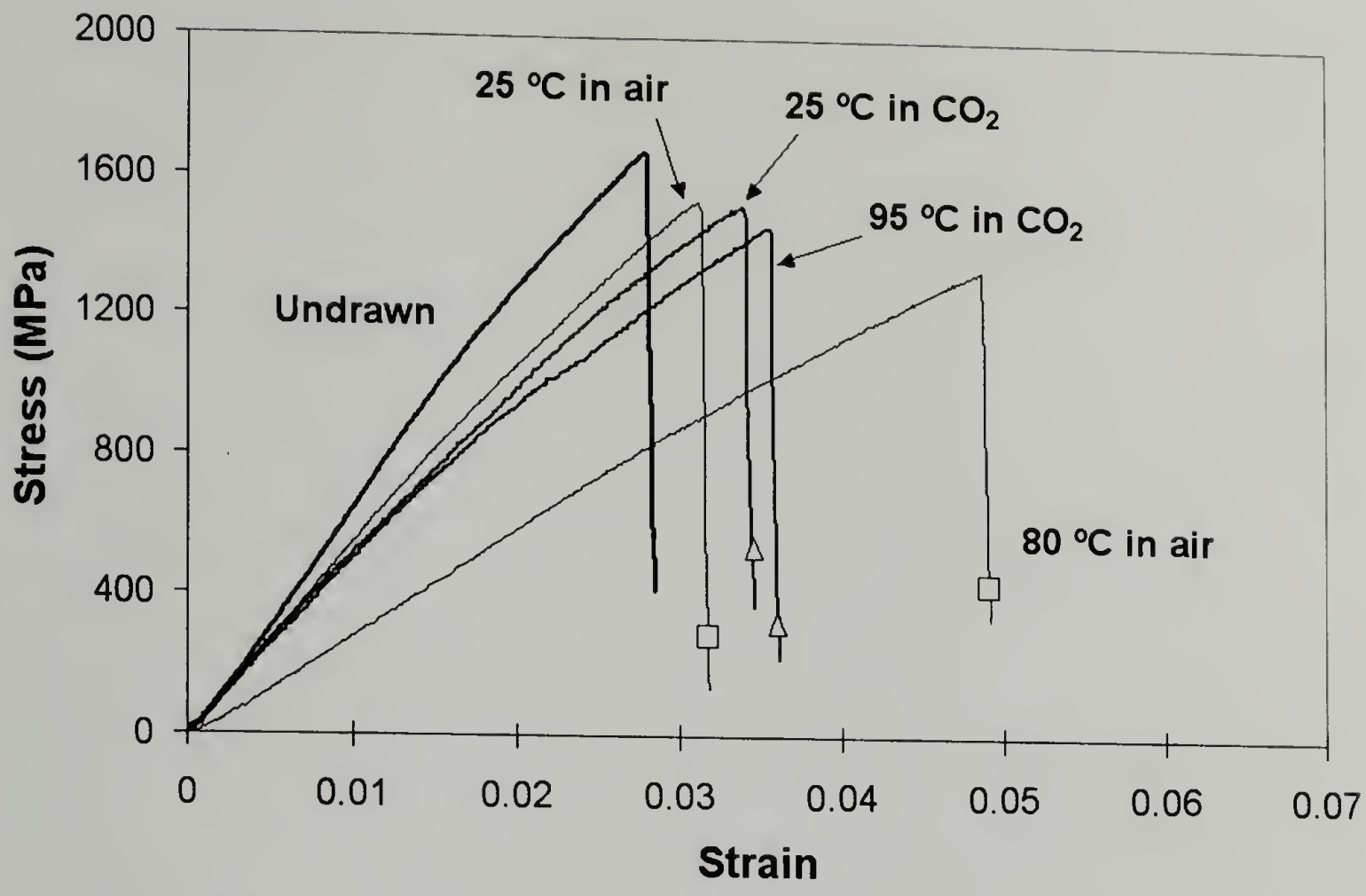

Figure 2.19. Single filament stress-strain curves of UHMWPE fibers treated at different processing conditions.

Evidently, the mechanical response of samples treated in $scCO_2$ remains approximately constant with increasing temperature. Both the elastic modulus and the strain at break remain unchanged at 50 GPa and 3.5% respectively, over the entire temperature range. This suggests again that the high-pressure environment created by the presence of $scCO_2$, helps to maintain the mechanical integrity of the fiber and so, the required macroscopic deformation to break the sample remains unaltered regardless of the processing conditions. This behavior is also observed for the case of the break stress as presented in figure 2.21.

In contrast, the behavior for the air-drawn samples is completely different. The mechanical properties are very temperature dependent in this case. As suggested in figures 2.20 and 2.21, both the elastic modulus and tensile strength are reduced in a significant manner with increasing temperature. Almost a 45% decrease in the elastic

modulus along with a 13% reduction in tensile strength is observed by increasing the processing temperature to 80 °C. The larger draw ratios observed in these samples correlate with their higher crystallinity, as described below.

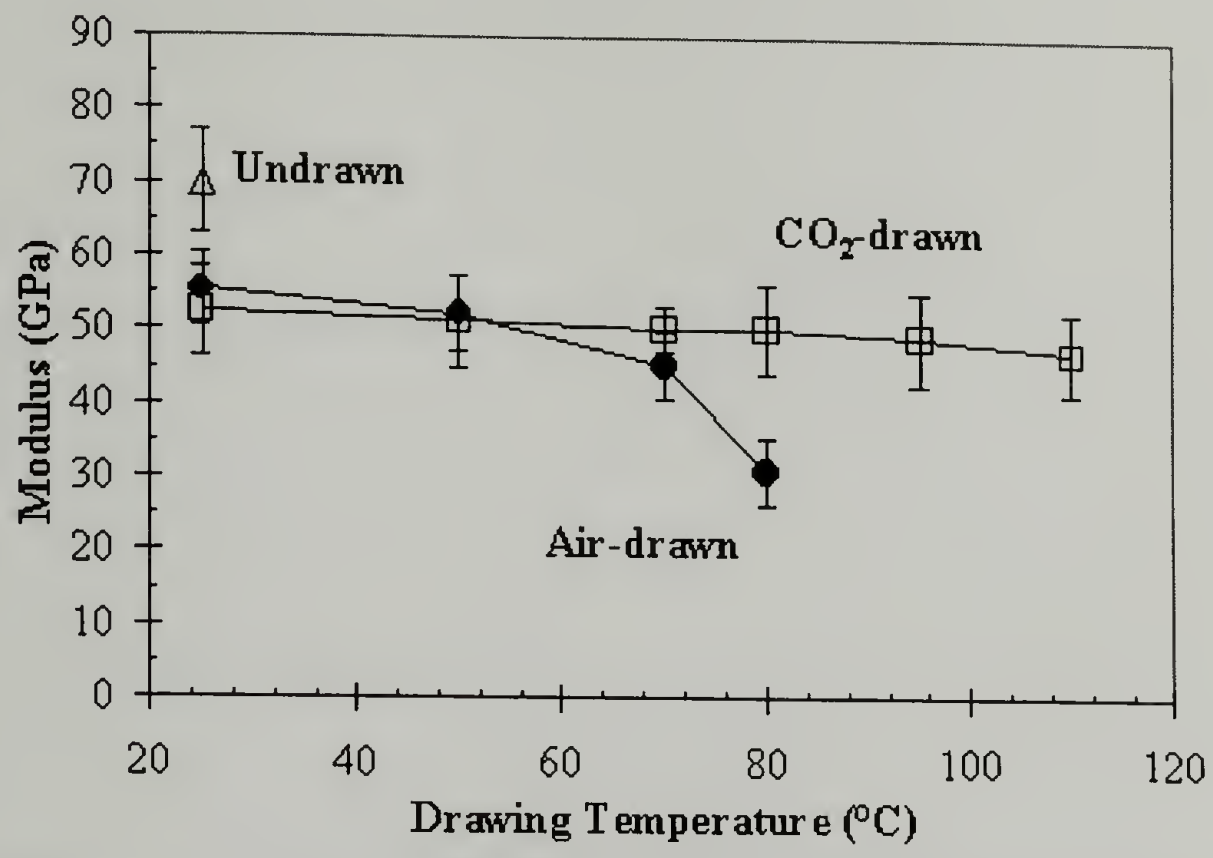

Figure 2.20. Elastic modulus of UHMWPE fibers treated at different processing conditions.

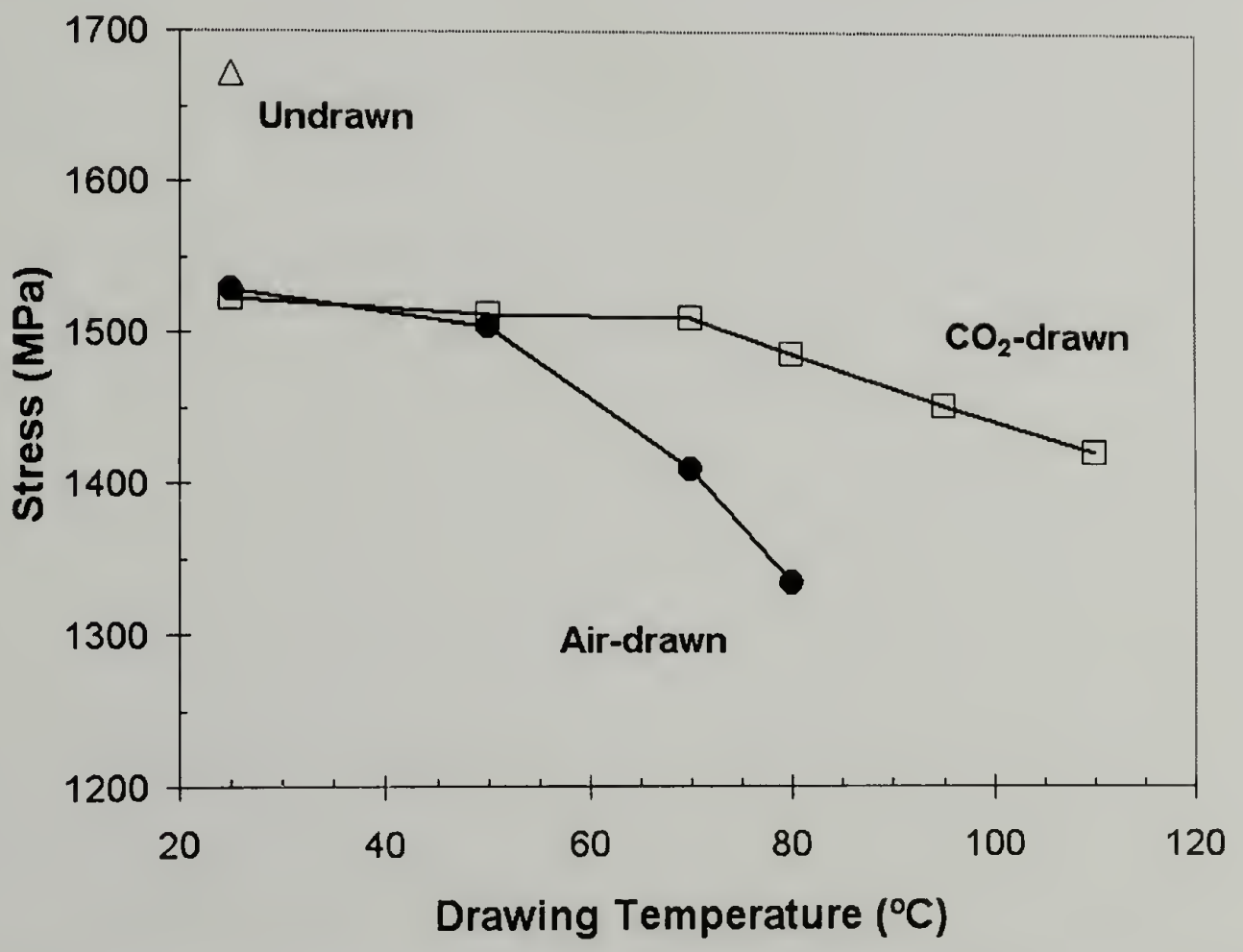

Figure 2.21. Break stress of UHMWPE fibers treated at different processing conditions.

Sample	Modulus (GPa)	Strain at break (%)	Break stress (MPa)
Undrawn UHMWPE	69.9	2.7	1672
25 °C in Air	55.4	3.15	1528
50 °C in Air	52.2	3.26	1503
70 °C in Air	45.1	4.14	1409
80 °C in Air	30.8	4.70	1334
25 °C in CO_2	52.4	3.40	1522
50 °C in CO_2	51.1	3.39	1512
70 °C in CO_2	50.2	3.42	1509
80 °C in CO_2	50.1	3.46	1485
95 °C in CO_2	48.9	3.57	1452
110 °C in CO_2	46.9	3.55	1421

Table 2.6. Single filament properties of UHMWPE fibers at different processing conditions.

However, as depicted in figures 2.20 and 2.21, it seems that the macroscopic deformation imposed by drawing, promotes an overall decrease in the mechanical properties with respect to the undrawn sample. For the specific case of the $scCO_2$-drawn samples, this reduction in the mechanical properties is compensated by the fact that the processing range is increased in a considerable manner (30 °C).

2.4 Discussion

These results overall suggest that the deformation in $scCO_2$ is different from that observed at ambient pressure. The high-pressure along with the presence of $scCO_2$ promote significant differences in the deformation process, which reflect in the final thermal and drawing behavior. Drawing in air appears to involve the deformation of an

orthorhombic unit cell along the entire process. The macroscopic deformation imposed to the sample promotes some strain-induced crystallization, which is responsible for the increased crystallinity of these samples, as detected by DSC. The deformation is highly temperature dependent in this case, as judged by the considerable increase in the draw ratios for the case of air-drawn samples. In this case, the addition of new crystals to the existing crystalline lamellae is restricted due to the low mobility of chains within the orthorhombic unit cell. The newly formed crystals either grow between the existent lamellae or as extended single chains, this later possibility being specifically valid for polyethylene.[23] These two situations inevitably promote internal constraints in the sample. In any of these cases, the newly formed orthorhombic crystals will tend to expand to the more mobile hexagonal phase during heating before transforming into the melt phase, relaxing the stress imposed by the constraints.[16] This being the reason for the appearance of the melting endotherm at 150 °C in these samples during the DSC experiments. At ambient conditions, however, no hexagonal phase is present and only the orthorhombic unit cell is present, as confirmed by WAXS.

The deformation in $scCO_2$ appears to involve a crystal-crystal transformation, from the orthorhombic unit cell to the more mobile hexagonal phase due to the high-pressure environment (20.7 MPa). It is well known that the mobility of the hexagonal phase is related with the degrees of freedom for rotations around the c-axis of the fiber, but that the deformation along the chain backbone is somewhat restricted.[15,16] If as suggested a hexagonal phase is formed in this case, lower macroscopic uniaxial deformations would be expected for $scCO_2$-treated samples. This is actually in agreement with the lower draw ratios observed experimentally. As a consequence, the amount of strain-induced

crystallization would also be reduced, suggesting that the crystallinity of these samples must remain unchanged with increasing drawing temperature, something also confirmed by DSC. Furthermore, since the hexagonal phase melt at a higher temperature[15], the presence of this phase when drawing in $scCO_2$ explains the observed increase in the processing temperature range. This suggests that either the presence of $scCO_2$ or the imposed hydrostatic pressure suppress the α-transition of UHMWPE fibers, shifting it to higher temperatures through a crystal-crystal transformation to the hexagonal phase.

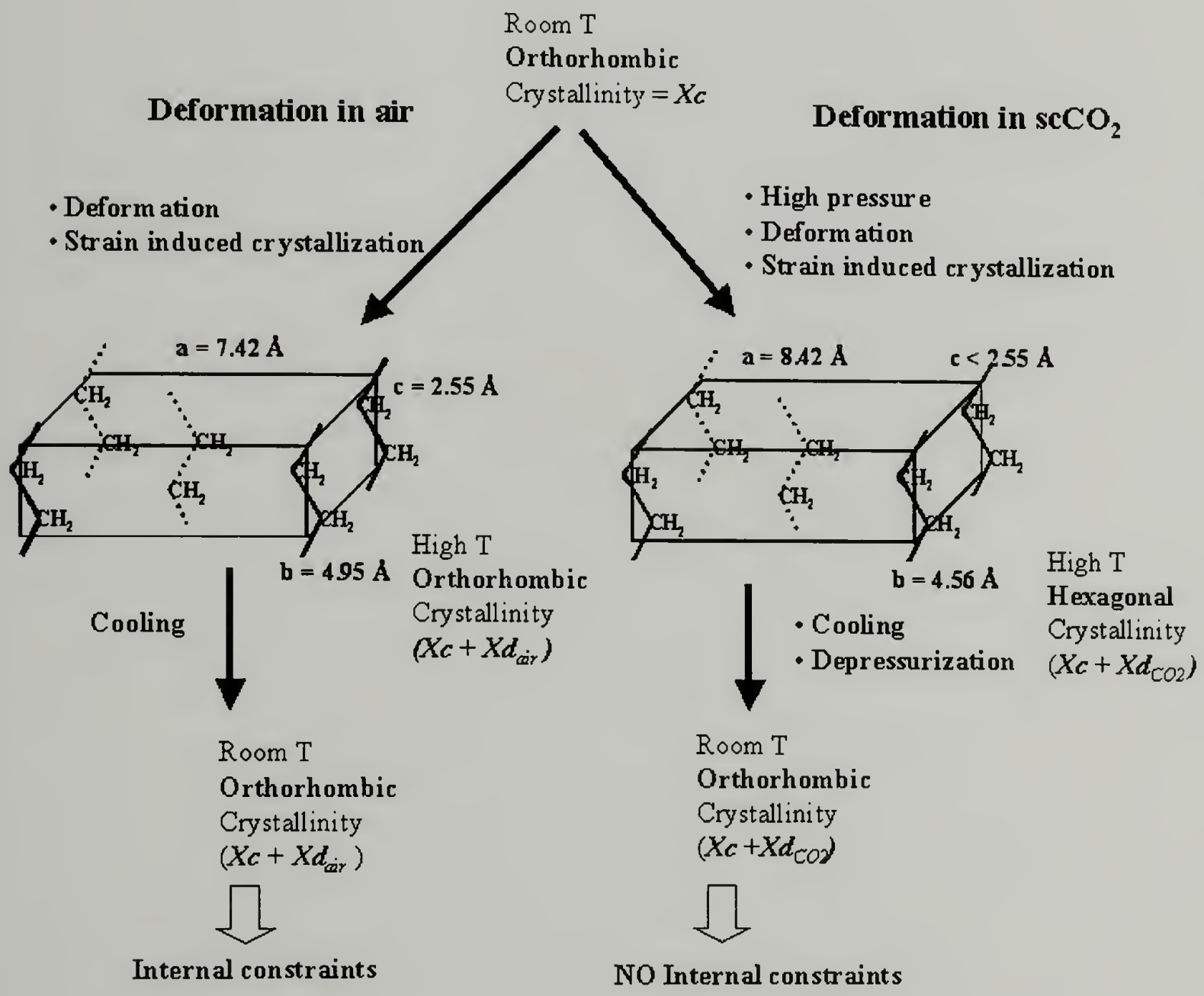

Figure 2.22. Suggested deformation mechanism of UHMWPE fibers in air and in $scCO_2$.

In contrast to the case of air-drawn samples, the newly formed crystals are added to the existing crystalline lamellae without internal constraints due to the high mobility of the hexagonal phase. Thus, no change in the thermal behavior is expected for samples treated in $scCO_2$ at different temperatures, as also confirmed experimentally by DSC. During depressurization, crystals within the sample return to the original orthorhombic phase, as suggested by WAXS. The suggested deformation mechanism is presented graphically in figure 2.22.

2.5 Deformation at high pressures- hydrostatic effects

To confirm that the behavior described before is related only to hydrostatic effects promoted by the supercritical conditions of CO_2, drawing experiments at different pressures were conducted.

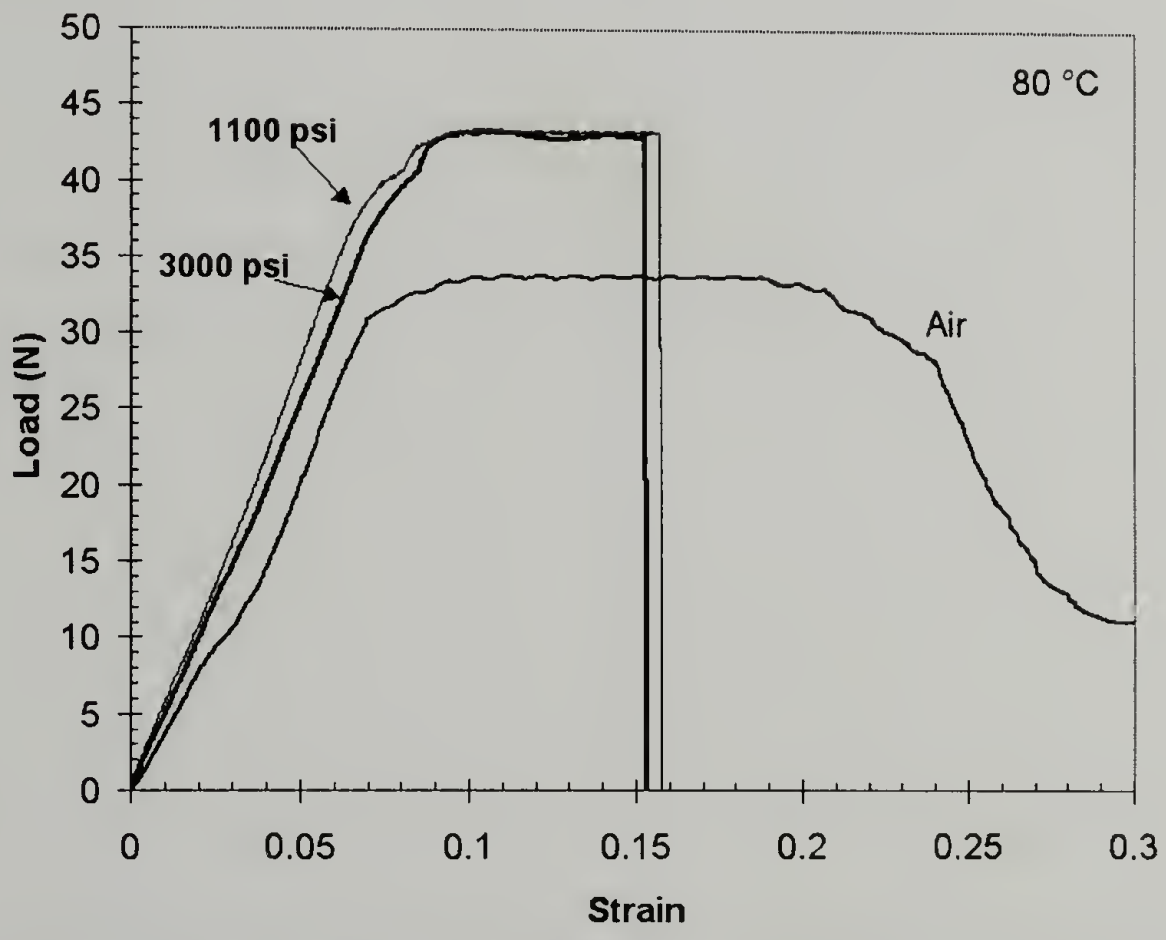

Figure 2.23. Drawing behavior observed at 80 °C using different pressures. The behavior in air is shown for comparison.

The *in-situ* drawing behavior is presented in figure 2.23 using of two different pressures at 80 °C. As shown, the response in $scCO_2$ appears to be independent of the pressure, and clearly the temperature dependence observed in the air-drawn sample is not observed in CO_2 even at lower pressures.

The thermal behavior of samples obtained at different pressures is presented in figure 2.24, where again a bimodal melting behavior is observed. In this case, an increase in pressure appears to restrict the amount of hexagonal crystals created during the heating process, which as suggested before are an indirect way of quantifying the amount of internal constraints in the sample. This observation supports the idea of the high-pressure environment stabilizing the crystalline structure during deformation, shifting to the hexagonal phase reducing the strain-induced crystallization process.

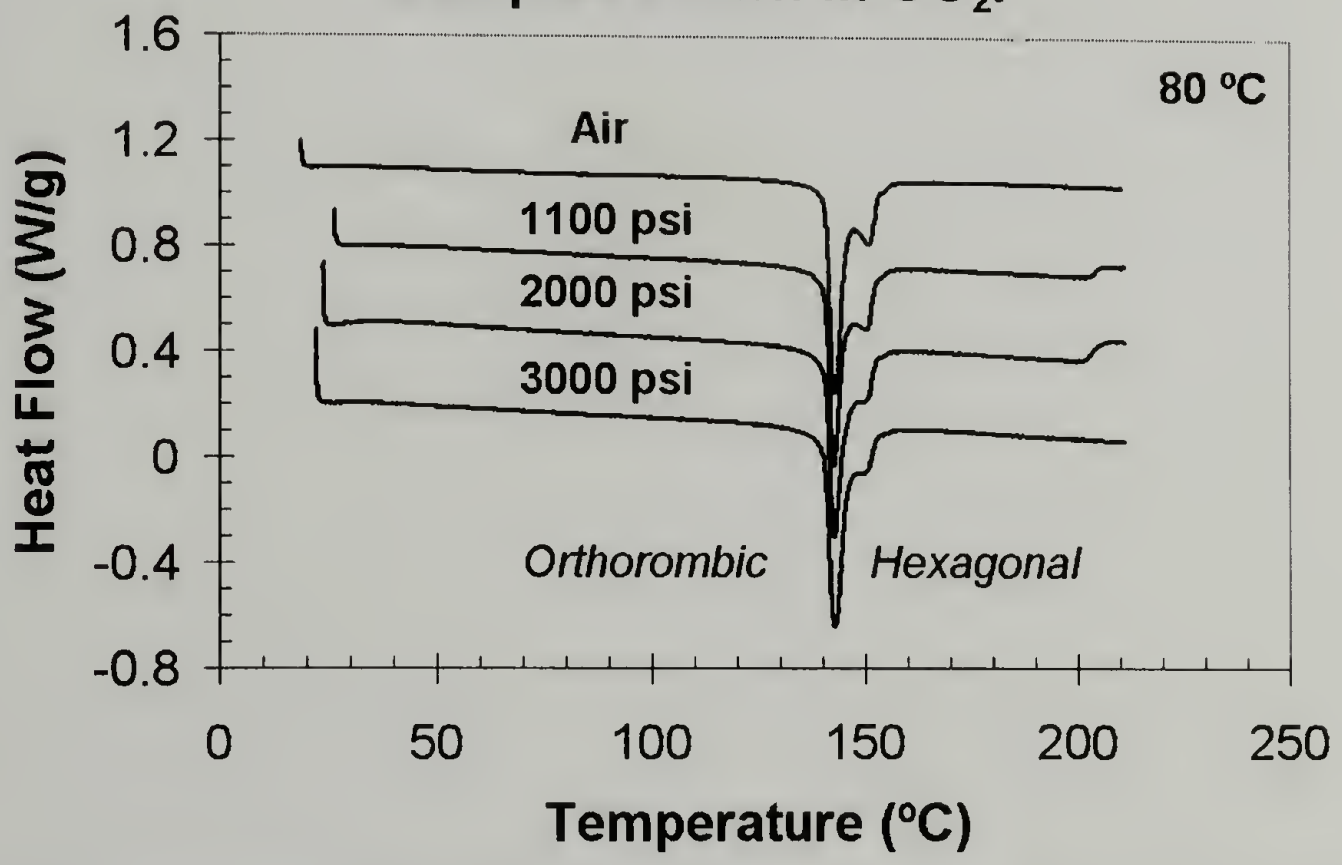

Figure 2.24. Thermal behavior for UHMWPE fibers drawn in $scCO_2$ at 80 °C using different pressures. The behavior in air is shown for comparison.

As suggested in figure 2.25 this effect is more evident at higher pressures and the crystalline composition reflects a slight pressure dependence. This difference, however, is comparable to the precision of the instrument and might be entirely related to experimental conditions.

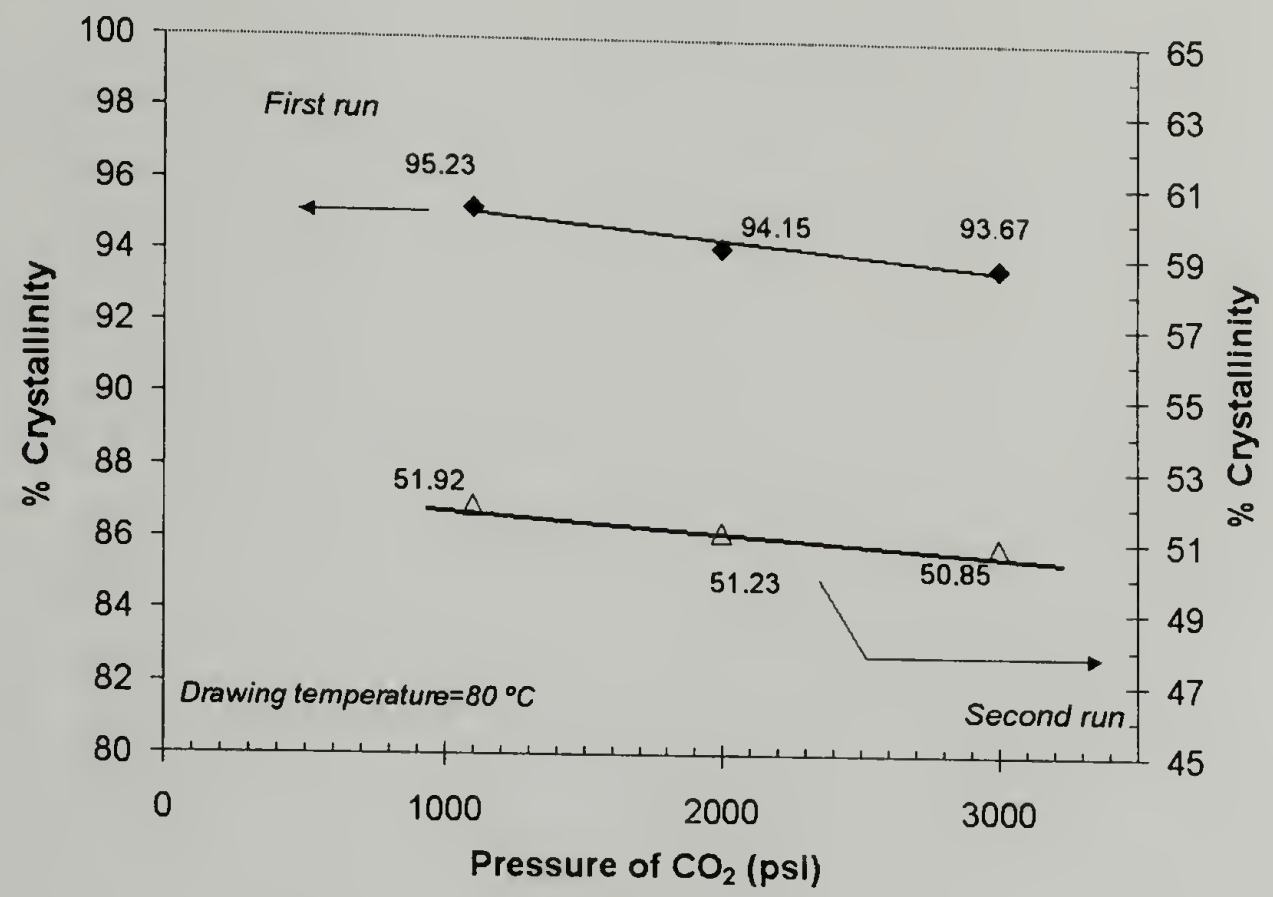

Figure 2.25. Crystallinity percent for UHMWPE fibers drawn in $scCO_2$ at 80 °C using different pressures.

To prove further the hydrostatic nature of the results observed in this work, drawing experiments in high-pressure nitrogen were conducted. The results are presented in figure 2.26, and as shown, they suggest indeed the hydrostatic origin of our observations in $scCO_2$. As shown in this figure, samples deformed in CO_2 or N_2 at the same pressure (3000 psi) show almost exactly the same drawing response. Almost the same apparent elastic modulus and draw stress is obtained in both samples. Furthermore, the extreme weakening observed at high temperatures (80 °C) in air-drawn samples is not present for samples drawn at high pressures regardless of the pressurizing medium.

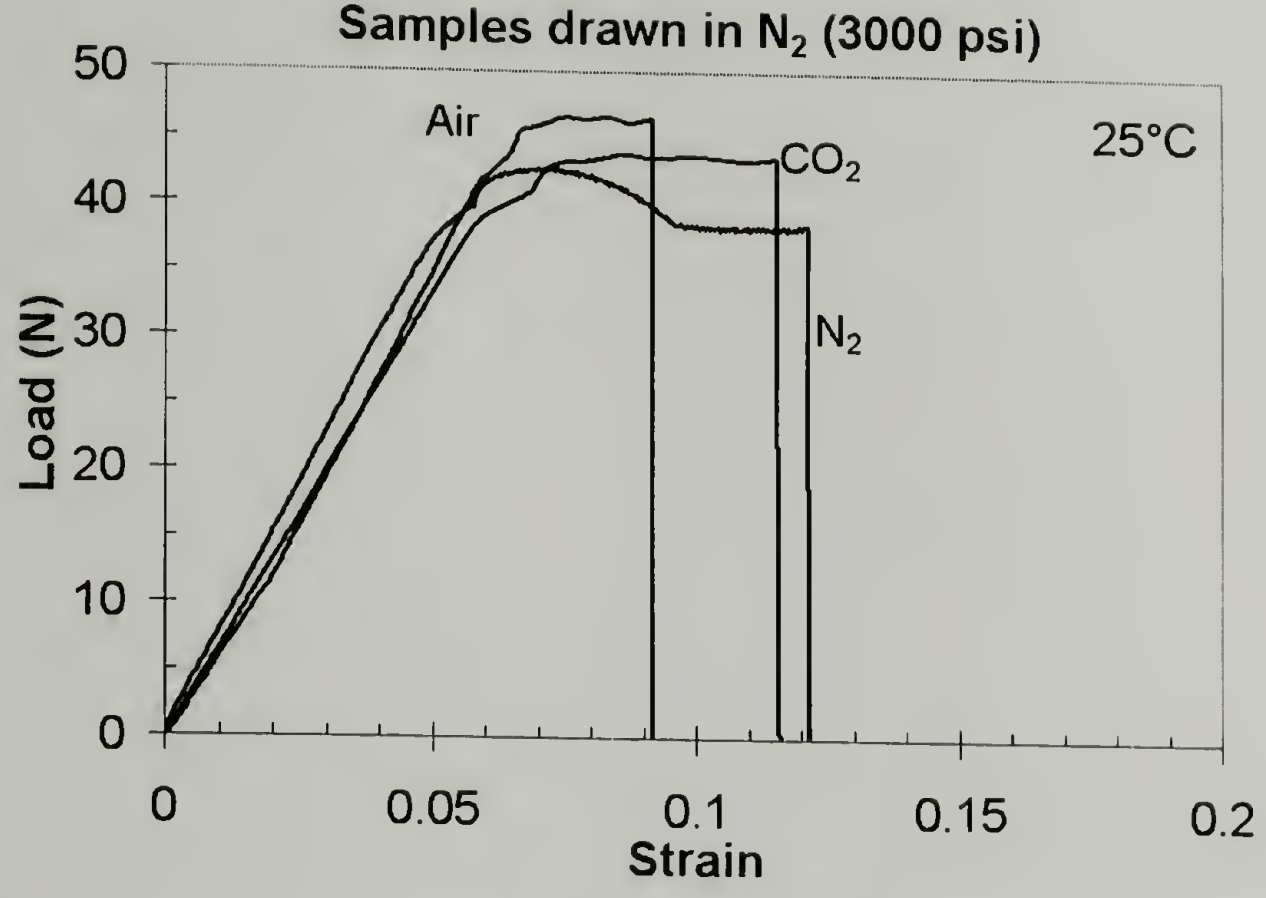

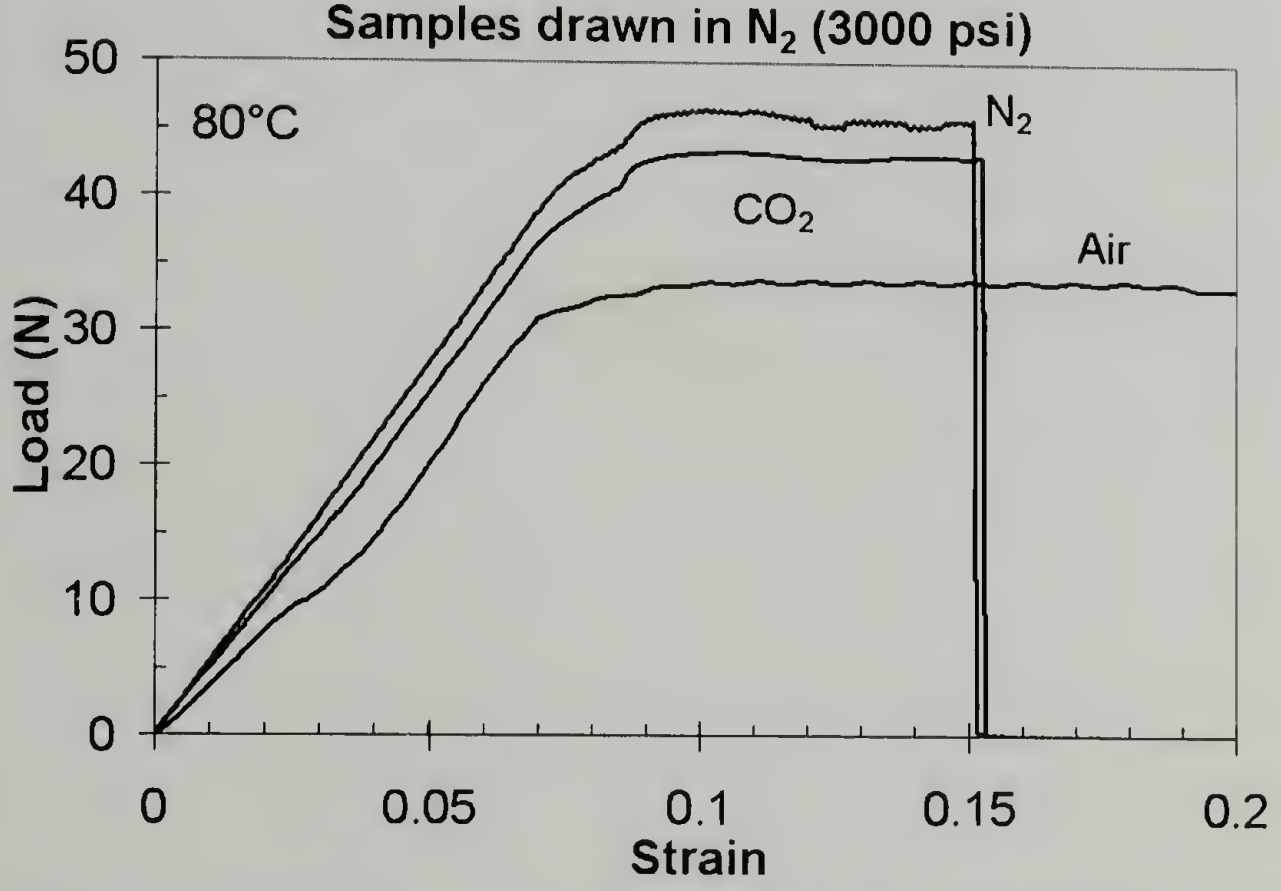

Figure 2.26. Drawing behavior observed at 25 °C and 80 °C using high-pressure nitrogen and $scCO_2$ at 3000 psi. The behavior in air (ambient pressure) is shown for comparison.

2.6 Conclusions

The drawing behavior of UHMWPE fibers in supercritical CO_2 ($scCO_2$) is compared to that in air at different temperatures. Both the mechanical properties and drawing behavior are altered when the deformation is conducted in the presence of $scCO_2$. Samples drawn in air show significant temperature dependence in their drawing properties. In contrast, $scCO_2$-drawn samples show a constant draw stress (286 MPa) and tensile strength (1500 MPa) over the entire temperature range. Apparently, the $scCO_2$ environment along with the imposed hydrostatic pressure helps to maintain the integrity of the fibers, allowing them to deform up to a certain extent without changing the draw stress. Modulus, strain at break and tensile strength are maintained essentially unaltered when the fiber is drawn in $scCO_2$, while significant weakening is observed for air-drawn samples with increasing temperature.

The thermal behavior of air-drawn samples is also dependent on the drawing temperature. DSC results show a development of a melting endotherm at 150 °C in air-drawn samples when increasing drawing temperature, suggesting the possibility of a development of an apparent hexagonal phase. In addition, a significant increase in crystallinity is observed in these samples. In contrast, no significant changes in the thermal behavior are observed in the $scCO_2$ treated samples. Apparently, the presence of $scCO_2$ promotes that the integrity of the crystalline phase remains unaltered regardless of the processing conditions.

WAXS results, however, suggest that no hexagonal phase is present at ambient conditions in any of the samples regardless of the processing conditions. An

orthorhombic unit cell is present in all the samples, showing two strong reflections (110_0 and 200_0), with no trace of the suggested hexagonal phase.

These results suggest that the appearance of the high-temperature melting peak in DSC is related to the internally constrained manner in which air-drawn samples crystallize. In contrast, samples deformed in $scCO_2$ are able to crystallize without internal constraints via the mobile hexagonal phase. The existence of this hexagonal unit cell during deformation in $scCO_2$ is consistent with the lower draw ratios experimentally confirmed for these samples, as well as with the increased processing temperature up to a value of 110 °C.

CHAPTER 3

FOAMING POLYETHYLENE IN SUPERCRITICAL CARBON DIOXIDE

A modified processing system has been used to process a variety of polymers in the presence of high-pressure carbon dioxide (CO_2). The system includes a conventional single screw extruder that has been modified to allow for high pressures created by the injection of CO_2. The new design includes a modified feed section that allows a given mass of polymer to interact with CO_2 prior and during the extrusion process. The inherent shear mixing and the presence of CO_2 allow for a specific control over the extrudate morphology. Some of the relevant parameters in the foaming process of polyethylene systems (HDPE and LDPE) are analyzed and specifically related to the processing conditions imposed in this system.

3.1 Introduction

The idea of using CO_2 particularly at supercritical conditions as an alternative processing aid in polymer extrusion has been analyzed extensively for the past two decades.[25-36] The interest in supercritical CO_2 ($scCO_2$) is a natural consequence of the fact that its inherent properties are very close to those required in a successful blowing agent. The phase diagram of CO_2 is presented in figure 3.1. The critical conditions for CO_2 correspond to 30.98 °C and 72.8 atm (1070 psi). Part of the scientific and commercial interest in $scCO_2$ is also related to the fact that these conditions are easily accessible even in traditional laboratory environments.

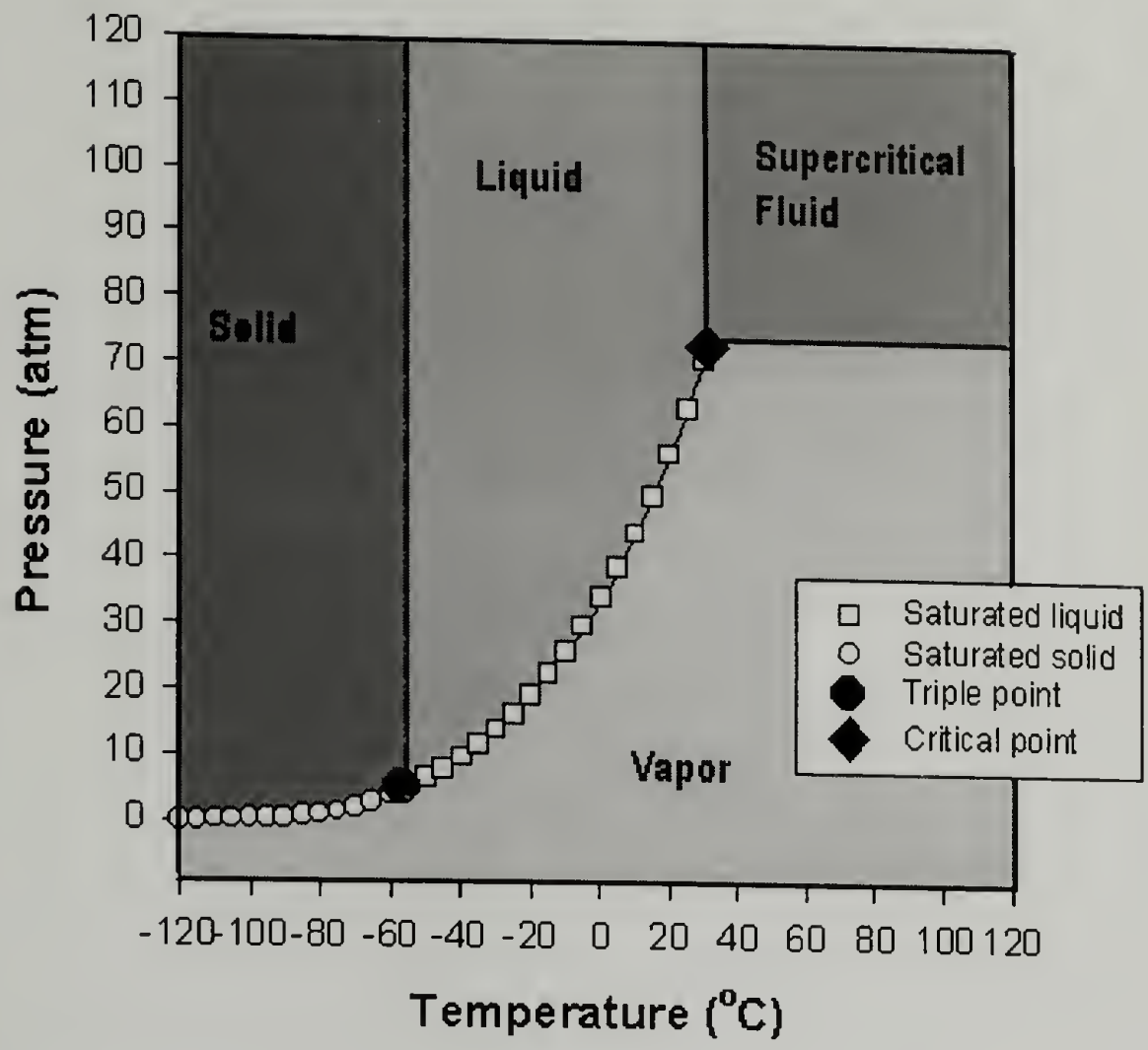

Figure 3.1. Phase diagram for carbon dioxide.

At supercritical conditions, CO_2 combines in a unique manner, properties from both liquid and gas states, exhibiting liquid-like densities along with low viscosities and high diffusion rates that are typical of a gas phase.[4-11,24] In addition, the low toxicity and flammability along with the reduced cost of CO_2 make it a real and environmentally friendly alternative for polymer processing. Because of its high compressibility, the solvent/plasticizer properties of CO_2, typically related to its density, can be tuned and controlled by small changes in temperature and pressure, acting as a "reversible plasticizer" that can be easily removed from the system during depressurization. A density-pressure diagram for CO_2 is presented in figure 3.2. During extrusion, CO_2 dissolves into a molten polymer under moderately high pressures, and diffuse away from the polymer substrate at ambient conditions, leaving the final product solvent-free, reducing the costs of solvent removal.[12]

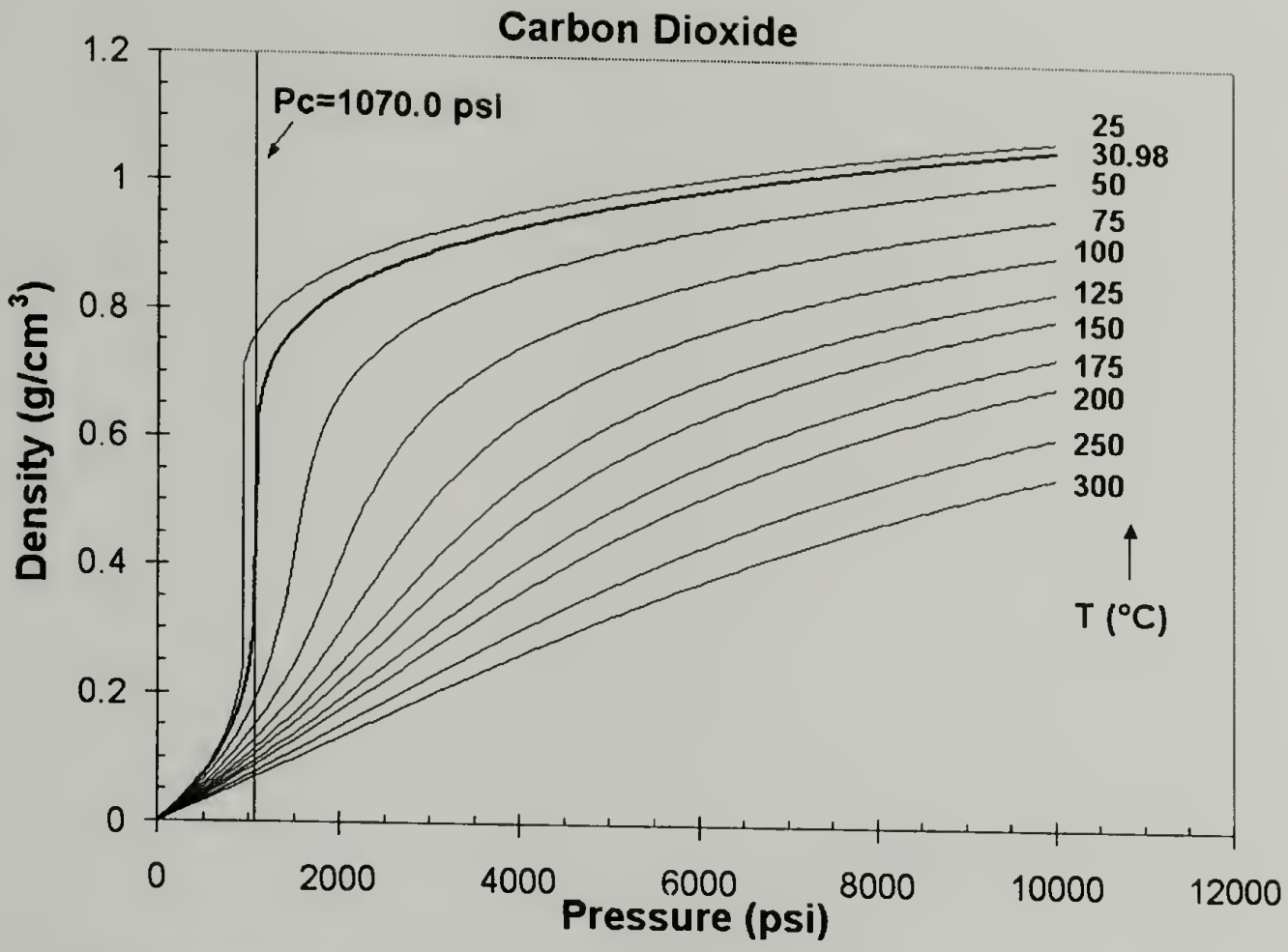

Figure 3.2. Density-pressure diagram for carbon dioxide.

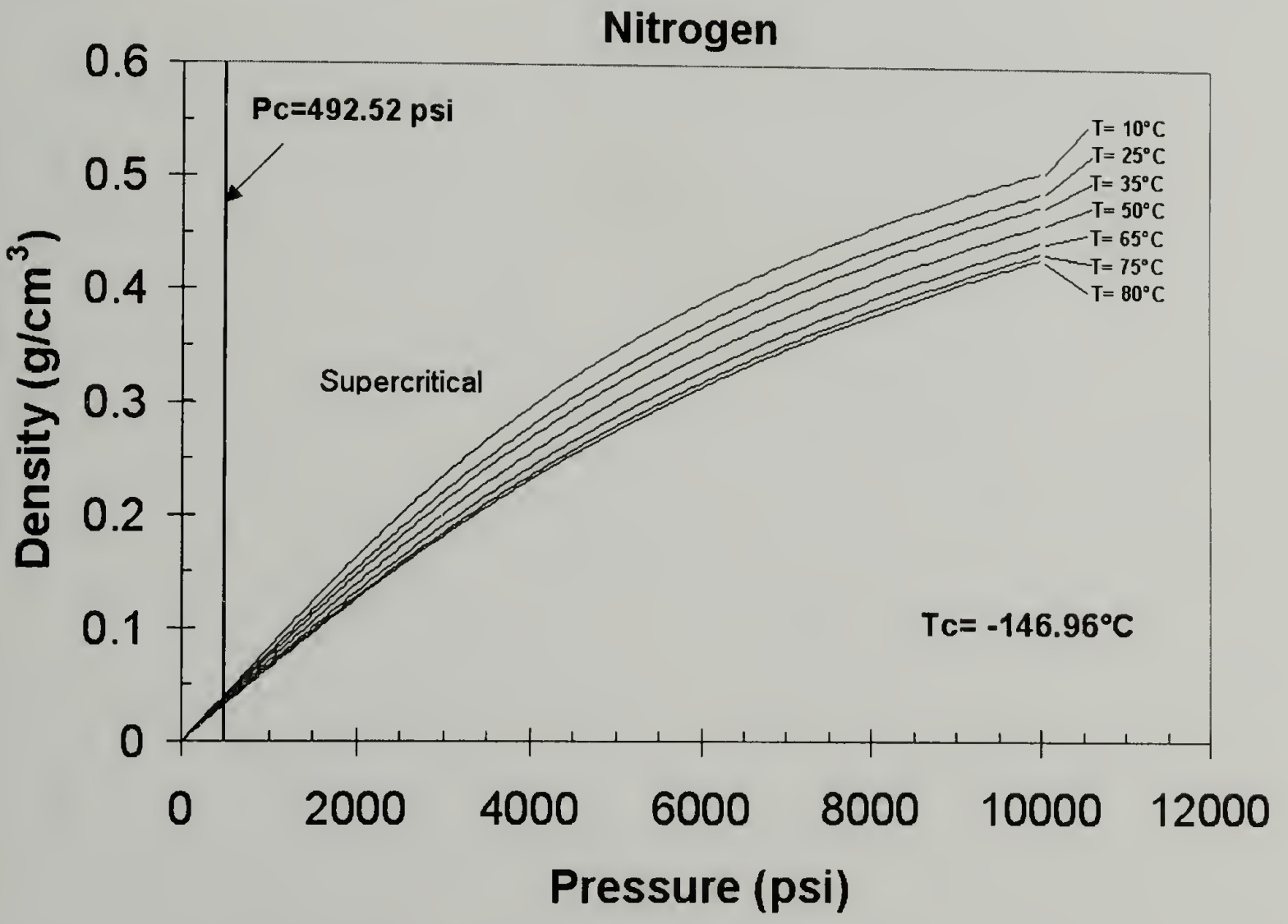

Figure 3.3. Density-pressure diagram for nitrogen.

Similar effects are difficult to be achieved by other conventional gases at high pressures due to their significantly lower density at the same conditions, which typically reduce their solvent properties in conventional polymers. This is shown in figure 3.3 for the case of nitrogen.

A vast amount of research, particularly in the area of polymeric foams, has been focused in studying the relation between the processing conditions in extrusion and the final polymer morphology when CO_2 is introduced.[25-36] As depicted graphically in figure 3.4, polymeric foams are comprised of a cellular structure created by the expansion of a blowing agent, which is usually a volatile gas or a liquid.[31] The type and initial concentration of the blowing agent, the pressure distribution in the polymer melt and the solubility and diffusivity of the gas in the polymer melt all have a direct effect on the final properties of the foam.

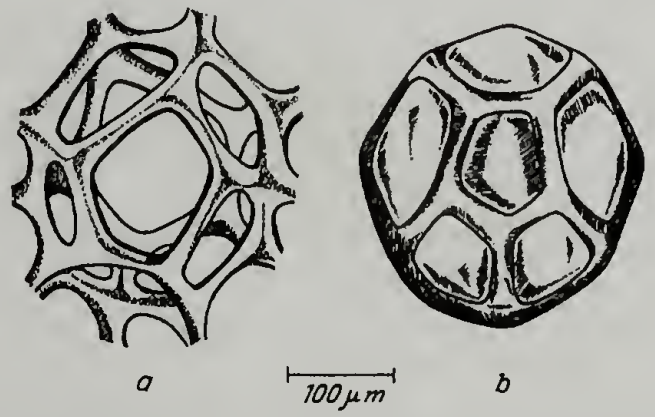

Figure 3.4. General foam morphology. Open and closed cell morphologies are typically observed depending on the material properties and processing conditions.[70]

The commercial approach to produce polymer foams by direct extrusion generally includes either single extrusion processes or tandem extrusion lines. In all cases a variety of steps are included in the process such as extrusion, mixing, cooling, expansion and aging of the final material. Typically, these steps are executed in systems with different configurations including single-screw extruders having a long screw or twin-screw extruder with additional mixing devices. In a tandem operation a primary extruder is used

to melt the resin and promote mixing with solid additives and blowing agents, and a secondary extruder is typically used to cool the mixture to the optimum foaming conditions.[70]

In general, improved mechanical properties are observed when a reduced cell size and an increase in the cell density are promoted. As mentioned in Chapter 1, microcellular polymer foams exhibit greatly improved mechanical properties due to their reduced cell size,[28] and a variety of nucleation strategies have been followed to produce microcellular materials.[27-36,71] Without a foaming agent, homogeneous nucleation occurs and nucleation is promoted through a thermodynamic instability in the process, which is commonly obtained through a pressure drop along the extrusion line.[28]

Suh[25] and Baldwin et al.[26] studied the feasibility of producing microcellular foams using a static mixer to promote the dissolution of the gas and a rapid heating element for cell nucleation. Park et al.[28] proposed a continuous process for the manufacture of low-density microcellular polymers, using a strategy both to control cell growth after nucleation and to prevent cell coalescence. Lee et al.[30] quantified the plasticization effect of CO_2 in the extrusion of polymer blends (PE/PS), suggesting that the dissolution of CO_2 into the polymer blend decreased the shear thinning behavior resulting in an increase of the power law index regardless of the CO_2 content.

All these studies have been done in conventional extrusion foaming systems as the one presented in figure 3.5, where $scCO_2$ is only used as a blowing agent and is introduced at later stages of the extrusion line, namely at the metering section of the extruder. Recent studies[34,36] have shown that direct processing parameters and material

properties such as melting temperature, chemical structure and molecular weight of the resin play an important role in the final morphology of the polymer.

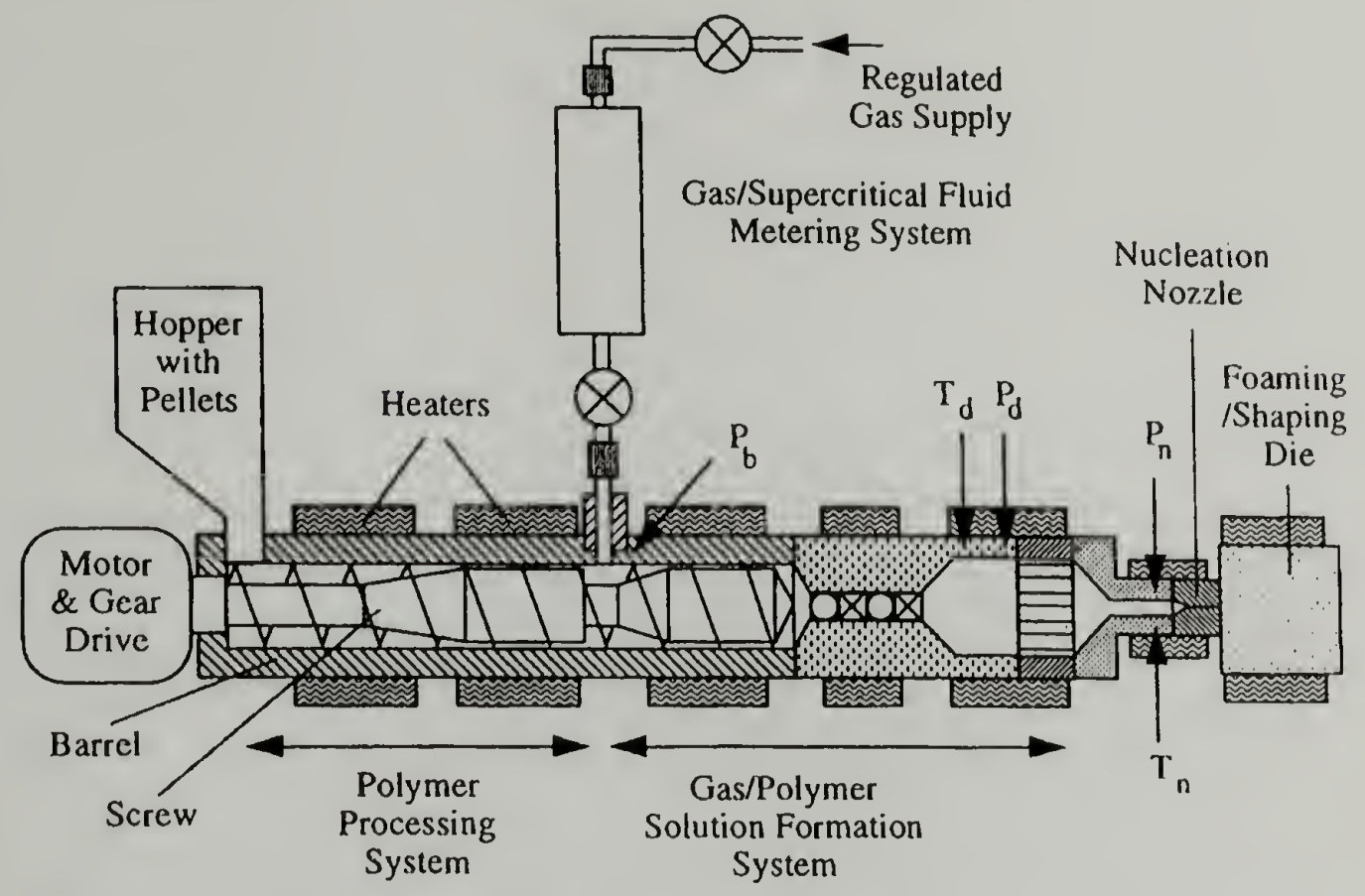

Figure 3.5. Conventional extrusion foaming system, showing the suggested morphology change during processing.[72]

3.2 Experimental

A single screw extruder (Randcastle RCP-025 Microtruder) with a working L/D ratio of 24 and a screw diameter of 6.35 mm (1/4 in.) is employed to process a variety of polymers. The extrusion system, as depicted in figure 3.6, has a vertical feeding with the screw driven through the metering section and no additional mixing devices. Temperature is controlled through four independent heaters located in the die and along the extruder barrel. A 1 mm tubular die is employed along with a take-up roller for the spinning of the final extrudate. The spinning rate is maintained in the range of 0-200 RPM.

Figure 3.6. Single screw extruder used in this study. (Randcastle Microtruder model 025).

The feed section in the extruder has been modified in order to allow for the high pressures promoted by the injection of CO_2. The new feed section, constructed primarily of standard high-pressure fittings, includes a modified hopper that allows a specific

amount of polymer to interact with CO_2 prior to the extrusion process. The conditions inside the hopper are precisely controlled: temperature is manipulated using a temperature controller and a pressure gauge directly attached to the feed section is used to monitor the internal pressure. CO_2 is injected using a high-pressure carbon dioxide pump (Hydro-Pac, Inc.) with a maximum discharge pressure of 286.84 MPa. A detailed diagram of the modified processing system is presented in figure 3.7.

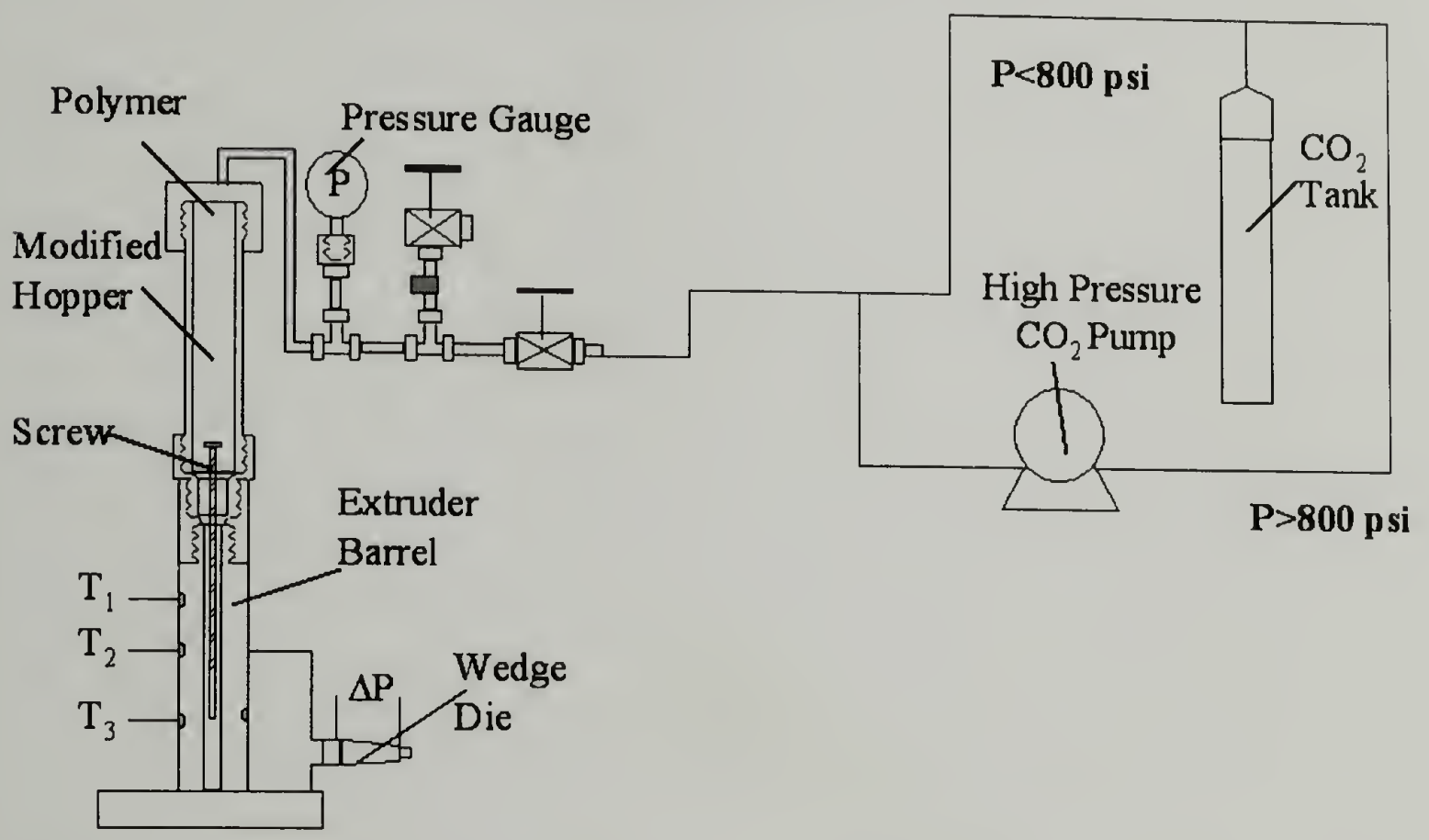

Figure 3.7. Detailed diagram of system for $scCO_2$-assisted polymer processing.

Differential Scanning Calorimetry (DSC) is used to study the thermal behavior of the polymers processed in our system. DSC experiments are carried out in a TA Instruments thermal analyst model 2910 DSC in the temperature range of 25-210°C at relatively slow heating rates (1-10 °C/min) in order to obtain a quantitative response of the thermal properties of each sample. The crystallinity of the samples is estimated by the ratio of their melting enthalpy and the theoretical heat of fusion for a perfect crystal of polyethylene (288.89 J/g).

The overall extrudate morphology obtained at different processing conditions is investigated using Scanning Electron Microscopy (SEM). Samples are cryo-fractured in liquid nitrogen and gold coated prior to the SEM analysis. SEM images are obtained using a Field Emission Scanning Electron Microscope (FESEM) JSM-6320FXV and a Scanning Electron Microscope model JEOL-CF-35 with a filament voltage of 20000 V.

3.3 Results and Discussion

In this study, polyethylene systems (LDPE and HDPE) are processed over a variety of conditions and are basically used as model polymers to understand the foaming process of a polymer in $scCO_2$, using the system described before. Results suggest that a specific control over the final extrudate morphology can be obtained using the modified processing system, and some of the important parameters that can be used to control the morphology are analyzed.

As shown in figure 3.7, the system allows for a semi-batch process in which a given mass of polymer is saturated in high-pressure CO_2 before and during extrusion. Factors such as processing temperature, saturation time and pressure of CO_2, and temperature distribution along the extrusion line are discussed in terms of their influence on the morphology of the final product.

A variety of morphologies are observed when processing a polymer, such as HDPE, in the described system, and in general the appearance of a certain foamed morphology is directly related to the processing conditions. As presented in figure 3.8, a smooth cross section is always obtained when no CO_2 is introduced, while the presence of CO_2 alters the extrudate morphology in a complex way introducing a foamed structure. Controlling

the processing conditions facilitates the production of foamed products, with controlled cell density (number of cells per unit area), average cell size and cell size distribution.

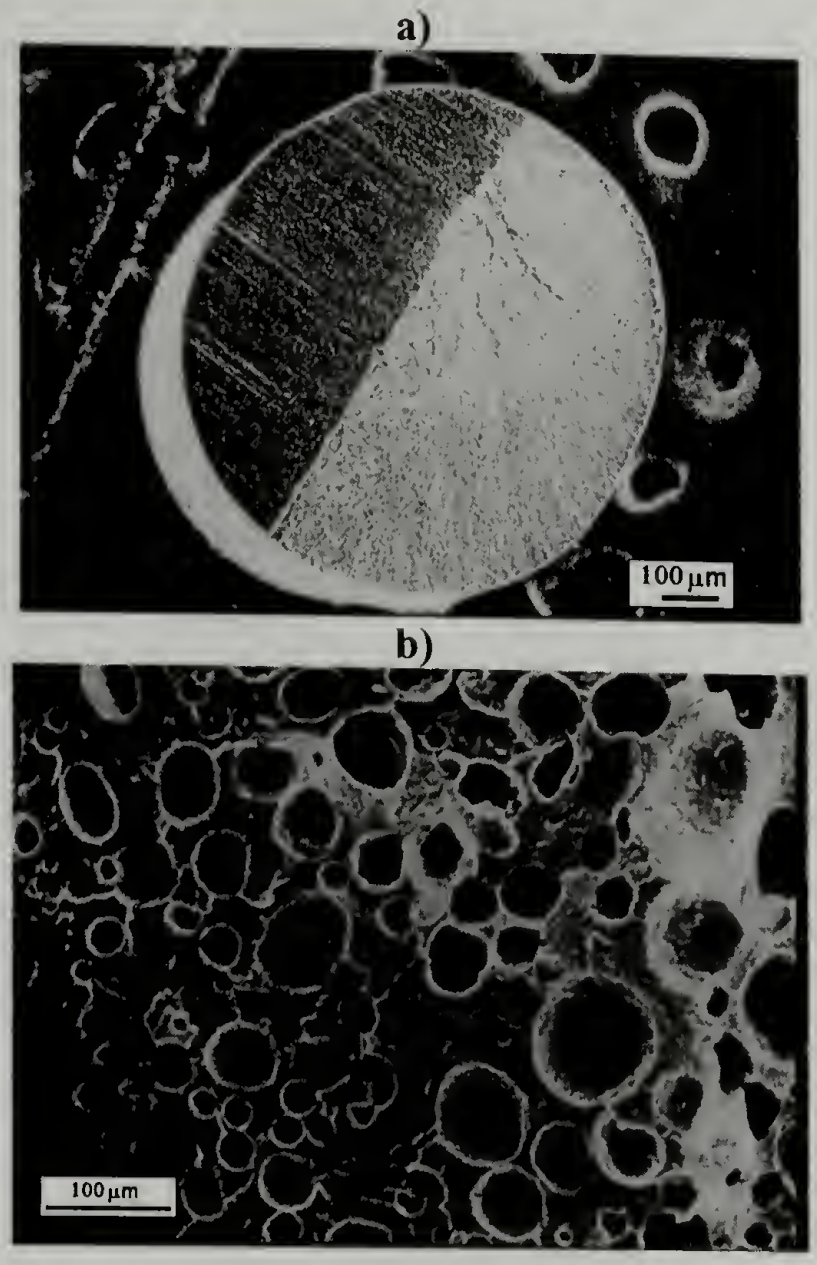

Figure 3.8. General morphology (SEM) of HDPE samples obtained at different conditions. a) Without CO_2 at 125 °C, and b) With CO_2 at 115 °C and 5.86 MPa.

Results using high-density polyethylene (HDPE) show that both the presence of CO_2 in the feed section and the diffusion rate of CO_2 in the polymer melt promote the appearance of a foamed structure. As shown in figure 3.9, if the material is saturated in CO_2 for a given time, cell nucleation is observed even at moderate pressures (3.44-5.86 MPa), which suggests that the diffusion rate of CO_2 into the melt controls the nucleation process. The modified design of our system allows for the free manipulation of the saturation time, facilitating the interaction of a polymer with $scCO_2$ prior to extrusion.

With a saturation time, the dissolution of CO_2 in the melt increases, and nucleation is dictated only by the processing conditions. When a favorable nucleation process is observed, specific control on the morphology can be achieved by altering several parameters in the system such as the temperature distribution and the saturation pressure.[73]

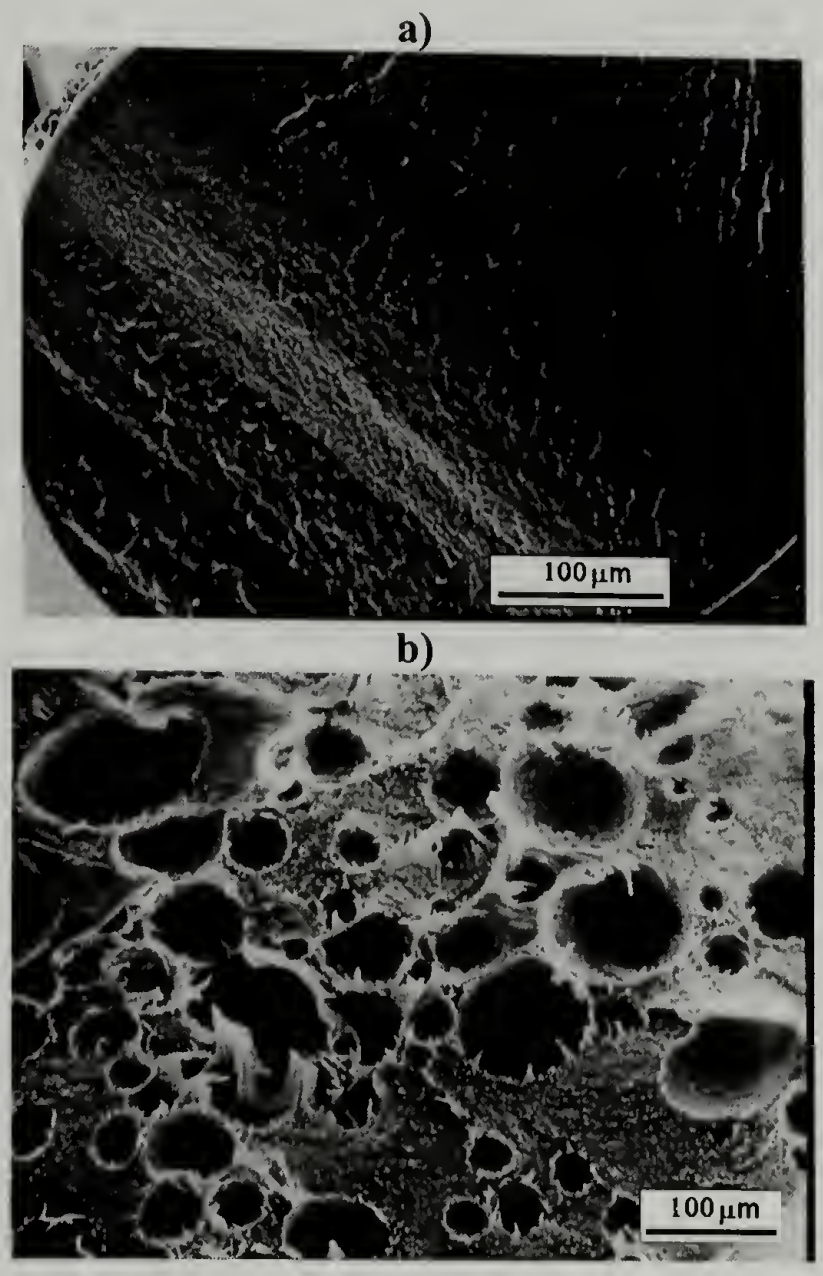

Figure 3.9. General morphology (SEM) of HDPE samples extruded at 145 °C with CO_2 (5.86 MPa) using various saturation times. a) 0 min, and b) 140 min.

Temperature appears to be the most important factor in controlling the nucleation process. In addition, it is also the easiest parameter to control given the characteristics of our system. Examples of the influence of temperature on the morphology are shown in figures 3.10 and 3.11, where by changing the temperature distribution in the system the

nucleation process is controlled, and polymer foams with different cell density and cell size are produced.

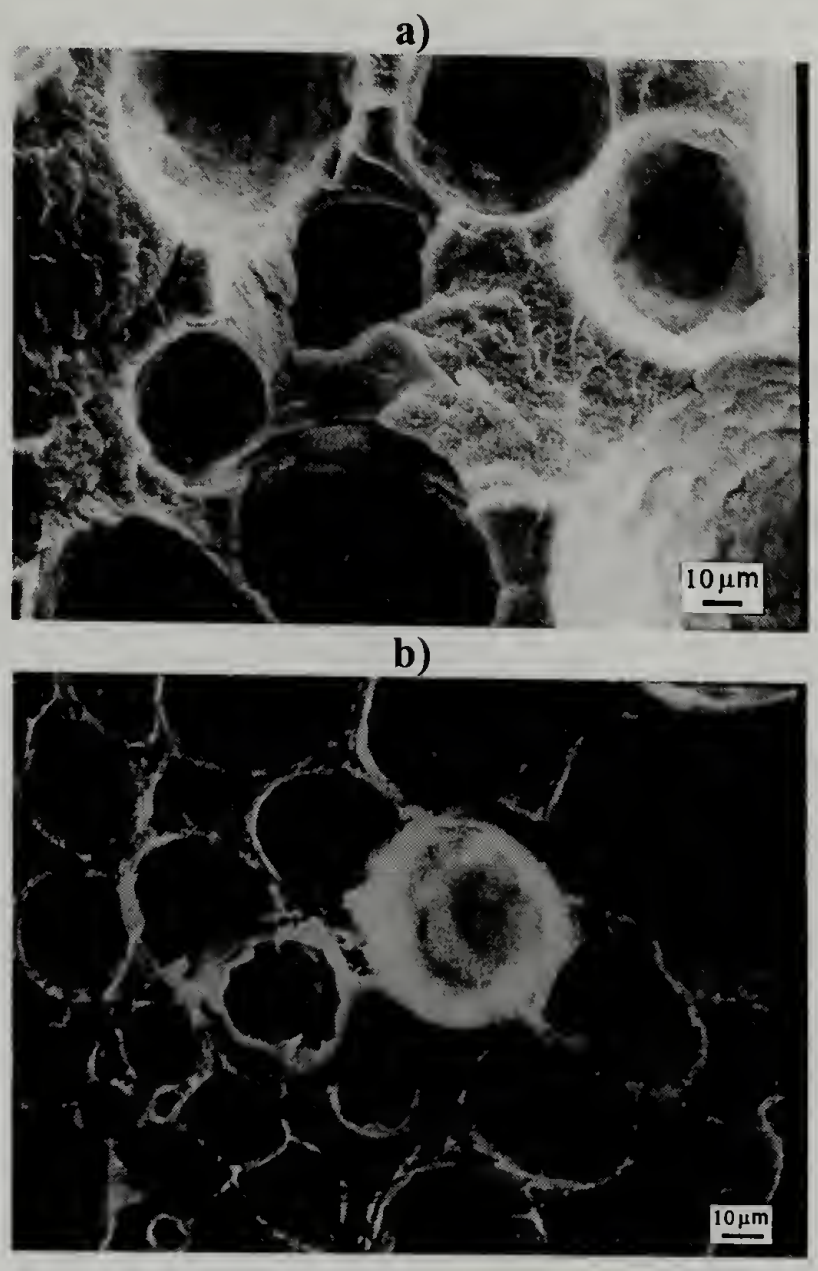

Figure 3.10. General morphology (SEM) of HDPE samples extruded with CO_2 at different die temperatures. a) 165 °C, and b) 115 °C.

Figure 3.11 shows both the average cell size and cell density of samples processed using different die temperatures. In all cases, a 140 min. CO_2 saturation time is used prior to extrusion in order to promote dissolution of gas in the polymer melt. As depicted in this figure, at a given saturation pressure (5.86 MPa), important differences are observed when the temperature is reduced, despite of the fact that the difference in CO_2 density within this temperature interval is small (0.090 kg/m^3 at 115°C, 0.076 kg/m^3 at 165°C and 0.071 kg/m^3 at 190°C). Significant changes are promoted when the temperature

approaches that of the melting point of the polymer. At low temperatures cell nucleation is promoted and systems with increased cell density and lower average cell size (30 μm) are produced. Additionally, since high-pressure CO_2 is introduced in the feed section, the hydrostatic pressure acts as a processing aid during extrusion and facilitates the processing of the polymer.

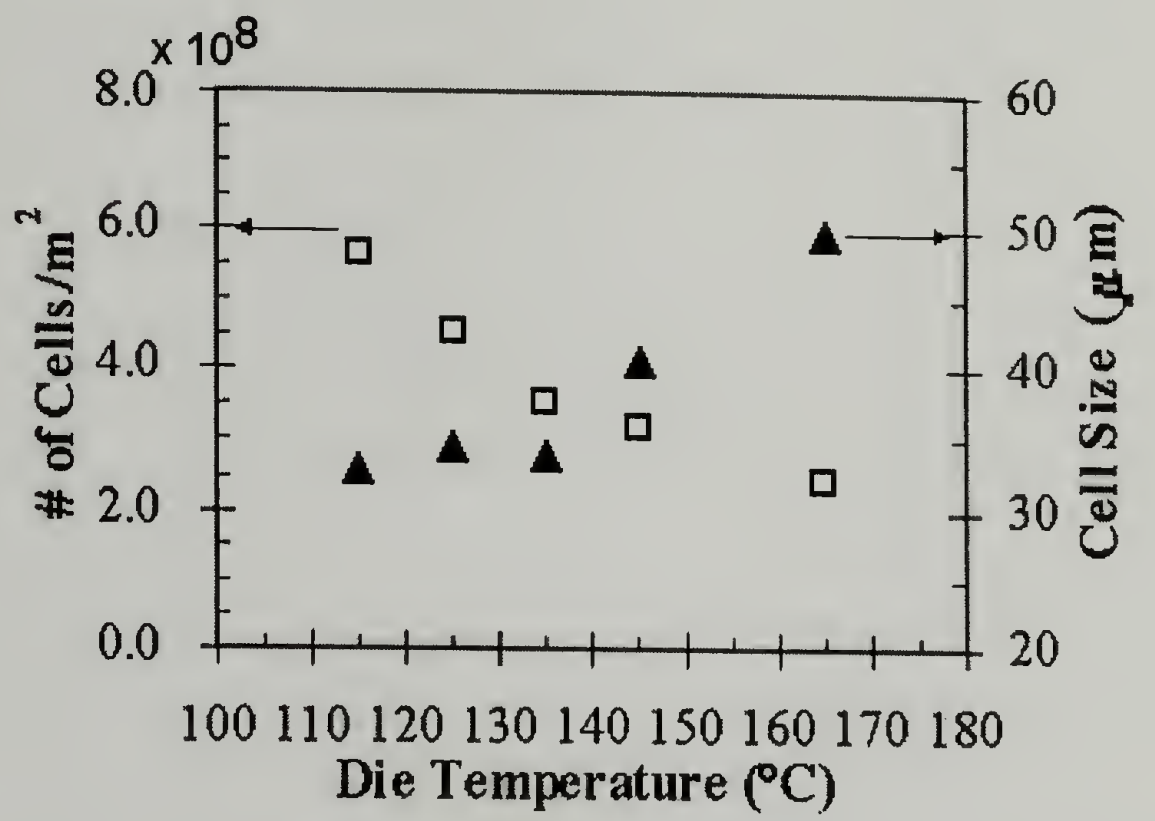

Figure 3.11. Influence of die temperature on the overall morphology of HDPE extrudates processed at 190 °C. (Saturation time=140 min, pressure of 5.86 MPa).

As shown in figure 3.11, polymer can be continuously processed at temperatures even below its melting point (127 °C for HDPE) when CO_2 is introduced, suggesting a significant amount of plasticization brought about by the presence of CO_2. These results suggest that the alternative design of the system allows not only for a specific control of the extrudate morphology, but it also provides a direct way to estimate the amount of plasticization in the system imposed by CO_2 at a certain conditions. This effect will be discussed in the following chapters where the plasticization process is actually used to process high molecular weight polymers and systems with increased melt viscosity.

Incipient dissolution of CO_2 into the melt is generally observed at high temperatures, as shown in figure 3.12 for the case of LDPE. At these conditions cell nucleation is ineffective and the presence of CO_2 is corroborated only by the appearance of bubbles at the outer surface of the sample. Lee et al.[27] have also observed this effect in foam rod experiments, where the rod surface has a much higher cell density than the center and it has been ascribed to additional shear effects. No difference is observed by decreasing the temperature from 205°C to 175°C.

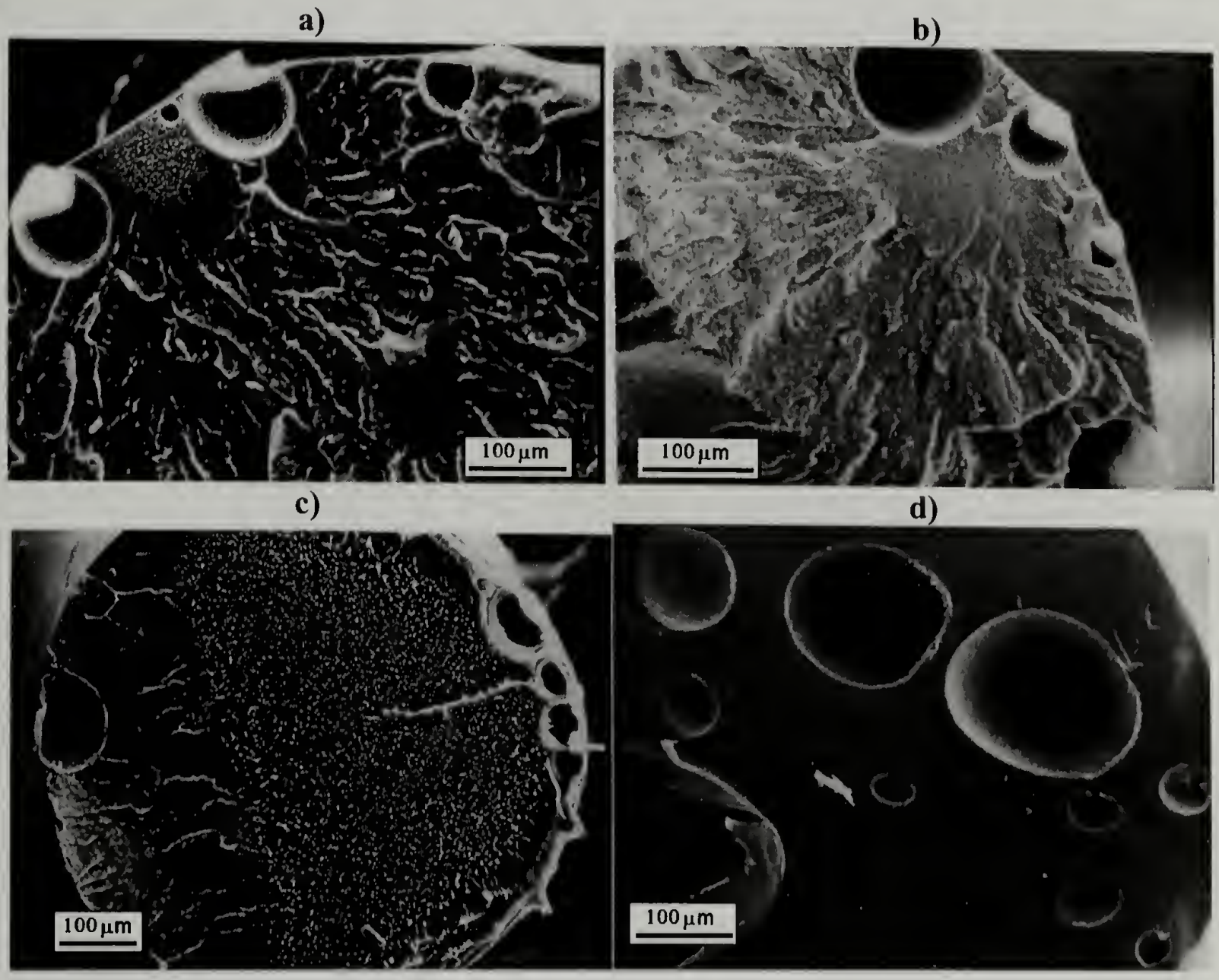

Figure 3.12. General morphology (SEM) of HDPE samples extruded with CO_2 at high temperatures. a) 175 °C and 3.44 MPa, b) 205 °C and 3.44 MPa, c) 205 °C and 13.79 MPa, and d) 205 °C and 3.44 MPa using a saturation time of 60 min.

This ineffective nucleation could be related to the low solubility of CO_2 in the polymer at such high temperatures, note that the density of CO_2 at 175°C and 205°C is 0.042 kg/m^3 and 0.039 kg/m^3, respectively. From this figure, it is evident that the morphology does not change even when the pressure is increased to 13.8 MPa, where CO_2 is in its supercritical regime, with a density of 0.170 kg/m^3, still too low to promote efficient dissolution and promote cell nucleation. Saturation of the material in CO_2 for 60 min. at 3.44 MPa slightly enhances cell nucleation, suggesting again that the rate of diffusion of CO_2 into the polymer plays an important role in controlling the morphology.

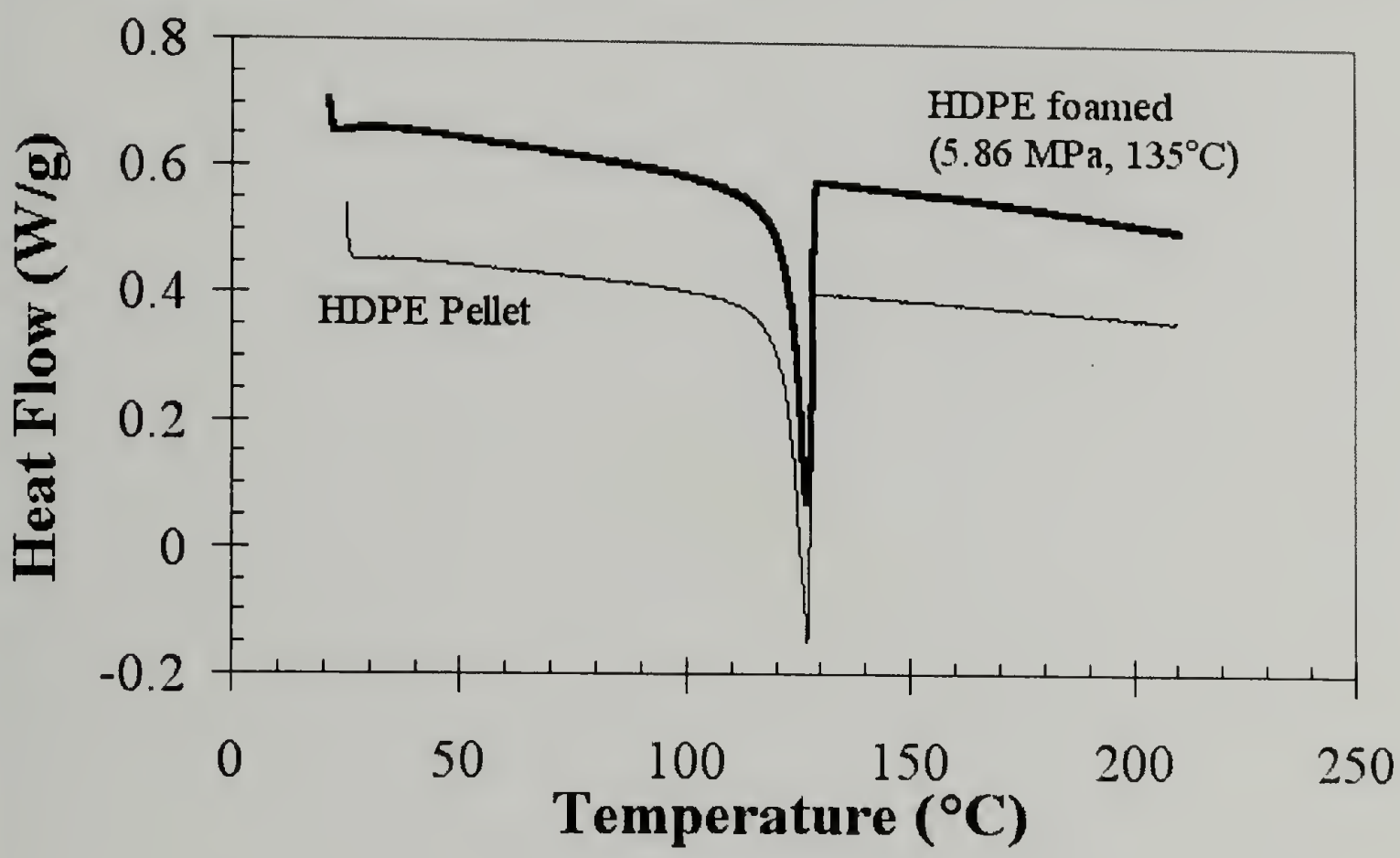

Figure 3.13. Thermal behavior (DSC) of HDPE foamed sample. For comparison the DSC trace of a HDPE pellet is included.

Foaming appears to have a negligible effect in the thermal behavior of polyethylene. DSC experiments of a HDPE pellet and a foamed sample processed at 5.86 MPa are compared in figure 3.13. The foamed structure in this latter sample is obtained when the die temperature is reduced to 135°C. No changes in the melting temperature and

crystallinity of the foamed sample with respect to the unfoamed material are observed. This can be a consequence of the high crystallization rate in HDPE, which suppresses any subsequent melt drawing and orientation during the foaming process.

In figure 3.14, the influence of the saturation pressure is analyzed. Evidently, pressure plays a significant role in the morphology of the final sample. Both samples are processed using the same temperature distribution with a die temperature of 135°C. Again, a 140 min. soaking time is imposed to maximize the dissolution of CO_2 into the polymer.

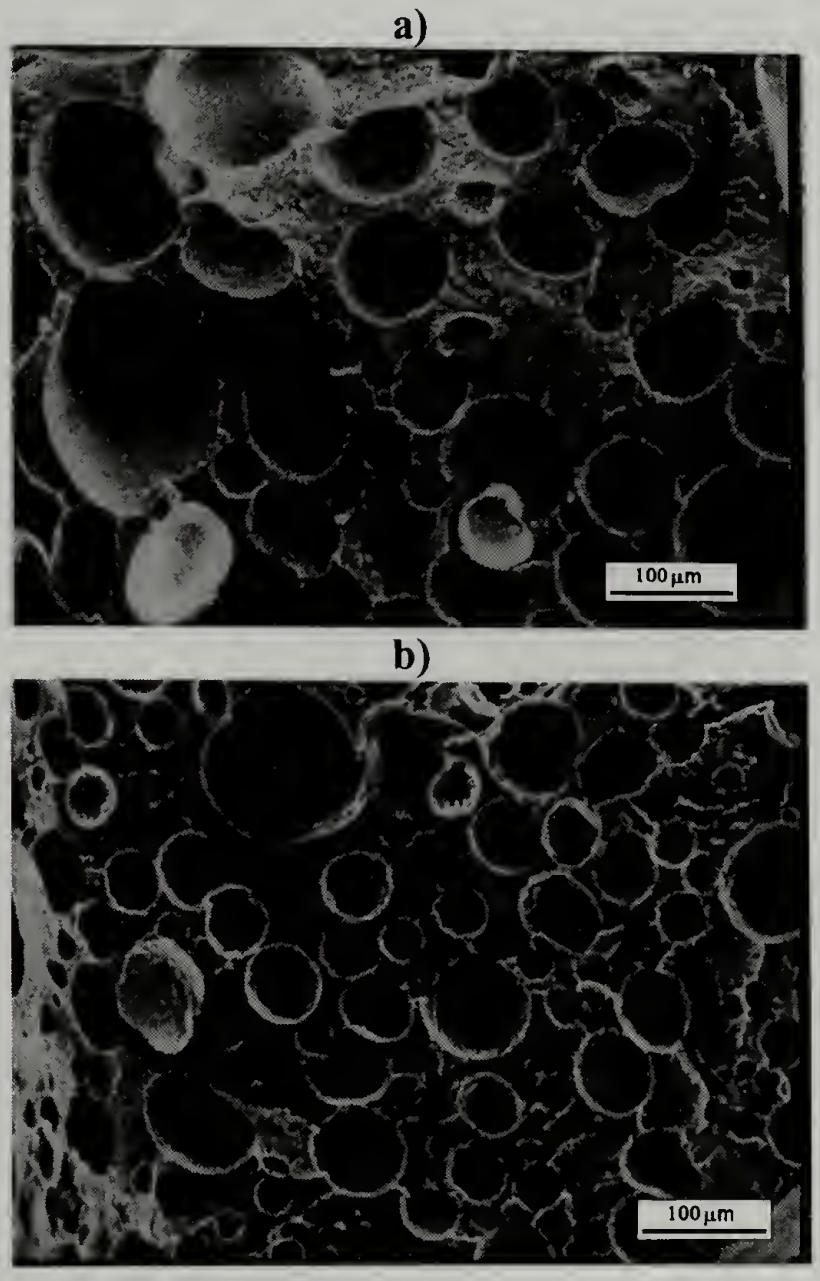

Figure 3.14. General morphology (SEM) of HDPE samples obtained at 135 °C using different saturation pressures. a) 5.86 MPa, and b) 10.34 MPa.

Cell nucleation is favored by increasing the pressure, promoting significant changes both in the cell density and cell size. The average cell size is decreased from 70 μm at 5.86 MPa to 25 μm at 10.34 MPa. Increasing the saturation pressure increases the concentration of CO_2 and as a consequence dictates its diffusion rate into the melt. In addition, an increased solubility of CO_2 is expected at high pressures, specifically above the critical point. As shown in table 3.1, at 135°C and 10.34 MPa, CO_2 is a supercritical fluid and its density (0.161 kg/m^3) is almost twice that observed at 5.86 MPa (0.084 kg/m^3).

Temperature (°C)	**Pressure (MPa)**	**Density (Kg/m^3)**
115	5.86	0.090
135	5.86	0.084
135	10.34	0.161
145	5.86	0.081
165	5.86	0.076
190	5.86	0.071

Table 3.1. CO_2 densities at different processing conditions used in this study.

It is important to point out that according to some of the previously shown figures a bimodal cell distribution is observed in many samples. This is a typical indication of the presence of additional nucleation mechanisms. The presence of large cells in the sample might be related to cell coalescence, which occurs after nucleation due to the low melt viscosity of polyethylene. This process, in combination with a heterogeneous nucleation mechanism promoted by the presence of a few small-sized impurities in the system is believed to be responsible for most of the large cells in the sample. The heterogeneous process is thermodynamically more favorable than the homogeneous nucleation mechanism, which is characterized by a typical thermodynamic barrier related with the

energy needed to create a nucleus surface, and it is believed to be responsible for the majority of the smaller voids.

Evidently, in addition to the parameters analyzed here, some other factors will definitely play a significant role in controlling the final foamed morphology. The experimental results presented above suggest that the nucleation of HDPE by $scCO_2$ is not a very favorable process and as a consequence the final foam morphology does not show a microcellular type of structure. The foam structure displays always a wide cell size distribution, showing lower cell densities and average cell sizes that are typically around 30-50 μm that result significantly larger than those observed in microcellular polymers (10 μm). As presented in figure 3.15, the intrinsic properties of the polymer dictate the final morphology. Foams with increased cell density and significantly lower cell sizes (some in the microcellular range) can be obtained in other polymers using our processing system. Evidently, the affinity of the polymer to CO_2, as in the case of fluoropolymers, promotes a larger dissolution of gas in the melt, increasing its concentration, promoting well-defined foam structures.

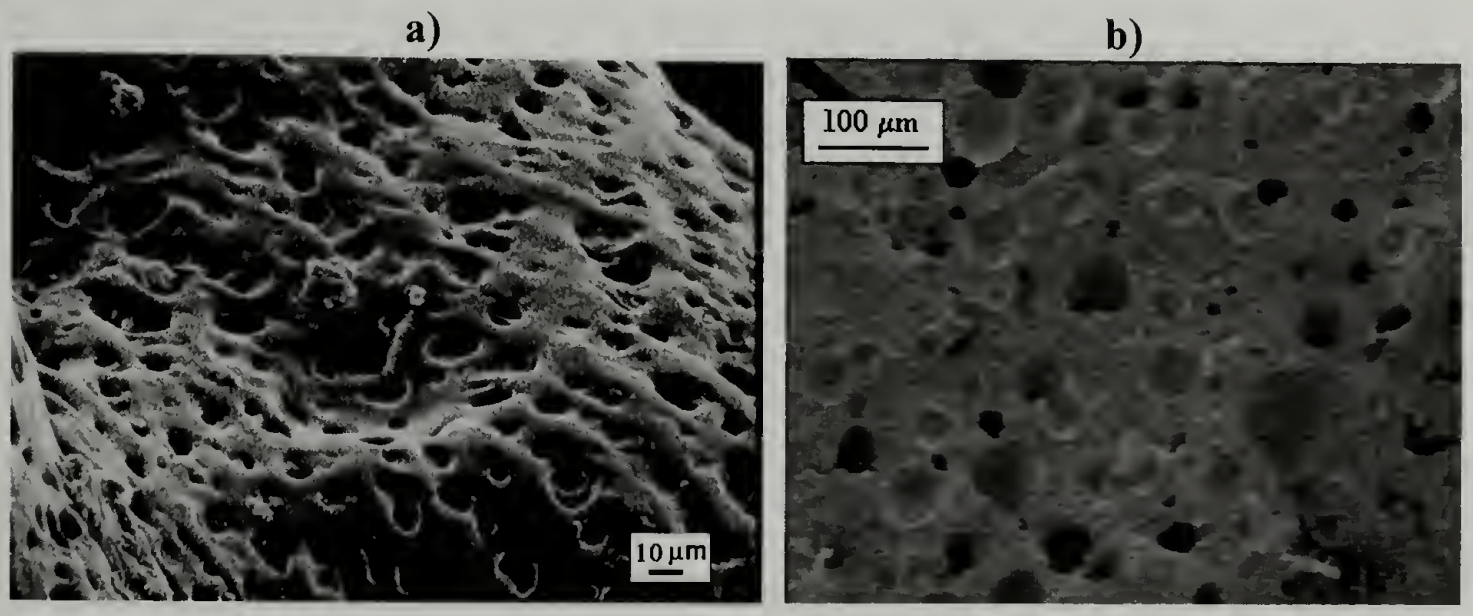

Figure 3.15. Typical closed cell morphology obtained in other polymers processed by $scCO_2$-extrusion. a) FEP, and b) PTT.

Additionally, the use of heterogeneous nucleators can enhance the foam structure in polyethylene-based systems, as shown in figures 3.16, 3.17, and 3.18, where 3 examples of using heterogeneous nucleators in HDPE systems are presented. These figures describe the morphology observed in polyethylene-based intercalated nanocomposites, produced by processing HDPE in CO_2 (135 °C, 5.86-10.34MPa) in the presence of clay nanoparticles. The specific details about the structure of these systems are given in Chapter 5, however, it is evident that the morphology of HDPE-clay systems is characterized by a better defined closed-cell structure, as compared to that observed in homogeneously nucleated HDPE systems.

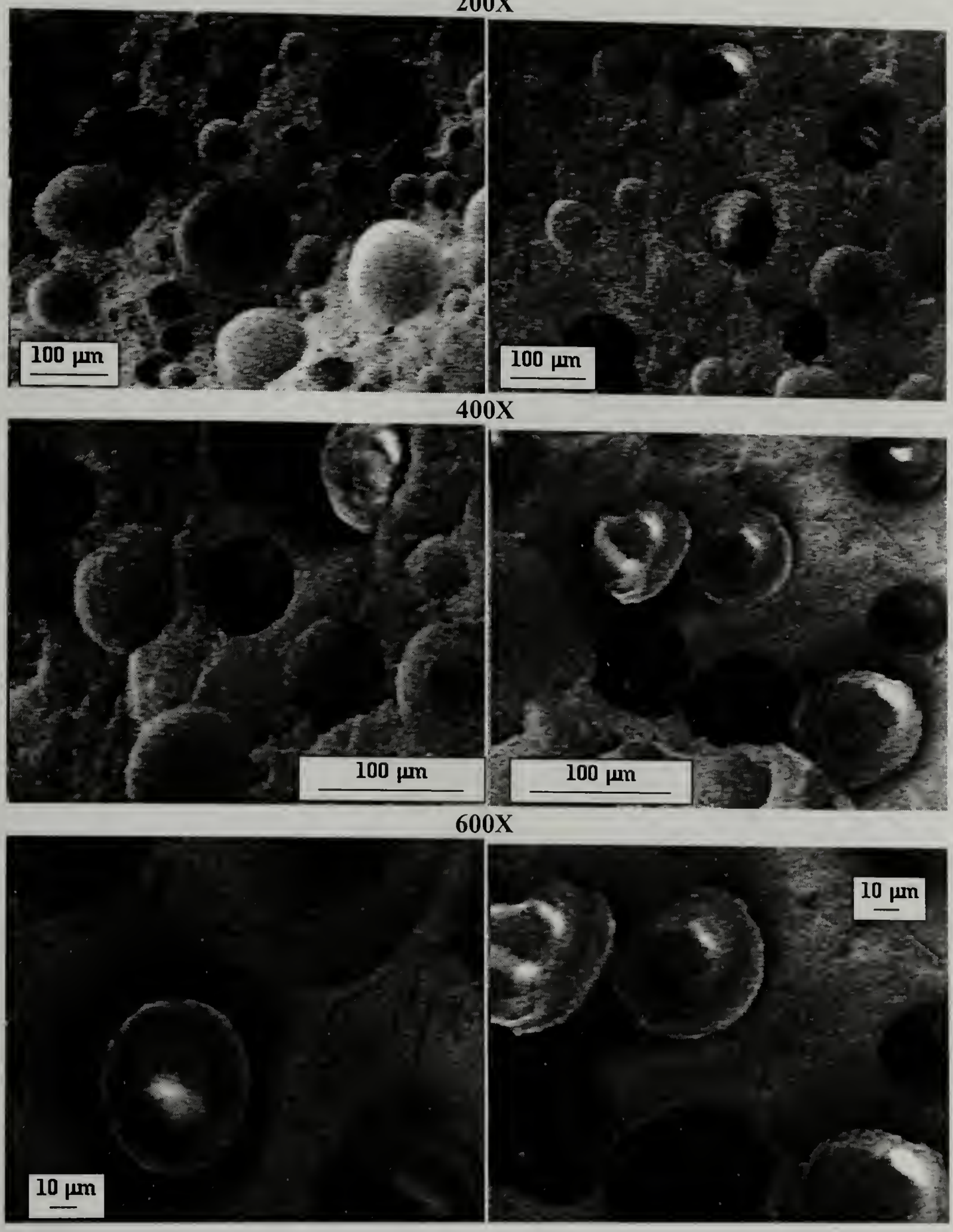

Figure 3.16. FESEM images of an HDPE sample processed with 0.5% MNa+ clay showing the typical closed-cell foamed structure.

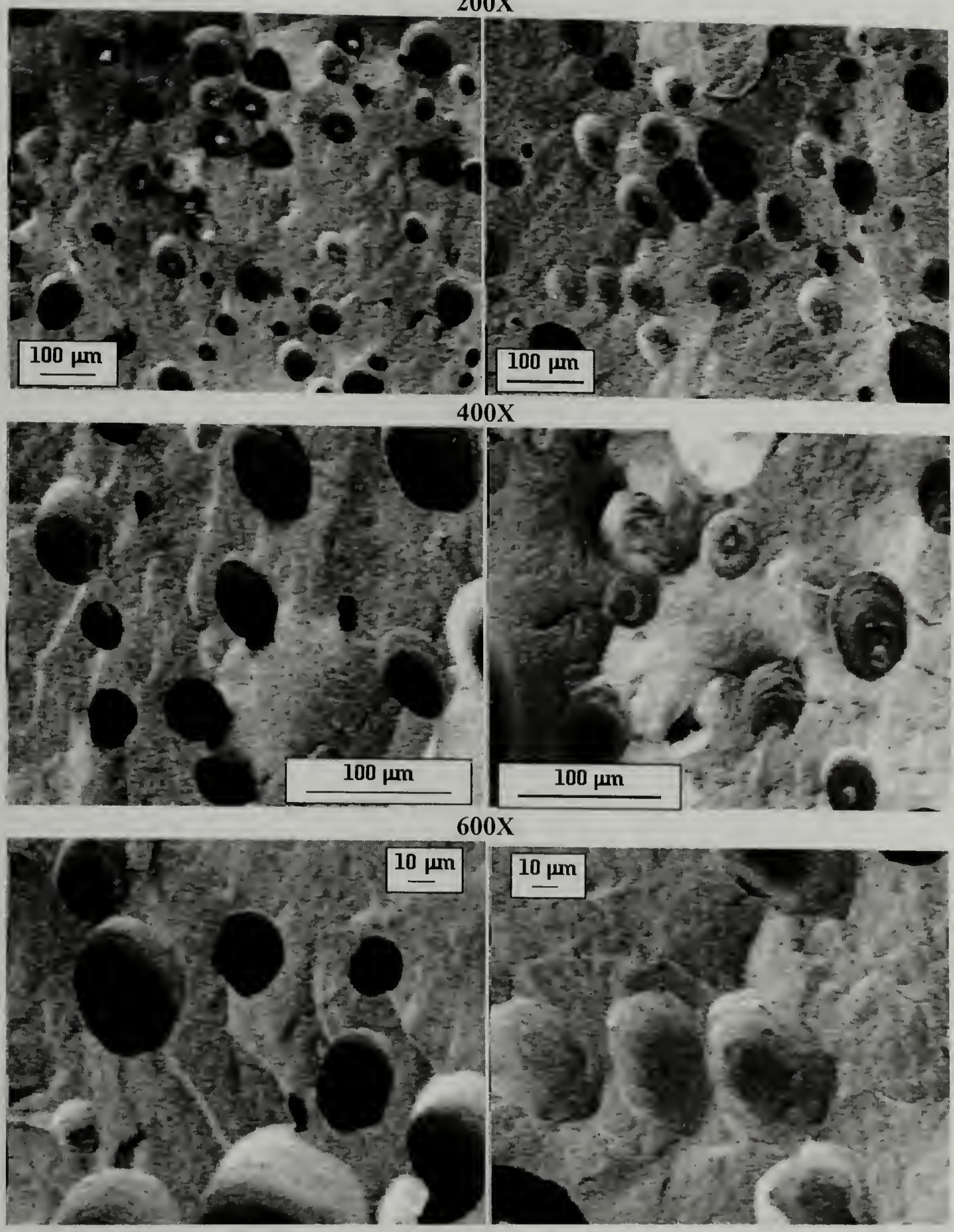

Figure 3.17. FESEM images of an HDPE sample processed with 10% MNa+ clay showing the typical closed-cell foamed structure.

200X

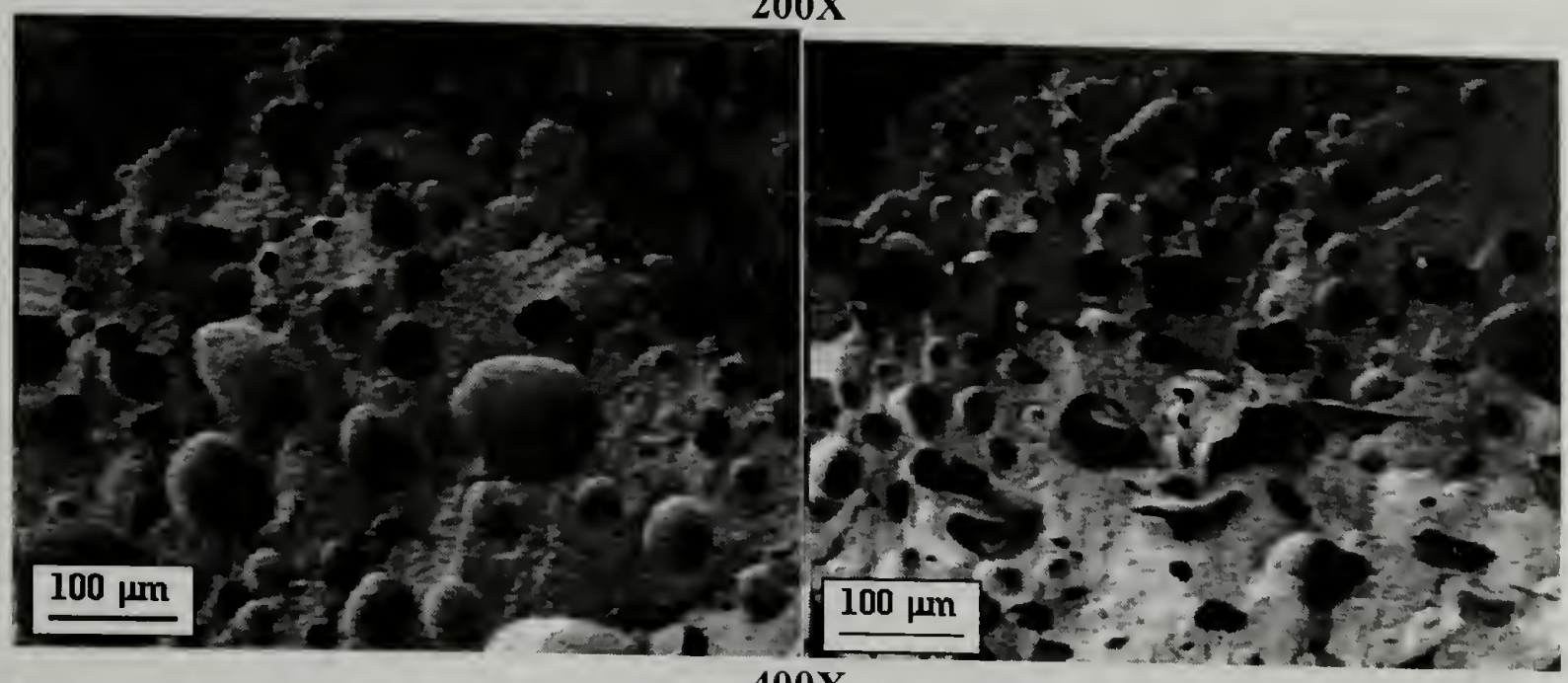

400X

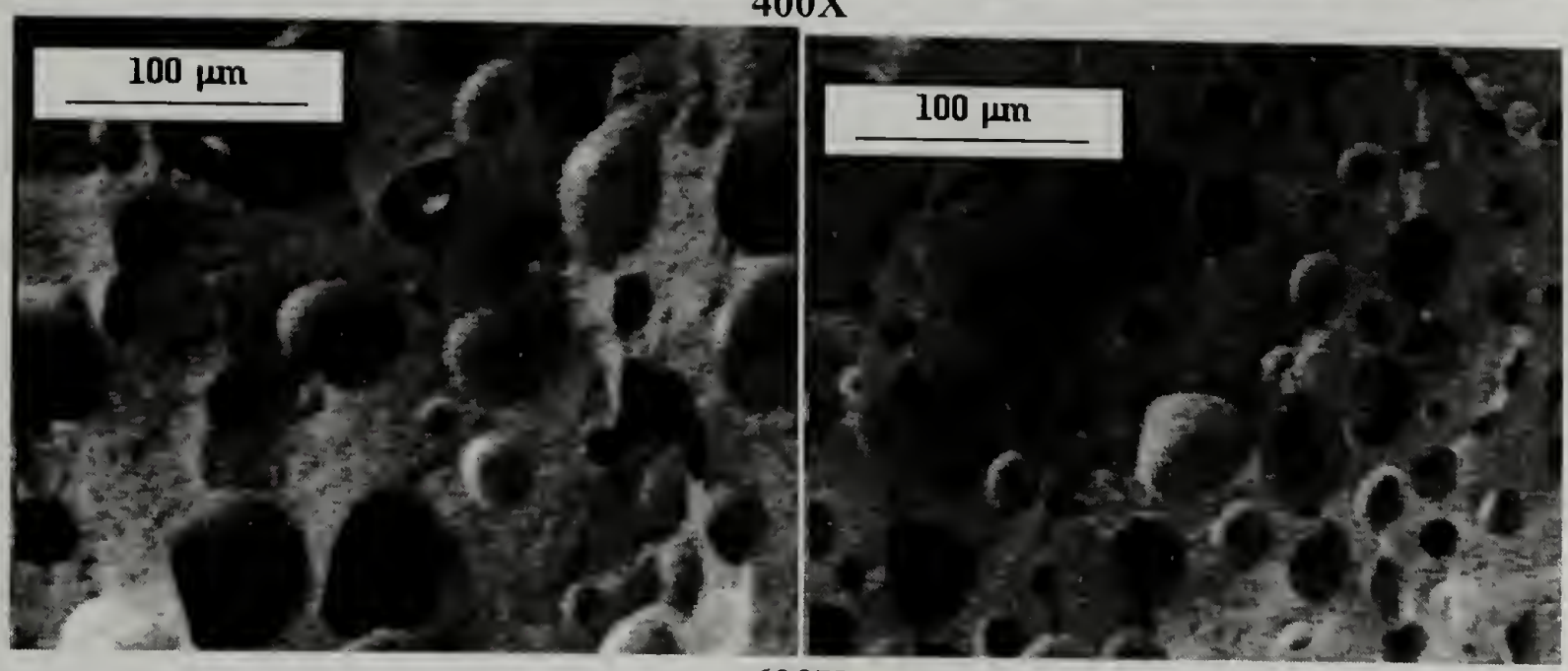

600X

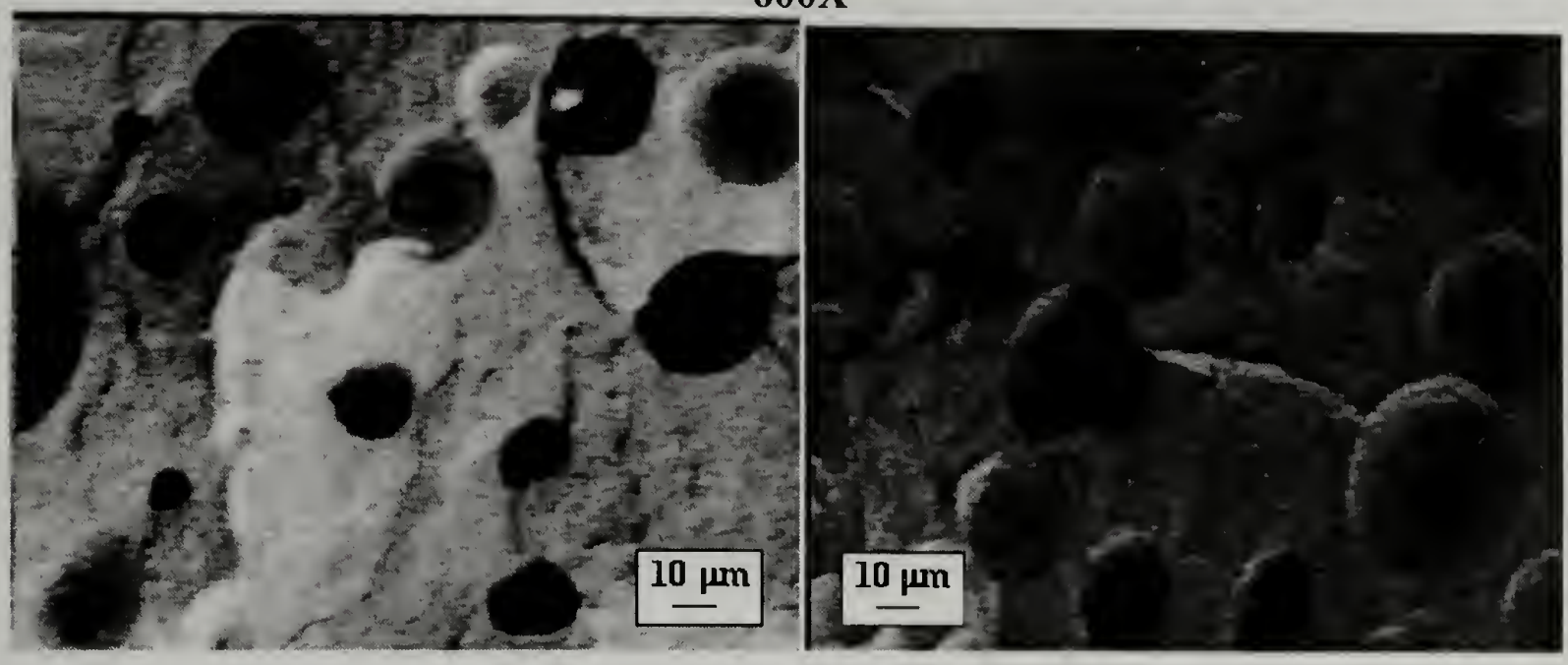

Figure 3.18. FESEM images of an HDPE sample processed with 1% M15A clay showing the typical closed-cell foamed structure.

As shown in figure 3.19, the presence of clay nanoparticles enhances the cell nucleation process and as a consequence, a significant increase in the cell density is observed at higher concentrations, until a critical clay concentration (~1%) is reached above which the cell density remains unchanged. It is found that the average cell size is primarily dictated by the concentration of clay and in a lower degree by the intrinsic physical properties of the clay employed. At any given clay concentration a narrow cell size distribution is observed, suggesting that most of the cells are nucleated at the same time, i.e. they are created by the same mechanism. The foaming process is significantly enhanced by the presence of clay particles that act as very effective heterogeneous nucleators, which provide available surface for nucleation, reducing the overall energy required to create a cell.

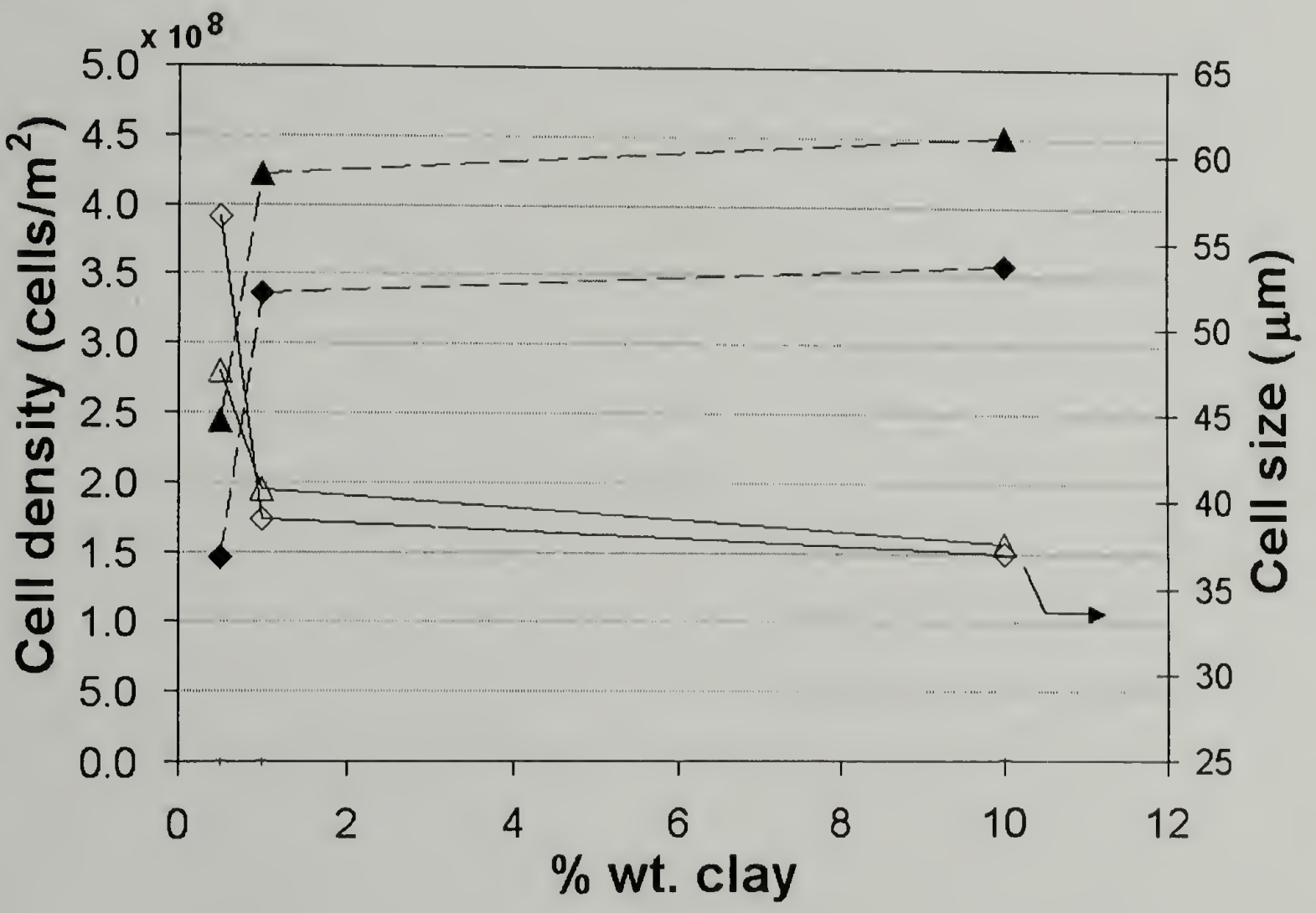

Figure 3.19. Cell densities and average cell size for HDPE samples at different amounts of clay (MNa+ clay (Δ) and M15A clay (◊)). Solid and open symbols are used to represent cell densities and average cell size respectively.

The observed densities in these systems remains unchanged regardless of the concentration of clay, as presented in table 3.2, suggesting that the amount of CO_2 dissolved is independent of the clay concentration, and so, the differences in the observed morphologies are only related to the nucleation process.

Sample	Clay	% wt. clay	Density
HDPE	MNa+	0.5	0.747
HDPE	MNa+	1.0	0.716
HDPE	MNa+	10	0.720
HDPE	M15A	0.5	0.677
HDPE	M15A	1.0	0.626
HDPE	M15A	10	0.651

Table 3.2. Observed densities in HDPE-clay systems at different concentrations of clay.

3.4 Conclusions

A modified processing system has been designed to process polymeric materials in the presence of high pressure CO_2. Several factors appear to have a direct effect on the final morphology of a polymer, however, the diffusion rate of CO_2 in the melt appears to dominate cell nucleation by controlling the amount of gas dissolved, so that foaming is favored by a saturation time in CO_2 prior to extrusion. When a favorable nucleation process is observed, specific control on the morphology can be achieved through several parameters in the system, including the temperature distribution and the saturation pressure.

CHAPTER 4

PROCESSING OF HIGH MELT VISCOSITY POLYMERS BY SUPERCRITICAL CARBON DIOXIDE-ASSISTED POLYMER PROCESSING

CO_2-assisted polymer processing is proposed as an alternative route for high melt viscosity and high-molecular weight polymers based on the plasticization effect of CO_2 and its direct effect on the melting behavior of semicrystalline polymers. A modified processing system has been used to process a variety of polymers in the presence of high-pressure CO_2. As presented in Chapter 3, the system includes an extruder that has been modified to allow for high pressures created by the injection of CO_2. Results suggest that this alternative design provides a new and easy route to melt-process high melt viscosity polymers of commercial importance such as PTFE, FEP and s-PS. The increased processability of these systems in CO_2 is related to the plasticization effect of CO_2 that has been quantified through a depression in the glass transition temperature according to the Chow model.

4.1 Introduction

As mentioned in Chapter 3, the idea of introducing $scCO_2$ in polymer extrusion as an alternative processing aid has been analyzed extensively for the past two decades.[25-36] Evidence of plasticization induced by $scCO_2$ can be found in the literature for a variety of polymer systems. As presented in figure 4.1, the plasticization effect is evident in PE/PS blends as suggested by Lee et al.[30], showing a significant reduction in the viscosity when $scCO_2$ is introduced in extrusion along with a definite change in the shear thinning

behavior, displaying a considerable increase in the power law index. Similar behavior has been observed in various systems, including amorphous PS homopolymer[74] and elastomeric systems such as PDMS[75] as shown in figure 4.2, where an increase in the concentration of CO_2 promotes a significant drop in the viscosity of the melt.

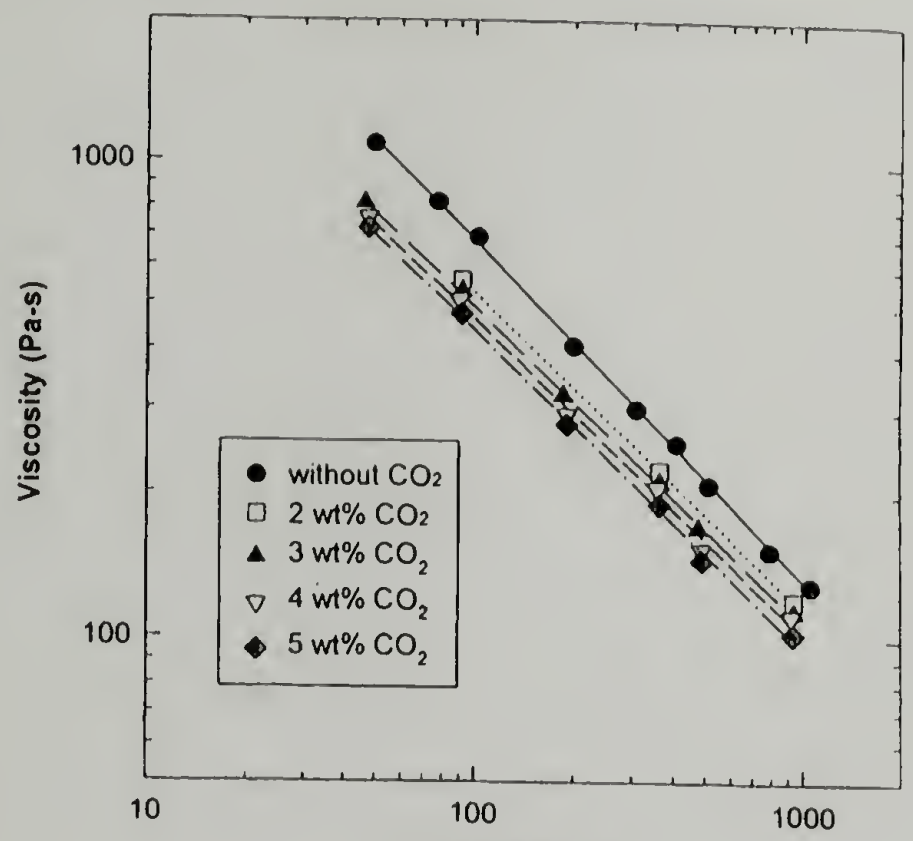

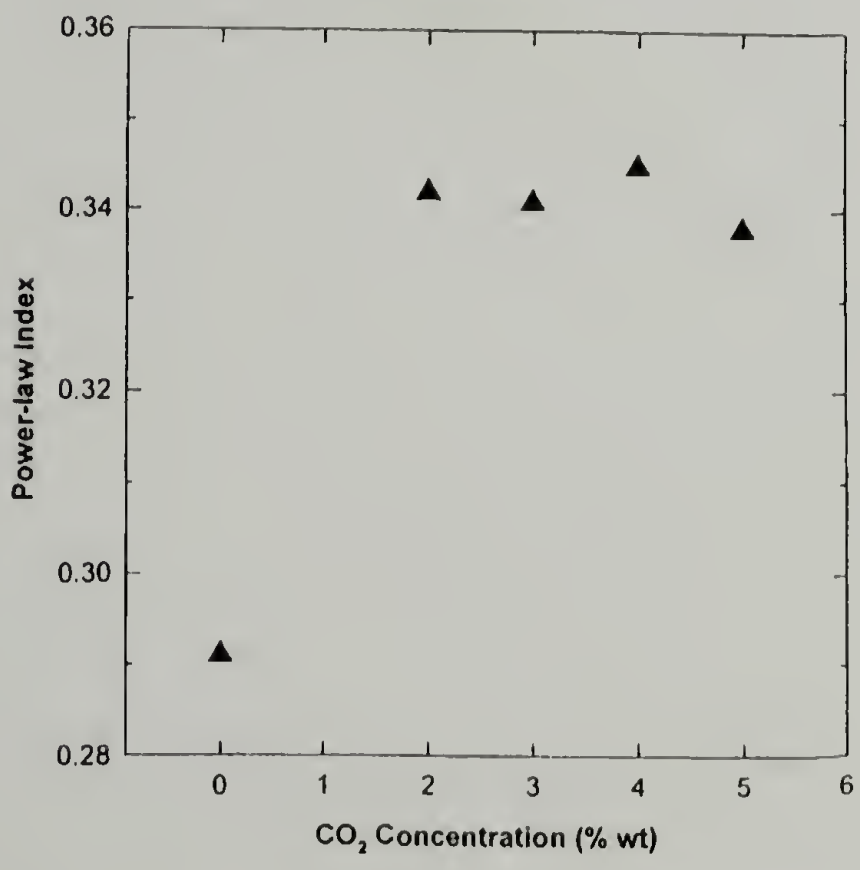

Figure 4.1. Evidence of plasticization induced by $scCO_2$ in PE/PS blends.[30]

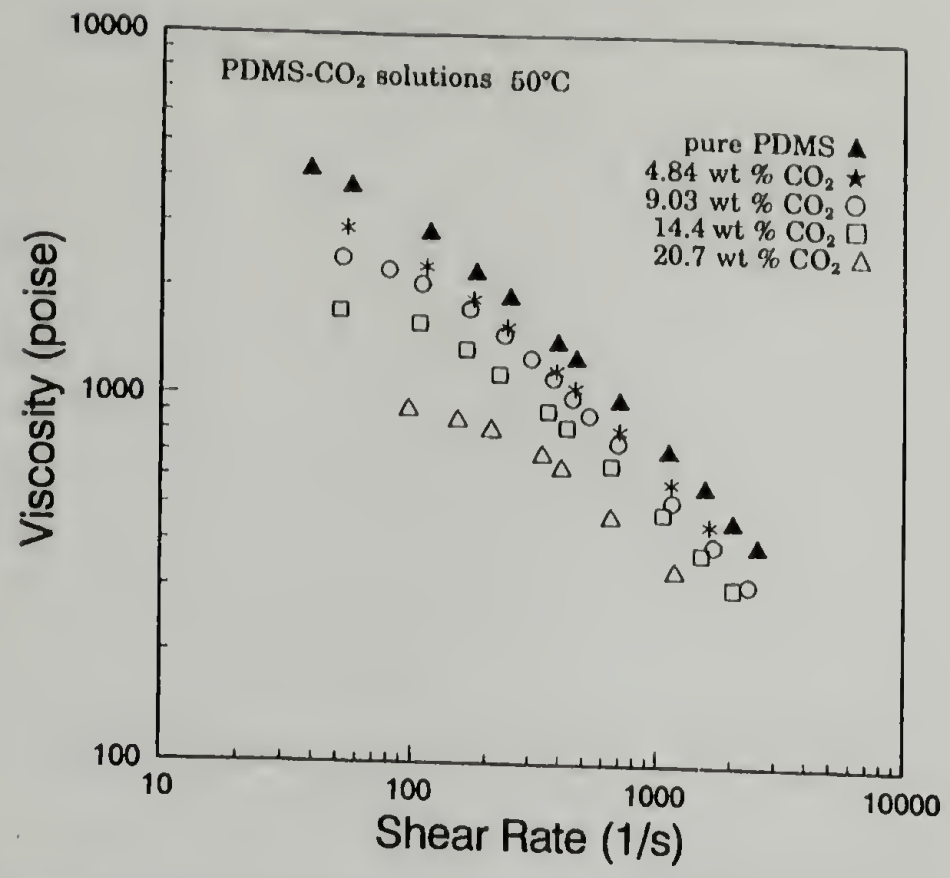

Figure 4.2. Evidence of plasticization induced by $scCO_2$ in PDMS.[75]

As described before, all these studies have been conducted in conventional extrusion foaming systems, as the one depicted in figure 3.5, where $scCO_2$ is introduced at later stages of the extrusion processes. This approach uses $scCO_2$ exclusively as a blowing agent and even though the plasticization effect has been recognized, it has never been exploited as a way to enhance the processability of high melt viscosity materials.

As described in figure 3.7, the interaction of $scCO_2$ with a polymer in our system can be specifically controlled even before the material enters the extrusion line, and as a consequence the plasticization process imposed by $scCO_2$ can be used to process materials that are difficult to process in conventional processing systems. In Chapter 3, a nucleation/processing strategy has been used for polyethylene systems in $scCO_2$, at temperatures very close or even below their melting point, suggesting that the processability of a given material could be dramatically increased when $scCO_2$ is introduced. In some cases this effect could be large enough to provide an alternative processing-route for high melt viscosity polymers.

In this work, CO_2-assisted polymer processing is employed for a variety of polymers at conditions very close or in the supercritical regime for CO_2. The results suggest that the alternative design of the system facilitates the melt processing of high melt viscosity polymers of commercial importance such as PTFE, FEP and s-PS. Polymeric foams down to the microcellular range are obtained in some cases, and a good understanding of the relation between the processing conditions and the final extrudate morphology is obtained, suggesting that the plasticization effect of CO_2 governs the processability of these materials, providing a new and easy route to melt process high melt viscosity polymers. Chow model's description of the plasticization phenomenon through an estimation of the glass transition depression in these systems has been used to correlate our experimental observations.

4.2 Experimental

The modified processing system described in Chapter 3 and presented in figure 3.7 is used to process a variety of high melt viscosity polymers. As mentioned before, the system includes a modified hopper that allows a specific amount of polymer to interact with CO_2 prior to the extrusion process.

Differential Scanning Calorimetry (DSC) is used to study the thermal behavior of the polymers processed in our system. DSC experiments are carried out in a TA Instruments thermal analyst model 2910 DSC at relatively slow heating rates (1-10 °C/min) in order to obtain a quantitative response of the thermal properties of each sample. The crystallinity of the samples is estimated by the ratio of their melting enthalpy and the theoretical heat of fusion for a perfect crystal of the corresponding polymer.

The overall extrudate morphology obtained at different processing conditions is investigated using Scanning Electron Microscopy (SEM). Samples are cryo-fractured in liquid nitrogen and gold coated prior to the SEM analysis. SEM images are obtained using a Field Emission Scanning Electron Microscope (FESEM) JSM-6320FXV and a Scanning Electron Microscope model JEOL-CF-35 with a filament voltage of 20 KV.

4.3 Results and Discussion

4.3.1 CO_2-assisted polymer processing and plasticization

A specific control over the final extrudate morphology can be obtained using the modified processing system described before. As presented in Chapter 3, results for HDPE suggest that both the presence of CO_2 and its diffusion rate into the melt promote the appearance of a foamed structure. When a favorable nucleation process is observed, several parameters can be used to control the morphology as shown in figure 3.11, where by changing the temperature distribution in the system the nucleation process is controlled, and polymer foams with different cell density and cell size are produced. As shown in this figure, when CO_2 is introduced, continuous processing can be achieved at temperatures as low as 115 °C, which is below the typical melting point in HDPE (127°C), suggesting a significant amount of plasticization brought about by the presence of CO_2.

As presented in Chapter 1, in order to quantify the plasticization effect of CO_2 in a given polymer we used the model proposed by Chow[37] that describes the plasticization phenomenon using a molecular interpretation of the glass transition temperature of polymer-diluent systems. Plasticization is described in terms of the glass transition

depression that occurs in a polymer-diluent system due to the presence of a small molecule diluent, such as CO_2, at low concentrations. The model provides an explicit expression for the glass transition depression (Tg/Tg_0) as the ratio of the glass transition temperature of a polymer-diluent system (Tg) to that of the pure polymer (Tg_0).

On the basis of both classical and statistical thermodynamics, Chow proposed the following expression to describe the glass transition depression.

$$\ln\left(\frac{T_g}{T_{g0}}\right) = \beta\left[(1-\theta)\ln(1-\theta) + \theta\ln\theta\right] \qquad (1)$$

where β, α are non-dimensional parameters given by

$$\beta = \frac{zR}{M_p \Delta C_{pp}} \qquad (2)$$

$$\theta = \frac{N}{N+L} = \frac{M_p}{2M_d}\frac{\omega}{1-\omega} = \frac{V_p}{2V_d}\frac{\phi}{1-\phi} \qquad (3)$$

where M_p and M_d are the molecular weights of the polymer repeating unit and diluent, respectively. ΔC_{pp} is the excess transition isobaric specific heat of the polymer, ω and ϕ represent the weight and volume fraction of diluent in the system, and V_p and V_d correspond to the molar volumes of the polymer repeating unit and diluent, respectively.

Equation (1) provides an explicit expression to quantify the plasticization of a polymer-diluent system in terms of intrinsic properties of the pure polymer and diluent. In our system, this expression can be used to quantify the amount of plasticization, using only two parameters that are either available in the literature or that can be easily estimated or prescribed by the processing conditions. It is easy to recognize that β is dependent only of the magnitude of ΔC_{pp}, a thermodynamic property of the polymer. On the other hand, θ depends on the weight fraction of CO_2 and since the conditions at the

hopper can be specifically controlled, the value of θ can be prescribed for each polymer system, setting the system to equilibrium conditions where the concentration of CO_2 is dictated by the equilibrium mass uptake of the polymer, as determined in conventional diffusion experiments.

Figure 4.3 shows the predictions of the Chow model, as described in equations (1-3), to the plasticization process of HDPE by CO_2. The parameters[39] and results obtained in this case are also summarized in table 4.1.

Polymer →	**Polyethylene**	**PTFE**	**FEP**	**Polystyrene**
Tg_0 (K)	237	200	180	358.5
ΔC_{pp} (J $g^{-1}K^{-1}$)	0.3708	0.0939	0.1361	0.2592
Mp (g mol^{-1})	28.04	100.02	106.52	104.15
Md (g mol^{-1})	44.09	44.09	44.09	44.09
Mp/Md	0.636	2.268	2.416	2.362
z	1	2	2	2
$Mp\Delta C_{pp}$ (J $mol^{-1}K^{-1}$)	10.4	9.4	14.75	27
Eq. Mass uptake of CO_2 (%)	6	3.5	4.4	11.8
ΔTg (K)	30.09	52.41	38.74	84.54
Tg (K)	206.91	147.59	141.26	273.96
Tg/Tg_0	0.8730	0.7379	0.7847	0.7641

Table 4.1. Summary of material properties, parameters and results obtained with the Chow model.

Chow model suggests the existence of a region in which the glass transition of the system is greatly affected by the presence of CO_2. The limit of this region is dictated by the amount of CO_2 that can be introduced into the polymer at equilibrium conditions. As shown figure 4.3, despite of the fact that the equilibrium mass uptake of CO_2 is rather small (6%), the glass transition depression is considerable and the ratio Tg/Tg_0 decreases to 0.8730. This value corresponds to an absolute change in glass transition of 30.09 °C, reducing the overall Tg of the system to 206.91 K. These calculations correlate very well with the experimental observations for HDPE, suggesting a significant amount of plasticization promoted by introducing CO_2 that enhances its processability at lower temperatures (even below the melting point).

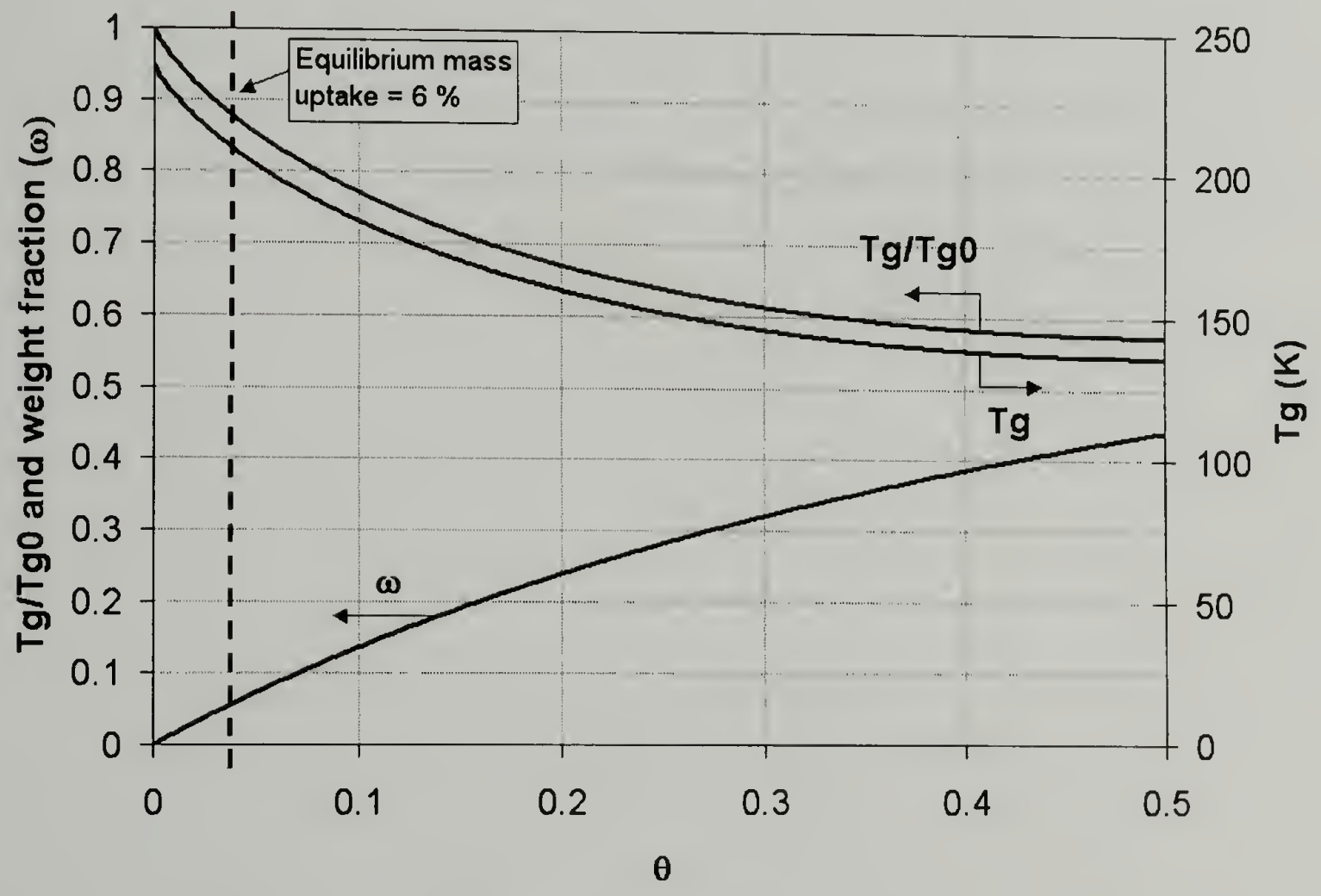

Figure 4.3. Glass transition depression (Tg/Tg_0) for the polyethylene-CO_2 system as predicted by the Chow model. The dashed line indicates the equilibrium mass uptake of CO_2 for the case of polyethylene (6%). Note that the relation between the weight fraction of CO_2 (ω) and the parameter θ is not linear.

These results suggest that the presence of CO_2 not only controls the final morphology, but it also facilitates the polymer processing through a combination of both plasticization and the imposed hydrostatic pressure acting as a processing aid during extrusion. This is a distinctive feature of our system, which enables the processing of high melt viscosity polymers, something impossible to achieve in a conventional extruder. Results obtained for syndiotactic polystyrene (s-PS), fluorinated ethylene propylene copolymer (FEP) and polytetrafluoroethylene (PTFE) using this alternative-processing route are discussed below.

4.3.2 Processing of high melt viscosity polymers

4.3.2.1 Polytetrafluoroethylene (PTFE)

Due to their high service temperatures and chemical inertness, fluoropolymers are a very attractive group of materials for CO_2-assited polymer processing. Two specific fluoropolymers are used in this study and their chemical structure is shown in figure 4.4.

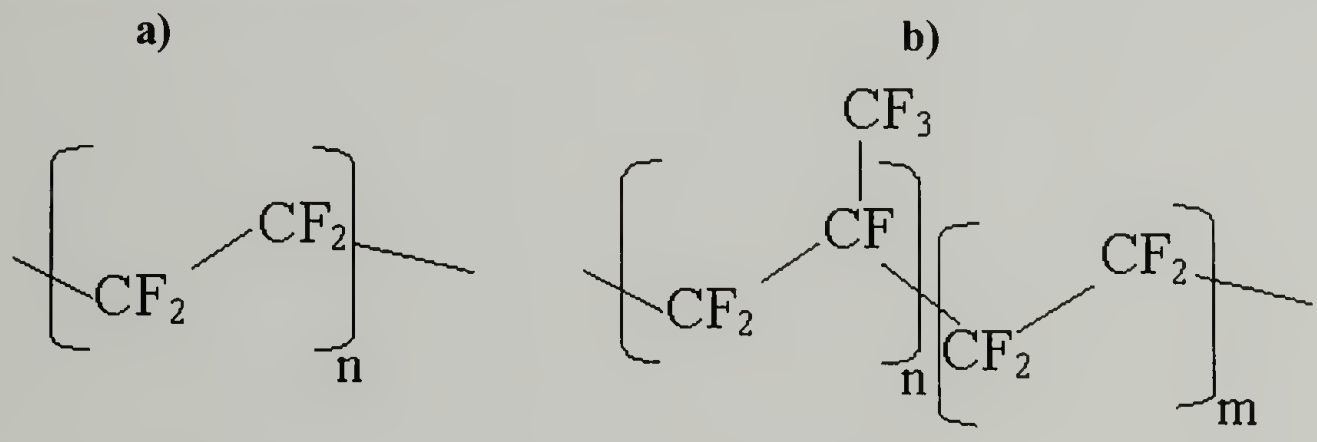

Figure 4.4. Chemical structure of fluoropolymers used in this study.
a) PTFE, Polytetrafluoroethylene (Polysciences, Powder 35 μm particle size, Teflon 7A)
b) FEP, Fluorinated ethylene propylene copolymer (Dupont, Pellets, FEP 4100).

In particular, polytetrafluoroethylene (PTFE) might be a good candidate for this alternative processing method due to its well-known affinity to CO_2. In general PTFE shows an extremely high molecular weight resulting in a melt viscosity, which is about

six orders of magnitude higher than that of most common thermoplastic polymers (10^{10}-10^{12} Pa s). The chemical inertness and stability as well as the low surface energy of PTFE is provided by its helical conformation, which creates an almost perfect cylindrical structure comprised of an outer layer of fluorine atoms surrounding a carbon based core.[42] Consequently, as mentioned in Chapter 1, the processing alternatives for PTFE are reduced to RAM extrusion and compression molding, and the possibility of an alternative and easy processing route for PTFE is of major relevance.

As presented in figure 4.5, processing of PTFE in conventional extruders is virtually impossible due to its extremely high melt viscosity. As a consequence, feeding problems are present and a continuous operation cannot be achieved. Without introducing $scCO_2$, the material remains in the feed section and is sintered at high temperatures. As shown in this figure the sintered material has the same thermal behavior as the original PTFE powder employed, since it does not undergoes melting during the sintering process.

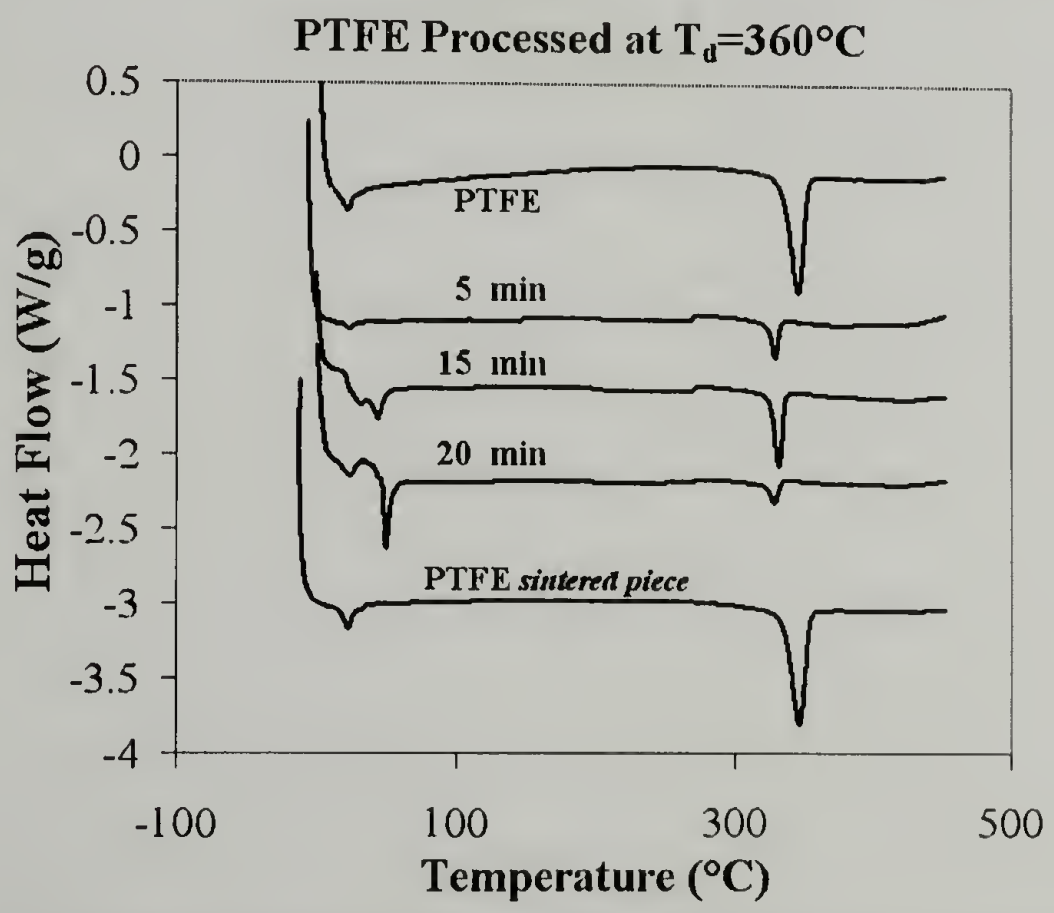

Figure 4.5. Typical feeding problems observed when attempting conventional extrusion processing in PTFE.

The sintered morphology is similar to that observed in commercially available PTFE products, as shown in figure 4.6, and is characterized by micron-sized PTFE aggregates held together by small fibril structures created during the sintering process.

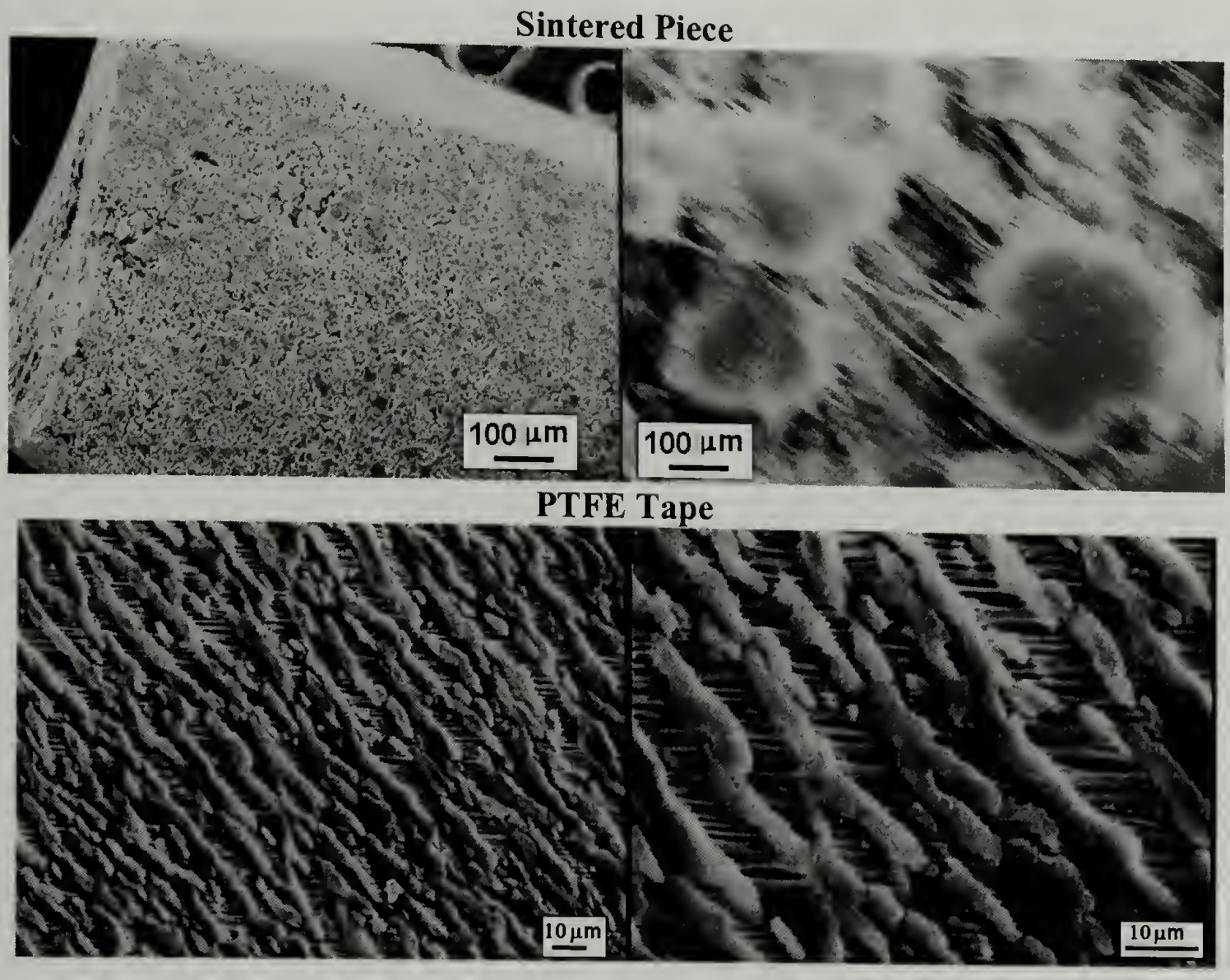

Figure 4.6. Morphology observed in sintered PTFE samples and its comparison with that observed in commercially available PTFE materials (PTFE tape).

As presented in figure 4.7 and table 4.2, the intrinsic characteristics of PTFE promote a very unique thermal behavior. A very high melting temperature is observed (345-350 °C) and the degree of crystallinity is typically between 60-90% depending on the crystallization conditions. However, once the material goes through a melting process, the crystallinity and melting temperature are significantly reduced as a consequence of the significant lost of molecular orientation during the melting process along with the fact

that due to the extremely high melt viscosity, the re-crystallization process becomes diffusion-controlled.

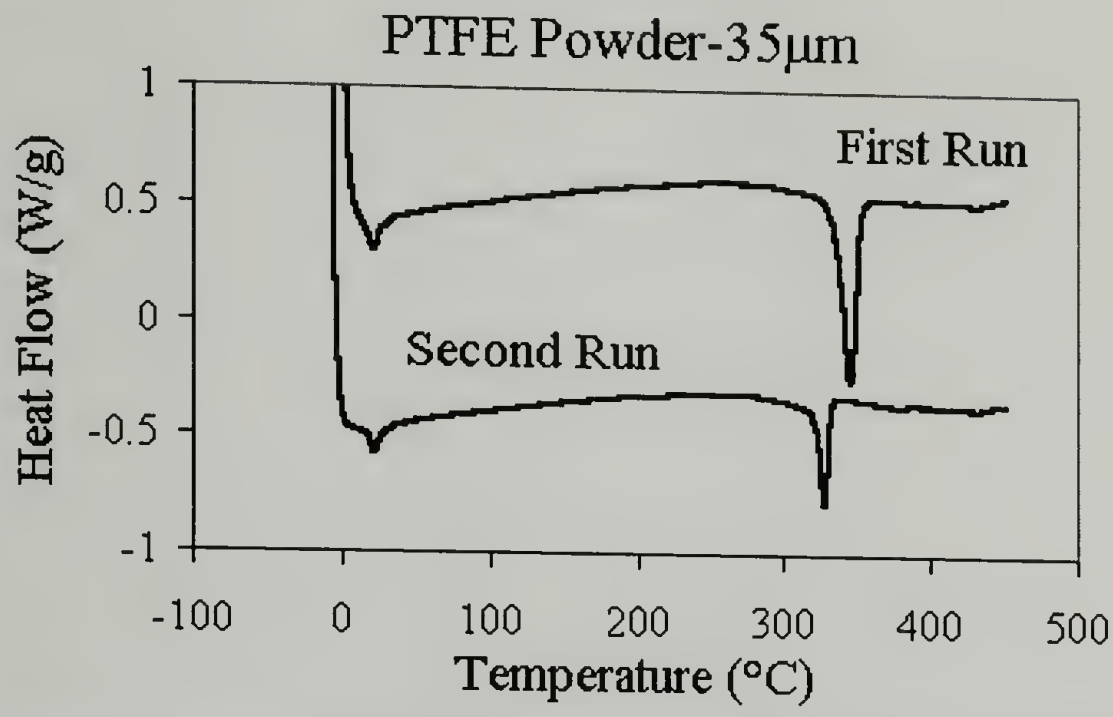

Figure 4.7. Thermal behavior of the PTFE powder used in this study.

Sample	Run	T1 (°C)	ΔH1 (J/g)	Tm (°C)	ΔHm (J/g)	Crystallinity (%)
PTFE	1	21.77	8.09	345.94	55.61	62.39
PTFE	2	22.23	5.33	327.88	21.13	25.91

Table 4.2. Thermal behavior of the PTFE powder used in this study.

PTFE powder with a particle size of 35 µm has been processed in our system in the presence of CO_2. Results suggest that despite the extremely high molecular weight of PTFE, a continuous processing is obtained when CO_2 is introduced, significantly enhancing the processability of PTFE in the presence of CO_2. The thermal behavior of the samples obtained with CO_2 is presented in figure 4.8 and table 4.3. As typically observed, the virgin polymer has a melting point of 345.94 °C with a corresponding degree of crystallinity of 62.4%, using a value of 102.1 J/g as the enthalpy of fusion for

100% crystalline PTFE.[43] In contrast, the melt-processed sample displays a lower degree of crystallinity (25.9%) and a significantly lower melting temperature (327.88°C).

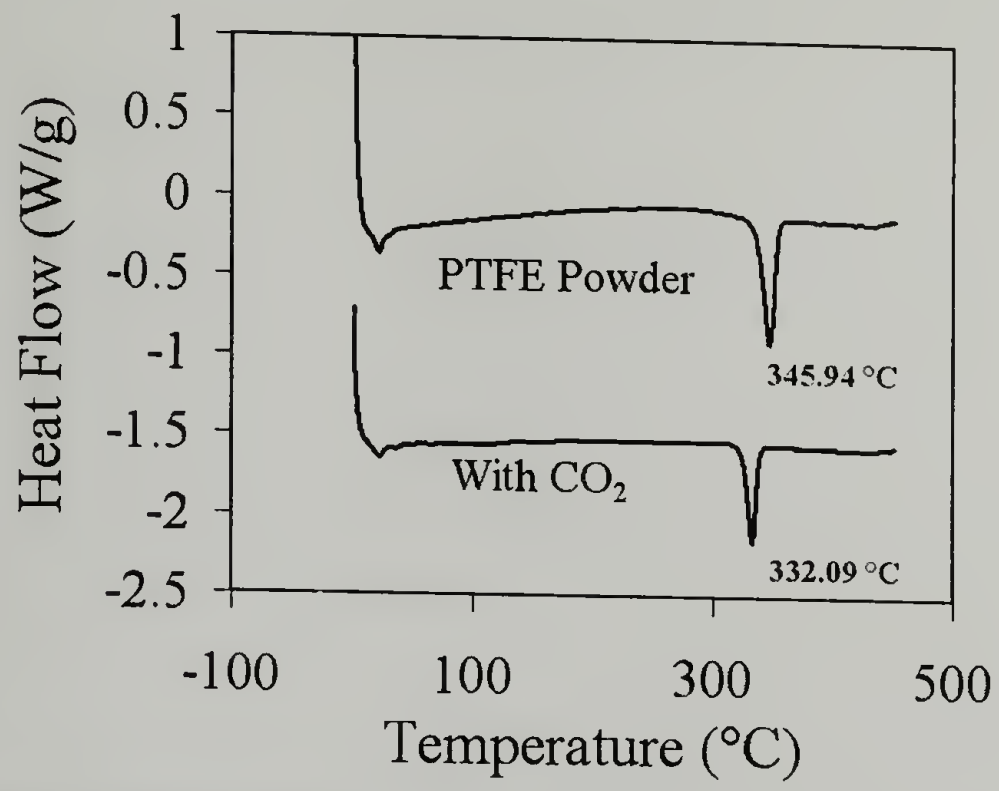

Figure 4.8. Typical thermal behavior of PTFE samples processed in our system at 360°C.

Sample	Tm (°C)	ΔHm (J/g)	Crystallinity (%)
PTFE Powder	345.94	55.61	62.39
PTFE Extruded with CO_2	332.09	32.32	36.22

Table 4.3. Typical thermal behavior of PTFE samples processed in our system at 360°C.

As described before, this dramatic change in the thermal response is evidence of the melting process of the sample during extrusion in $scCO_2$. After melting, the re-crystallization process is restricted due to the extremely high melt viscosity, and as a consequence, the crystallinity of the sample is significantly reduced. In this particular case, the melt viscosity is so high that upon melting more than 50% of the crystallinity is lost. The restricted re-crystallization process significantly reduces the typical crystal size, thus the lower melting point.

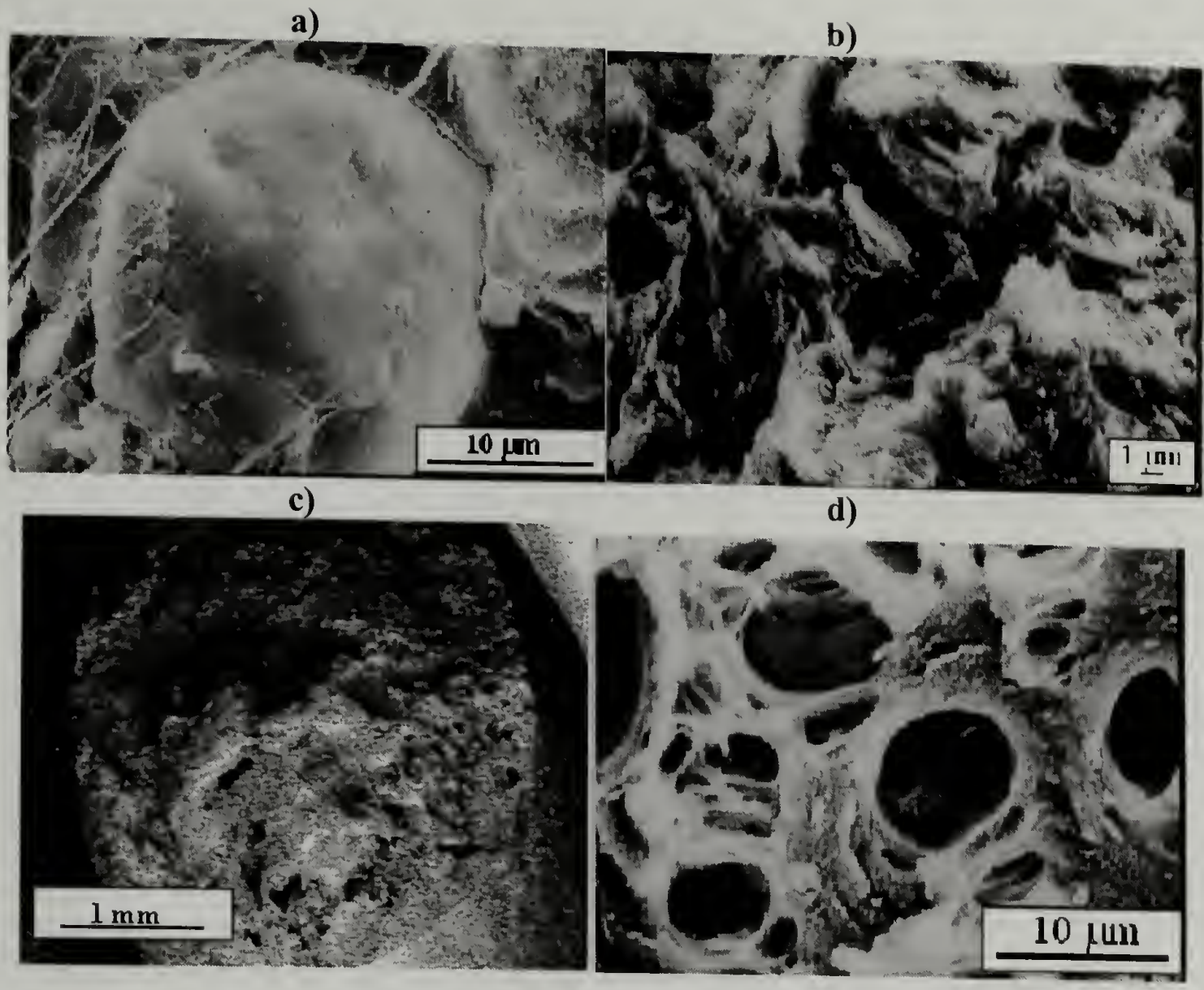

Figure 4.9. General morphology (SEM) observed in PTFE samples processed at different processing conditions. a) PTFE particle, b) Melt Pressed sample, c) $scCO_2$-extruded at 400 °C, and d) $scCO_2$-extruded at 360°C.

In addition to the thermal behavior, the presence of CO_2 has a direct effect on the morphology as shown in figure 4.9, where samples processed in $scCO_2$ display a well-defined foamed structure. The nucleation strategy suggested in Chapter 3, can also be applied to PTFE, and as presented in figure 4.10 control over the final foamed structure can be achieved by lowering the processing temperature, reducing in a significant way the amount of cell coalescence observed at high temperatures (400 °C). As in the case of HDPE, the final morphology can be specifically controlled though the processing conditions, so that a decrease in the die temperature allows for a specific control on the average cell size and cell density.[73] Also, as mentioned before, our design allows for a

given saturation time in CO_2 before processing that promotes cell nucleation even at moderate pressures (3.44 MPa), which suggests that even in the case of PTFE, the nucleation process can be tuned so that a specific control over the cell density and cell size can be obtained.

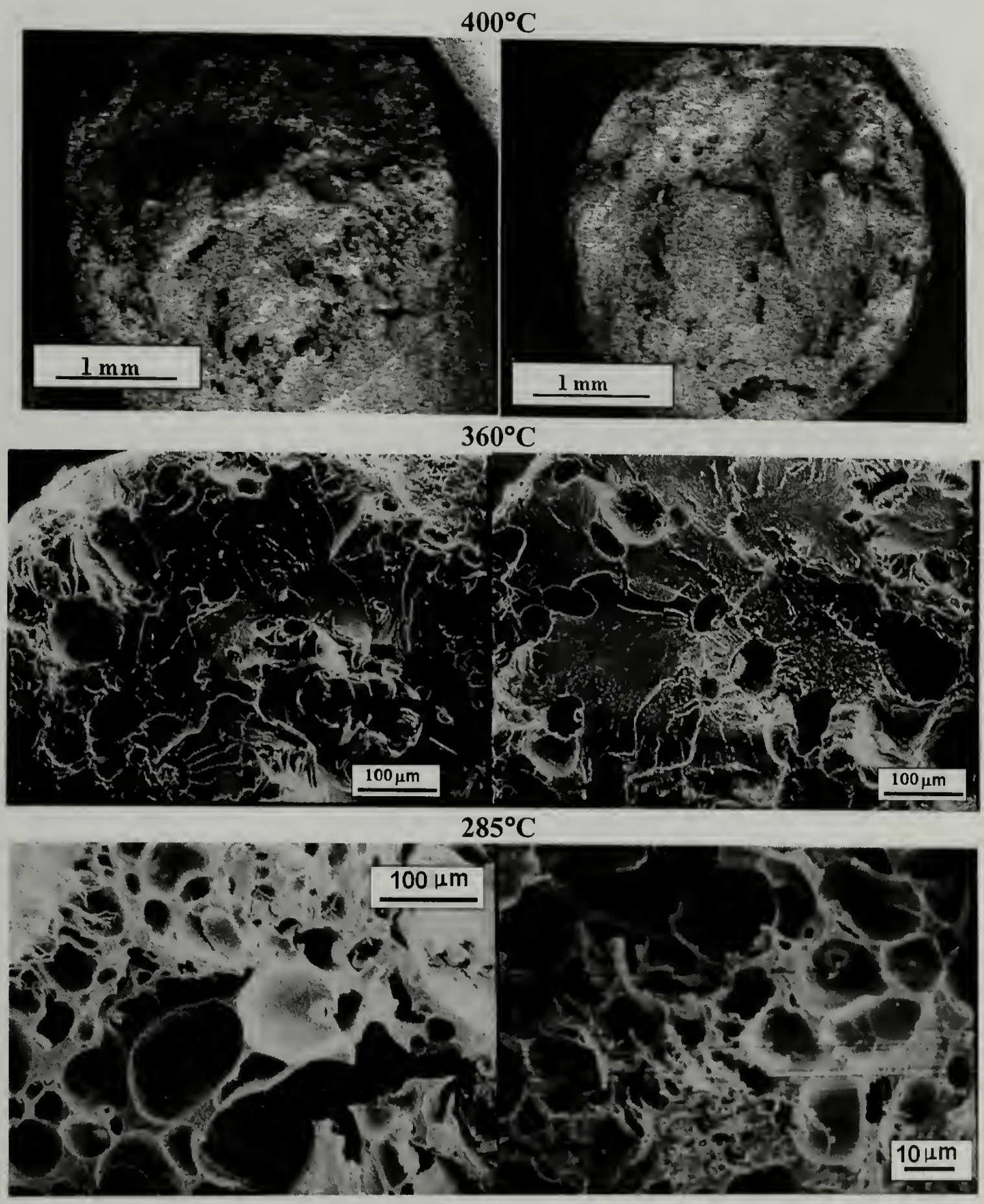

Figure 4.10. General morphology (SEM) observed in PTFE samples extruded in $scCO_2$ at different processing conditions.

A typical example of the final morphology observed in the PTFE extrudates is presented in figure 4.11. Well-defined foamed structures with enough cell integrity even at such high temperatures are obtained. This figure shows a SEM image of a PTFE sample obtained at 360 °C, in this particular case, the average cell size is below 10 μm, a cell size typically observed in microcellular materials.

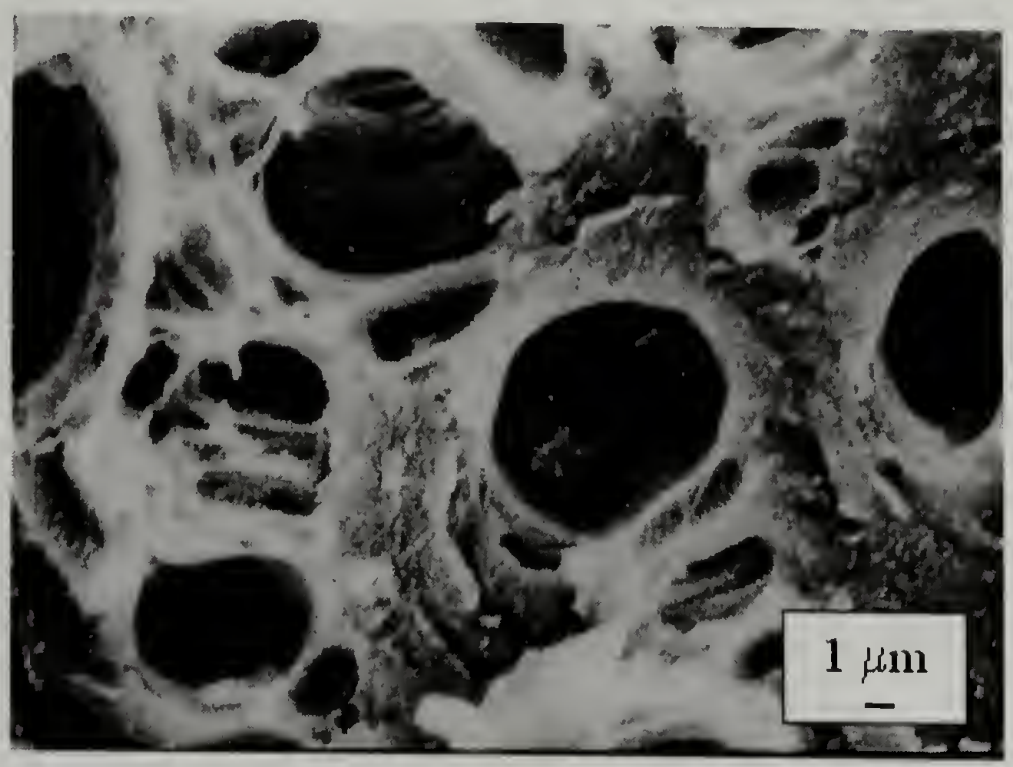

Figure 4.11. Overall morphology observed in PTFE samples processed at 360°C.

The high melt viscosity does not limit the processability of PTFE by this route, and a continuous process is observed even at temperatures below the polymer melting point (285 °C), suggesting a significant amount of plasticization by CO_2. Figure 4.12 shows the predictions of the Chow model for the plasticization process of PTFE by CO_2. The parameters used in this calculation are summarized in table 4.1 and include a value of 3.5% for the equilibrium mass uptake of CO_2 for PTFE[43] and a change in heat capacity during glass transition ($Mp\Delta C_{pp}$) of 9.4 $Jmol^{-1}K^{-1}$.[44-45] The model predicts the existence of a large plasticizing region that extends until the equilibrium mass uptake of CO_2 is reached, and again, despite of the fact that this value is very low (3.5%), the glass

transition of the system is significantly affected by CO_2, decreasing the magnitude of the ratio Tg/Tg_0 to 0.7379. This result corresponds to almost a 30% decrease in the Tg of the system, displaying an absolute change in glass transition of 52.41 °C, reducing the overall Tg of the system to 147.59 K. Once again, these calculations indicate that the plasticization effect of CO_2 is large enough to allow for a continuous processing of PTFE at lower temperatures using this alternative processing strategy.

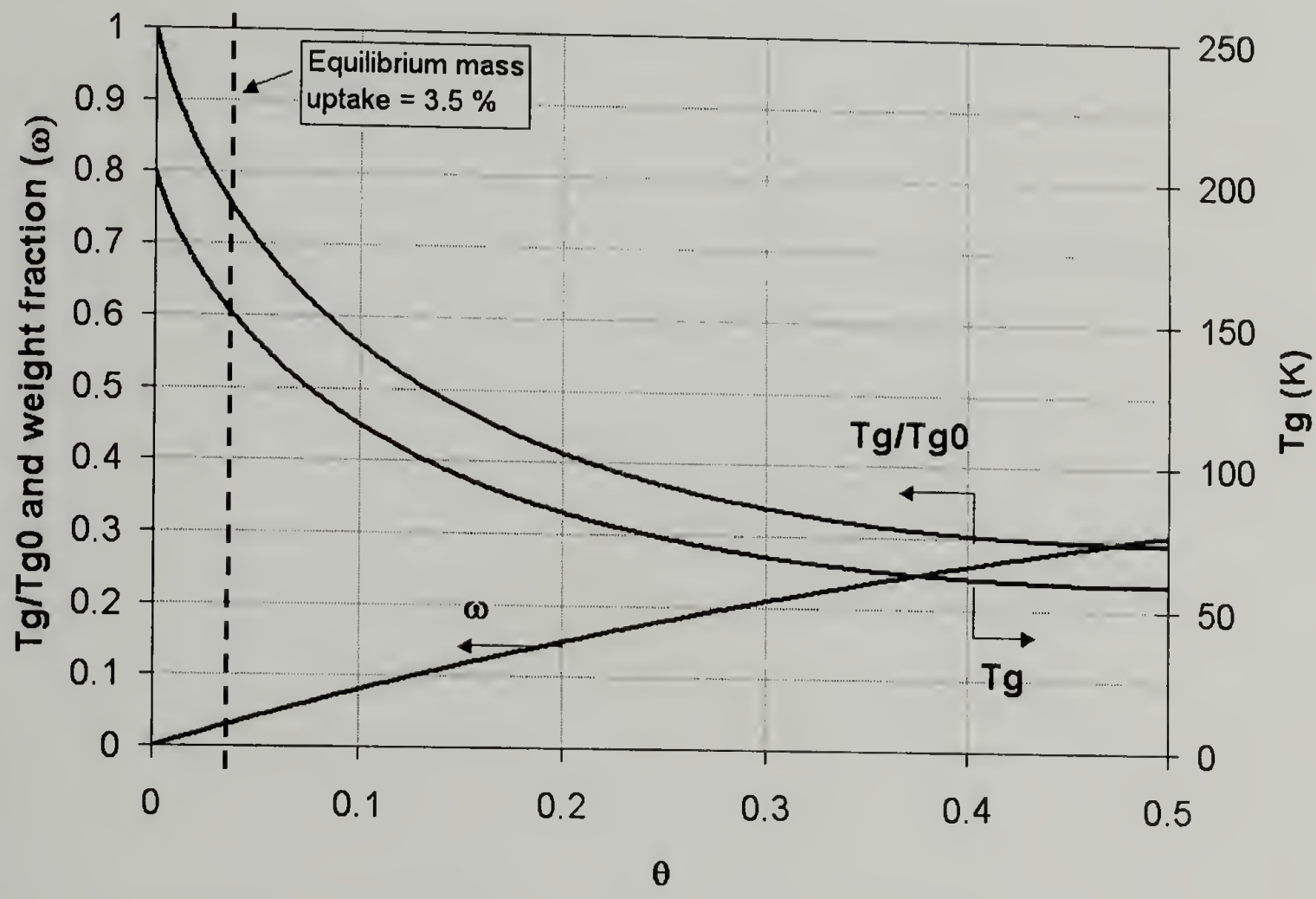

Figure 4.12. Glass transition depression (Tg/Tg_0) for the polytetrafluoroethylene-CO_2 system as predicted by the Chow model. The dashed line indicates the equilibrium mass uptake of CO_2 for the case of polytetrafluoroethylene (3.5%).

4.3.2.2 Fluorinated ethylene propylene copolymer (FEP)

As presented in figure 4.4, fluorinated ethylene propylene copolymer (FEP) is a random copolymer of tetrafluoroethylene (TFE) and hexafluoropropylene (HFP), with a structure very similar to that of PTFE except for the HFP units that are responsible for

significant changes in the physical properties of the system, acting as defects in crystallites that reduce the overall melting point to 260°C.[42] In addition, FEP systems are produced with significantly lower molecular weight than PTFE, and as a consequence, FEP has a reduced melt viscosity in comparison to PTFE that enhances its processability.

The thermal behavior of the FEP samples (13 % HFP) processed in our system is presented in figure 4.13. As shown in this figure, despite the similarity with PTFE, significant differences are observed in the general behavior of both polymer systems. The thermal behavior of the FEP samples appears to be independent of the processing conditions, such that the DSC traces of these materials are very similar regardless of the presence of CO_2. In addition, the thermal behavior of the melt-processed samples are almost identical of that observed in the virgin powder.

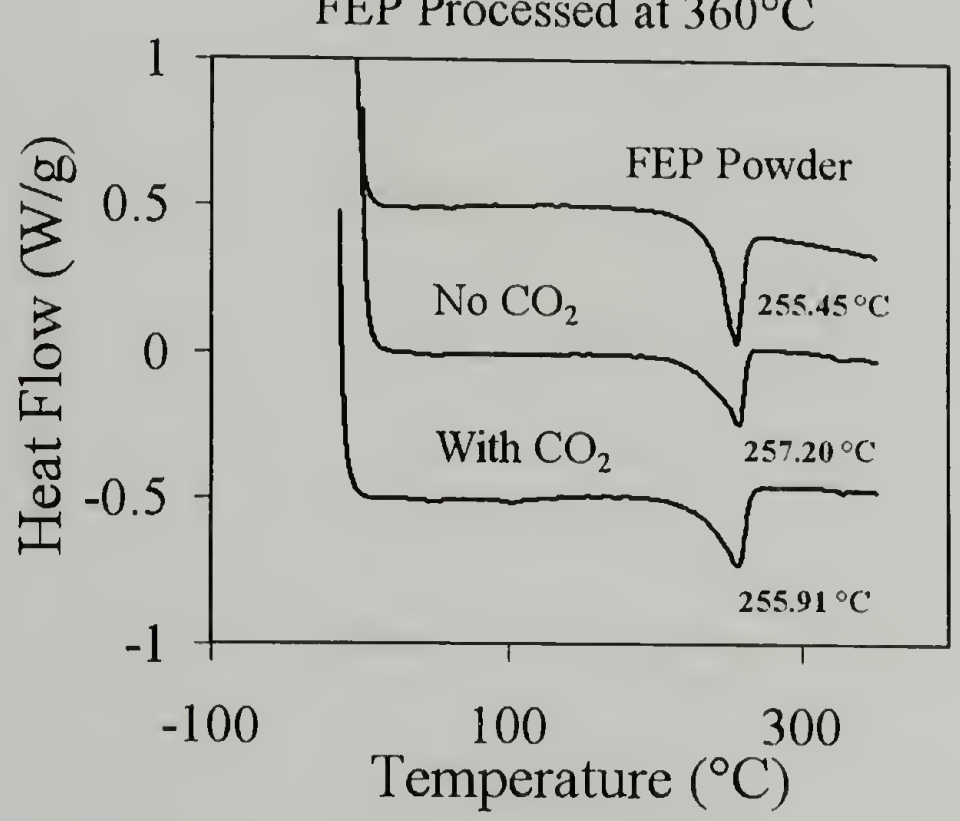

Figure 4.13. Typical thermal behavior of FEP samples processed in our system at 360°C.

As shown in table 4.4, the crystallinity of the virgin polymer in this case is around 41.38 %, using 92.94 J/g as the enthalpy of fusion for 100 % crystalline FEP.[46] This value is very similar to that observed in the samples processed with and without CO_2 (40.67

and 37.0 %, respectively), and it appears not to be affected in a significant way by the melting process. This general behavior is a consequence of the inherently larger processability of FEP that despite the high molecular weight does not restrict the re-crystallization process, so that most of the crystallinity in the sample can be recovered after melting.

Sample	Tm (°C)	ΔHm (J/g)	Crystallinity (%)
FEP	255.45	38.46	41.38
FEP Extruded without CO_2	257.20	34.39	37.0
FEP Extruded with CO_2	255.91	37.80	40.67

Table 4.4. Thermal behavior of FEP samples processed in our system at 360°C with and without $scCO_2$.

The enhanced processability of FEP facilitates in a significant manner the specific control of the morphology of the FEP extrudates when CO_2 is introduced. In this case, despite of the high temperatures, the nucleation process can be enhanced by lowering the die temperature promoting an increase in the cell density and decreasing the cell size.

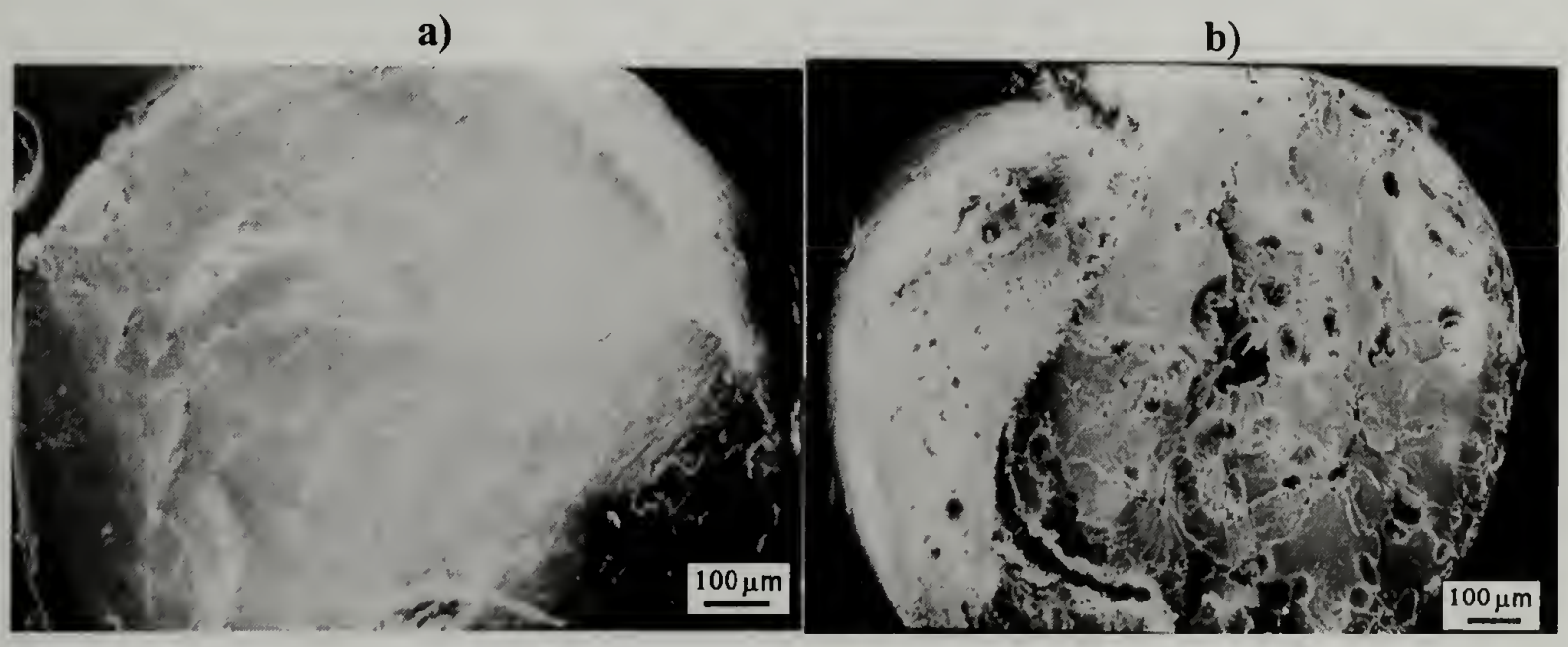

Figure 4.14. General morphology (SEM) obtained in FEP samples processed at 360°C. a) Without CO_2, and b) with CO_2.

As shown in figure 4.14, at high temperatures (360°C) the foamed structure is evident but a significant amount of cell coalescence is present, however, at lower temperatures (285°C) the cell structure is better defined and the integrity of the cells increases. The morphology at 285°C is shown in figure 4.15, displaying a well-defined closed cell structure with a typical average cell size is around 10 μm.

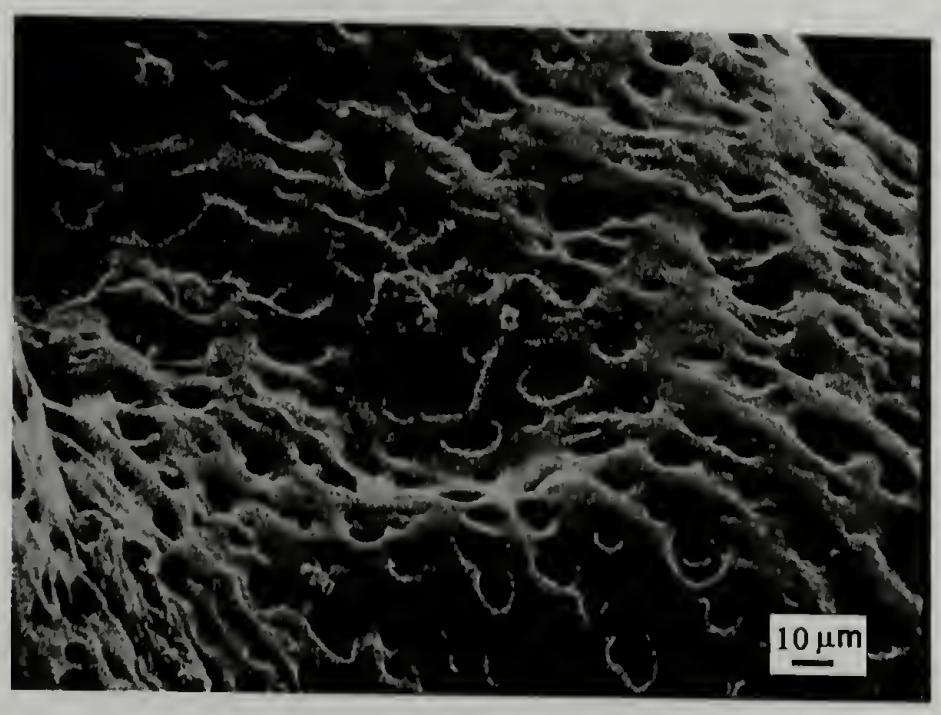

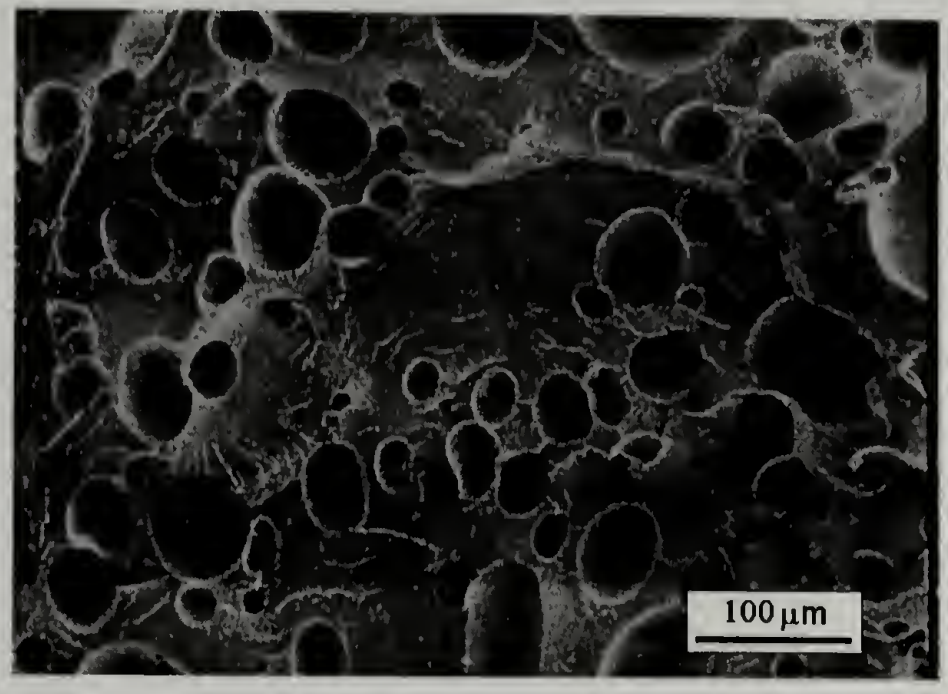

Figure 4.15. Typical closed cell morphology obtained in FEP at 285°C.

Once again, a continuous process is obtained in FEP samples, however, in this case the high melt viscosity restricts the processability of FEP to temperatures above 285 °C, regardless of the presence of CO_2. This observation suggests that plasticization in this

case is not as important as in the case of PTFE, so that the glass transition depression observed in FEP due to the presence of CO_2, should be lower that that of PTFE at equilibrium conditions.

The plasticization process of FEP by CO_2 can also be described the Chow model. In this case, however, no available data is found in the literature regarding the heat capacity change of FEP at the glass transition (ΔC_{pp}). As presented in figure 4.16, using the additivity concept of the heat capacities of linear polymers proposed by Gaur and Wunderlich[47-48] a change in heat capacity during glass transition ($Mp\Delta C_{pp}$) can be estimated.

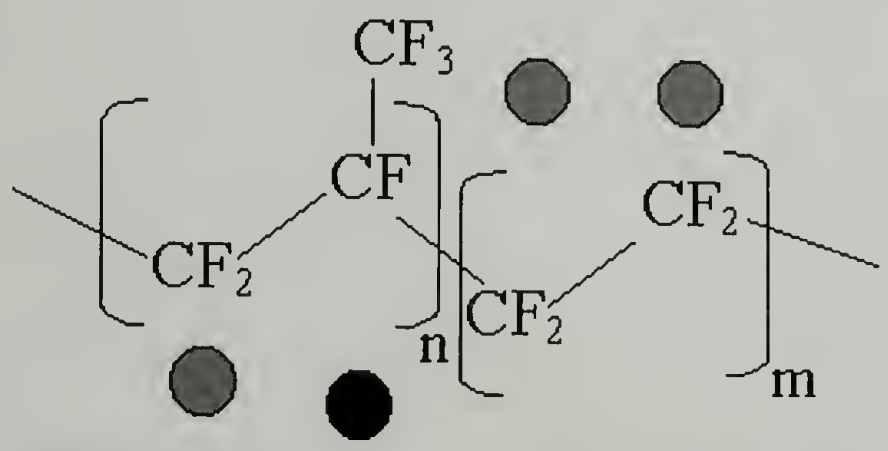

Units	Repeating unit	% mol
TFE		87
HFP		13

Structure	# beads	$Mp\Delta C_{pp}$ (J/molK)
	1	11.3
	4	45.2

Figure 4.16. Additivity concept of linear polymers applied to FEP to determine the heat capacity at Tg.[47-48]

This calculation is based on the fact that since the concentration of HFP units in the copolymer is known, their contribution to the heat capacity can be estimated. According to this theory, a dimer containing one unit of HFP attached to one of TFE creates a 4-bead structure with a corresponding $Mp\Delta C_{pp}$ of 45.2 $Jmol^{-1}K^{-1}$. In contrast, a single-bead

structure is created when two TFE units are attached to each other. In this case, the structure is identical to a PTFE dimer and so the corresponding $Mp\Delta C_{pp}$ is 9.4 $Jmol^{-1}K^{-1}$. Given the concentration of HFP units in the copolymer (13%), a value of 14.75 $Jmol^{-1}K^{-1}$ is estimated.

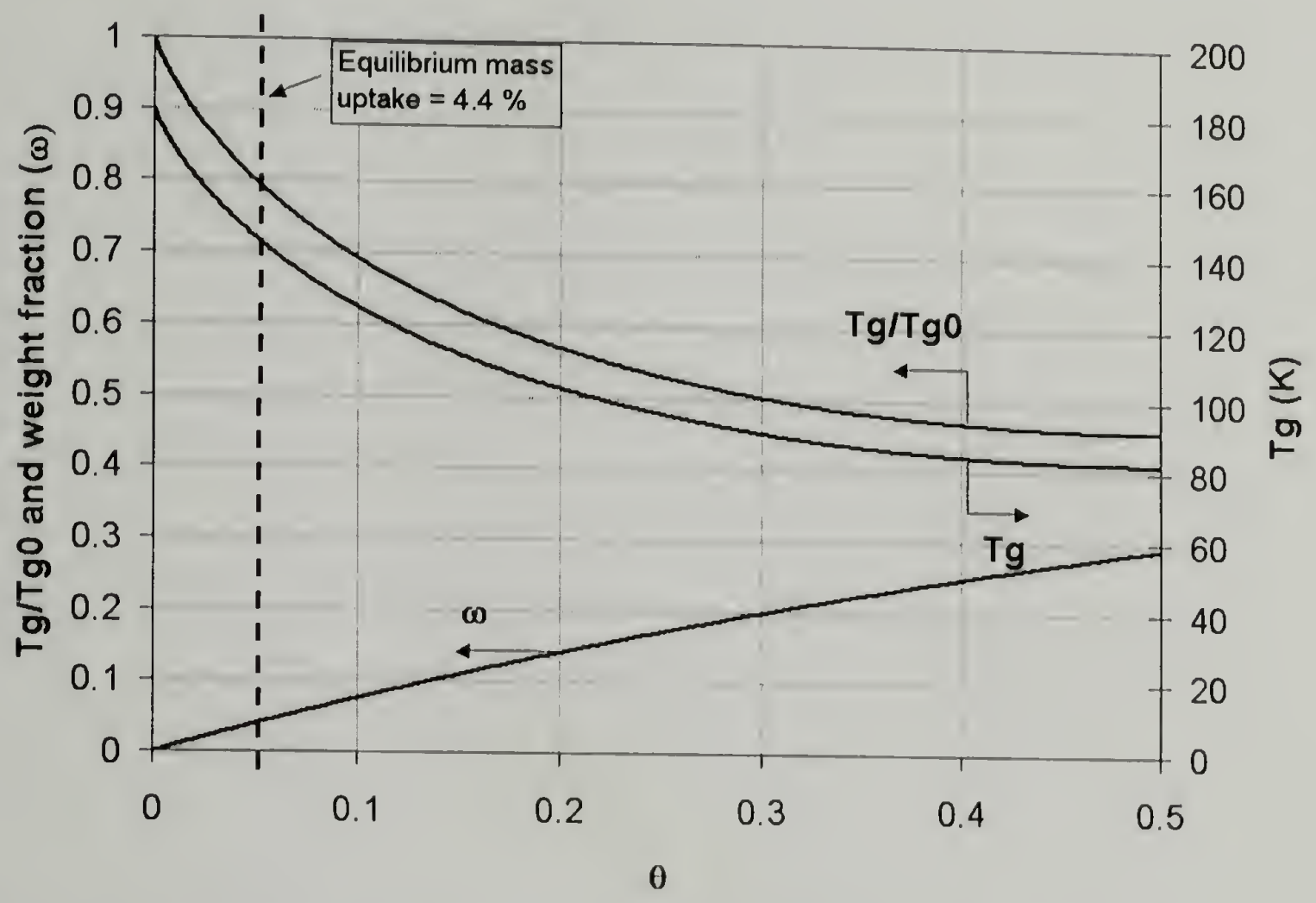

Figure 4.17. Glass transition depression (Tg/Tg_0) for the FEP-CO_2 system as predicted by the Chow model. The dashed line indicates the equilibrium mass uptake of CO_2 for the case of FEP (4.4%).

Figure 4.17 shows the results obtained using the parameters in table 4.1 for the case of FEP. The predictions correlate very well with the experimental observations, showing the existence of a large plasticizing region limited by the equilibrium mass uptake of CO_2 (4.4 %). The important observation here is that despite of the fact that this value is larger than that observed in PTFE (3.5 %), the model predicts that at equilibrium conditions, the value of the glass transition depression ratio Tg/Tg_0 is 0.7847, which corresponds to an absolute change in glass transition of 38.71 °C, less than that observed in PTFE. These

results indicate that even though the plasticization process of FEP by CO_2 is large, it is less important than that observed in PTFE and due to the high melt viscosity of the system it is not enough to allow for a continuous processing at temperatures close the melting point.

4.3.2.3 Syndiotactic Polystyrene (s-PS)

In addition to fluoropolymers, high melt viscosity polyolefins are also good candidates to be processed using this route. An example of these materials is syndiotactic polystyrene (s-PS), a relatively new semicrystalline plastic with a high melting point (>250ºC), suggesting higher service temperatures than common plastics. The relevance of s-PS as an engineering polymer is that the amount of crystallinity, the type of crystal structure and morphology can be controlled by the crystallization conditions. Thus, as mentioned in Chapter 1, a consistent strategy for melt process s-PS is of great relevance, since the properties that make s-PS an attractive material (high temperature mechanical properties, low permeability, good chemical resistance) are strongly affected by the amount and distribution of the crystalline phase.

Figure 4.18 describes the typical thermal behavior of the s-PS samples processed in our system. As in the case of FEP, the thermal behavior appears to be independent of the processing conditions, and so the DSC trace of a sample processed with CO_2 differs slightly from that of the s-PS virgin powder employed. However, due to the lack of additional mixing devices in the extruder, processing without the addition of CO_2 is almost impossible due to the high molecular weight, so a comparison between samples processed with and without CO_2 cannot be achieved in this case. The crystallinity of the

virgin polymer in this case is 47.76 %, using 53.2 J/g as the enthalpy of fusion of 100 % crystalline s-PS.[49] Again, as in the case of FEP, this is very similar to the value observed in CO_2-processed samples (48.10 %), suggesting that the re-crystallization process is not restricted despite the high molecular weight, so that after melting most of the crystallinity in the sample can be recovered. In addition, as shown in table 4.5, no significant changes in the melting point are observed.

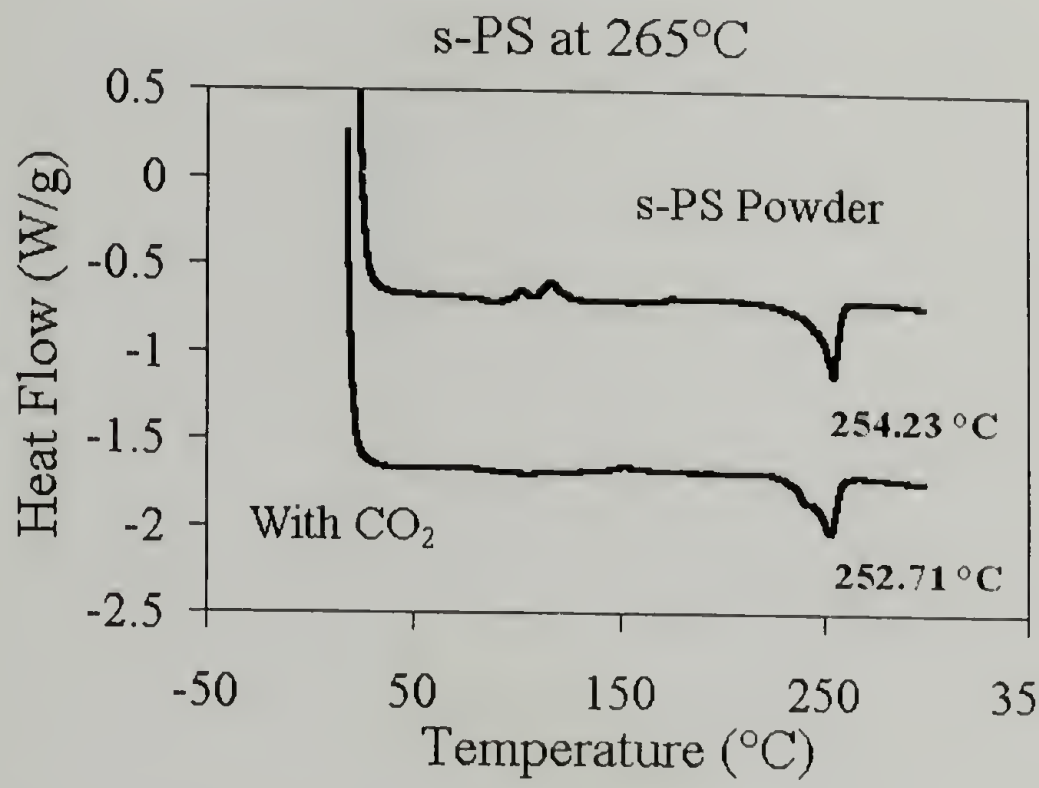

Figure 4.18. Typical thermal behavior of s-PS samples processed in our system using $scCO_2$ at 265°C.

Sample	Run	Tm (°C)	ΔHm (J/g)	Crystallinity (%)
sPS	1	254.23	25.41	47.76
sPS	2	252.71	25.59	48.10

Table 4.5. Thermal behavior of s-PS samples processed in our system using $scCO_2$ at 265°C.

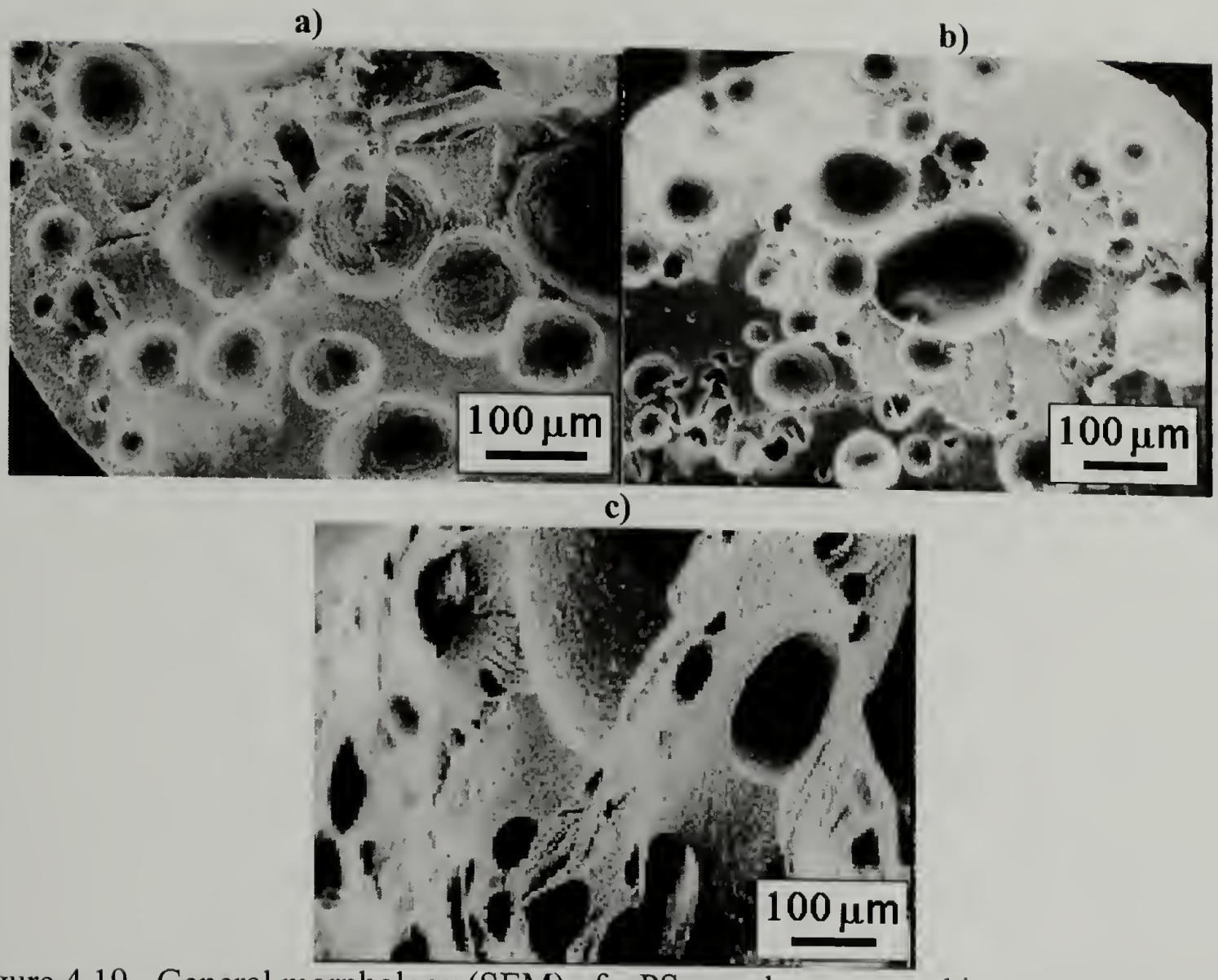

Figure 4.19. General morphology (SEM) of s-PS samples processed in our system using $scCO_2$ at different conditions. a) 275°C, b) 265°C, and c) 255°C.

As in any other systems, the overall morphology of s-PS extrudates can be controlled via the processing conditions, and given the right conditions a well-defined foam structure is observed, showing increases in the cell density at lower temperatures. These results are shown in figure 4.19.

Despite the high melt viscosity of s-PS, a continuous process is obtained with CO_2, suggesting a considerable amount of plasticization. This plasticizing properties of $scCO_2$ in s-PS systems has been reported by Handa at al.[40], as shown in figure 4.20, where a systematic depression in the glass transition temperature is observed in s-PS samples saturated in CO_2 at various pressures. In this case, however, the processability is limited at temperatures very close to the melting point (255 °C) where the high melt viscosity

prohibits a continuous processing. Again, this observation suggests that the plasticization process in this case is not as significant as in the case of PTFE, and that the glass transition depression observed in s-PS due to the presence of CO_2, should be very similar or slightly larger than that observed in the case of FEP.

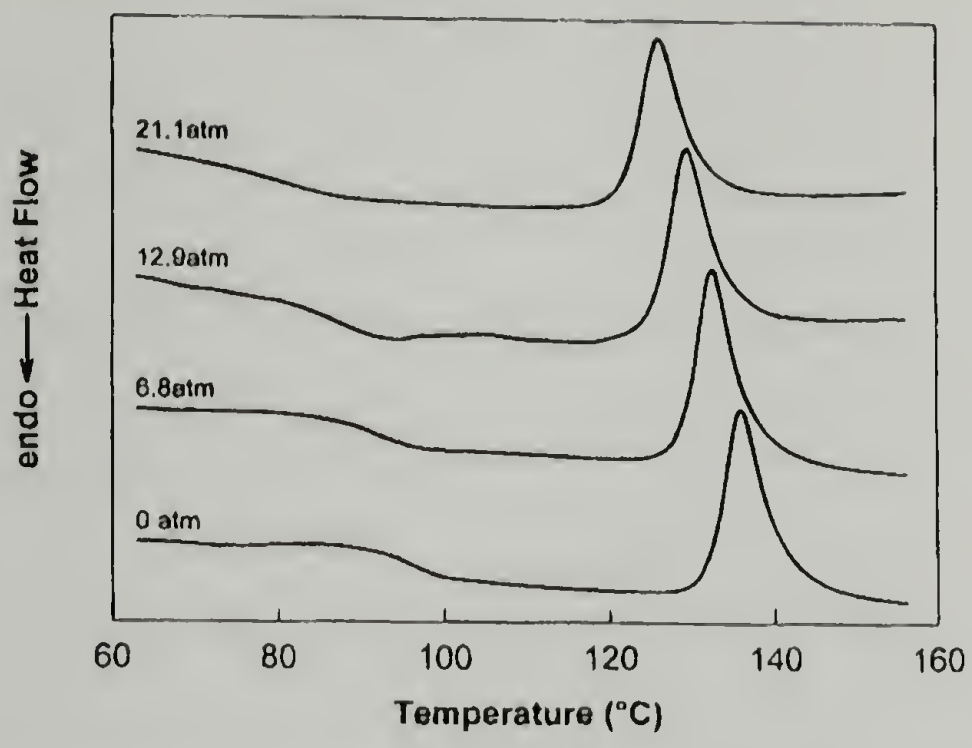

Figure 4.20. Plasticization observed in sPS samples at various CO_2 pressures. Glassy sPS was saturated with CO_2 at 35 °C at the indicated pressure before scanning.[40]

Figure 4.21 shows the predictions to the plasticization process of s-PS by CO_2 using the Chow model. In this particular case, it is important to point out that since specific details on tacticity or crystallinity are not prescribed in the model, and since no available data is found in the literature regarding the heat capacity change (ΔC_{pp}) or equilibrium mass uptake of CO_2 for s-PS, the parameters employed in this figure correspond to those of amorphous polystyrene.[40,46] The predictions, however, correlate very well with the experimental observations, showing a large plasticizing region limited by the equilibrium mass uptake of CO_2 (11.8 %). In this case, the value of the glass transition depression ratio Tg/Tg_0 is 0.7641, which corresponds to a smaller change than that of PTFE. These results indicate that even though the mass uptake of CO_2 is very large in this case, the

plasticization process of s-PS by CO_2, as judged by the ratio Tg/Tg_0 is larger than that observed in FEP but smaller than in the case of PTFE, which correlates exactly with the observed processability of these systems.

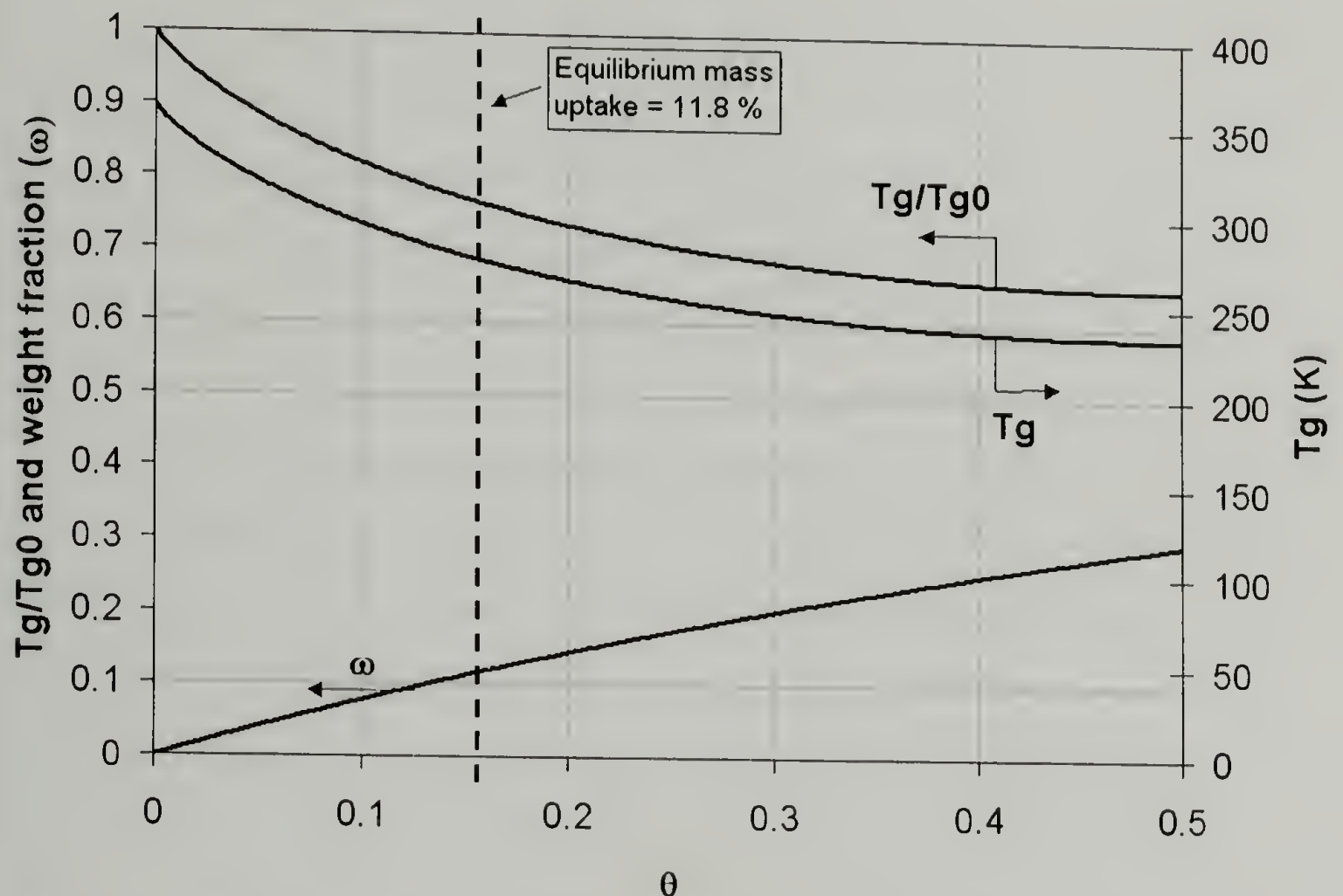

Figure 4.21. Glass transition depression (Tg/Tg_0) for the polystyrene-CO_2 system as predicted by the Chow model. The dashed line indicates the equilibrium mass uptake of CO_2 for the case of polystyrene (11.8%).

4.3.3 Plasticization and the effect of CO_2 on the melting behavior of semicrystalline polymers

As described before, the Chow model appears to be appropriate to describe the plasticization process of a polymer in the presence of CO_2. The predictions of the model for the polymers used in this study are shown in figure 4.22. The presence of CO_2 promotes a depression in the glass transition that is dependent of the intrinsic properties of the system. The rate of depression is very large for the case of PTFE, displaying a very

pronounced slope, while the smallest rate of depression is observed in s-PS. In contrast, the largest equilibrium mass uptake of CO_2 is observed in s-PS (11.8 %) while the smallest value corresponds to PTFE. In this regard, it appears that the overall plasticization process is dictated by a combination of the rate of depression in the glass transition and the equilibrium mass uptake of CO_2 for a given polymer.

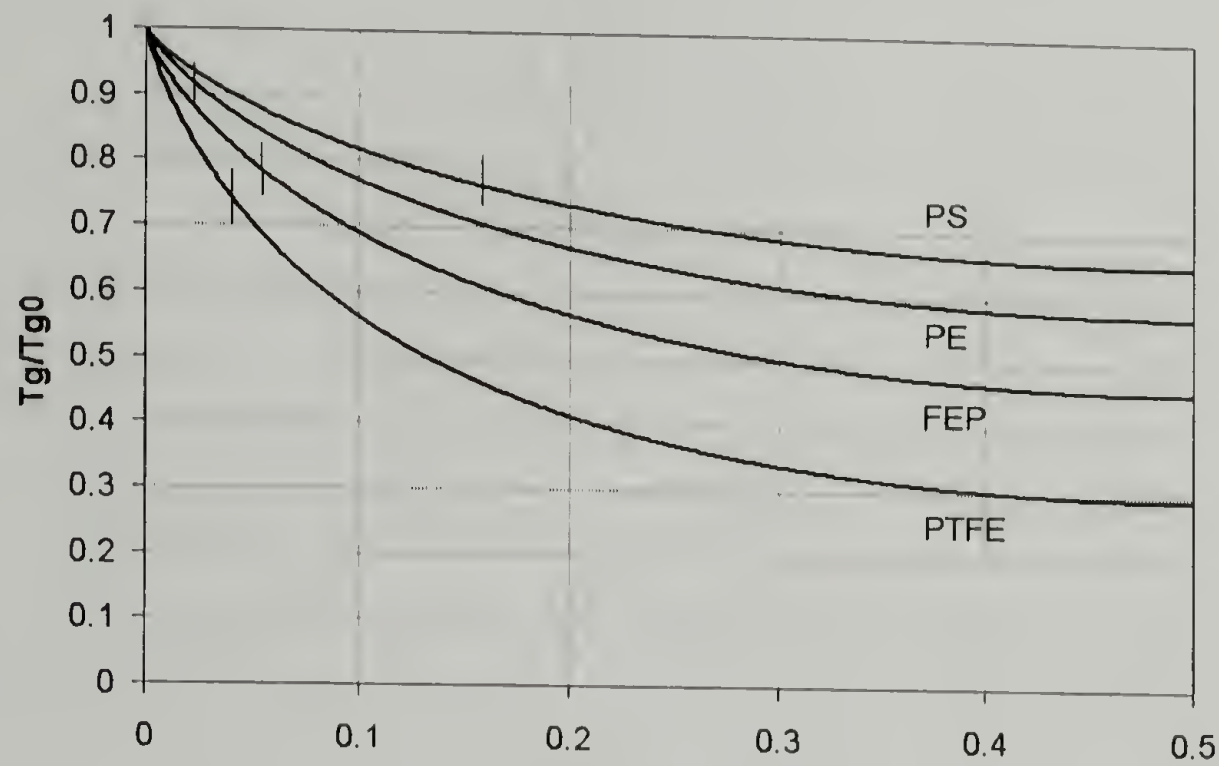

Figure 4.22. Chow model predictions of the glass transition depression (Tg/Tg_0) for the polymers used in this study. The marks indicate the equilibrium mass uptake of CO_2 for the corresponding polymer.

As proposed in the Chow model, the plasticization process can be quantified by the ratio Tg/Tg_0, which appears to correlate well with the experimental observations. As presented in figure 4.23, the processability of these systems is directly related to the magnitude of Tg/Tg_0, suggesting that the amount of CO_2 plasticization in PTFE is larger than that observed in any of the systems studied here, thus its increased processability at lower temperatures.

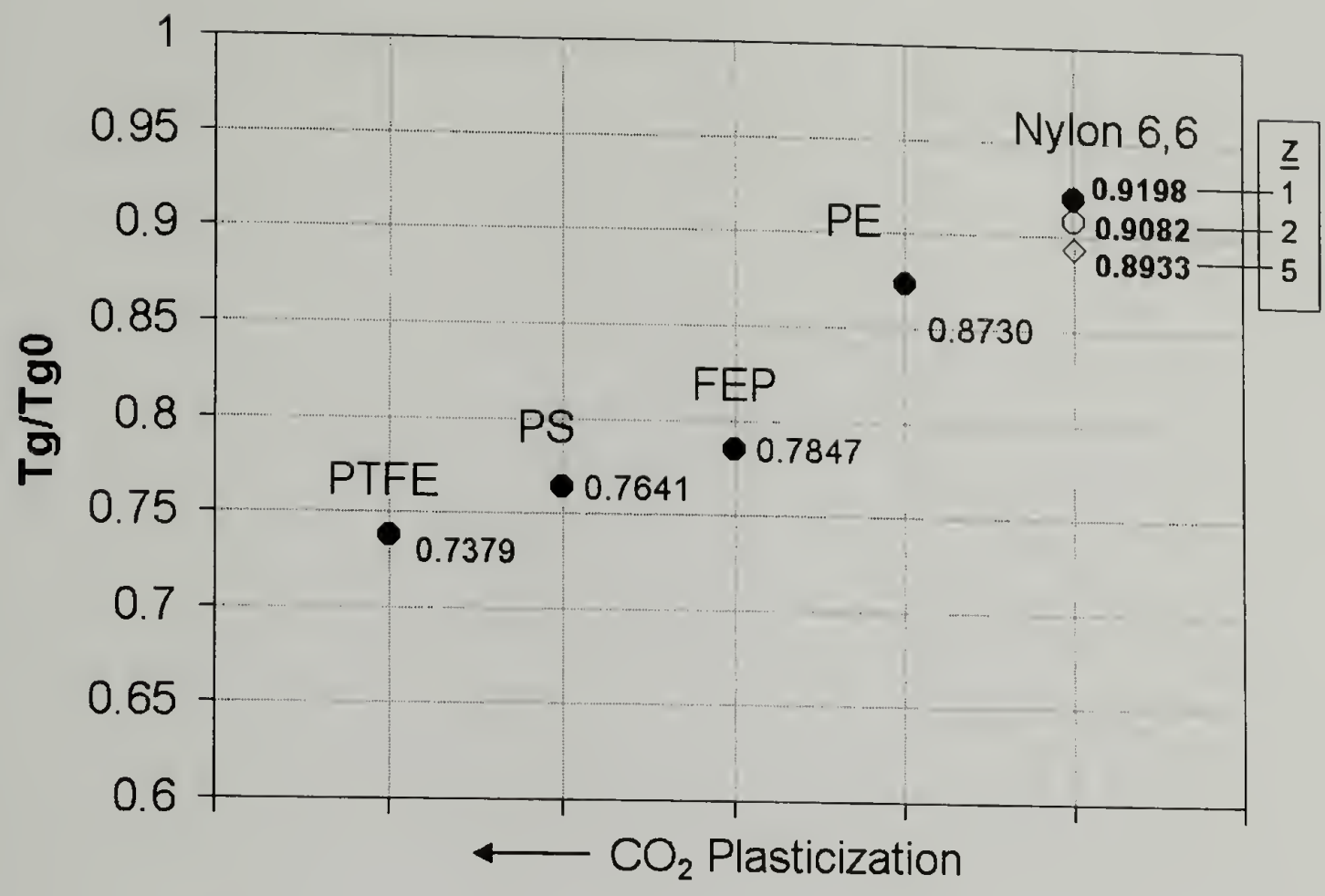

Figure 4.23. Plasticization process of CO_2 for various polymers as estimated by the Chow model. As shown, the experimental observations suggest a direct relation between the glass transition depression (Tg/Tg_0) and the processability of these systems in CO_2.

While the plasticizating effect of CO_2 in a variety of polymers has been reported extensively in the literature, the effects of CO_2 on the crystallization and melting temperatures have only been analyzed for a few systems.[40-41] In general, the behavior of the crystallization temperature (Tc) is consistent with that observed for Tg, showing a linear decrease with an increase of CO_2 pressure. However, as mentioned in Chapter 1, for the specific case of s-PS, Handa and Zhang[41] have shown that CO_2 promotes crystallization of glassy s-PS into its various crystalline forms (α and β) as well as to induce crystal-crystal transformations between them at a temperature below the melting temperature of the α form. These transitions could only be understood if the α crystals undergo melting at a depressed temperature before transforming into the β form. Crystal-

crystal transformations have been also reported by us[24], in high-modulus UHMWPE fibers when deformed in supercritical CO_2.

Using high-pressure DSC techniques Handa and Zhang[41] have shown in fact that CO_2 has a direct effect on the melting behavior of semicrystalline polymers. This is shown in figure 4.24, where a significant depression in the melting point is evident in the presence of dissolved CO_2. The melting temperature depression is dependent on the solubility of the gas, showing no change in Tm when CO_2 was replaced with N_2. A rapid decrease in Tm is observed initially by increasing the pressure of CO_2 until the hydrostatic contribution of CO_2 dominates, making the change in Tm smaller at elevated temperatures. The same behavior is observed in PET samples,[40] as presented in figure 4.25, suggesting that the depression in melting temperature is dictated by both the polymer-gas interactions and the intrinsic crystal characteristics.

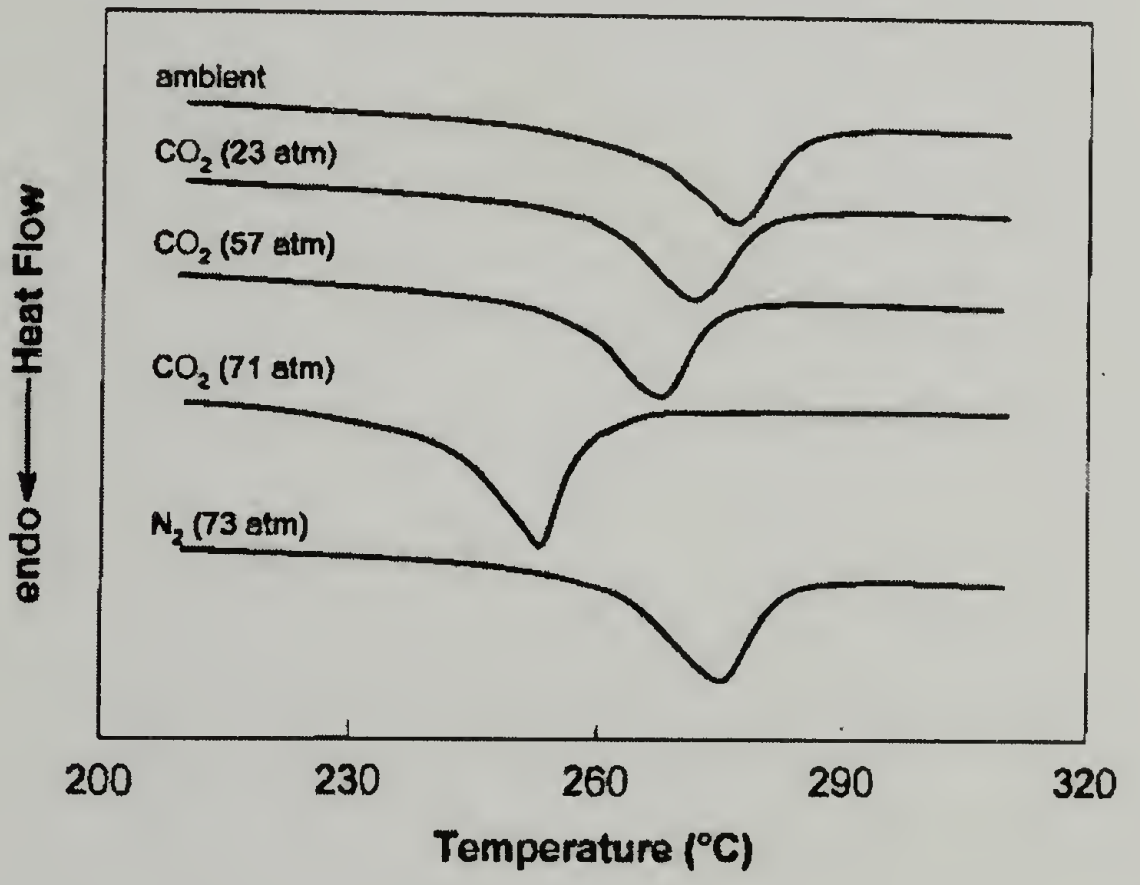

Figure 4.24. DSC scans under various gas pressures on sPS crystallized from the melt state.[41]

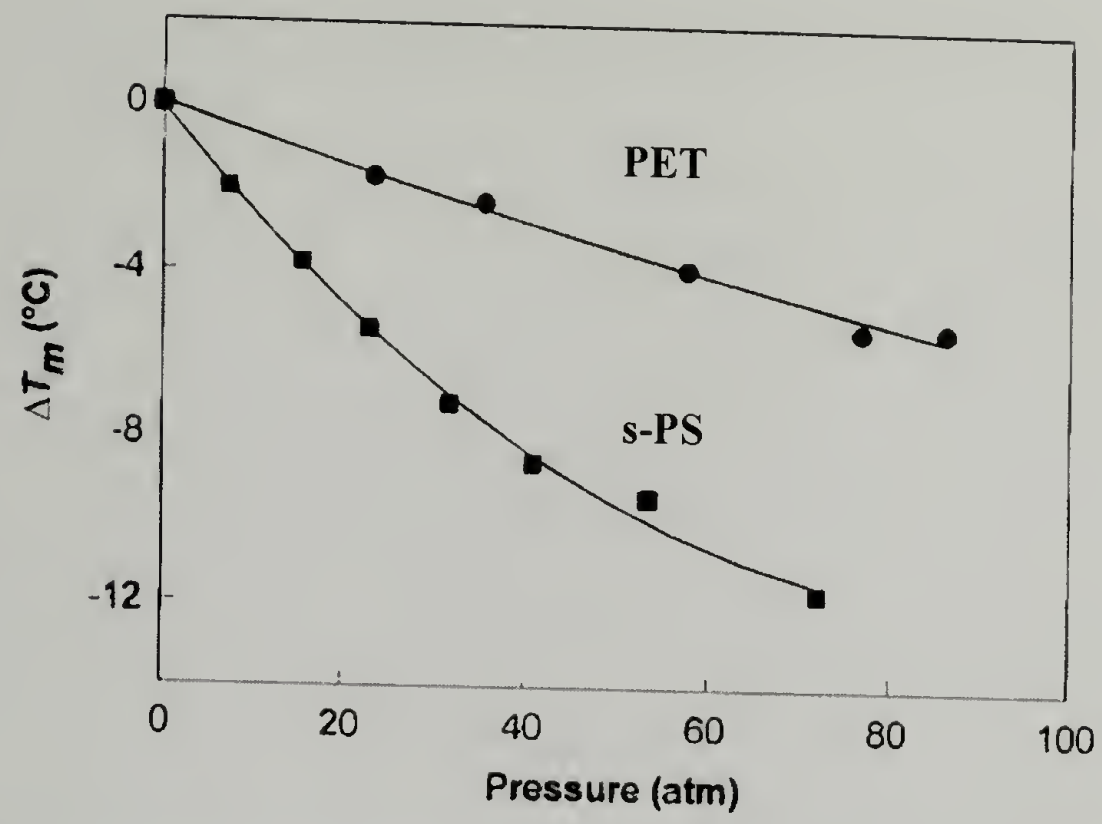

Figure 4.25. Tm depression in melt-crystallized sPS and PET as a function of CO_2 pressure.[40]

The decrease in Tm has been related to an increase in the specific surface free energy δe caused by the dissolved CO_2. Using the Thomson-Gibbs equation, the change in melting temperature is given by

$$Tm = Tm^0\left(1 - \frac{2\delta e}{l\Delta h}\right) \qquad (4)$$

where Tm^0 is the melting point of an infinitely large crystal, l is the lamellar thickness and Δh is the heat of fusion per unit volume. Since Tm, l and Δh are generally constant, the change in Tm is attributed to δe.

This behavior is expected to occur in other polymer-gas systems also whenever the gas sorption and the plasticization effect are pronounced. As discussed before, the plasticization by CO_2 is significant for the systems studied here (PTFE, FEP and s-PS), so that a direct effect on the melting behavior of these systems is expected to occur. This effect might certainly help to explain the enhanced processability in systems such as

PTFE where a continuous process is obtained even at temperatures below the typical melting point.

Furthermore, as shown in figure 4.26, when PTFE is saturated in CO_2 below its melting point at relatively small pressures for a certain amount of time, the resulting material displays a decreased melting point, suggesting in fact that at these conditions there is a direct effect of CO_2 on the melting behavior of PTFE. In this case, the well-known affinity to CO_2 contributes to the gas sorption, displaying a considerable plasticization effect, which as suggested before, might be accompanied with a significant depression in the melting temperature. As mentioned before, the plasticization process appears to be smaller in the case of FEP, so that a lower effect on the melting behavior is expected in this case, which correlates well with the lower processability of this system as compared to PTFE and s-PS.

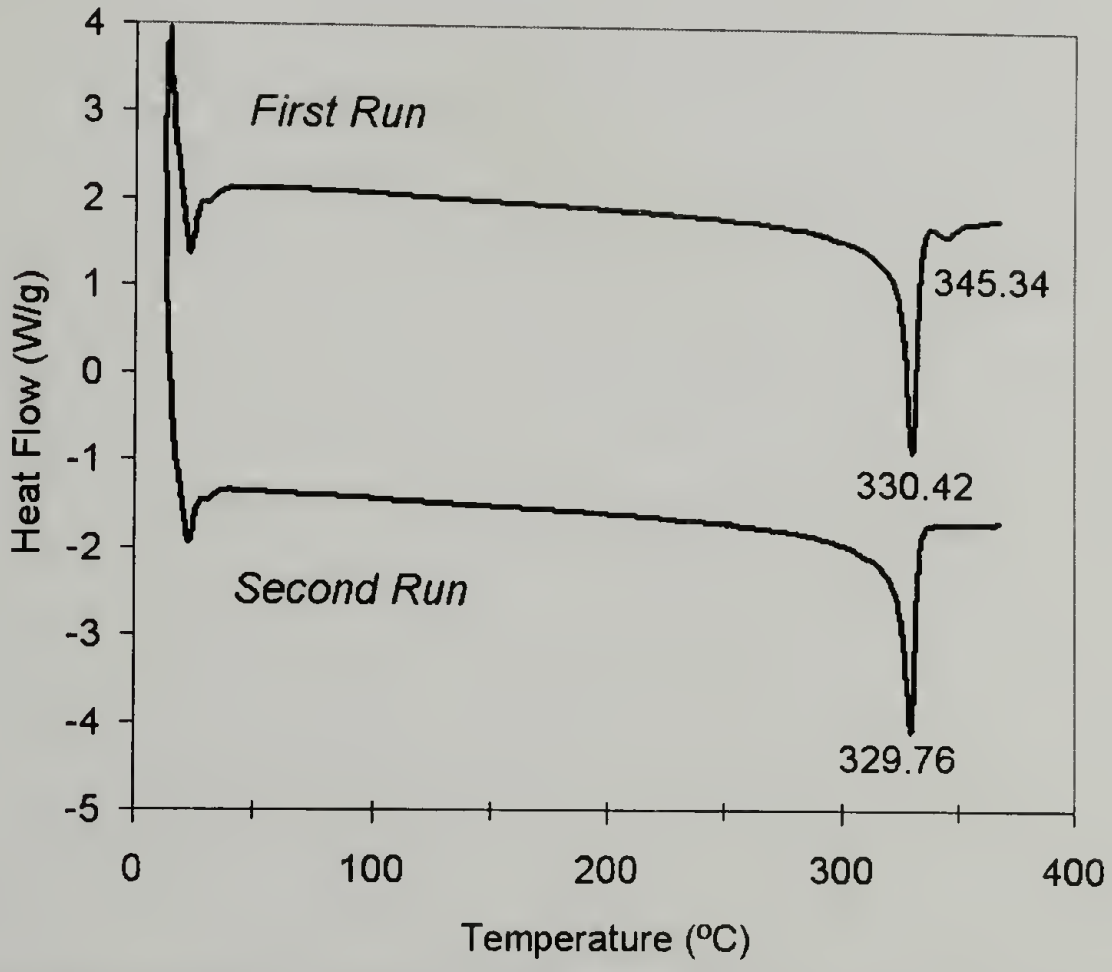

Figure 4.26. Thermal behavior of PTFE sample saturated in CO_2 at 330 °C for 6.5 hrs at relatively small pressures (5.51 MPa). Shown are the first and second traces obtained in the DSC.

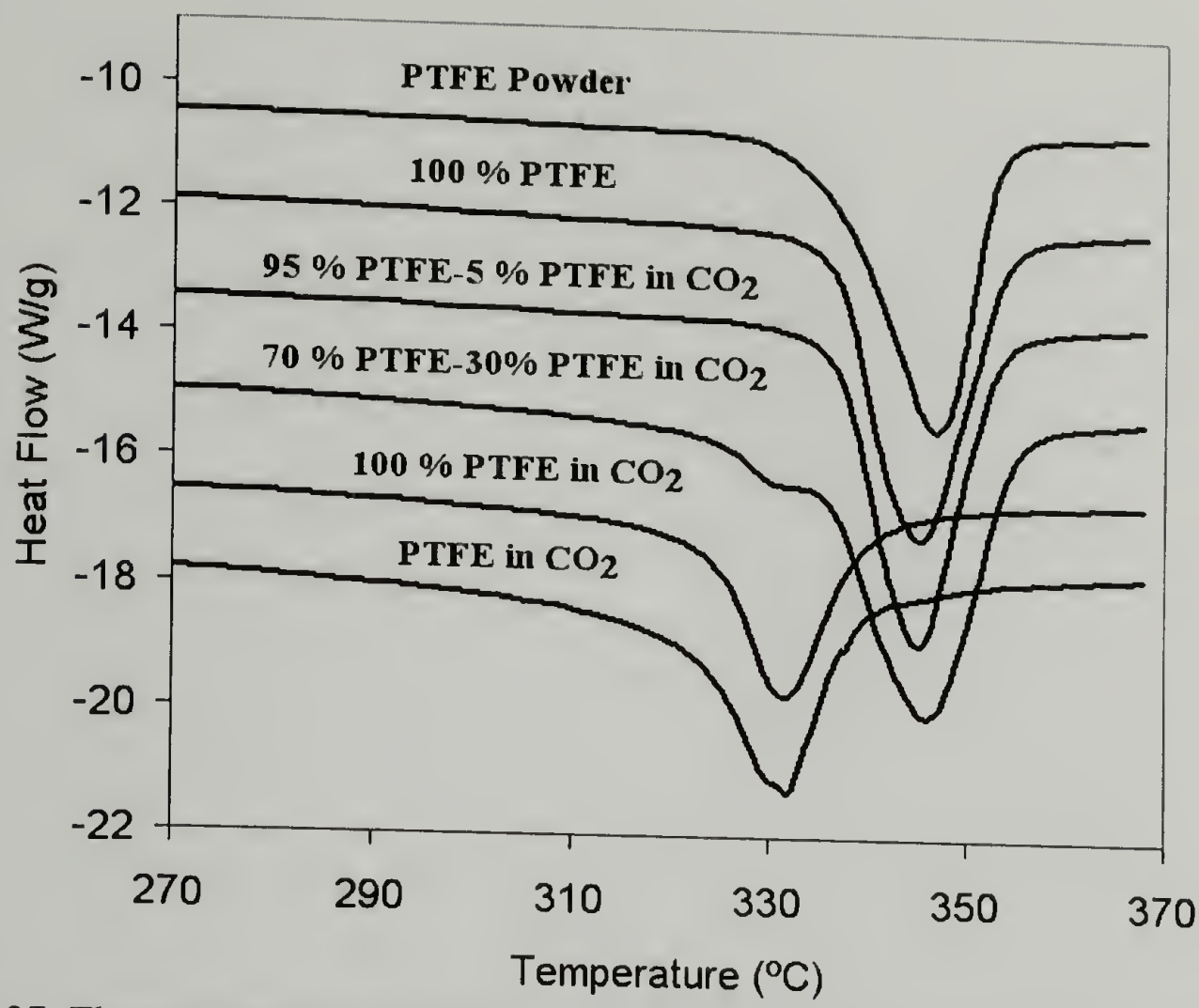

Figure 4.27. Thermal behavior of PTFE samples prepared using PTFE powder and the PTFE extrudate obtained after extrusion in CO_2. For comparison, the DSC traces of the pure PTFE powder and the PTFE extrudate in CO_2 are included.

The clear difference in the thermal behavior and more specifically in the melting behavior between PTFE samples processed with and without CO_2, can be easily observed in figure 4.27. Films containing various amounts of material processed in CO_2 are prepared, and as shown in this figure, lower melting points are systematically obtained when the concentration of material processed in CO_2 is increased.

4.4 Conclusions

In this chapter, CO_2-assisted polymer processing is presented as an effective alternative to process high melt viscosity polymers. This alternative route combines both the plasticization effect and the hydrostatic contribution, brought about by the presence of CO_2, enhancing in a significant way the processability of a polymer-CO_2 system. Despite their high melt viscosity, high molecular weight and inherent physical properties of the systems analyzed here (s-PS, FEP and PTFE), a continuous process is obtained in CO_2 using a modified processing system. Several factors appear to have a direct effect on the final morphology of a polymer, however, the diffusion rate of CO_2 in the melt appears to dominate cell nucleation by controlling the amount of gas dissolved, so that foaming is favored by a saturation time in CO_2 prior to extrusion.

The increased processability is directly related to the plasticization process of the polymer due to the presence of CO_2 and to the direct effect that dissolved CO_2 might have on the melting temperature through an increase in the specific surface free energy of the system. The amount of plasticization has been quantified using the model proposed by Chow, suggesting that the improved processability of high melt viscosity materials in the presence of CO_2 can be related to the glass transition depression ratio (Tg/Tg_0). The plasticization process appears to be dependent of the intrinsic properties of the polymer and its interaction with CO_2, being predominantly large for the case of PTFE.

CHAPTER 5

POLYMER-CLAY NANOCOMPOSITES PREPARED IN SUPERCRITICAL CARBON DIOXIDE

In this chapter, an alternative route to prepare polymer-clay nanocomposites using supercritical carbon dioxide ($scCO_2$) is described. The presence of clay nanoparticles significantly influences the morphology, foaming process and crystallization of a polymer when processed in $scCO_2$. Polymer nanocomposites are successfully produced in the presence of $scCO_2$ even when favorable interactions between the polymer and the clay are not present. The effect of $scCO_2$ on the intercalation process is analyzed for a variety of polymer systems both with modified and unmodified clays. By controlling the hydrophilicity of the polymer and clay systems, specific understanding of the effect of $scCO_2$ on the structure and morphology of the nanocomposites is obtained. Experimental results show significant increases in the clays d-spacings for $scCO_2$-treated samples. This behavior is consistent regardless of the nature of the polymer, showing significant amounts of intercalation even in purely hydrophobic polymers.

5.1 Introduction

Nanotechnology has recently gained a lot of attention leading the way to better and unique materials for almost any type of application.[52-53,58,64] Current alternatives to improve the mechanical and physical properties of existing engineering polymers include the use of nanotechnology to incorporate diverse inorganic materials into engineering polymer systems producing polymer nanocomposites that in many cases provide an alternative for better mechanical and physical properties. Although most of the current

developments in polymer-clay nanocomposites are focused in obtaining fully exfoliated structures, recent investigations[62] suggest, however, that since most of the material improvements in nanocomposites come from interactions on the molecular scale and since toughening occurs over a specific length scale, effective toughening mechanisms require a specific filler size that may not be achieved by individual nanoscale particles.[63] As a consequence, it is suggested that the extremely reduced scale of a fully exfoliated structure may not be favorable for toughening. In contrast, an intercalated system where polymer has entered into the galleries between silicates but has not fully delaminated them, may promote considerable interaction between silicate layers thereby achieving the length scale necessary for toughening.

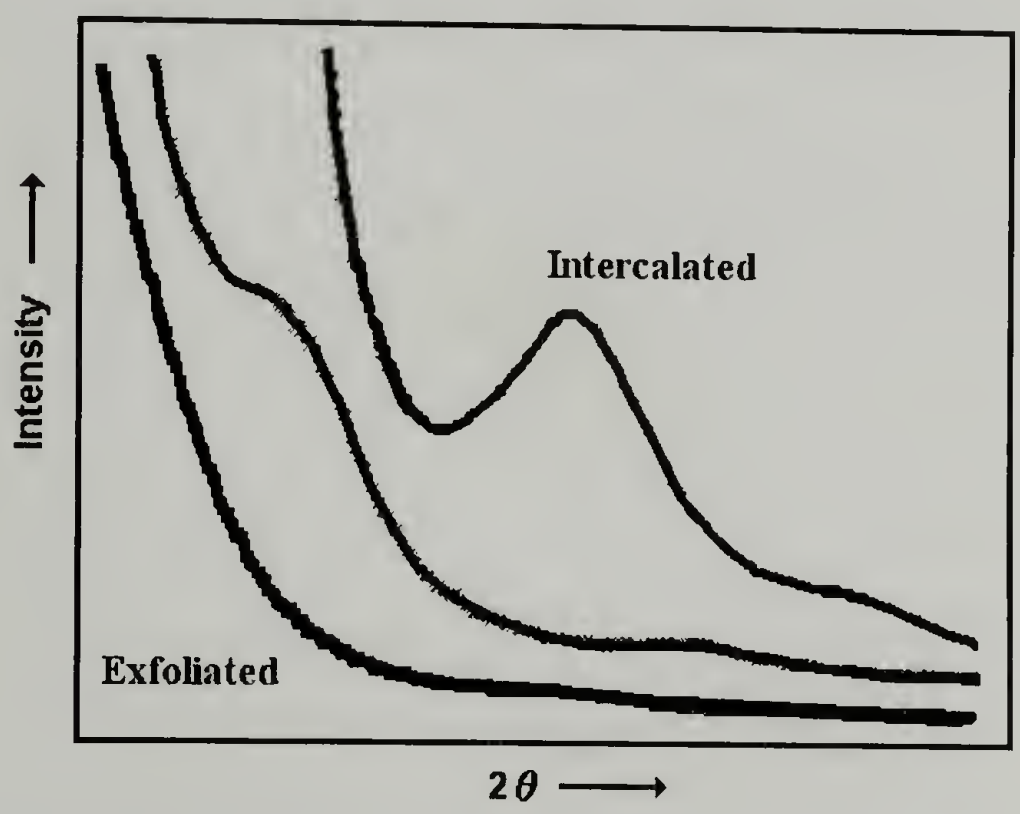

Figure 5.1. General WAXS pattern for intercalated and exfoliated polymer-clay nanocomposites.

As depicted in figure 5.1, WAXS is often used to discern between the structure of a nanocomposite. In an exfoliated nanocomposite the silicates are homogenously dispersed throughout the polymer matrix with little or no interaction between individual platelets, consequently the diffraction pattern show no particular reflection at low angles. In

contrast, the intercalated morphology is characterized by a distinct peak in the x-ray diffraction pattern, signifying the presence of a lamellar structure and retention of order within the silicate domains. This morphology is created after one or two polymer chains have entered into the gallery spacing, increasing the d-spacing.

In order to overcome the enormous entropic barrier associated to polymer intercalation, different approaches can be followed to produce intercalated systems. In this thesis, an alternative route to prepare polymer nanocomposites introducing $scCO_2$ in a conventional melt processing system is presented.[76,77,78] As shown in figure 5.2, a variety of routes are followed to access polymer-clay nanocomposites with either intercalated or exfoliated structures. This chapter focuses in describing the specific contribution of $scCO_2$ to the melt intercalation process of a polymer into clay systems without the use of compatibilizers to enhance the interactions between the polymer and the clay employed. Results suggest that the presence of $scCO_2$ promotes significant changes in the properties of a system that may enhance the ease of polymer intercalation when layered nanosilicates are introduced as nanoscopic filler materials. A specific study of the effect of $scCO_2$ on the melt intercalation process as well as on the final structure and morphology of polymer-clay nanocomposites is obtained by tuning the hydrophilicity of the polymer and clay systems. Intercalated polymer nanocomposites are successfully produced with $scCO_2$, even when favorable interactions between the polymer and the clay are not present. This behavior is consistent regardless of the nature of the polymer, showing significant amounts of intercalation even in purely hydrophobic polymers.

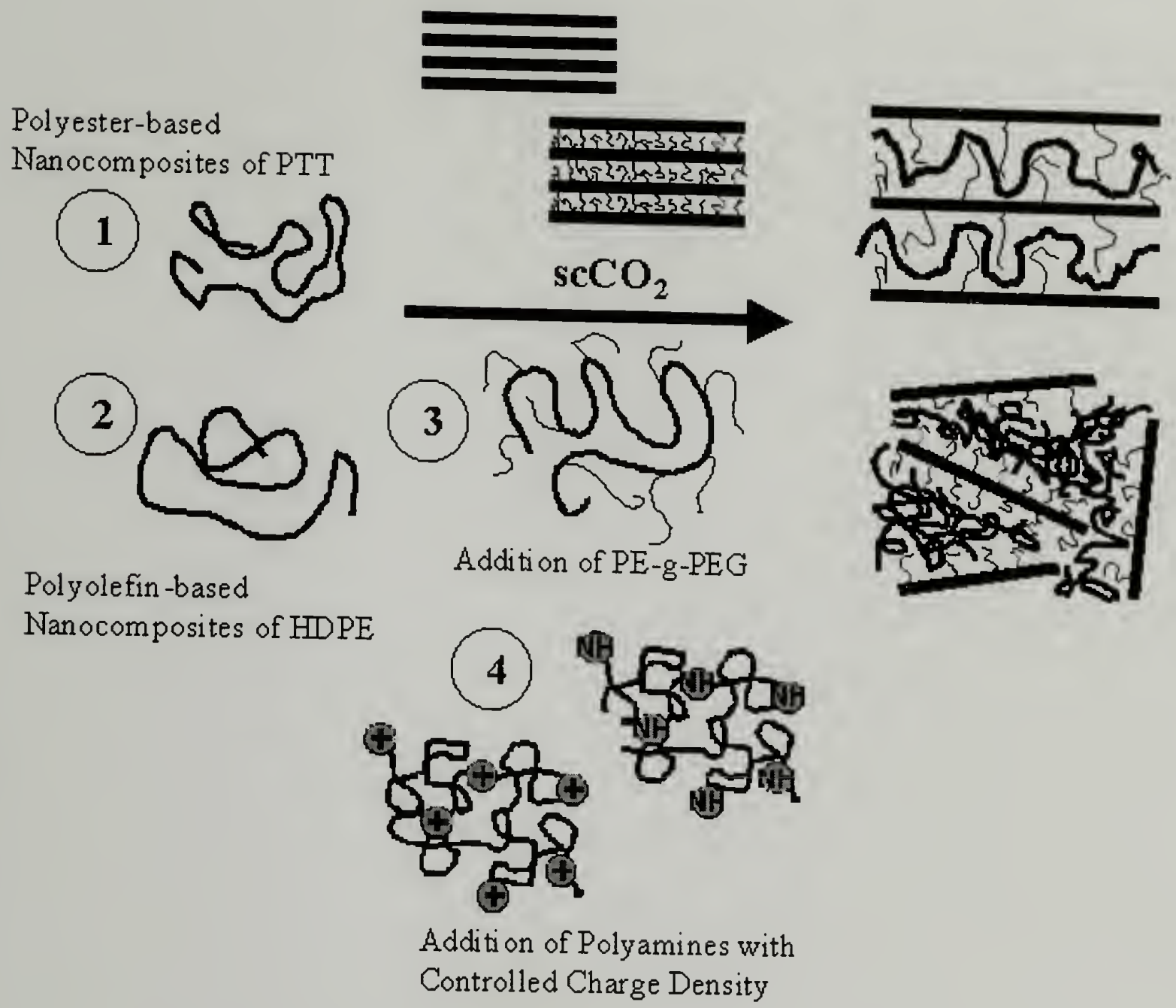

Figure 5.2. Different routes proposed in this study to produce polymer-clay nanocomposites.

5.2 Experimental

Materials. As shown in table 5.1, a variety of clay systems, particularly from the montmorillonite group, are commercially available. In this study, two specific clay systems are used : unmodified montmorillonite (MNa+) and a surface modified montmorillonite (M15A), both obtained from Southern Clay Products, Inc. The modified clay (M15A) is a surface modified montmorillonite from a cation exchange reaction wherein sodium from natural montmorillonite is replaced by a long alkylammonium salt. Both modified and unmodified clays are kept at 50°C under vacuum. High-density

polyethylene (HDPE) resin was obtained from The Dow Chemical Company in the form of pellets and was used as received. Poly(trimethylene terephtalate) (PTT) pellets were obtained from Shell Chemical Company and are dried at 50°C for at least 24 hours before processing.

Clay	Modifier	Structure of modifier	D_{001} spacing (nm)	Relative Hydrophobicity
M15A	**2M2HT**	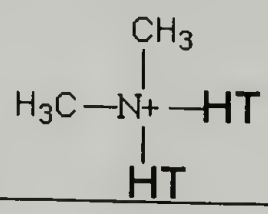	**3.15**	**Most Hydrophobic**
M20A	2M2HT	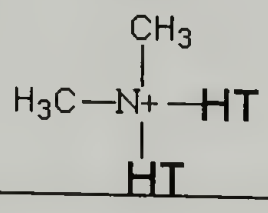	2.42	
M93A	M2HT	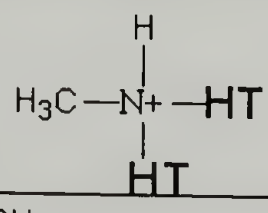	2.36	
M25A	2MHTL8	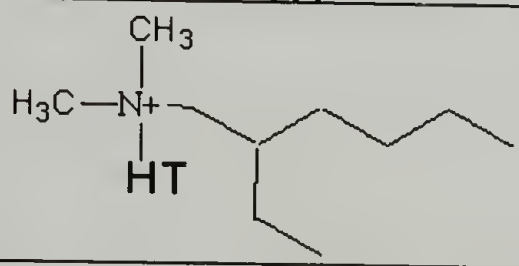	1.86	
M10A	2MBHT	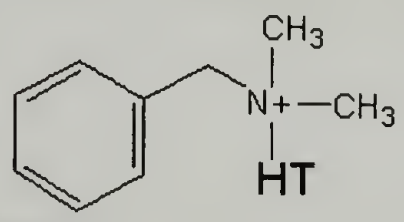	1.92	
M30B	MT2EtOH	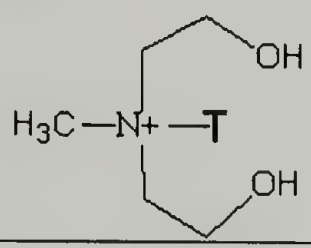	1.85	
MNa+	**None**	**Na+**	**1.17**	**Most Hydrophilic**

Table 5.1. Commercially available montmorillonite clay systems. Marked in bold are the systems used in this study.

Extrusion Experiments. The modified processing system described in Chapter 3 is employed to process a variety of polymers with high-pressure CO_2 in the presence of clay nanoparticles.[51] As mentioned before, the extruder has been modified in order to allow for the high pressures promoted by the injection of $scCO_2$, having a new feed section, which includes a modified hopper that allows a specific amount of polymer to interact with $scCO_2$ before processing.

Thermal Analysis. The thermal behavior of the samples is analyzed using Differential Scanning Calorimetry (DSC). DSC experiments are done using a TA Instruments thermal analyst model 2910 DSC at a heating rate of 10°C/min. The crystallinity of the samples is estimated by the ratio of their melting enthalpy and the corresponding theoretical heat of fusion for a perfect crystal.

Morphology. Wide-angle x-ray scattering (WAXS) experiments are done using a Siemens D500 Diffractometer with an operating voltage of 40 kV and a total current of 30 mA. The overall morphology is investigated using a Field Emission Scanning Electron Microscope (FESEM) model JSM-6320FXV and a Scanning Electron Microscope (SEM) model JEOL-CS-35 with a filament voltage of 20 kV. Samples are cryo-fractured in liquid nitrogen and gold coated prior to the SEM analysis. TEM experiments are conducted in a JEOL-200CX with an accelerating voltage of 200 kV, using cryomicrotomed thin sections (40 nm) of existing samples.

5.3 Results and Discussion

5.3.1 Polyester-based nanocomposites of poly(trimethylene terephthalate) (PTT)

$ScCO_2$-assisted polymer processing is used to prepare polyester-based nanocomposites of poly(trimethylene terephthalate) (PTT). Using our modified system PTT is processed in CO_2 (5.86-10.34 MPa) in the presence of either unmodified (MNa+) or modified (M15A) clay at 210°C.[51,76-78] To understand the specific effect of $scCO_2$ on the overall morphology, thermal behavior and structure of these systems, PTT-clay systems are also prepared by melt pressing.

The melt intercalation of PTT into a clay system is graphically presented in figure 5.3. As in any other case, in order for the polymer to diffuse into the clay galleries to produce an intercalated or exfoliated structure, it has to overcome a very large entropic barrier, related to the confinement of the polymer into the clay structure. In the case of melt intercalation, this is done typically by promoting favorable interactions between the polymer and the groups in the clay.

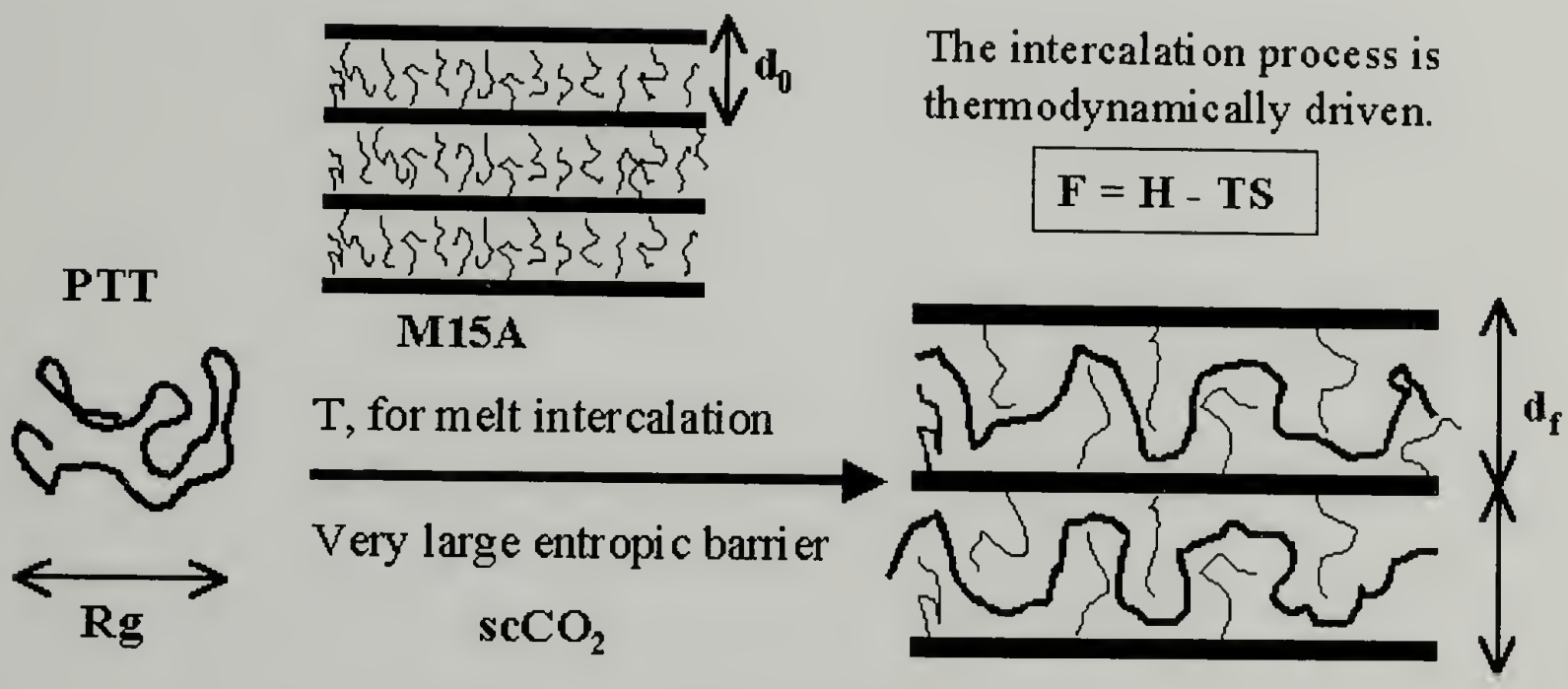

Figure 5.3. Graphical representation of melt-intercalation process of PTT assisted by $scCO_2$ in M15A clay systems.

As shown in figure 5.4, PTT-clay systems produced in CO_2 display a foamed morphology with a typical closed-cell structure where the average cell size is dictated primarily by the clay concentration. The cell density (cells/unit area) is increased at higher clay concentrations and narrow cell size distributions are generally observed, suggesting that the nanoparticles enhance nucleation through an effective heterogeneous process.

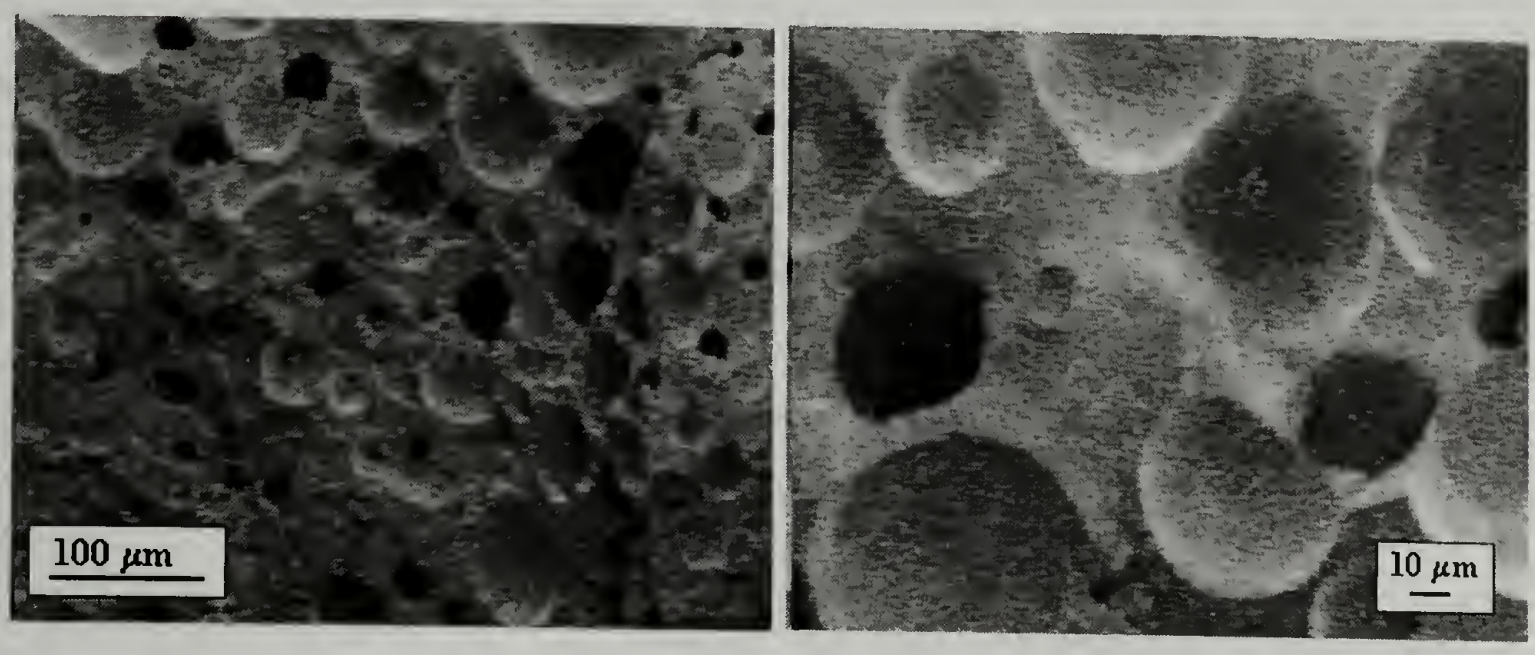

Figure 5.4. General Morphology (SEM) of PTT-M15A systems produced by extrusion with $scCO_2$.

In figures 5.5 and 5.6 the thermal behavior of PTT systems processed at different conditions is presented. For the case of melt-pressed samples, the thermal behavior, shown in figure 5.5, appears to be independent of the concentration of clay, displaying a Tg around 49°C and a melting temperature of 229°C. In contrast, as presented in figure 5.6, a significant amount of orientation is suggested in samples processed in $scCO_2$, displaying an additional crystallization peak after Tg. This transition appears regardless of the presence of clay or its chemical nature and in fact, appears to be attenuated at high clay concentrations. Evidently, in addition to the foaming process, the crystallization of PTT is also altered by the presence of particles that provide available surface for crystallization. Regardless of the clay system employed, the overall crystallinity increases

with the concentration of clay. The increase in crystallinity is considerable (15%), and as shown in this figure appears to be dependent of the clay concentration.

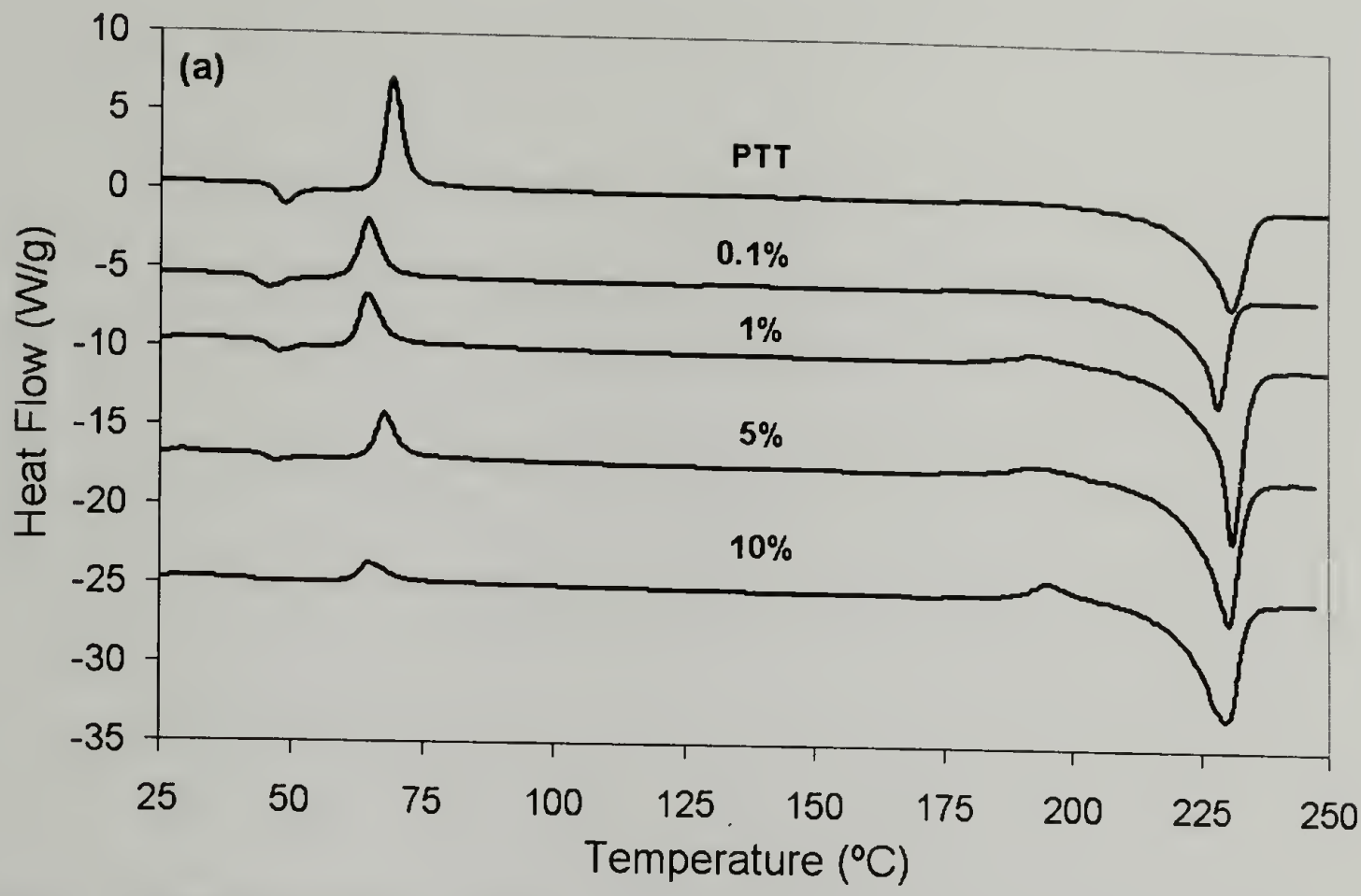

Figure 5.5. Thermal behavior of PTT-MNa+ systems prepared by melt pressing at different concentrations of clay.

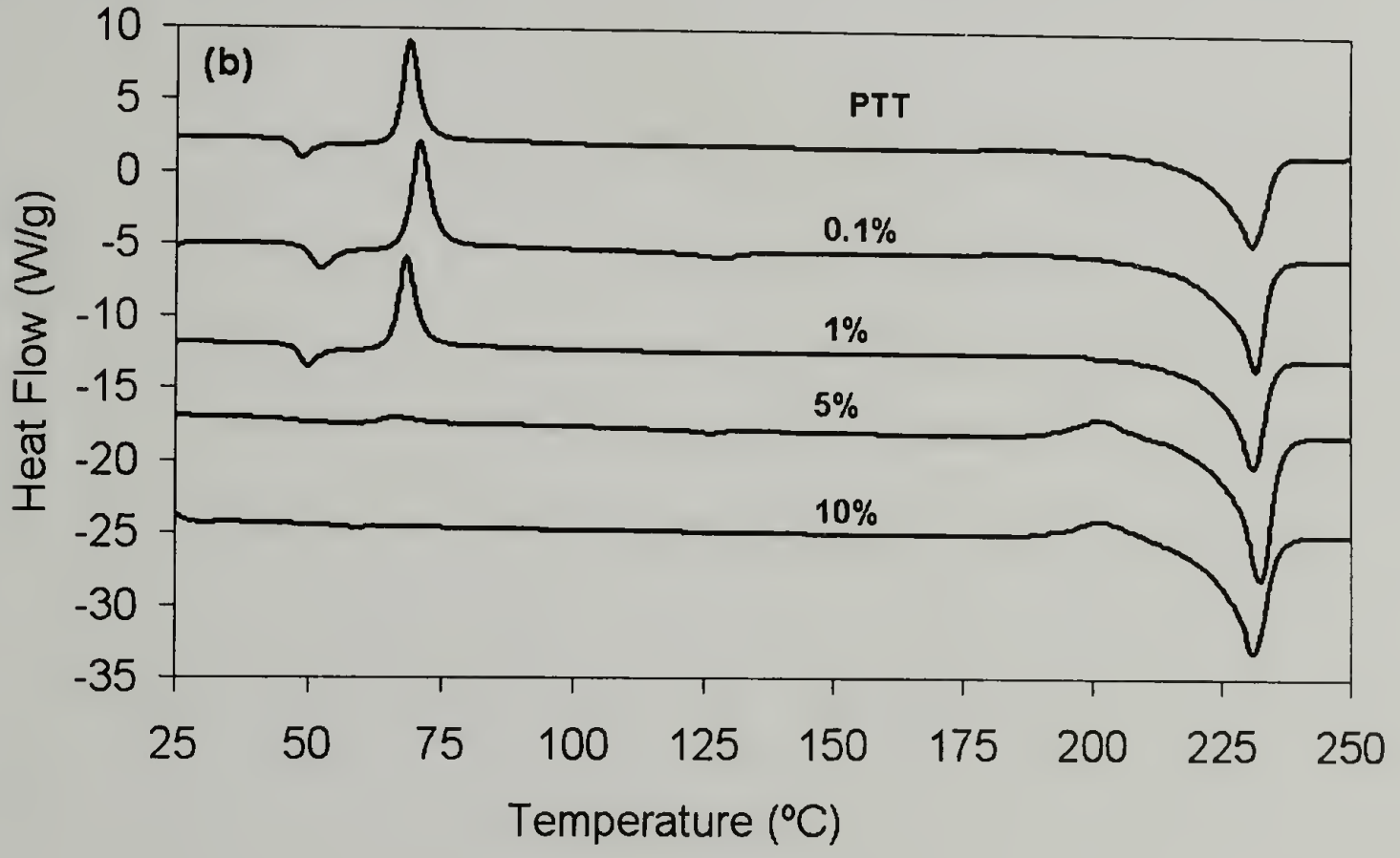

Figure 5.6. Thermal behavior of PTT-MNa+ systems processed at 210 °C in $scCO_2$. Values indicate the weight percent concentration of clay.

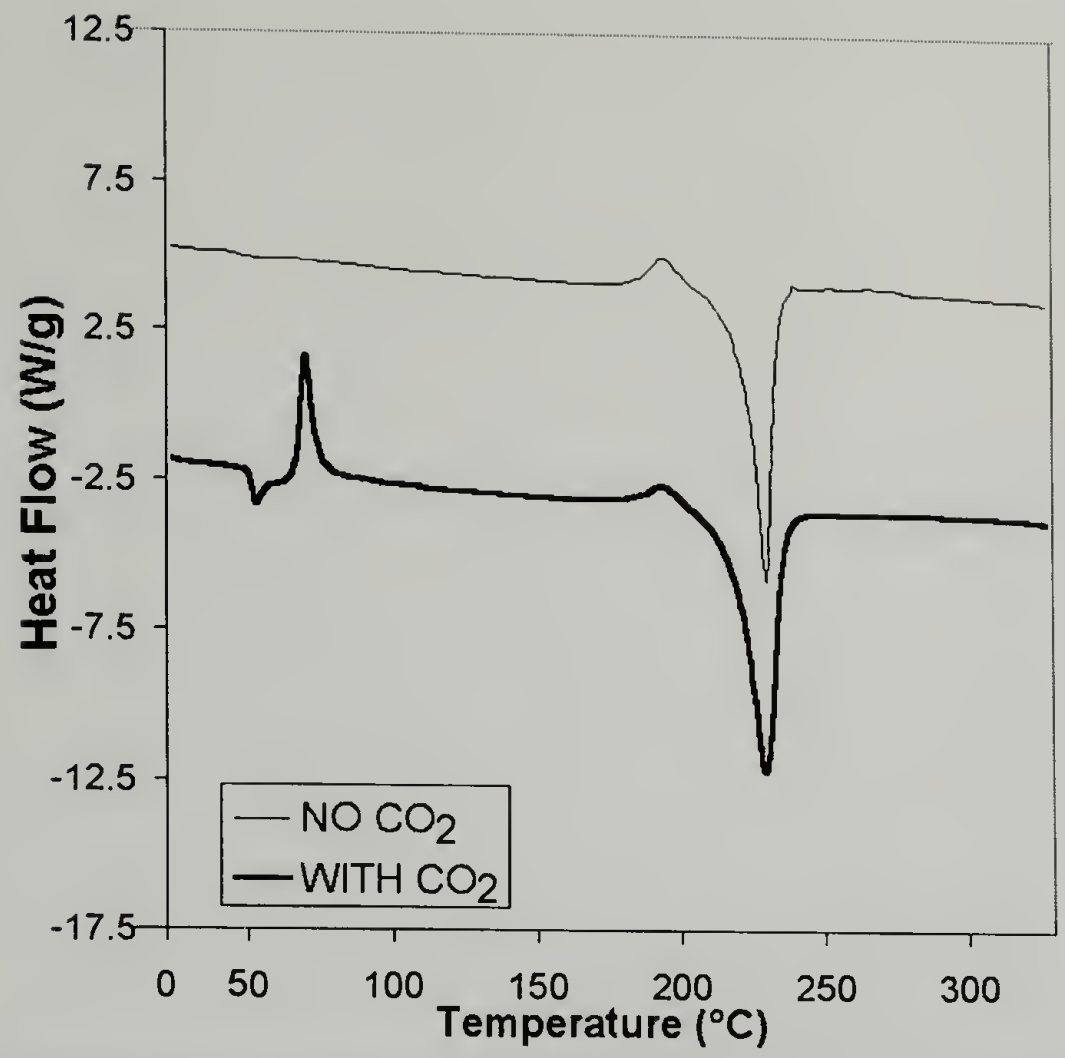

Figure 5.7. Thermal behavior of PTT-M15A systems produced by extrusion with and without $scCO_2$.

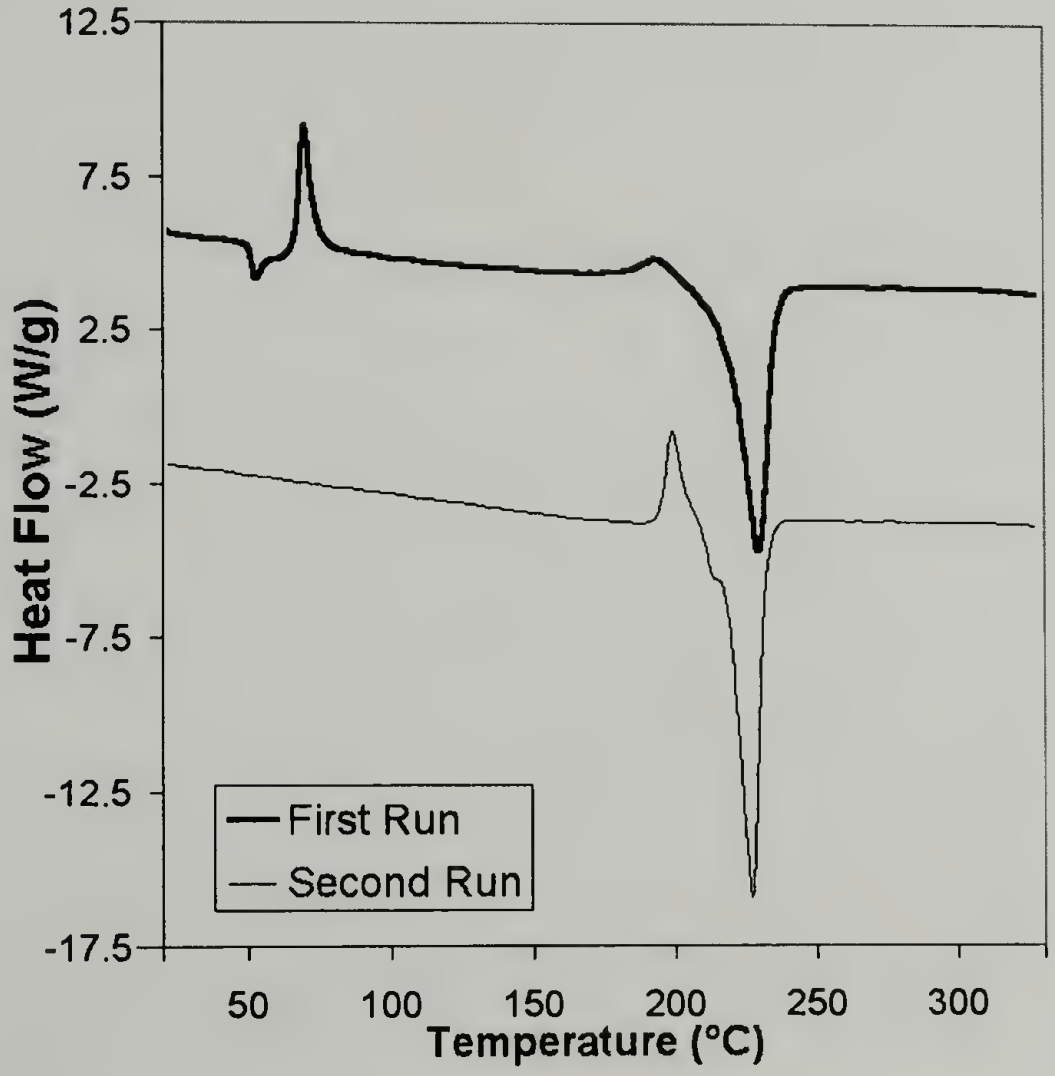

Figure 5.8. Thermal behavior of PTT-M15A systems produced by extrusion with $scCO_2$.

This additional transition is related to the $scCO_2$-processing and as shown in figure 5.7, it is not present in PTT-clay systems produced by conventional extrusion. In fact, as presented in figure 5.8, the molecular orientation induced during the extrusion in $scCO_2$ is completely lost during the melting process. In this regard, it is important to point out that as presented in figure 5.9, if the general foam morphology obtained after $scCO_2$-extrusion is completely removed by post-melt pressing, the thermal behavior of the resulting material will also be affected as presented in figure 5.10. The melt-pressed sample will only display a Tg and the molecular orientation will be lost after the melting process as described before.

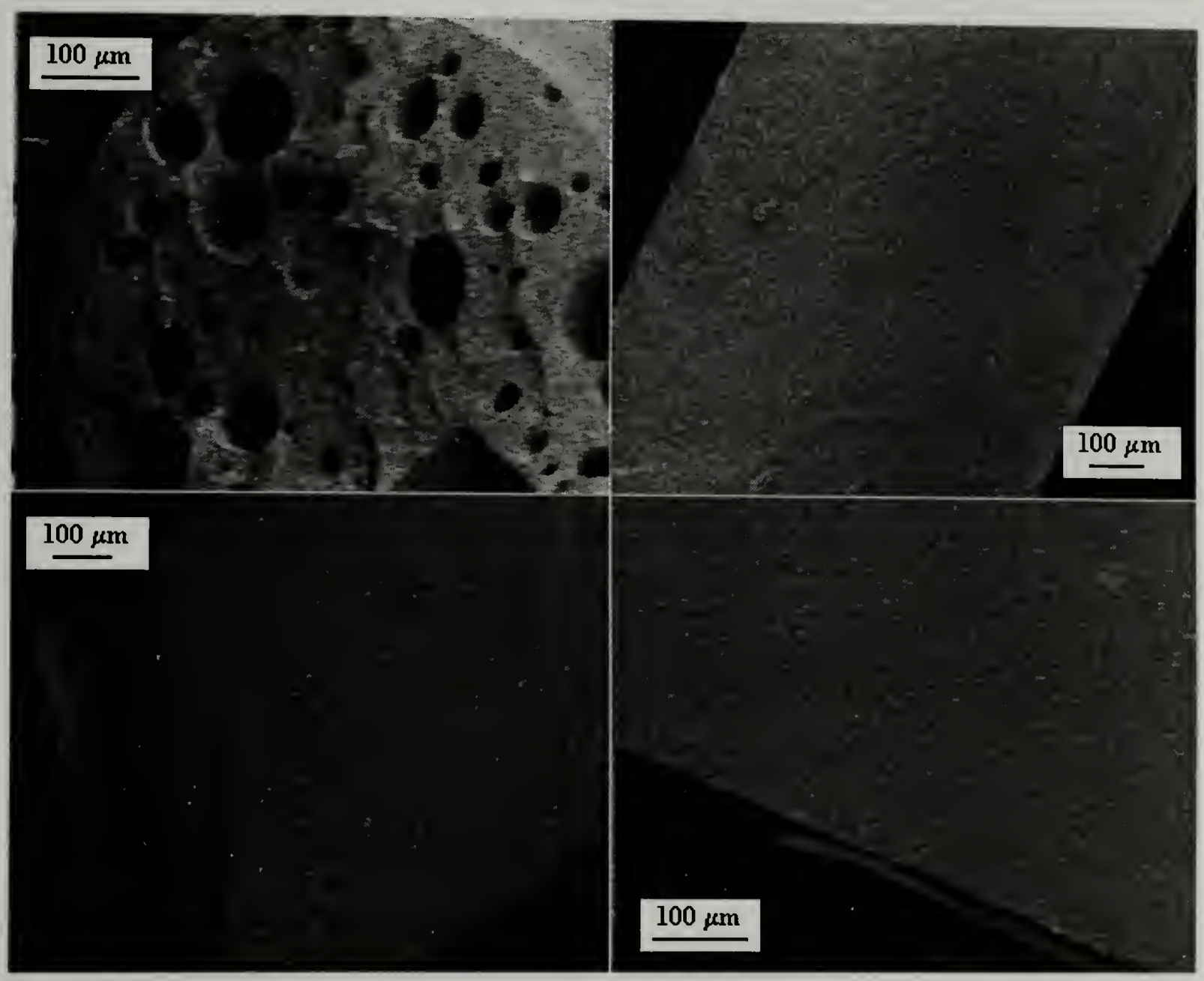

Figure 5.9. General Morphology (SEM) observed in PTT-M15A systems produced by extrusion with $scCO_2$ after post-melt pressing.

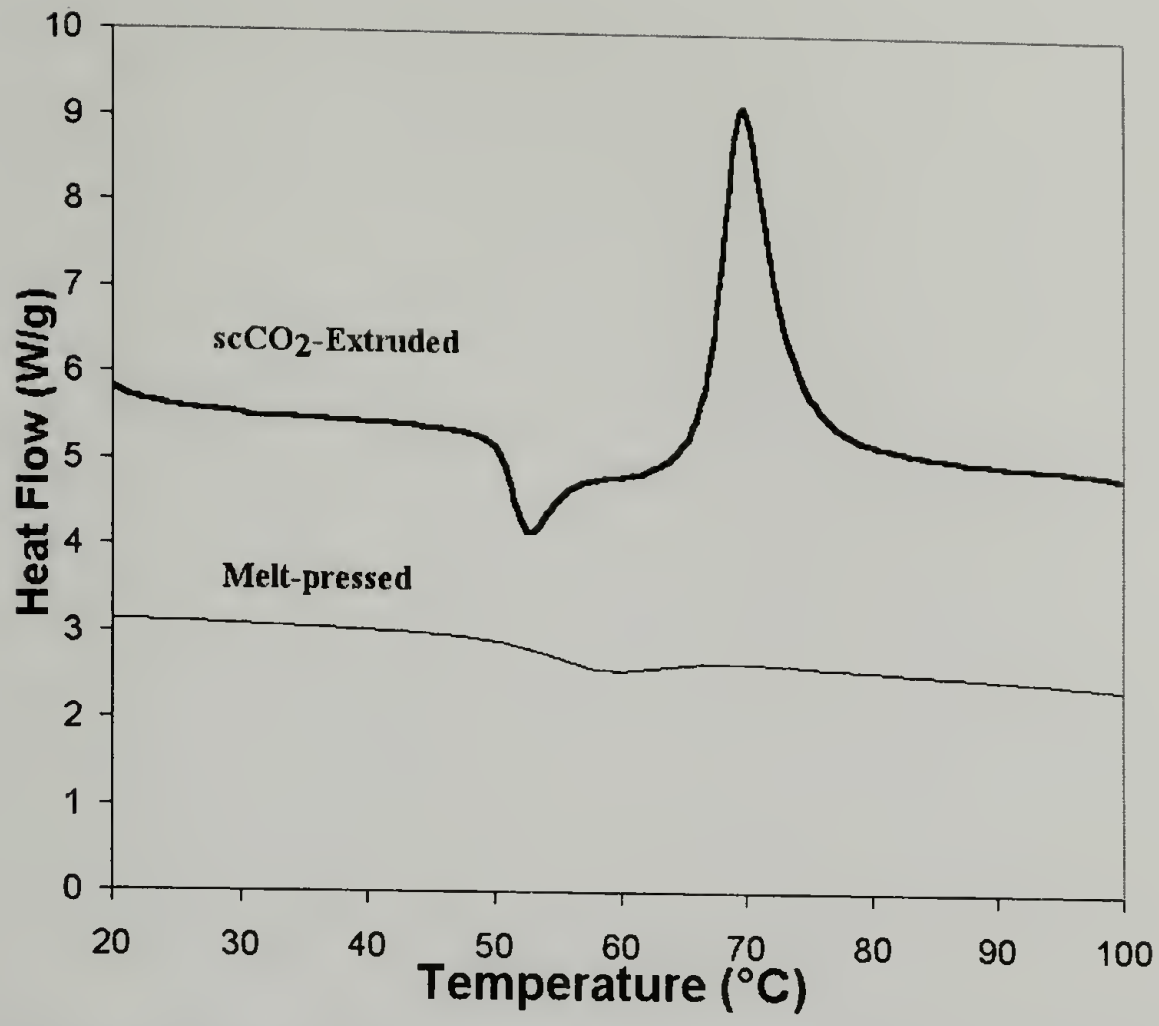

Figure 5.10. Thermal behavior (DSC) observed in PTT-M15A systems produced by extrusion with $scCO_2$ after post-melt pressing.

Intercalation of polymer chains into the clay galleries is monitored through changes in the basal spacing of the clay employed using WAXS. Some examples of the corresponding scattering patterns obtained for PTT samples prepared with both clay systems are presented in figure 5.11.

Results for the case of PTT-M15A clay systems are depicted in figure 5.12, and summarized in table 5.2. In this figure, a direct influence of the presence of $scCO_2$ on the basal spacing of the clay can be observed. As presented in table 5.2, regardless of the processing conditions, melt intercalation is evident when the modified clay is used, due to its larger d-spacing, its increased hydrophobicity and its inherent favorable interactions between the alkylammonium salt in the clay and PTT.[66]

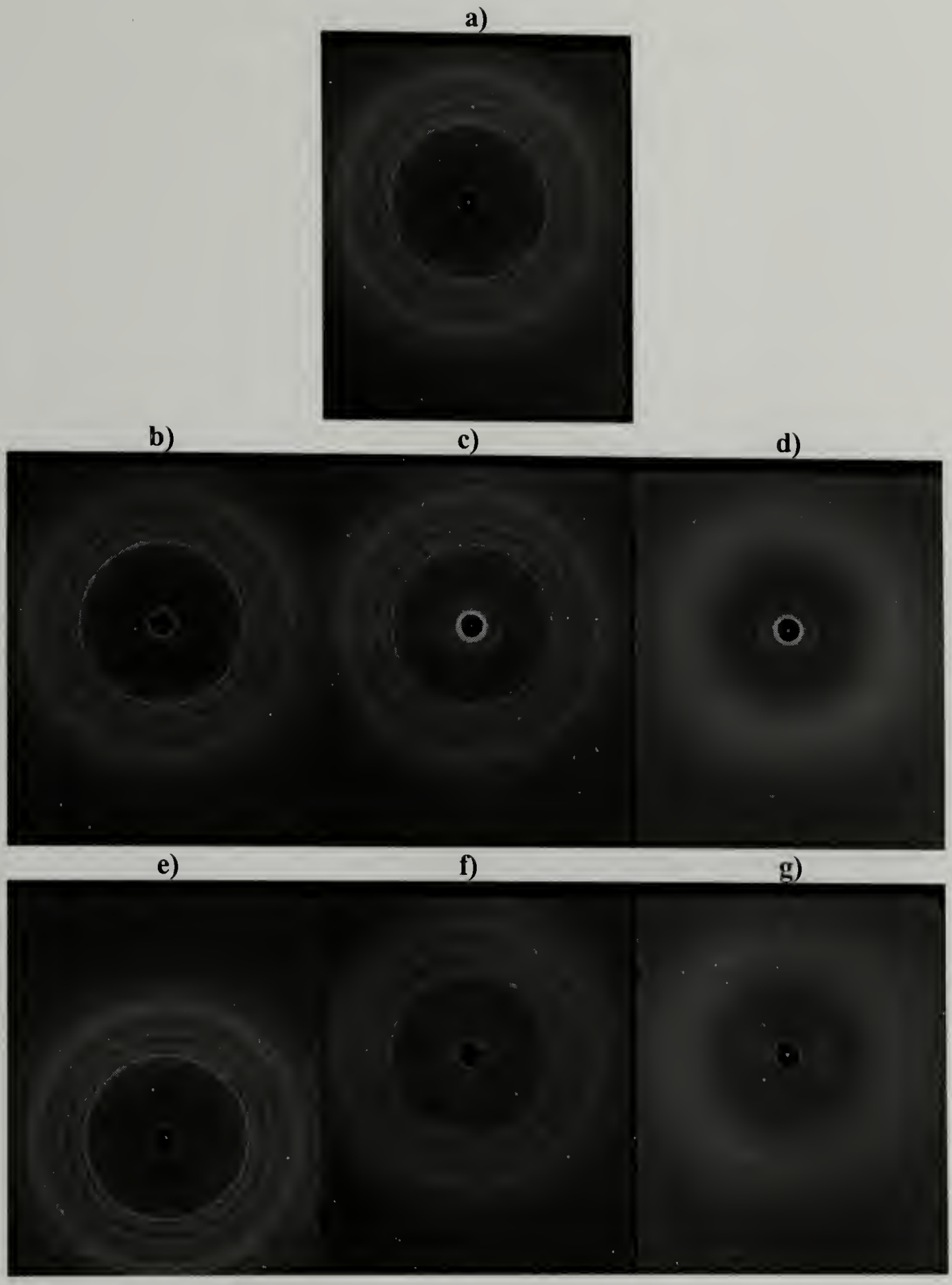

Figure 5.11. WAXS patterns for PTT samples obtained at different conditions using both types of clay. Shown are the corresponding results for a) PTT, b) PTT-M15A melt pressed (1 % wt. clay), c) PTT-M15A melt pressed (10 % wt. clay), d) PTT-M15A extruded with $scCO_2$ (10 % wt. clay), e) PTT-MNa+ melt pressed (1 % wt. clay), f) PTT-MNa+ melt pressed (10 % wt. clay), g) PTT-MNa+ extruded with $scCO_2$ (10 % wt. clay).

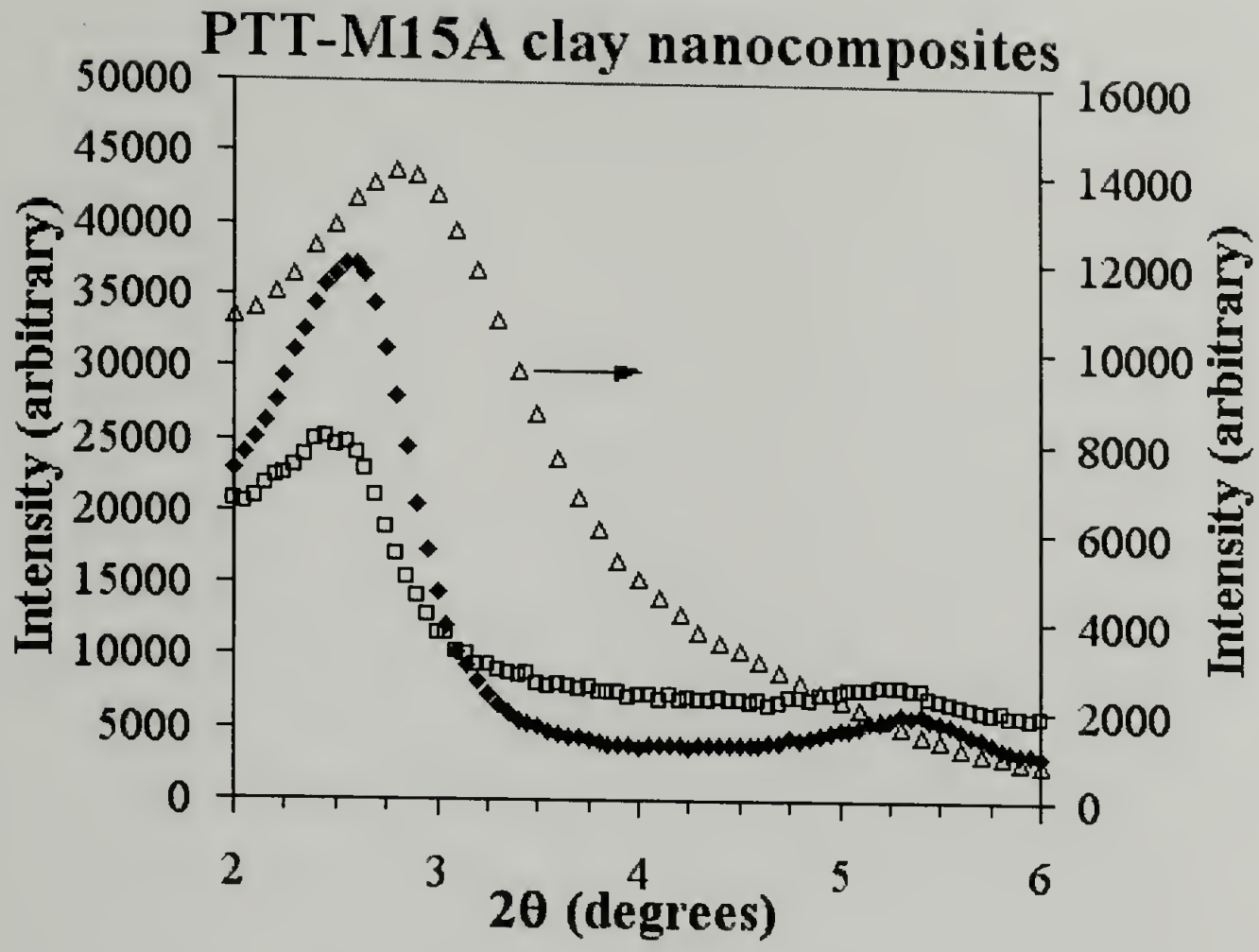

Figure 5.12. WAXS results for PTT-M15A nanocomposites obtained by melt intercalation. Pure MNa+ clay (Δ); PTT-M15A system without CO_2 (♦); PTT-M15A system produced with CO_2 (□).

As compared with that of the pure M15A clay, the typical d-spacing of the polymer systems prepared with and without $scCO_2$ is increased in a significant manner, suggesting in fact the diffusion of polymer chains into the clay galleries. A 10% increase is observed when comparing the typical d-spacing of the PTT-clay nanocomposite prepared without CO_2 and that of the pure M15A clay. However, it is very important to point out that a more pronounced change is generally observed when $scCO_2$ is introduced, where the d-spacing changes from 30.46 Å to 36.06 Å (a 20% increase), as shown in table 5.2. This suggests a direct contribution of the presence of $scCO_2$ to the melt intercalation process, implying that in systems where a favorable enthalpic interaction is present, the addition of $scCO_2$ can enhance the degree of intercalation.

Polymer	Process	Clay	% wt. clay	2θ (degrees)	d-spacing (Å)
-	-	M15A	100	2.90	30.46
PTT	Extrusion	M15A	10	2.60	33.98
PTT	$ScCO_2$-extrusion	M15A	10	2.45 1.41	36.06 62.71

Table 5.2. WAXS results of PTT-M15A systems produced by extrusion with and without $scCO_2$ showing the additional signals at low angles.

In fact, as presented in figure 5.13, when a wider range in scattering angles is analyzed, the scattering pattern of the material processed in $scCO_2$, reveals that the degree of intercalation is much larger, showing a clear reflection at 1.41 degrees, which corresponds to a d-spacing of 62.71 Å. As shown in this figure, systems produce without $scCO_2$ do not reveal further degree of intercalation.

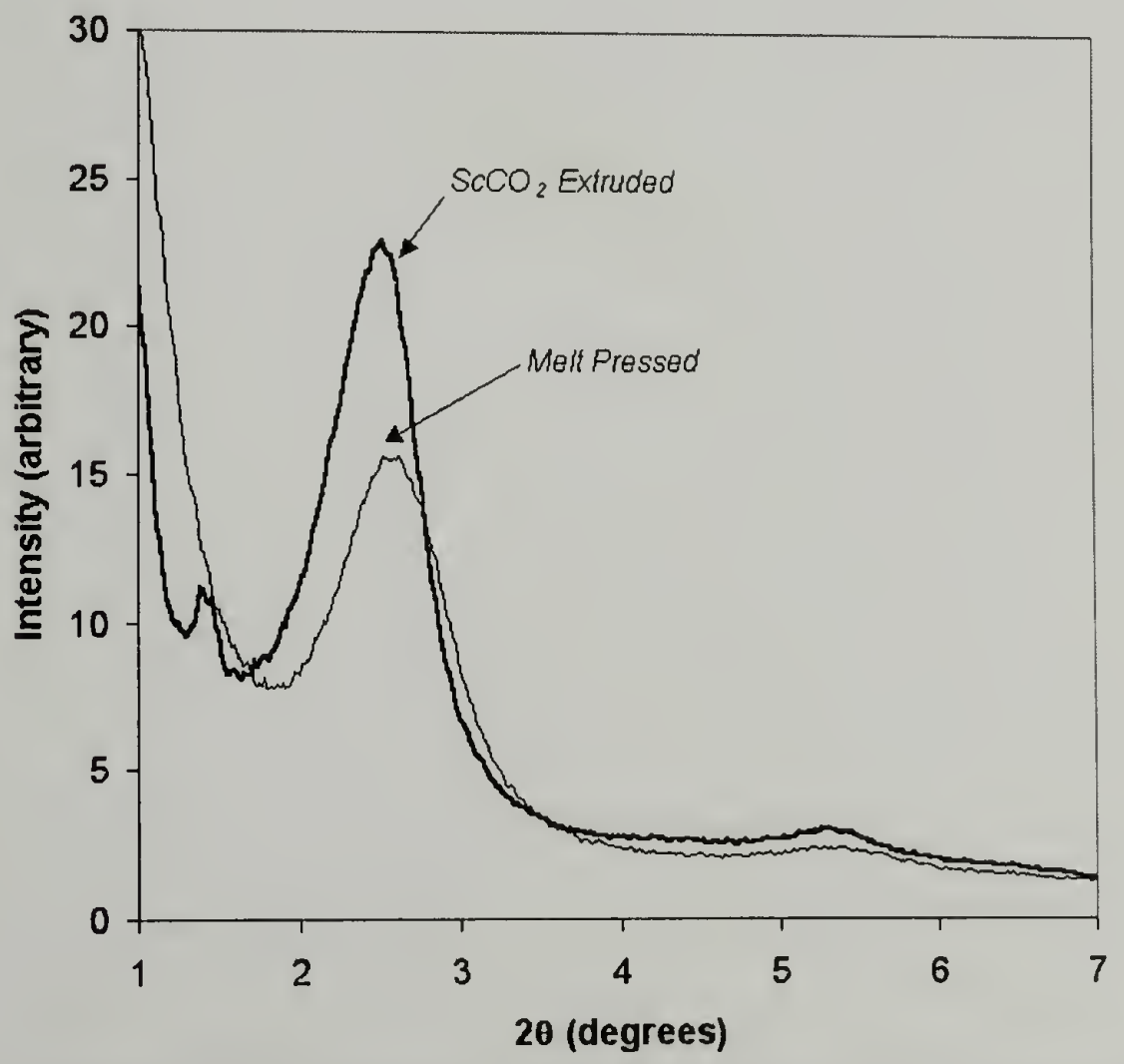

Figure 5.13. WAXS results of PTT-M15A systems produced by melt pressing and extrusion in $scCO_2$.

In systems containing unmodified clay (MNa+), the influence of $scCO_2$ on the intercalation process is significant and, as shown in figure 5.14, appears to control completely the degree of intercalation.

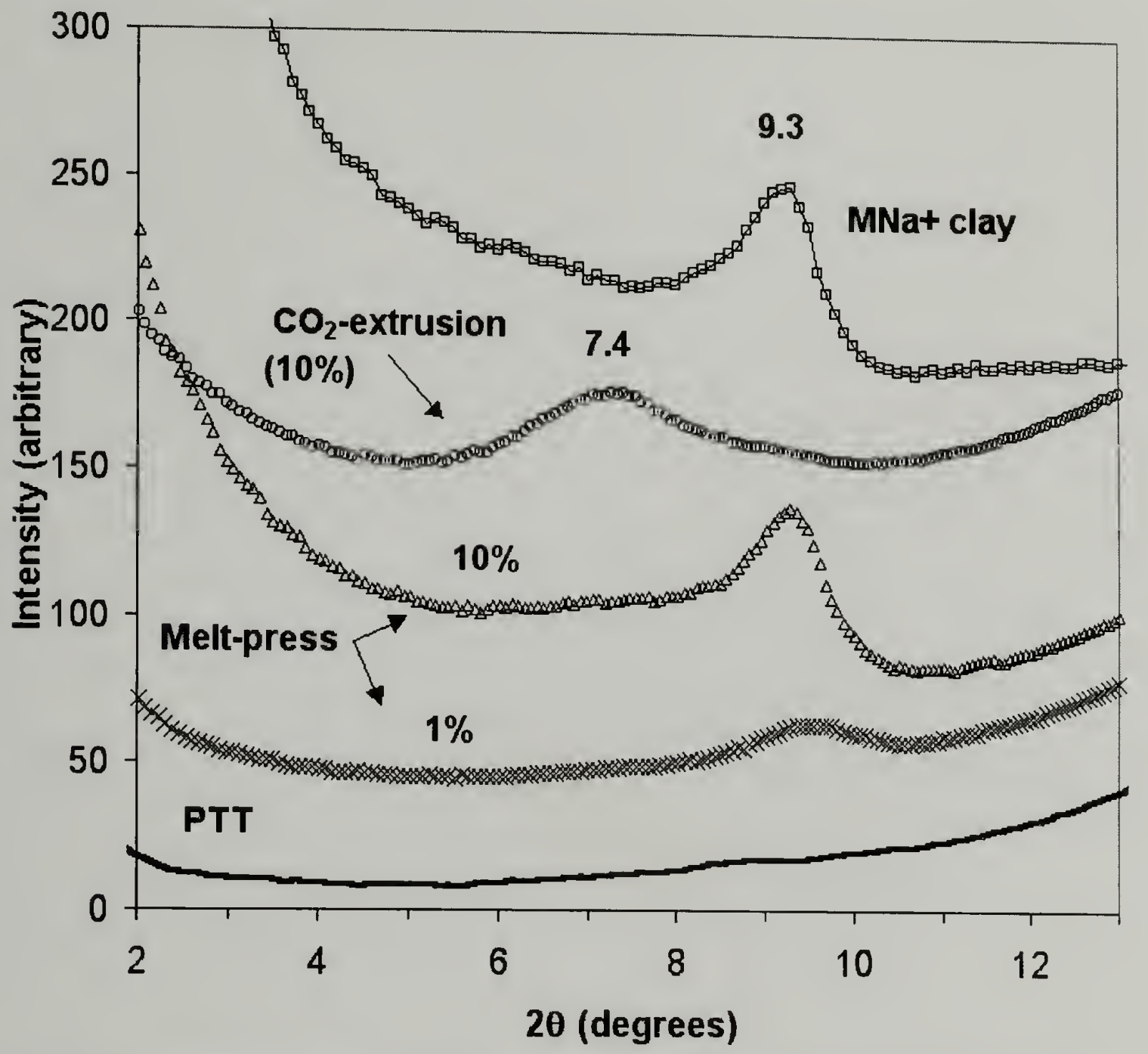

Figure 5.14. WAXS results of PTT-MNa+ systems produced by melt pressing and extrusion in $scCO_2$.

Intercalation appears only in $scCO_2$-processed samples showing a 20% increase in the clay d-spacing. In contrast, as presented in table 5.3, melt-pressed systems prepared with different concentrations of clay show no change in d-spacing. The observed reflections are well defined showing a distinctive maximum even at small clay concentrations, suggesting that the ordered intercalated structure in the clay lattice is maintained after

processing. Since the polymer-clay interactions in this case are limited due to the high degree of hydrophilicity of the clay, these results suggest a direct evidence of the influence of $scCO_2$ in the intercalation process.

Polymer	**Process**	**Clay**	**% wt. clay**	**2θ (degrees)**	**d-spacing (Å)**
-	-	MNa+	100	9.30	9.51
PTT	Melt Press	MNa+	1	9.34	9.46
PTT	Melt Press	MNa+	10	9.28	9.52
PTT	Extrusion	MNa+	10	9.30	9.51
PTT	$ScCO_2$-extrusion	MNa+	10	7.40	11.93

Table 5.3. WAXS results of PTT-MNa+ systems produced by melt pressing, extrusion and extrusion in $scCO_2$.

5.3.2 Polyolefin-based nanocomposites of high-density polyethylene (HDPE)

To understand the specific contribution of $scCO_2$ to the melt intercalation process, high-density polyethylene (HDPE) samples are prepared in CO_2 at 135°C (5.86-10.34MPa) in the presence of both types of clay (MNa+ and M15A). The melt intercalation of HDPE into a clay systems is graphically presented in figure 5.15. In this case, in addition to the very large entropic barrier that the polymer has to overcome to diffuse into the clay galleries, as a consequence of the hydrophobicity of the polymer, favorable interactions between the polymer and the hydrophilic clay systems are not expected, decreasing the possibilities for melt intercalation. Thus, by monitoring changes in the typical d-spacing of these systems, a clear understanding of the specific contribution of $scCO_2$ to the melt intercalation process can be obtained.

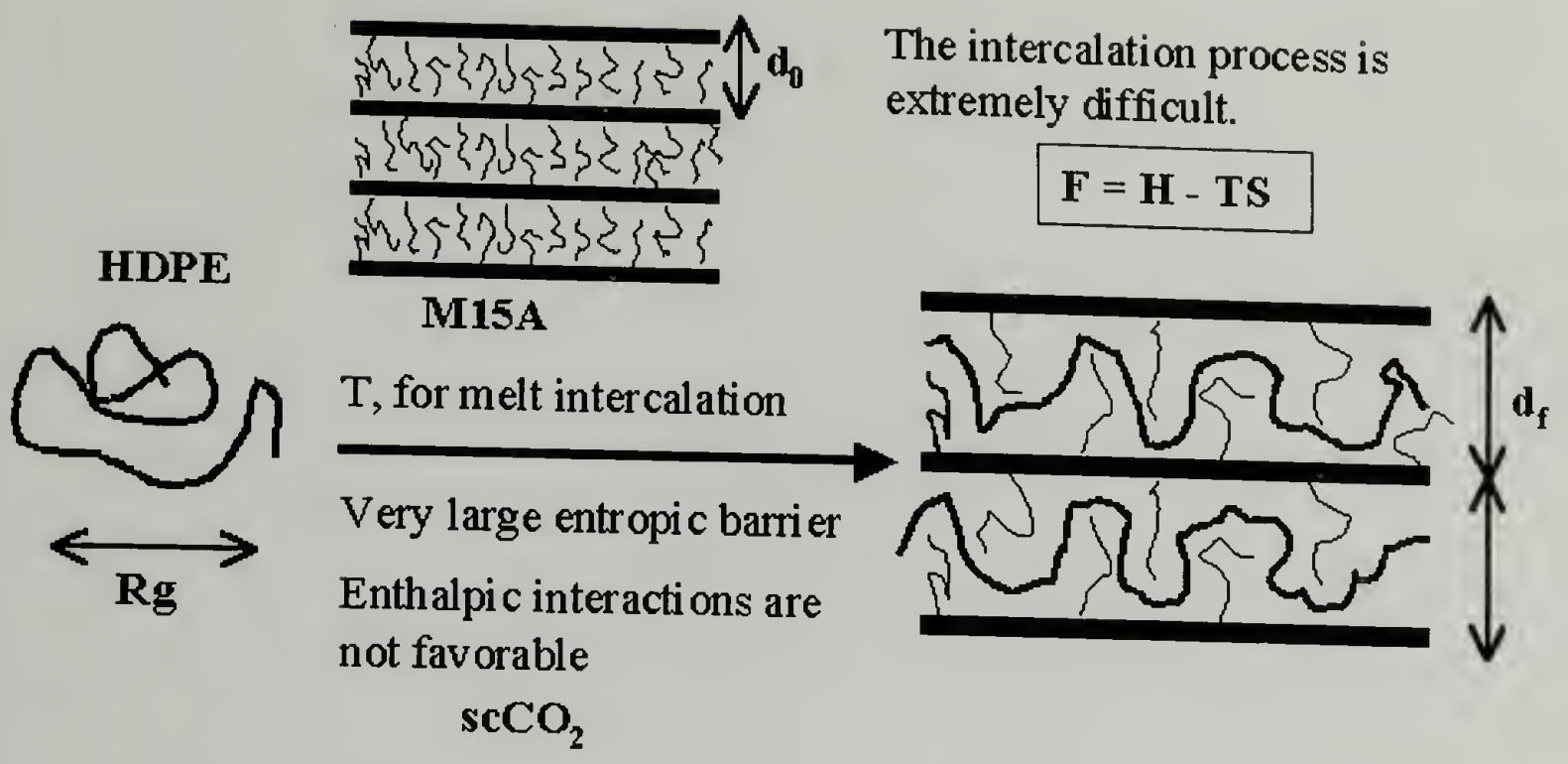

Figure 5.15. Graphical representation of melt-intercalation process of HDPE assisted by $scCO_2$ in clay systems.

The morphology of HDPE-clay systems obtained at these conditions is presented in figure 5.16. As shown in this figure, the overall morphology is characterized by a closed-cell foamed structure, which is consistent with that observed for the PTT-clay systems described before. As described in Chapter 3, it is evident that the presence of the clay nanoparticles enhances the cell nucleation process and as a consequence, a significant increase in the cell density is observed at higher clay concentrations. As mentioned in Chapter 3, this occurs until a critical clay concentration (~1%) is reached above which the cell density remains unchanged. The average cell size is dictated primarily by the concentration of clay and at any given concentration of clay a narrow cell size distribution is observed. As suggested in Chapter 3, the clay nanoparticles act as very effective heterogeneous nucleators, providing available surface for nucleation reducing the overall energy required in this process.

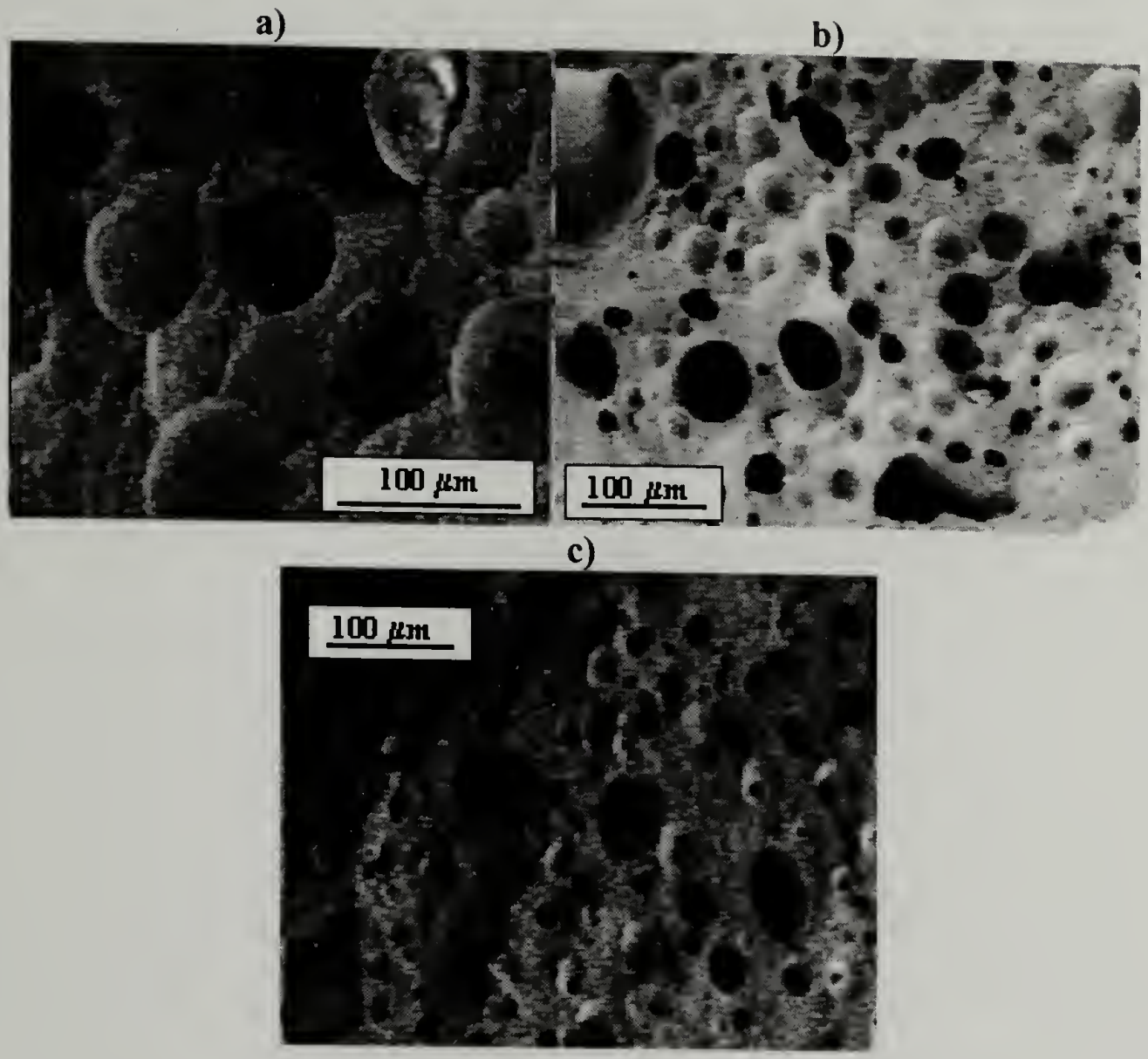

Figure 5.16. FESEM images of HDPE samples processed with different amounts of clay. a) HDPE with 0.5 % MNa+ clay, b) HDPE with 1 % M15A clay, c) HDPE with 10 % M15A clay.

In addition to foaming, the crystallization process follows a very similar trend and it is also altered significantly by the presence of clay, as presented in figure 5.17, where crystallinity values obtained by DSC for samples with different clay concentrations are shown. A considerable increase in crystallinity (from 41% to 60%) is observed even at relatively small clay concentrations (<1%). However, further addition of clay does not change the overall crystallinity, which reaches a plateau around 63%.

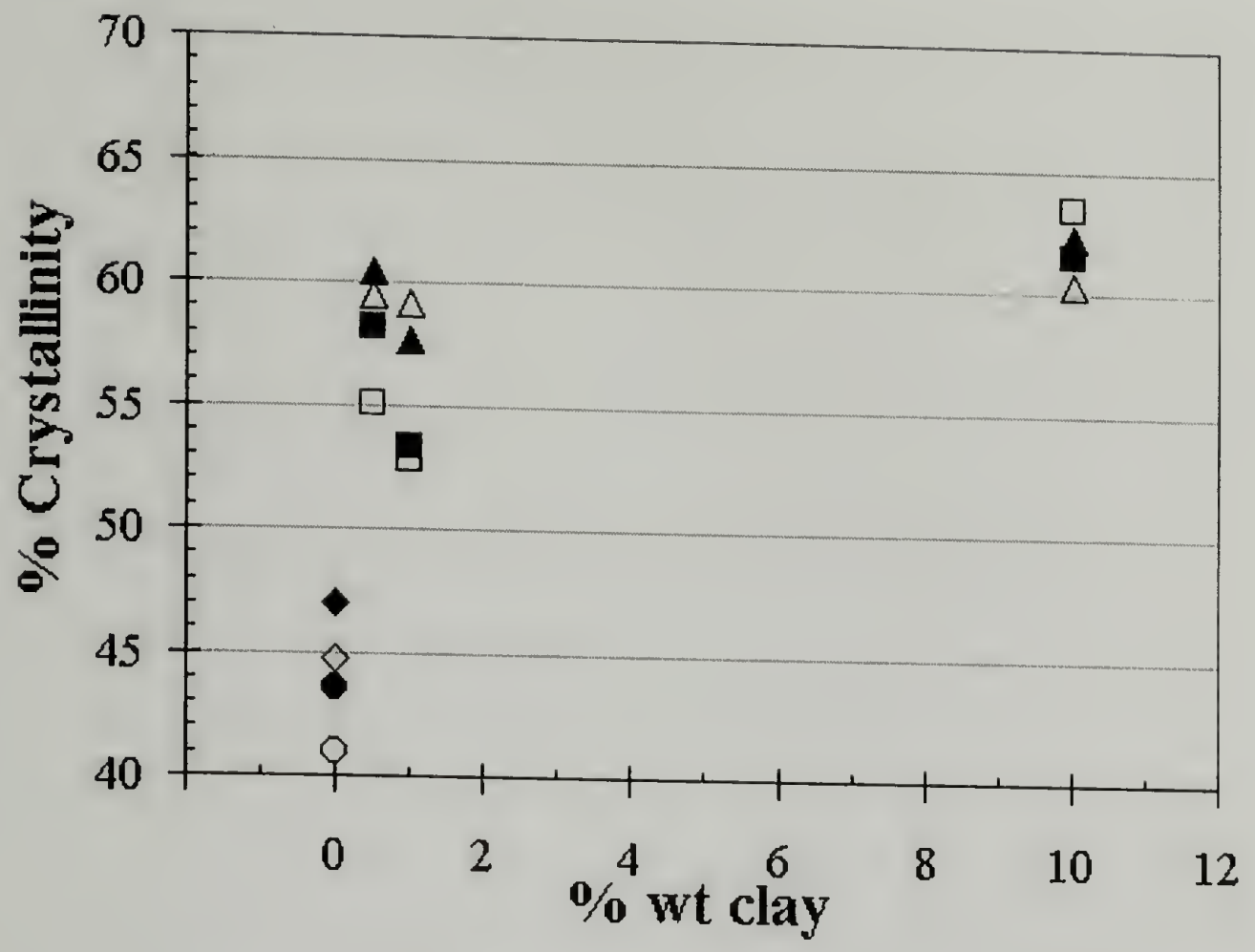

Figure 5.17. Crystallinity of HDPE samples processed at 135°C with clay nanoparticles. Not foamed (O); foamed without clay (◊); processed with MNa+ clay (□); processed with M15A clay (Δ). Solid and open symbols represent results obtained during the first and second DSC scans, respectively.

From these results it is difficult to observe significant differences between systems prepared with different clays (MNa+ or M15A), suggesting that regardless of their chemical structure, the crystallization process is mainly determined by the presence of particles that provide available surface for crystallization. The considerable increase in crystallinity suggests the possibility of a pronounced change in the mechanical properties of these systems with respect to those typically observed in HDPE.

The addition of clay does not modify the melting point regardless of the clay system employed, as shown in figures 5.18 and 5.19, where the DSC traces of HDPE-clay systems at different clay concentrations are compared to those observed in conventional HDPE and a material processed in $scCO_2$ without the addition of clay.

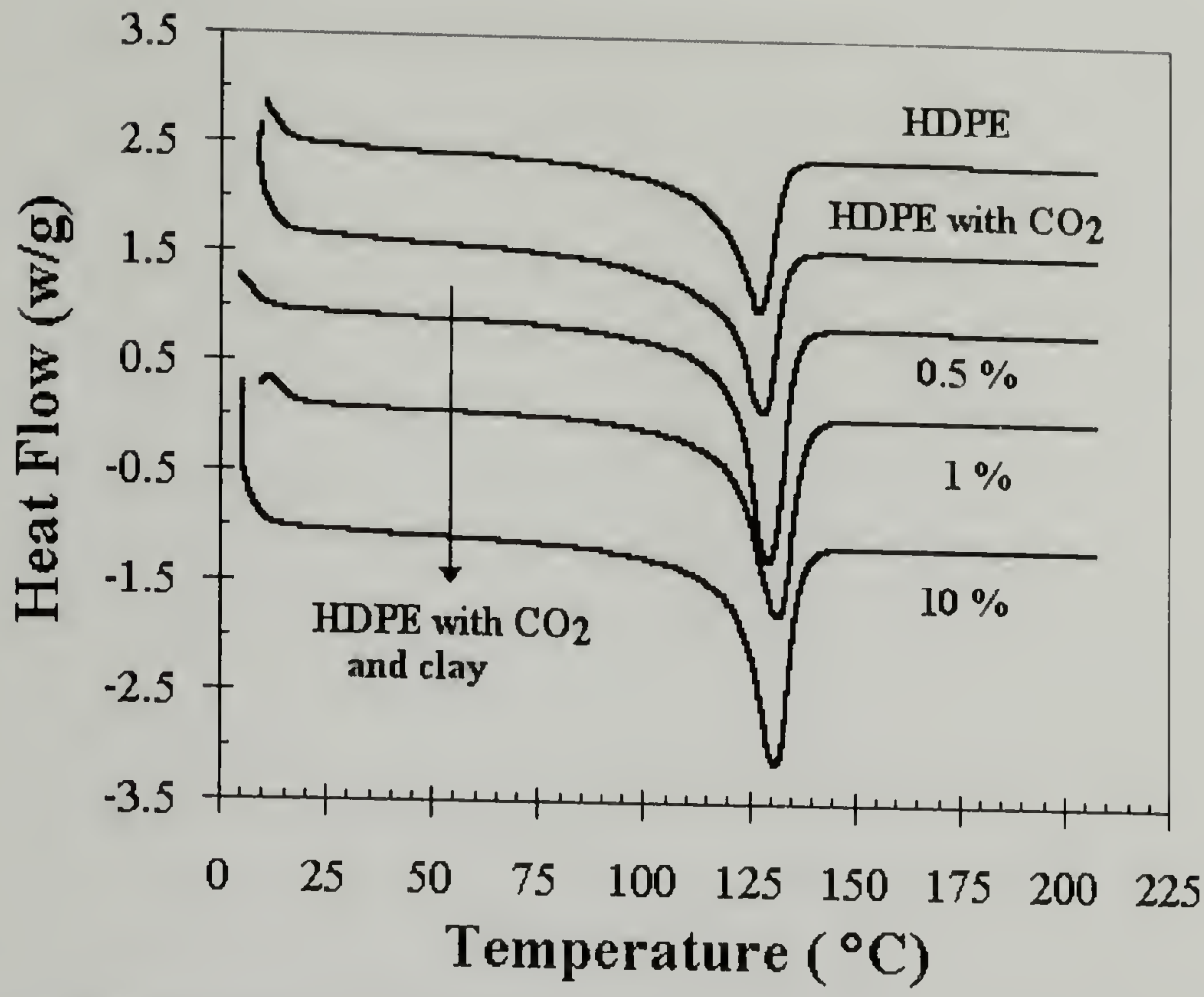

Figure 5.18. Thermal behavior of HDPE samples processed in $scCO_2$ using various amounts of MNa+ clay. For comparison, DSC traces of HDPE and HDPE with CO_2 are also included.

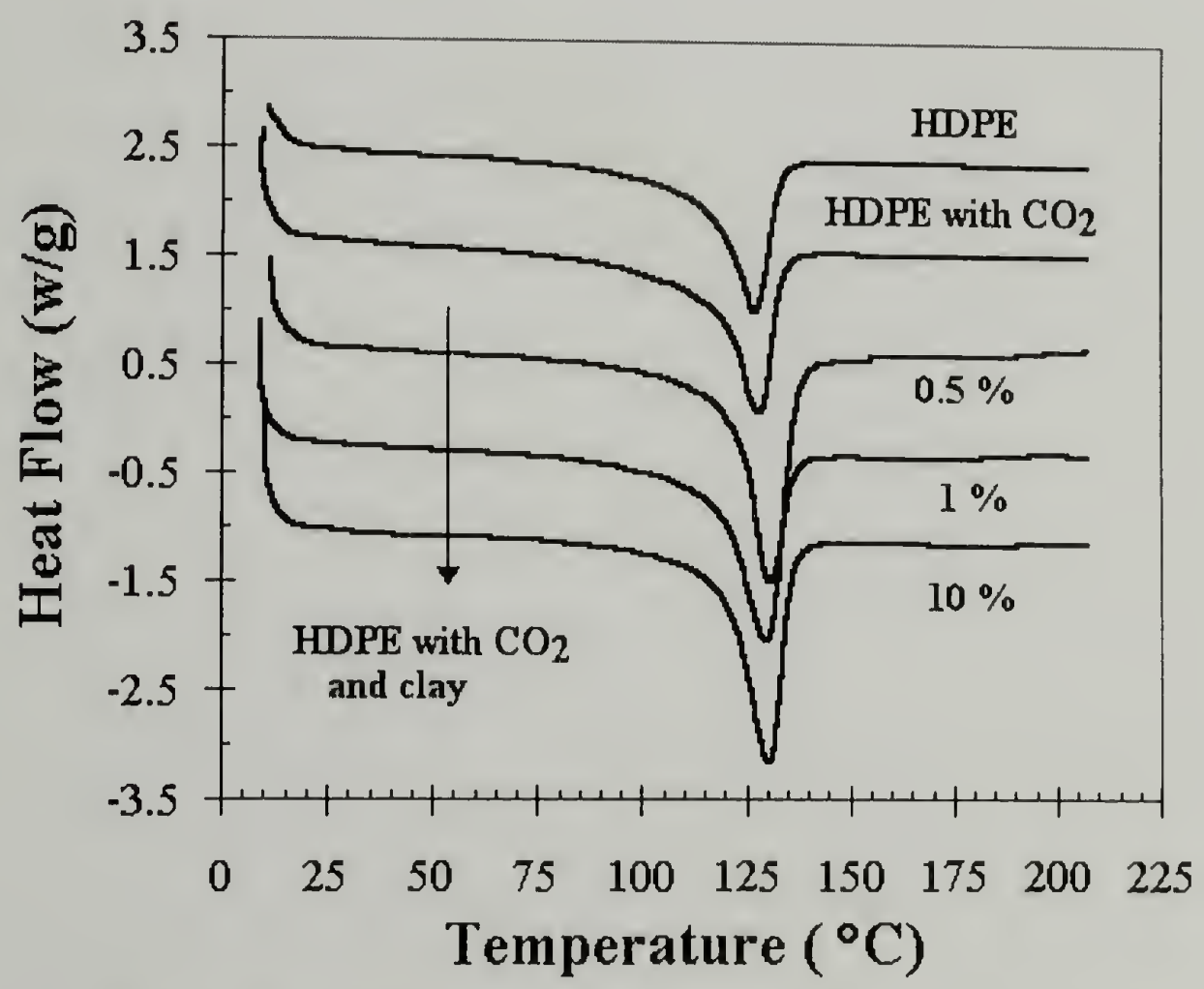

Figure 5.19. Thermal behavior of HDPE samples processed in $scCO_2$ using various amounts of M15A clay. For comparison, DSC traces of HDPE and HDPE with CO_2 are also included.

As mentioned before, the structure of these systems is analyzed by monitoring the position of the 001 plane in the clay structure by WAXS. The results are summarized in table 5.4, showing that $scCO_2$ has a significant influence on the intercalation process, promoting significant changes on the basal spacing of the clay. In figure 5.20, it is evident that regardless of the concentration of unmodified clay (MNa+), the principal reflection of the clay appears at lower scattering angles (from 9.3 to 7.0), suggesting a 33% increase in the clay d-spacing when the material is processed in $scCO_2$. Since no interactions between the polymer and the clay are expected in this case, this result shows direct evidence of the influence of $scCO_2$ to the melt intercalation process, and so in the final structure of the system. As shown in figure 5.21, the observed reflections are well defined showing a distinctive maximum even at small clay concentrations, suggesting that the ordered intercalated structure in the clay lattice is maintained after processing.

Polymer	**Type of clay**	**% wt. clay**	**2θ (degrees)**	**d-spacing (Å)**
-	MNa+	100	9.3	9.51
-	M15A	100	2.9	30.46
HDPE	MNa+	0.5	7.0	12.63
HDPE	MNa+	1	6.9	12.81
HDPE	MNa+	10	7.0	12.63
HDPE	M15A	0.5	2.55	34.64
HDPE	M15A	1	2.55	34.64
HDPE	M15A	10	2.70	32.72

Table 5.4. WAXS results for HDPE-clay systems obtained at various clay concentrations.

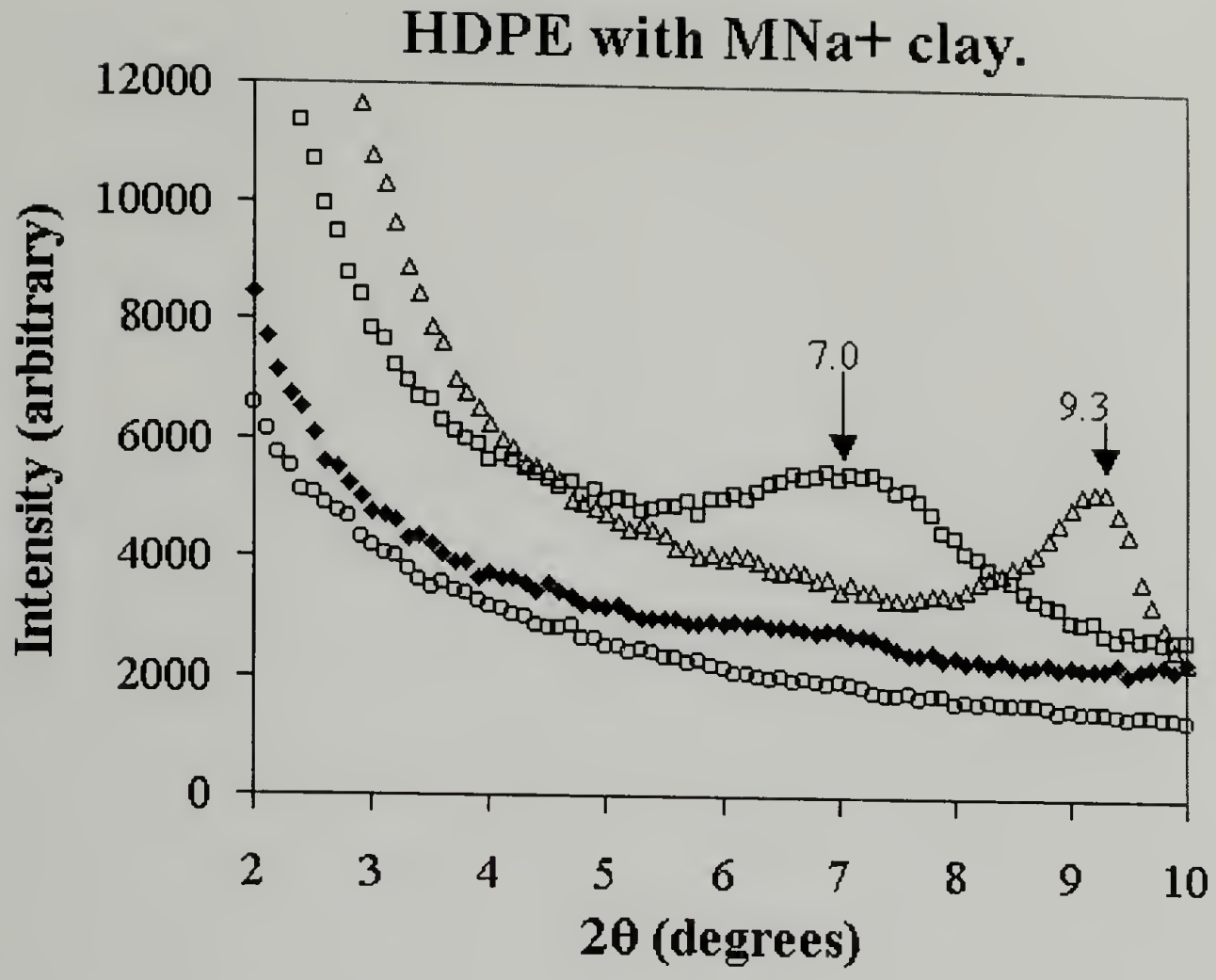

Figure 5.20. WAXS results for HDPE samples processed with MNa+ clay. Pure MNa+ clay (Δ); HDPE-0.5% clay (O); HDPE-1% clay (♦); HDPE-10% clay (□).

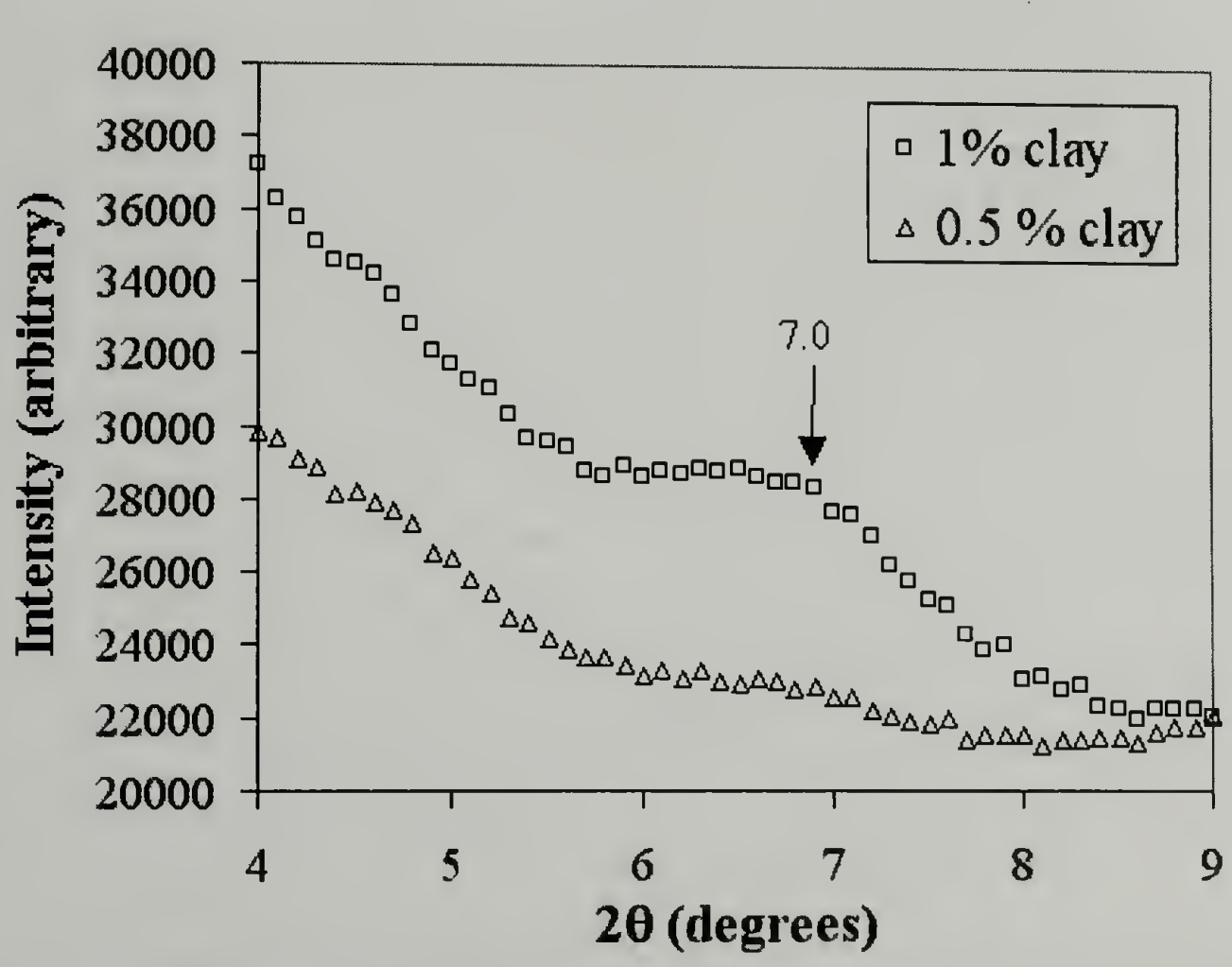

Figure 5.21. WAXS results for HDPE samples processed with MNa+ clay. Shown are the results for low clay concentration samples using 300 seconds/degree as the exposure time.

These observations are extremely important, suggesting that by processing in $scCO_2$, melt intercalation of a purely hydrophobic polymer into the galleries of a purely hydrophilic clay system can be promoted, creating intercalated polymer nanocomposites that are not accessible by traditional routes.

This behavior is consistent regardless of the nature of the clay and a similar behavior is observed in samples processed with the modified M15A clay, as shown in figure 5.22, where once again, the position of the principal reflection of the clay shifts to lower scattering angles in HDPE-clay systems. In this case, as presented in table 5.4, the typical d-spacing of the clay is increased from 30.46Å to 34.64Å. Again since no melt intercalation is expected, these results quantify the specific influence of $scCO_2$ in the morphology of these systems.

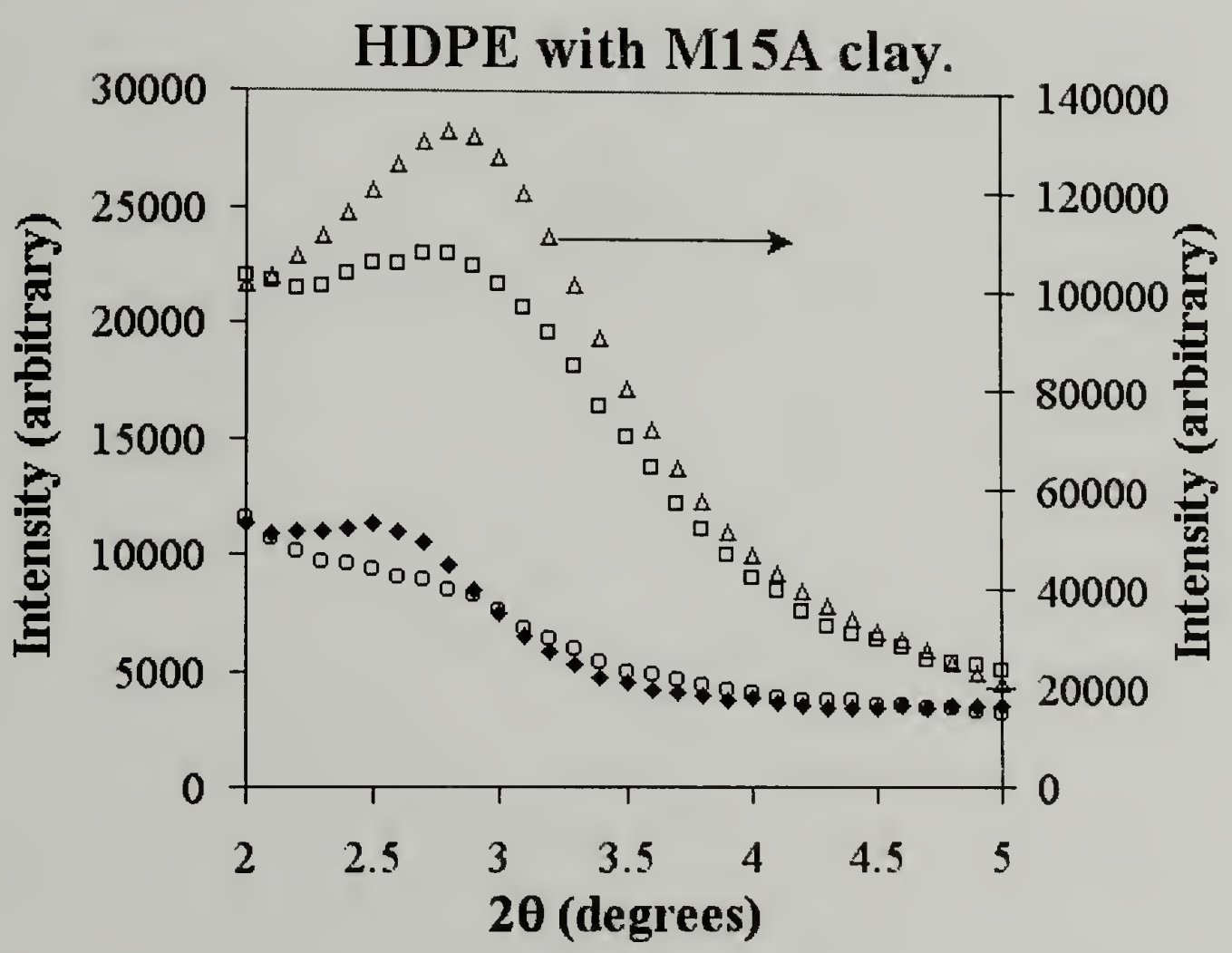

Figure 5.22. WAXS results for HDPE samples processed with M15A clay. Pure M15A clay (Δ); HDPE-0.5% clay (O); HDPE-1% clay (♦); HDPE-10% clay (□).

. The importance of the energetic interactions between the clay and polymer systems are systematically studied in Chapter 6, where a specific understanding of the effect of $scCO_2$ is obtained by controlling the hydrophilicity of the polymer and clay systems, hence controlling the enthalpic interactions between the two.

5.4 Conclusions

A modified processing system[51,76-78] has been employed to successfully produce polymer-clay nanocomposites in $scCO_2$. Polymer nanocomposites of commercially relevant systems can be produced via $scCO_2$-assisted polymer processing. Experimental results suggest that the presence of clay nanoparticles has a significant influence on the morphology, crystallization and foaming process of a polymer when processed in $scCO_2$. The effect of $scCO_2$ has been analyzed in a variety of polymer systems processed both with modified M15A and unmodified MNa+ clay. A significant increase in the basal spacing of the clay is observed when $scCO_2$ is introduced, suggesting that $scCO_2$ has a measurable effect on the clay dispersion and the melt intercalation of a polymer into clay nanoparticles.

The effect of $scCO_2$ on the melt intercalation process as well as on the final structure and morphology of polymer-clay nanocomposites is obtained by tuning the hydrophilicity of the polymer and clay systems. Intercalated polymer nanocomposites are successfully produced when $scCO_2$ is introduced, showing a significant increase in the basal spacing of the clay even when there are no favorable interactions between the polymer and the clay. Results suggest that the intercalation process is considerably enhanced by $scCO_2$, showing significant increases in the clays d-spacings (40-100% increase) and in some

cases controlling the rate at which the intercalation process takes place. This effect is evident regardless of the nature of the polymer, showing significant amounts of intercalation even in purely hydrophobic polymers, suggesting that the presence of $scCO_2$ can be used to enhance the melt intercalation process. This opens up the possibility of using this technique to produce nanocomposites in systems that either have been traditionally rejected in this area due to thermodynamic limitations or those in which a need for material properties enhancements is of commercial importance. The produced intercalated structures might promote considerable interactions between silicate layers at the molecular scale that may influence the physical and material properties of the composite, providing property-enhancing characteristics at scales inaccessible for traditional filler materials.

CHAPTER 6

POLYMER-CLAY NANOCOMPOSITES PREPARED IN SUPERCRITICAL CARBON DIOXIDE USING CHEMICALLY-DESIGNED COMPATIBILIZERS

In this chapter, polymer nanocomposites of commercially relevant systems are prepared via the combination of $scCO_2$-assisted polymer processing and the addition of chemically-designed polymeric systems that enhance the interaction between the polymer and clay, acting as compatibilizers for melt intercalation. Results suggest that this method can be used as an effective route to produce polymer nanocomposites, with specific control over the degree of intercalation and in some cases allowing access to exfoliated structures. The properties and structure of nanocomposites prepared by the addition of two types of compatibilizers is described.

6.1 Introduction

As mentioned in Chapter 5, current alternatives to improve the mechanical and physical properties of existing engineering polymers include the preparation of polymer nanocomposites incorporating diverse inorganic materials into a variety of polymers. In order to overcome the enormous entropic barrier associated to polymer intercalation, different approaches have been followed and described in the literature to produce intercalated and exfoliated systems.[52-62] In Chapter 5, supercritical carbon dioxide ($scCO_2$)-assisted polymer processing has been described as a new alternative route to prepare polymer nanocomposites.[76-78] Results indicate that $scCO_2$ enhances the ease of polymer intercalation into layered nanosilicates, and its effect on the final structure of

polymer-clay nanocomposites has been studied by tuning the hydrophilicity of the polymer-clay systems, obtaining intercalated structures even in purely hydrophobic polymers.

In this Chapter, another route to intercalated and exfoliated nanocomposites of commercially relevant polymers is presented. Polyolefin-based nanocomposites are obtained using specifically designed compatibilizers to enhance the interaction between the polymer and clay. Two specific polymeric compatibilizers are used: a) amphiphilic graft copolymers of polyethylene and poly(ethylene glycol) (PE-g-PEG) produced by ring-opening metathesis polymerization of poly(ethylene glycol)-substituded cyclooctene macromonomers,[67] and b) polyamines with controlled amine density, produced by chemical modification of a variety of nylon systems[68], including Nylon 6/6, Nylon 6/9, and Nylon 4/6, which after reduction, materials with inherent affinity to the clay and increased hydrophilicity are obtained.

Results suggest enhanced intercalation when these systems are introduced and in fact this effect is more pronounced when the polymer is processed in $scCO_2$. This method suggests a direct route to control specifically the polymer-clay interactions that could be used to produce nanocomposites with well-defined structure.

6.2 Experimental

Materials. As described in Chapter 5, unmodified (MNa+) and surface modified (M15A) montmorillonite, obtained from Southern Clay Products, Inc. are employed. Both systems are kept under vacuum at 50°C before used. The modified clay (M15A) is produced by cation exchange wherein sodium from natural montmorillonite is replaced

by a long alkylammonium salt. High-density polyethylene (HDPE) resin was obtained from The Dow Chemical Company in the form of pellets and was grinded into powder or used as received. Whatman Nylon 6/6 membranes (0.45 μm), Hydrochloric acid (37%) and formic acid (88%) were purchased from Fisher. Nylon 4/6 and 6/9 pellets, tetrahydrofuran (THF), borane-THF complex (1M), morpholine and sodium hydroxide were obtained from Aldrich

Extrusion Experiments. The modified processing system[51] described in Chapter 3 is employed to process a variety of polymers with $scCO_2$ in the presence of clay nanoparticles and the chemically designed compatibilizers.

Reduction of Nylons. Nylon membranes were chemically reduced by the reaction of Nylon-film surfaces with BH_3·THF to produce polyamine systems with controlled charge density.[68] Nylon 6/6 membranes were used as received while Nylon 4/6 and 6/9 membranes were fabricated by diffusion-induced phase separation.

Materials Characterization. Differential Scanning Calorimetry (DSC) is used to analyze the thermal behavior of the samples, using a TA Instruments thermal analyst model 2910 DSC at a heating rate of 10°C/min. The crystallinity of the samples is estimated by the ratio of their melting enthalpy and the corresponding theoretical heat of fusion for a perfect crystal. Wide-angle x-ray scattering (WAXS) experiments are done in a Siemens D500 Diffractometer using an operating voltage of 40 kV and a total current of 30 mA. The overall morphology is investigated using a Field Emission Scanning Electron Microscope (FESEM) model JSM-6320FXV and a Scanning Electron Microscope (SEM) model JEOL-CS-35 with a filament voltage of 20 kV. Samples are cryo-fractured in liquid nitrogen and gold coated for 3-4 min prior to the SEM analysis. TEM experiments

are conducted in a JEOL-200CX with an accelerating voltage of 200 kV, using cryomicrotomed thin sections (40 nm) of existing samples.

6.3 Results and Discussion

6.3.1. Polymer nanocomposites prepared by the addition of polyethylene-g-poly(ethylene glycol)(PE-g-PEG) systems

As suggested in Chapter 5, specific understanding of the effect of $scCO_2$ on the structure and morphology of the nanocomposites can be obtained by controlling the hydrophilicity of the polymer and clay systems, hence controlling the enthalpic interactions between the two. In this regard, introducing the PE-g-PEG amphiphilic copolymers can be used to specifically control of the overall hydrophilicity of a polymer system.

The synthesis of the amphiphilic graft copolymers used in this case is presented in figure 6.1. The copolymers have a hydrophobic backbone as a result of the cyclooctene monomer used that enhances their interaction with hydrophobic polymers. Their structural similarity with polyolefins makes these systems very good candidates to be used in combination with this type of materials. In addition, a hydrophilic group (PEG) has been introduced to the backbone as a consequence of the ring-opening metathesis polymerization of the PEG-substituted monomer. Several synthetic strategies can be followed to control the degree of hydrophilicity of these systems, including the control of the grafting density of PEG groups onto the hydrophobic backbone and/or the specific length (molecular weight) of the PEG groups in the copolymer. Both situations lead to specific control of the hydrophilicity of the system, and as described later, they can be

used to influence the degree of interaction between a polymer and a given clay system. The copolymers by themselves are intractable and difficult to produce in substantial quantities, but their use as compatibilizers is extremely successful as described in this chapter.

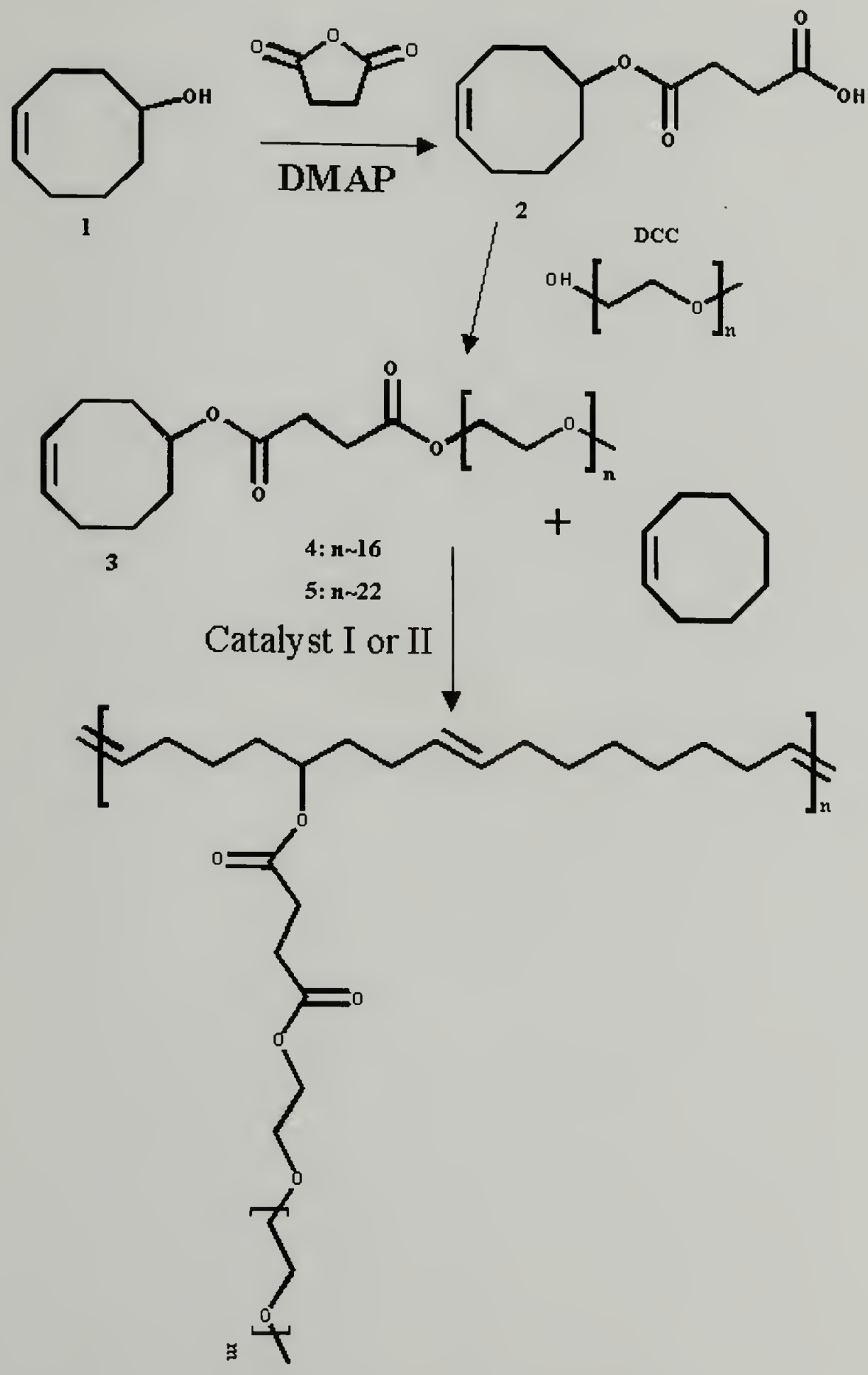

Figure 6.1. Synthesis of amphiphilic PE-g-PEG copolymers.[67]

Two particular materials with different concentration of PEG groups (2% and 5%) have been used. PE-g-PEG systems with 5% PEG have been mainly employed to understand the contribution of the enhanced hydrophilicity in a system on the degree of intercalation. These results allowed us to use copolymers with 2% PEG in a very efficient way, tuning the ratio of clay/PEG in the system, thus adjusting the degree of intercalation to produce materials that could help us to understand the influence of structure on the final properties of the composite.

The thermal behavior of the two PE-g-PEG systems is presented in figure 6.2 and summarized in table 6.1.

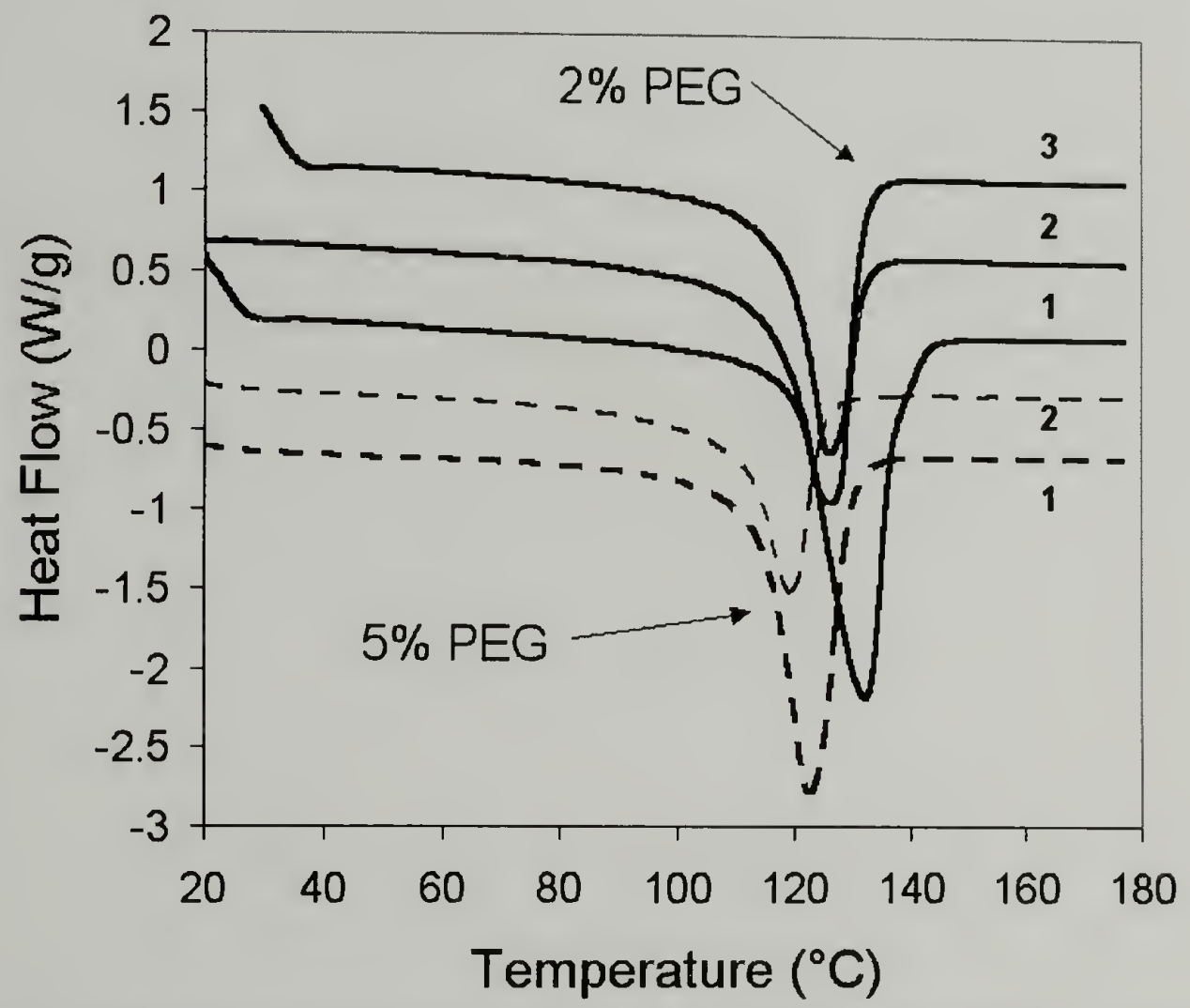

Figure 6.2. Thermal behavior of PE-g-PEG systems with different PEG concentration. Numbers indicate the first, second and third runs in the DSC for each sample.

As shown, the thermal behavior is altered by the amount of PEG groups in the copolymer. 2% PEG systems show increased melting points and crystallinity as

compared to 5% PEG systems. As expected, the melting behavior approaches that observed in polyethylene at low PEG concentrations. Significant reduction in the overall crystallinity is observed during the melting process due to the high molecular weight of the copolymers that restricts in a significant manner the re-crystallization process.

Sample	% PEG	Run	Tm (°C)	ΔHm (J/g)	Crystallinity (%)
PEgPEG	2	1	132.21	165.5	57.28
PEgPEG	2	2	126.24	120.7	41.78
PEgPEG	2	3	125.96	124.5	43.09
PEgPEG	5	1	122.65	153.1	52.98
PEgPEG	5	2	119.46	92.03	31.85

Table 6.1. Thermal behavior of PE-g-PEG systems with different PEG concentration. Degree of crystallinity is calculated with respect to polyethylene using 288.89 J/g as the theoretical heat of fusion.

As mentioned earlier, these materials are difficult to produce in substantial quantities, however, they can be used in combination with other polymers to enhance the hydrophilicity. In this regard, HDPE/(PE-g-PEG) blends are used and as mentioned before, the overall hydrophilicity of the HDPE/(PE-g-PEG) blend is controlled through the concentration of PEG groups, which is adjusted in a precise manner during the synthesis.[67]

Using 5% PEG copolymers, HDPE/(PE-g-PEG) blends are processed in our modified system at 135°C using CO_2 (pressures between 5.86-10.34 MPa) in the presence of various clay systems. Evidently, the presence of $scCO_2$ and that of the clay nanoparticles enhance the nucleation process and as a consequence, foamed structures with a typical

closed cell morphology are obtained[76]. In general, as described in previous sections, higher concentrations of clay significantly affect the cell density and primarily dictate the average cell size regardless of the type of clay employed, suggesting that heterogeneous nucleation brought about by the presence of clay is the principal foaming mechanism.

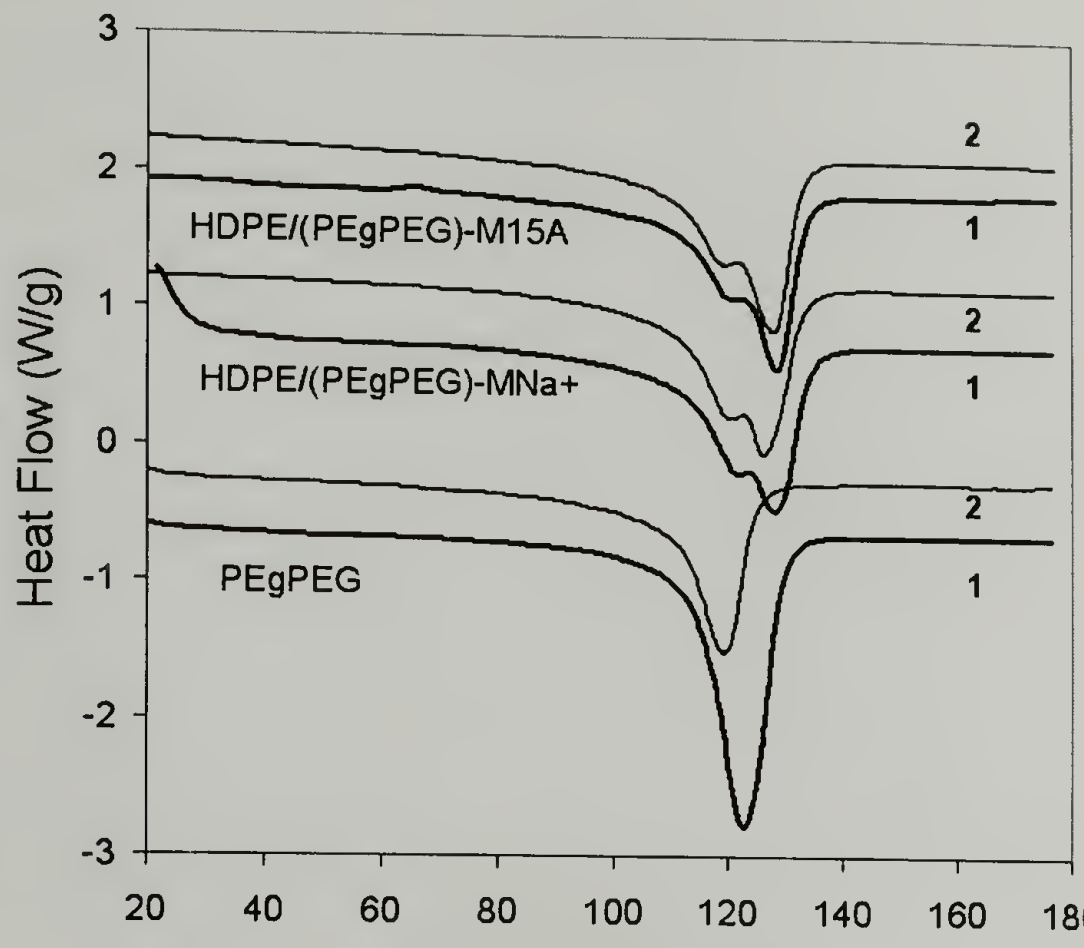

Figure 6.3. Thermal behavior of HDPE/PE-g-PEG (5% PEG) blends produced by extrusion with $scCO_2$ using different clay systems. Results for the pure PE-g-PEG copolymers are included for comparison. Numbers indicate the first and second runs in the DSC for each sample.

Figure 6.3 shows the thermal behavior of the HDPE/(PE-g-PEG) blends processed in $scCO_2$, using 5% PEG systems. As shown in this figure, the systems display two characteristic melting endotherms, and the thermal behavior is independent on the nature of the clay used in the process. The low-temperature melting peak at around 119°C corresponds to the melting of the polyethylene units in the PE-g-PEG copolymers, while at 127°C the melting transition of the HDPE systems is observed, as shown in table 6.2.

Again, a lower crystallinity is observed after the melting process due to the high molecular weight of the copolymers that restricts the re-crystallization process. From these results, it is difficult to identify differences between systems prepared with different clay systems, suggesting again that regardless of their chemical structure, the crystallization process is mainly determined by the presence of particles that provide available surface for crystallization.

Sample	Clay	Run	Tm (°C)	ΔHm (J/g)	Tm^2 (°C)	Crystallinity (%)
HDPE		1	-	172.4	128.53	59.66
HDPE		2	-	183.4	127.31	63.46
PEgPEG		1	122.65	153.1	-	52.98
PEgPEG		2	119.46	92.03	-	31.85
HDPE-PEgPEG	MNa+	1	120.83	126.32	128.17	48.56
HDPE-PEgPEG	MNa+	2	119.68	123.6	126.29	47.52
HDPE-PEgPEG	M15A	1	119.67	116.13	128.58	44.65
HDPE-PEgPEG	M15A	2	118.46	119.8	128.08	46.06

Table 6.2. Thermal behavior of HDPE/PE-g-PEG (5% PEG) blends produced by extrusion with $scCO_2$ using different clay systems. For comparison HDPE and pure PE-g-PEG are included. Degree of crystallinity is calculated with respect to polyethylene using 288.89 J/g as the theoretical heat of fusion. The heat of fusion of the blends includes both endotherms.

WAXS analysis is done in HDPE/PE-g-PEG blends prepared at different conditions, to understand the effect of the enhanced hydrophilicity on the structure of the blends. The behavior of these blends is also compared to that observed in PE-g-PEG samples prepared by melt-pressing using the same concentration of clay, to understand the specific contribution of the hydrophilic PEG groups on the degree of intercalation.

As shown in figure 6.4, it appears that the increased hydrophilicity in the copolymers (PE-g-PEG), brought about by the hydrophilic PEG groups, is not enough to promote intercalation. Melt-pressed samples of pure PE-g-PEG with clay at various processing times do not show evidence of a change in the basal spacing of the clay, as shown in table 6.3. These observations suggest that the chemical nature and relative hydrophilicity of the polymer does not provide enough energy to drive the intercalation process.

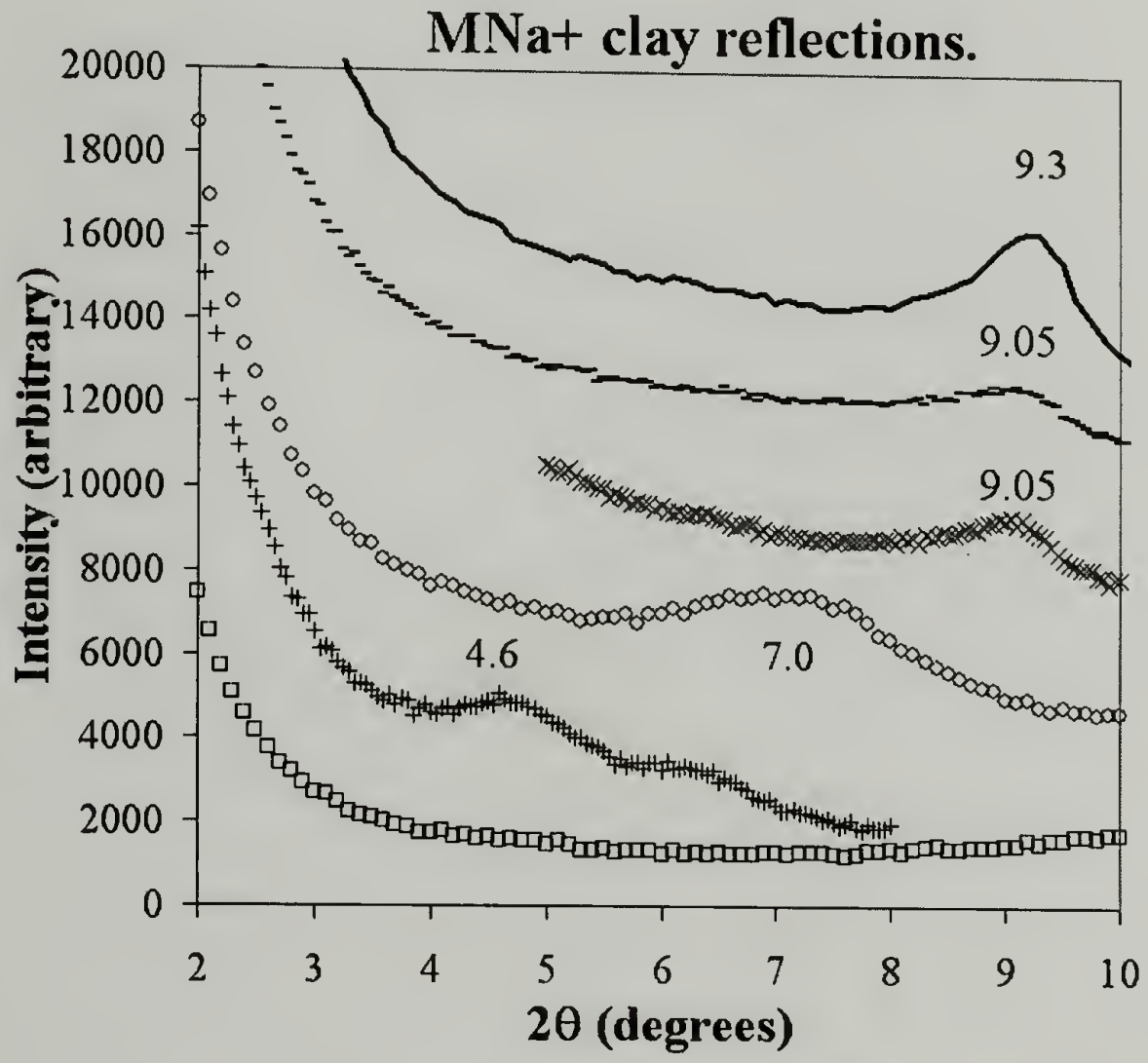

Figure 6.4. WAXS results for polyethylene samples processed with MNa+ clay. Pure MNa+ clay (—), HDPE/(PE-g-PEG) blend melt-pressed for 15 min.(-), HDPE/(PE-g-PEG) blend melt-pressed for 45 min.(x), HDPE-10% clay processed in $scCO_2$ (O), HDPE/(PE-g-PEG) blend processed in $scCO_2$ (+), PE-g-PEG pure copolymer (□).

In contrast, intercalation is evident even in completely hydrophobic systems such as HDPE when processed in $scCO_2$, and the principal reflection of the clay changes from 9.3 to 7.0 (see Chapter 5). In fact, these results suggest that when a pure hydrophilic clay

system is used (MNa+), the change in the basal spacing of the clay is dictated by the presence of $scCO_2$ regardless of the nature of the polymer.

Sample description	**Type of clay**	**2θ (degrees)**	**d-spacing (Å)**
PE-g-PEG	-	-	-
Pure MNa+ clay	MNa+	9.3	9.51
PE-g-PEG Melt-pressed 15 min	MNa+	9.05	9.77
PE-g-PEG Melt-pressed 45 min	MNa+	9.05	9.77
HDPE Extruded with $scCO_2$	MNa+	7.0	12.63
HDPE/(PE-g-PEG) Extruded with $scCO_2$	MNa+	4.6	19.21

Table 6.3. WAXS results for various polyethylene-clay systems prepared with MNa+ clay. Shown are results for PE-g-PEG samples prepared by melt-pressing as well as HDPE and HDPE/PE-g-PEG blends prepared by $scCO_2$-extrusion. (Clay concentration 10%, PE-g-PEG copolymer with 5% PEG).

Experimental results suggest, however, that combining both effects ($scCO_2$-processing and enhanced hydrophilicity) can systematically control the degree of intercalation. In fact, when HDPE/(PE-g-PEG) blends are processed in $scCO_2$, the hydrophilicity of the system is enhanced by the PE-g-PEG copolymers, as a consequence, a more pronounced change in the scattering angle is observed and the maximum reflection appears at 4.6 degrees. As presented in table 6.3 this latter change in scattering angle corresponds to a 100% increase in the clay d-spacing, which represents a direct evidence of the influence of $scCO_2$ in the final morphology of the system.

It is important to point out that, when a completely hydrophilic clay is used (MNa+), intercalation appears only in $scCO_2$-processed samples, suggesting that even though the PE-g-PEG systems may be used to enhance the thermodynamic interactions between the polymer and the clay, $scCO_2$ has a predominant effect on the intercalation process, providing specific control over the degree of intercalation.

A similar behavior is observed in samples prepared with the modified clay (M15A), as presented in figure 6.5. In these systems, however, favorable interactions between the alkylammonium salt in the clay and the more hydrophilic PE-g-PEG systems occur. As a consequence, significant degrees of intercalation are observed even in melt-pressed PE-g-PEG samples. The intercalation process is evident and a considerable increase in the clay d-spacing is observed after melt pressing for 240 min.

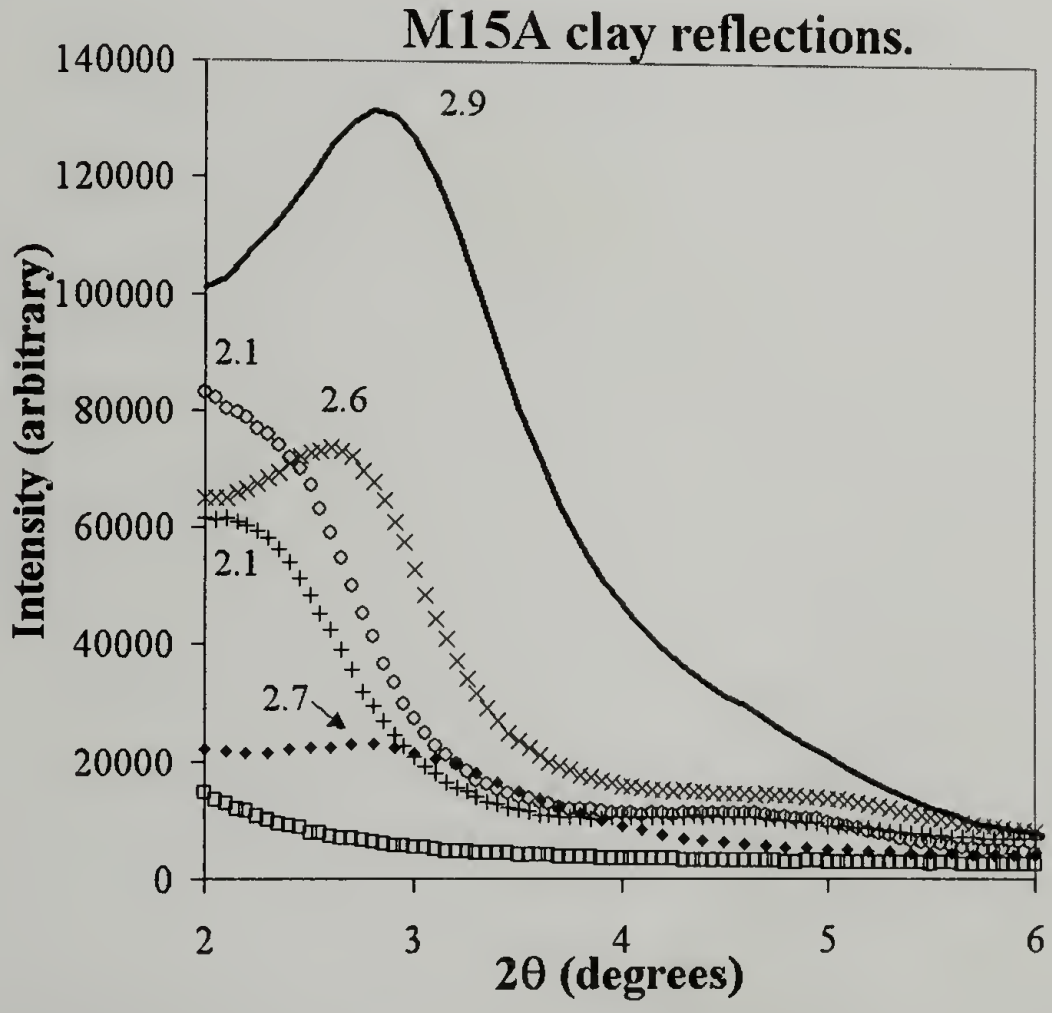

Figure 6.5. WAXS results for polyethylene samples processed with M15A clay. Pure M15A clay (—), HDPE/(PE-g-PEG) blend melt-pressed for 140 min.(x), HDPE/(PE-g-PEG) blend melt-pressed for 240 min.(o), HDPE-10% clay processed in $scCO_2$ (♦), HDPE/(PE-g-PEG) blend processed in $scCO_2$ (+), PE-g-PEG pure copolymer (□).

Also in this case, processing in $scCO_2$ appears to have a significant effect in the intercalation process and so in the structure of the nanocomposites. As shown in table 6.4, the presence of $scCO_2$ appears to control the rate at which intercalation takes place, obtaining the same degree of intercalation at smaller times during a single extrusion operation. After processing with $scCO_2$ (140 min. aprox.), the clay d-spacing changes from 30.46 Å to 42.07 Å, suggesting that even in this case, where a favorable enthalpic interaction is present, the addition of $scCO_2$ enhances the kinetics of the melt intercalation process.

Sample description	**Type of clay**	**2θ (degrees)**	**d-spacing (Å)**
PE-g-PEG	-	-	-
Pure M15A clay	M15A	2.9	30.46
PE-g-PEG (melt-pressed 140 min)	M15A	2.6	33.98
PE-g-PEG (melt pressed 240 min)	M15A	2.1	42.07
HDPE with $scCO_2$	M15A	2.7	33.72
HDPE/(PE-g-PEG) processed with $scCO_2$	M15A	2.1	42.07

Table 6.4. WAXS results for various polyethylene-clay systems prepared with M15A clay. Shown are results for PE-g-PEG samples prepared by melt-pressing as well as HDPE and HDPE/PE-g-PEG blends prepared by $scCO_2$-extrusion. (Clay concentration 10%, PE-g-PEG copolymer with 5% PEG)

As depicted in figure 6.6, the morphology of these systems, analyzed by TEM, suggests the presence of regions of high clay concentration dispersed throughout the polyethylene matrix. Within these regions, as supported by WAXS, the clay platelets

maintain their typical layered structure, as described in figures 6.4 and 6.5, and intercalation of polymer chains into the clay is monitored through changes in the basal clay spacing.[76-78]

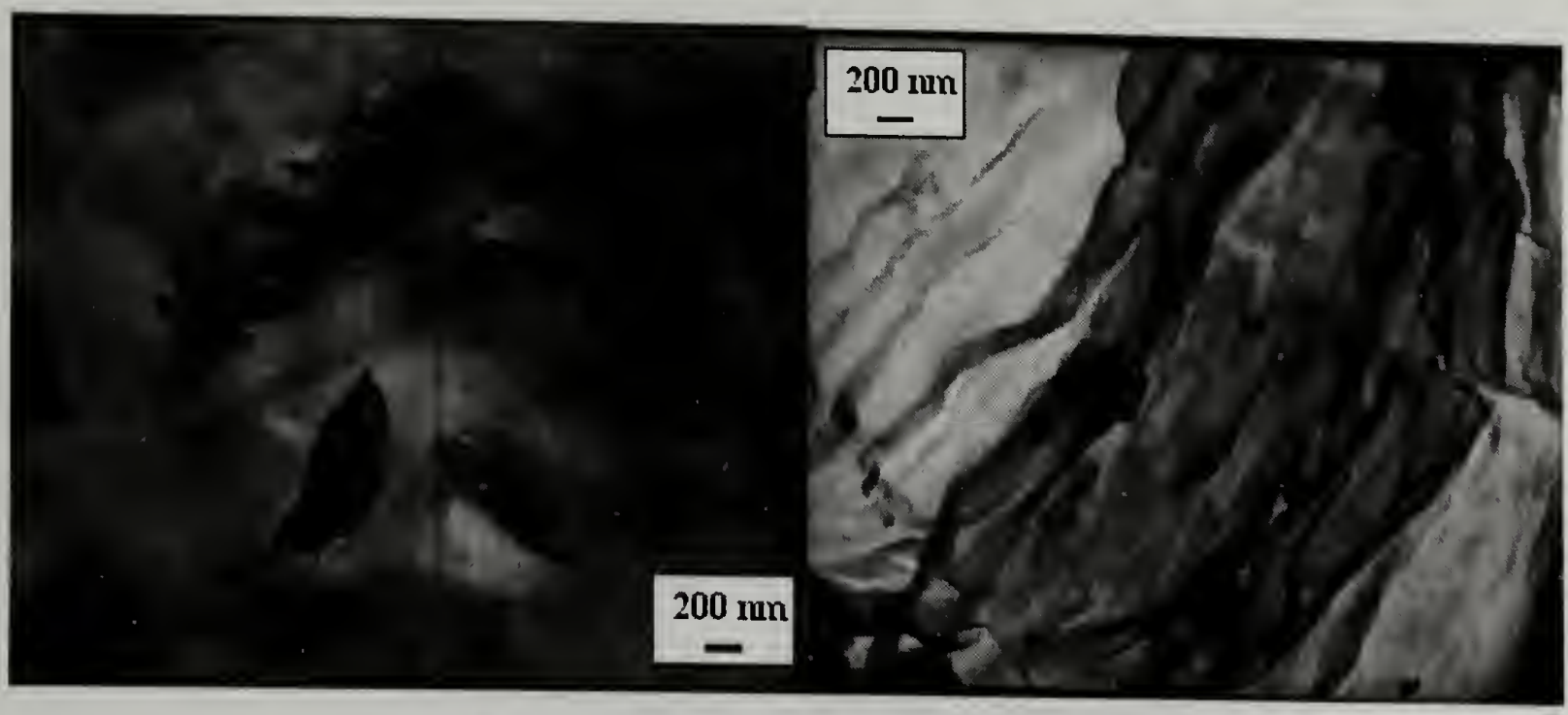

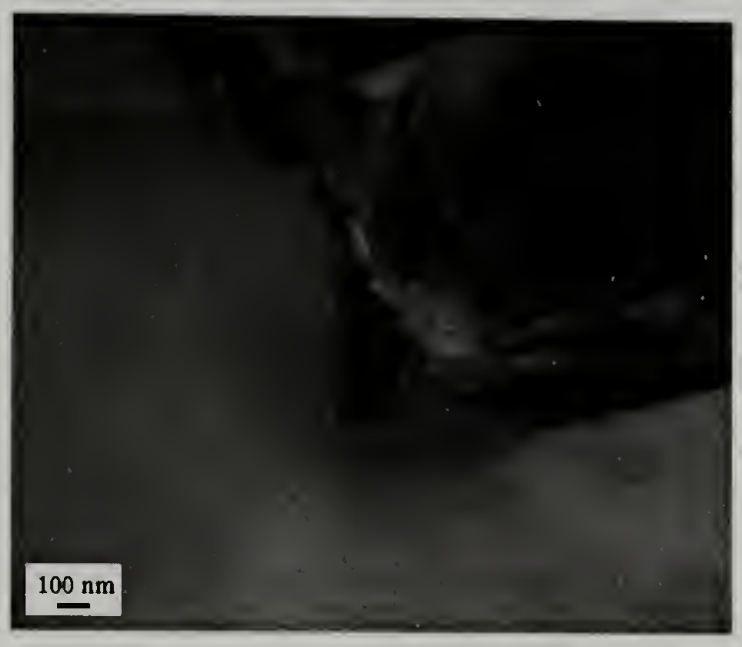

Figure 6.6. TEM images of an HDPE/(PE-g-PEG) sample processed in $scCO_2$. In these images there is evidence of regions of high clay concentration and layered structures in the surface of the sample due to the presence of the clay dispersion in the polymer matrix.

The morphology presented in figure 6.6, correlates with that typically observed in intercalated systems as shown in figure 6.7, for the case of epoxy systems. However, as shown in figure 6.6, clay aggregation is evident in these systems, and micron-sized clay agglomerates are observed. This morphology suggests that the clay dispersion is not completely homogeneous, probably due to the high concentration of clay (10%),

something that could have a detrimental effect on the physical properties of the composite.

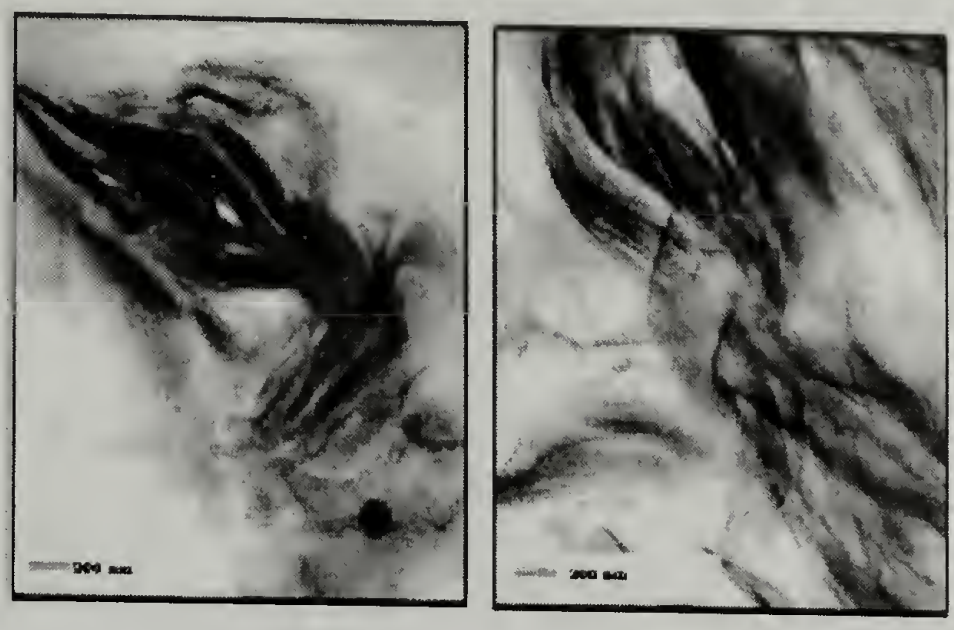

Figure 6.7. TEM images of intercalated structures.[62]

Now, as mentioned before, 2% PEG systems are used to understand the influence of the intercalated/exfoliated structure on the final properties of these composites.

As described before, the thermal behavior of the 2% PEG copolymers is similar to that observed in polyethylene. However, as shown in table 6.5, significant differences between these two systems exist. PE-g-PEG and HDPE samples, prepared in the presence of both types of clay by melt pressing differ both in melting points and overall crystallinity. HDPE systems in general show larger values of crystallinity and higher melting points, suggesting the specific contribution of the PEG groups to the crystalline behavior of the PE-g-PEG copolymers, reducing both the crystal size and the perfection of the crystals, and probably acting as defects in the crystallization process. The contribution of clay to the overall crystallinity in these systems is not evident, which might be related to the incipient mixing during melt-pressing that promotes non-homogeneous dispersion of the clay.

Sample	Tm (°C)	ΔHm (J/g)	Crystallinity (%)
HDPE	131.76	190.7	66.01
HDPE-MNa+	132.60	162.8	62.61
HDPE-M15A	134.21	158.5	60.96
PEgPEG	130.68	127.9	44.27
PEgPEG-MNa+	128.79	120.1	46.19
PEgPEG-M15A	129.63	124.6	47.92

Table 6.5. Thermal behavior comparison between PE-g-PEG (2% PEG) and HDPE systems obtained by melt-pressing with different clay systems. Degree of crystallinity is calculated with respect to polyethylene using 288.89 J/g as the theoretical heat of fusion.

In this regard, it is believed that the dispersion of the clay in these samples, and as a consequence, the intercalation process, might be promoted at longer processing times. To understand the influence of processing time on both the thermal behavior and structure of the composite, pure PE-g-PEG samples are prepared with clay (10%) by melt-pressing using various processing times. The results in terms of the thermal behavior are presented in table 6.6.

Sample	Clay	Time (min)	Tm (°C)	ΔHm (J/g)	Crystallinity (%)
PE-g-PEG	MNa+	45	128.79	112.8	43.37
PE-g-PEG	MNa+	140	129.67	110.5	42.48
PEgPEG	M15A	45	129.63	118.6	45.61
PEgPEG	M15A	140	128.84	111.2	42.76
PEgPEG	M15A	240	129.25	116.3	44.72

Table 6.6. Thermal behavior of PE-g-PEG (2% PEG) systems obtained after melt-pressing at different processing times using both types of clay. Degree of crystallinity is calculated with respect to polyethylene using 288.89 J/g as the theoretical heat of fusion.

From this table, it is evident that the thermal behavior is independent of the processing time, and also, similar values of melting point and crystallinity are obtained regardless of the type of clay employed, suggesting again that the chemical nature of the clay is irrelevant for the crystallization process, which is only dictated by the availability of particles to nucleate.

Sample	2θ (degrees)	d-spacing (Å)
MNa+	9.3	9.51
PE-g-PEG	N/A	N/A
PE-g-PEG/MNa+ (45 min melt press)	9.33	9.46
PE-g-PEG/MNa+ (140 min melt press)	9.28	9.52
M15A	2.9	30.46
PE-g-PEG/M15A (45 min melt press)	2.18	40.47
PE-g-PEG/M15A (140 min melt press)	2.41	36.61
PE-g-PEG/M15A (240 min melt press)	2.25	39.21

Table 6.7. WAXS results of PE-g-PEG-clay systems produced by melt-pressing using different processing times (PE-g-PEG copolymer with 2% PEG).

According to WAXS, the structure of these systems does not show significant changes as well. In fact, no intercalation is detected for systems with the unmodified clay (MNa+). These results correlate with our previous observations in 5% PEG systems, suggesting that the enhanced hydrophilicity of these copolymers is not sufficient to overcome the energy required in the intercalation process, and that in general, the hydrophilic nature of the MNa+ clay restricts the intercalation process. In these systems,

as shown in table 6.7, the d-spacing remains unchanged (9.5 Å). In contrast, systems prepared with the modified clay M15A show a definite increase in the basal spacing of the clay, changing from 30.5 Å to values around 40 Å. As discussed before, the affinity between the hydrophilic PEG group in the copolymer and the modified clay, promotes a better interaction between the two, which is enough to overcome the energetic penalties of intercalation.

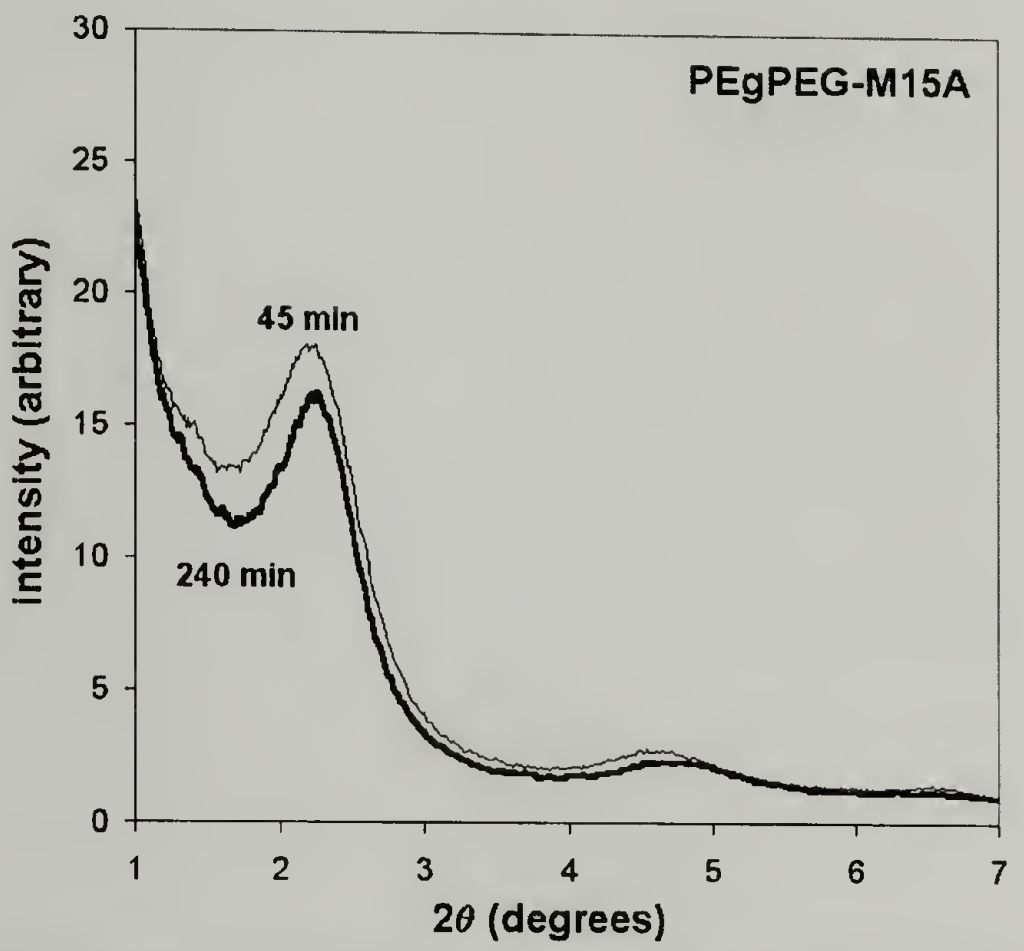

Figure 6.8. WAXS results of PE-g-PEG/M15A clay systems produced by melt-pressing using different processing times (PE-g-PEG copolymer with 2% PEG).

However, it is important to realize that the degree of intercalation is not dictated by the processing time, and apparently the structure obtained at 45 min. is almost identical to that observed after 240 min., suggesting that a processing time of 45 min. is enough to reach an equilibrium condition. The scattering pattern of these two samples is shown in figure 6.8.

From the results obtained previously in 5% PEG systems, it is evident that the clay concentration used (10%) is too large, promoting significant aggregation of the clay that,

as mentioned before, could lead to detrimental properties. To overcome this, copolymers with 2% PEG are used in a very efficient way to prepare HDPE/PE-g-PEG blends, reducing the clay concentration (from 10% to 4%), tuning the ratio of clay/PEG in the system, with the expectation of adjusting the degree of intercalation to produce materials that could help us to understand the influence of structure on the final properties of the composite.

The thermal behavior of these blends, processed with and without CO_2 using both clay systems is summarized in table 6.8. As compared with the behavior presented in figure 6.3 for 5% PEG copolymers, where a bimodal melting behavior is observed, these systems show only one melting endotherm due to the small concentration of copolymer in the blend.

Sample	Clay	Tm (°C)	ΔHm (J/g)	Crystallinity (%)
HDPE-PEgPEG Extruded with CO_2	MNa+	132.13	160.7	57.94
HDPE-PEgPEG Extruded without CO_2	MNa+	133.39	155.1	55.92
HDPE-PEgPEG Extruded with CO_2	M15A	132.31	159	57.33
HDPE-PEgPEG Extruded without CO_2	M15A	131.92	163.3	58.88

Table 6.8. Thermal behavior of HDPE/PE-g-PEG (2% PEG) blends produced by extrusion with and without $scCO_2$ using different clay systems. Degree of crystallinity is calculated with respect to polyethylene using 288.89 J/g as the theoretical heat of fusion.

The effect of the copolymer is shown in the slightly reduced crystallinity as compared to the typical values observed in HDPE systems. Once again, it appears that the chemical

nature of the clay does not affect the thermal behavior, and the melting points and crystallinity is similar for all the samples included in this table.

Now, in terms of structure, as presented in figure 6.9 and table 6.9, once again the use of $scCO_2$ appears to promote significant improvements in the melt intercalation process even in systems where the completely hydrophilic clay (MNa+) is used. As shown in figure 6.9, the shift in the principal reflection of the clay to lower angles is evident, moving from 9.3 to 6.45 degrees, which as presented in table 6.9 corresponds to a 43 % increase in the clay d-spacing, expanding the clay from 9.51 Å to 13.68 Å.

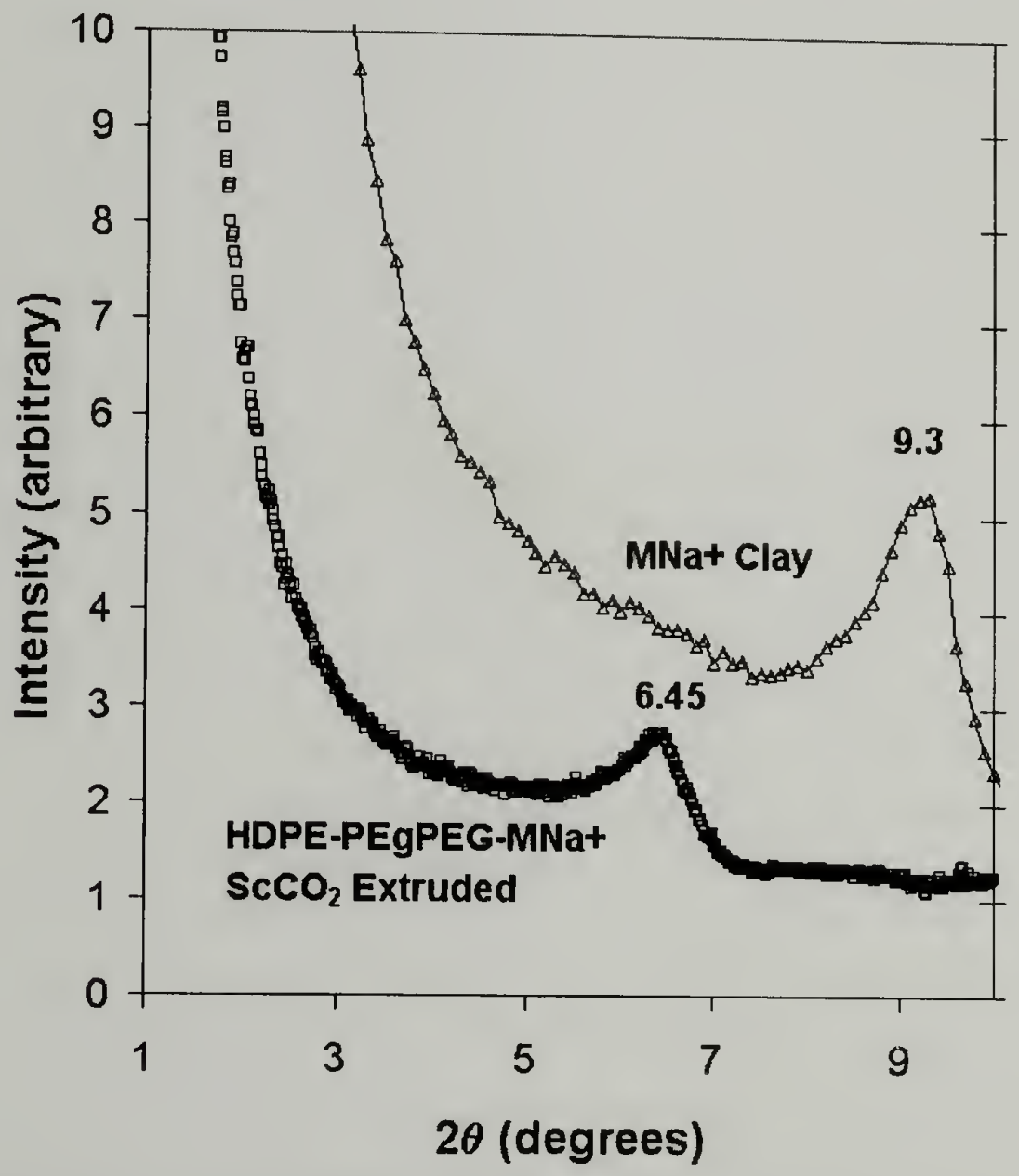

Figure 6.9. WAXS results of HDPE/PE-g-PEG blends produced by $scCO_2$-extrusion using MNa+ clay. (PE-g-PEG copolymer with 2% PEG).

Sample	2θ (degrees)	d-spacing (Å)
MNa+	9.3	9.51
HDPE-MNa+ in CO_2	7.0	12.63
HDPE/PE-g-PEG blend with MNa+ Extruded without CO_2	9.3	9.51
HDPE/PE-g-PEG blend with MNa+ Extruded in CO_2	6.45	13.68

Table 6.9. WAXS results of HDPE/PE-g-PEG blends produced by scCO_2-extrusion using MNa+ clay. (PE-g-PEG copolymer with 2% PEG).

As shown in this table, this change is even larger than that observed in HDPE, described in Chapter 5, suggesting a clear contribution of the presence of the copolymer on the degree of intercalation. Apparently by reducing the amount of clay used, the ability of the PE-g-PEG copolymers to enhance the interactions with the clay increases, having a direct effect on the intercalation process. It is important to note again that the intercalation is only observed in scCO_2-extruded samples, and as shown in table 6.9, conventional extrusion (without CO_2) does not render an intercalated structure, having no effect on the clay d-spacing.

As in the case of 5% PEG systems, the use of modified M15A clay significantly enhances the degree of intercalation. As presented in figure 6.10, in this case intercalation is evident even in systems prepared by conventional extrusion due to the favorable interactions between the modified clay and the PE-g-PEG, which enhances the interactions with the clay in a very efficient manner.

The structure of the system prepared by conventional extrusion is such that the dispersion of the clay is high but it is not completely homogeneous (partially exfoliated), and individual clay platelets still have enough interaction between them to be able to

show a typical basal spacing between them (partially intercalated). In other words, this structure is basically a mixture between an intercalated and an exfoliated system, where the degree of intercalation is extremely large, showing a pronounced change in the d-spacing, as shown in table 6.10.

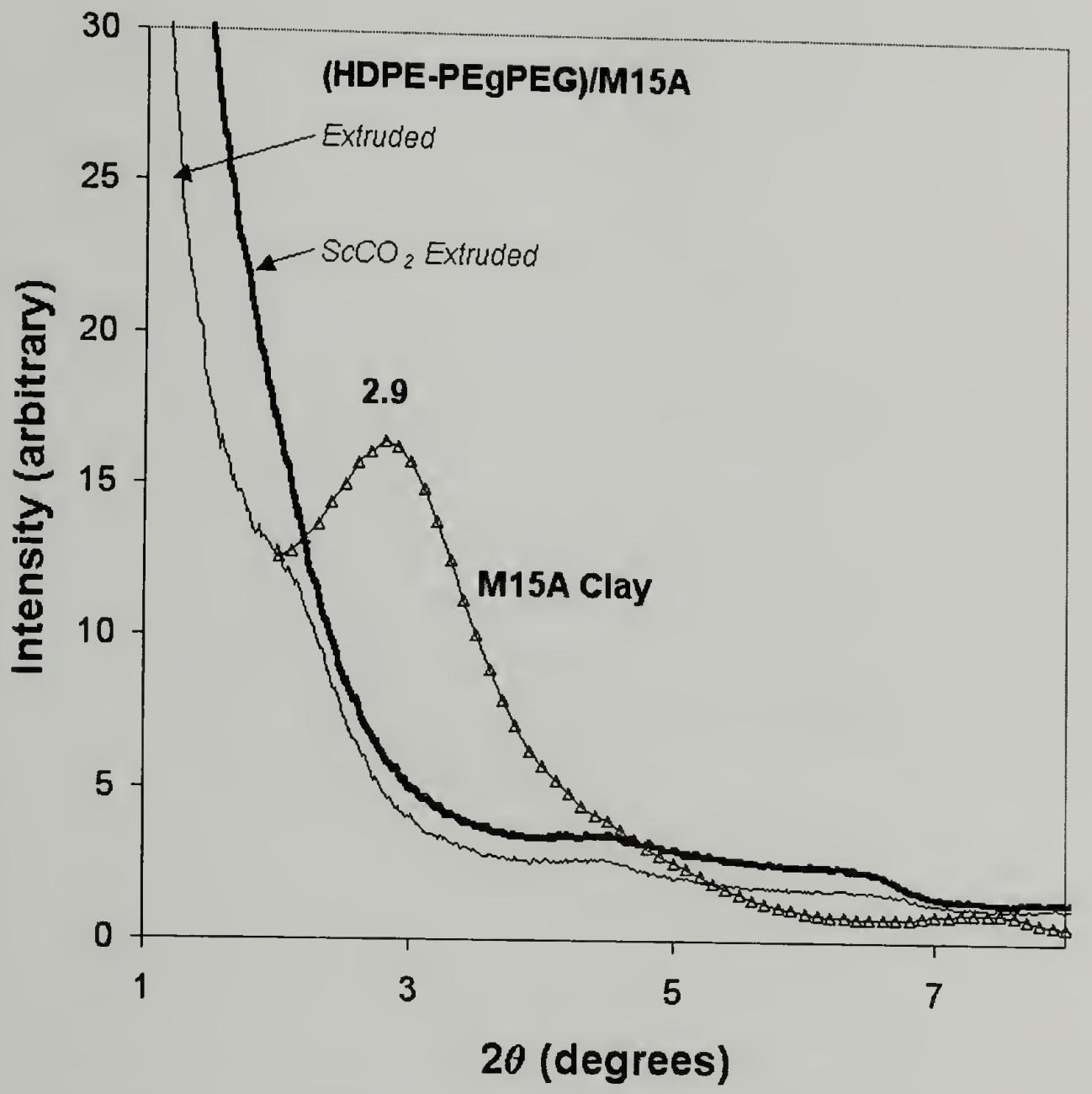

Figure 6.10. WAXS results of HDPE/PE-g-PEG blends produced by extrusion with and without $scCO_2$ using M15A clay. (PE-g-PEG copolymer with 2% PEG).

In contrast, the scattering pattern of the system prepared by $scCO_2$-extrusion shows a dramatic intensity fall at low angles, displaying no reflection in this range. In this system there is no indication of a characteristic scattering distance in this range, showing in fact, that the order of the clay has been completely lost due to complete intercalation of the polymer.

This structure corresponds to a completely exfoliated system where the dispersion of the clay throughout the polymer matrix is homogeneous and the individual clay platelets are not able to interact between them any more.

Sample	2θ (degrees)	d-spacing (Å)
M15A	2.9	30.46
HDPE/PE-g-PEG blend with M15A clay processed without CO_2	1.49	59.22
HDPE/PE-g-PEG blend with M15A clay processed with CO_2	N/A	Exfoliated

Table 6.10. WAXS results of HDPE/PE-g-PEG blends produced by extrusion with and without $scCO_2$ using M15A clay. (PE-g-PEG copolymer with 2% PEG).

Dynamic Mechanical Analysis (DMA) is used to study the effect of the structure of all the systems described in this section on their final properties. Rectangular samples of 1.25 in by 0.5 in (1/16 in thick) are prepared and analyzed using a single cantilever beam clamp in a DMA 2980 Dynamic Mechanical Analyzer from TA Instruments. In general, samples are subjected to two different experiments: a) a temperature sweep from –140 °C to 80 °C at a deformation frequency of 1 Hz and a heating rate of 3 °C/min. and b) a frequency sweep at room temperature (25 °C) in the range of 100-0.1 Hz.

Figures 6.11 and 6.12 describe the behavior of PE-g-PEG samples prepared by melt-pressing in the presence of both types of clay (10%). As described before in table 6.10, the structure of these systems show significant differences. The PE-g-PEG system prepared with the modified M15A clay displays an intercalated structure, while a

conventional composite morphology is observed in the presence of the MNa+ clay, without any indication of intercalation.

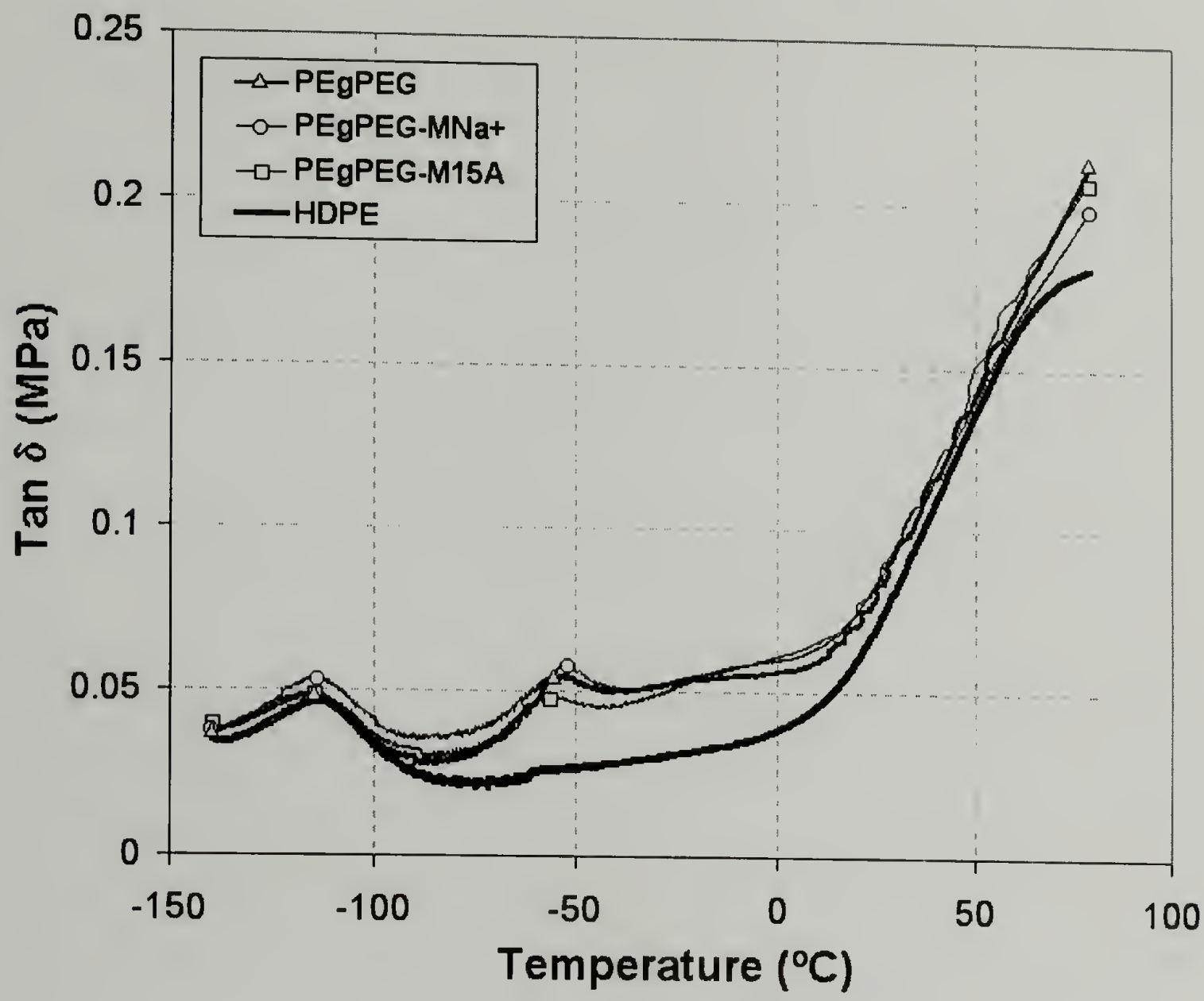

Figure 6.11. Tan δ of PE-g-PEG systems produced by melt pressing (Copolymer with 2% PEG). Included for comparison is the behavior observed in HDPE.

The behavior of Tan δ (G''/G') with temperature is presented in figure 6.11. In general, PE-g-PEG systems display two glass transitions as judged by the maximum values obtained at around –115 °C and –55 °C, suggesting the appearance of microphase separation in these systems, related directly to the grafted structure and the amphiphilic nature of the copolymers. As shown in this figure an immiscible blend behavior is observed where at low temperatures the PE blocks, from both HDPE and the copolymer, go through their glass transition, while the PEG blocks from the copolymer stay in the

glassy state and display a clear glass transition at higher temperatures. This becomes evident when the behavior of pure HDPE is analyzed, where this latter transition is not present. In addition, the transition for the PE blocks is so broad, that as mentioned before is impossible to distinguish between HDPE and the PE blocks in the copolymer at this heating rate. As presented in table 6.11, the presence of clay promotes almost no effect on the Tg of these systems, and in fact, a slight decrease on Tg is observed in the conventional composite (with MNa+), where as the Tg of the intercalated system prepared with M15A remains unchanged.

Sample	Tg (PE) (°C)	Tg (PEG) (°C)	% Crystallinity
PEgPEG	-114.98	-55.43	44.27
PEgPEG-MNa+	-115.46	-51.43	46.19
PEgPEG-M15A	-115.71	-55.02	47.92
HDPE	-113.99	N/A	66.01

Table 6.11. Tg (from DMA) and % crystallinity for PE-g-PEG systems produced by melt-pressing (Copolymer with 2% PEG). Included for comparison are the values for HDPE.

The behavior for the storage modulus is presented in figure 6.12. At low temperatures the storage modulus of the PE-g-PEG systems is significantly higher than that observed in pure HDPE, due to the presence of PEG groups that remain in their glassy state at these conditions. However, an important observation is that the traditional composite system, prepared with unmodified MNa+ clay, displays a higher modulus than both the pure PE-g-PEG copolymer and the composite prepared with M15A. Apparently these results suggest that for the case of the PE-g-PEG/MNa+ system the traditional composite morphology, having micron-sized clay particles dispersed in the polymer matrix, without any type of interaction between the clay and the polymer, confers improved properties as

compared to the pure PE-g-PEG copolymer. As shown in figure 6.12, the increase at the lowest temperature is around 12 %. In contrast, the intercalated morphology observed in the PE-g-PEG/M15A system has no effect on its bulk properties. This lack of improvements in the properties appears to be related to the thermal behavior and stability of the modified M15A clay at typical processing temperatures. This effect will be described more in detail later in this section.

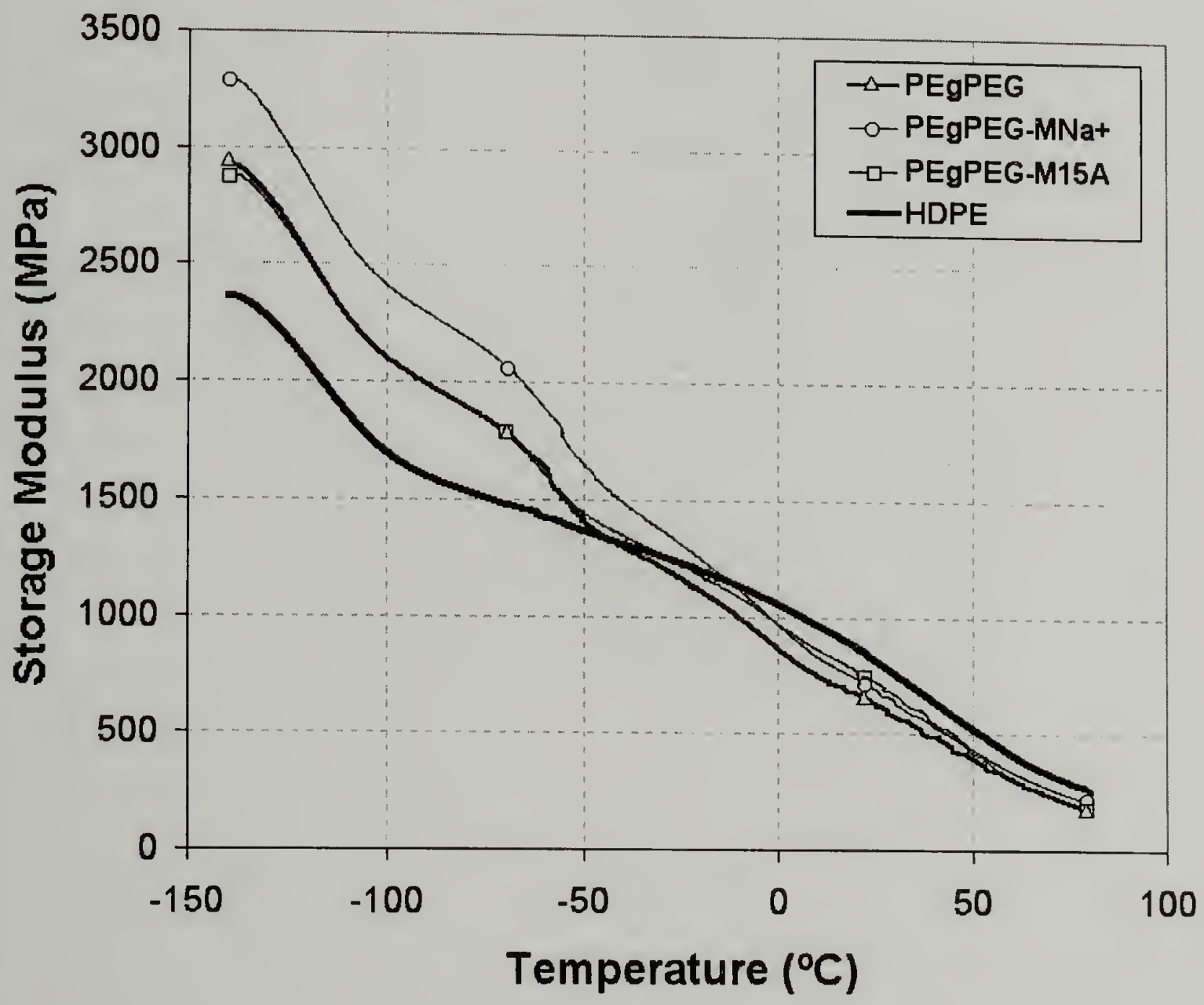

Figure 6.12. Storage Modulus of PE-g-PEG systems produced by melt pressing (Copolymer with 2% PEG). Included for comparison is the behavior observed in HDPE.

Now, as suggested before, using M15A clay in the processing of HDPE/PE-g-PEG blends has allowed access to both intercalated and exfoliated systems (figure 6.10). It is now of relevance to understand the specific influence of these morphologies in the bulk properties of these systems. The behavior of Tan δ for HDPE/PE-g-PEG blends prepared by extrusion with and without $scCO_2$ using M15A clay is presented in figure 6.13. As described earlier, in the presence of M15A clay, HDPE/PE-g-PEG blends produced by conventional extrusion display a highly intercalated structure, where as, $scCO_2$-extrusion produces blends with a completely exfoliated structure where the dispersion of the clay is homogeneous throughout the polymer matrix.

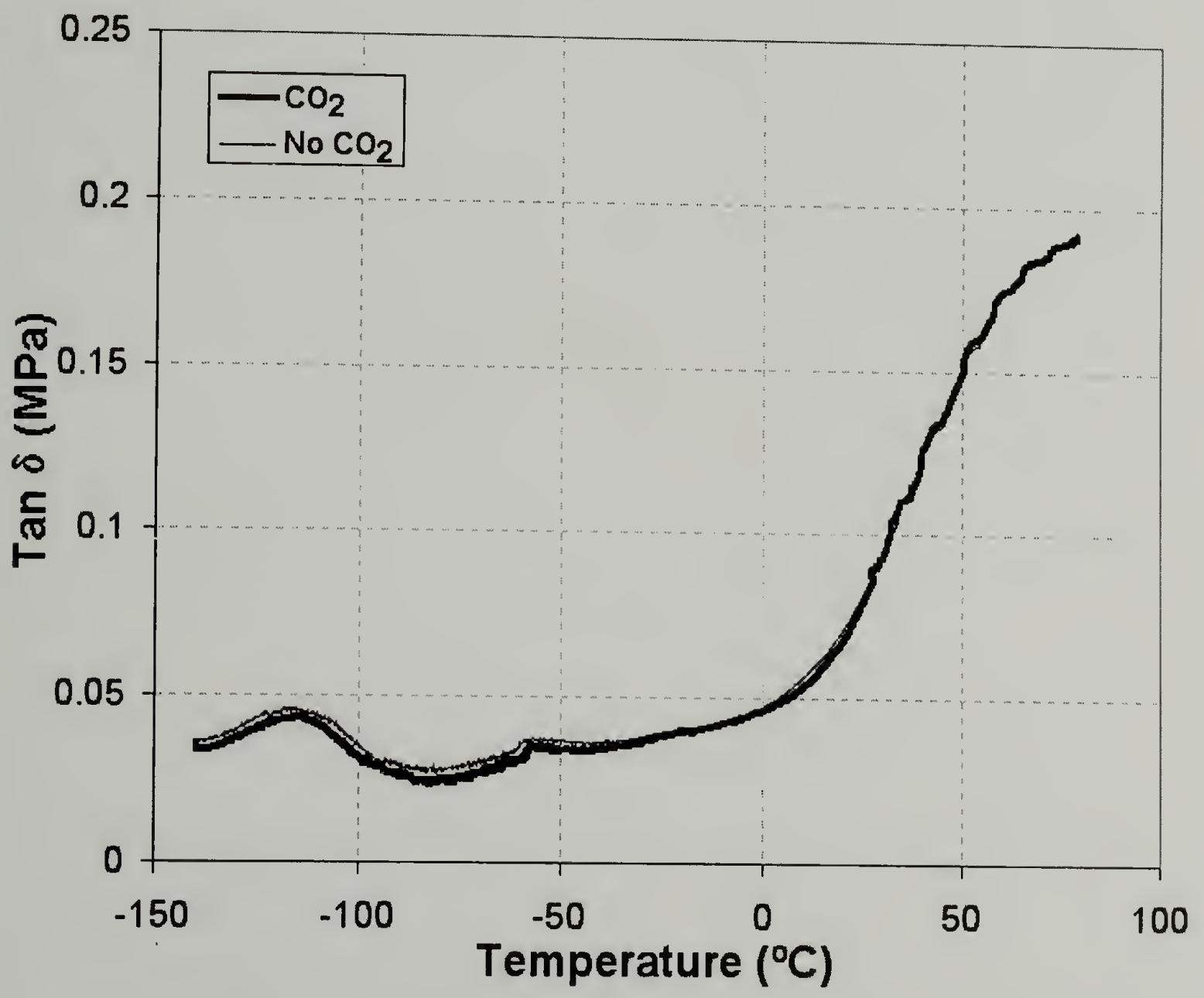

Figure 6.13. Tan δ of HDPE/PE-g-PEG blends produced by extrusion with and without $scCO_2$ using M15A clay. (Copolymer with 2% PEG).

As shown in this figure, once again an immiscible blend behavior is observed regardless of the structure, displaying two glass transitions temperatures (around –115 °C and –55 °C), suggesting the appearance of microphase separation, related to the grafted architecture and amphiphilic nature of the copolymers. Also no effect on the Tg of these systems is observed, as presented in table 6.12.

Sample	Tg (PE) (°C)	Tg (PEG) (°C)	% Crystallinity
PEgPEG	-114.98	-55.43	44.27
HDPE-PEgPEG blends with M15A clay Extruded without CO_2	-117.07	-56.98	58.88
HDPE-PEgPEG blends with M15A clay Extruded with CO_2	-115.32	-56.44	57.33
HDPE	-113.99	N/A	66.01

Table 6.12. Tg (from DMA) and % crystallinity HDPE/PE-g-PEG blends produced by extrusion with and without $scCO_2$ using M15A clay. (Copolymer with 2% PEG). Included for comparison are the values for HDPE and PE-g-PEG.

For these systems, the behavior of the storage modulus is presented in figure 6.14. Once again, results suggest that the bulk properties are almost independent of the clay dispersion and the structure of the nanocomposite. Differences between these two systems are only evident at low temperatures, where as expected, the storage modulus of the system prepared by $scCO_2$-extrusion (exfoliated) is higher than that produced by conventional extrusion (intercalated). As shown in this figure, the difference in modulus between these two systems at the lowest temperature is only around 5 %. Although this difference is very small, it represents an increase of 20% in modulus with respect to pure HDPE, reaching the properties observed in the pure PE-g-PEG copolymer, which as described before is intractable and difficult to produce in substantial quantities.

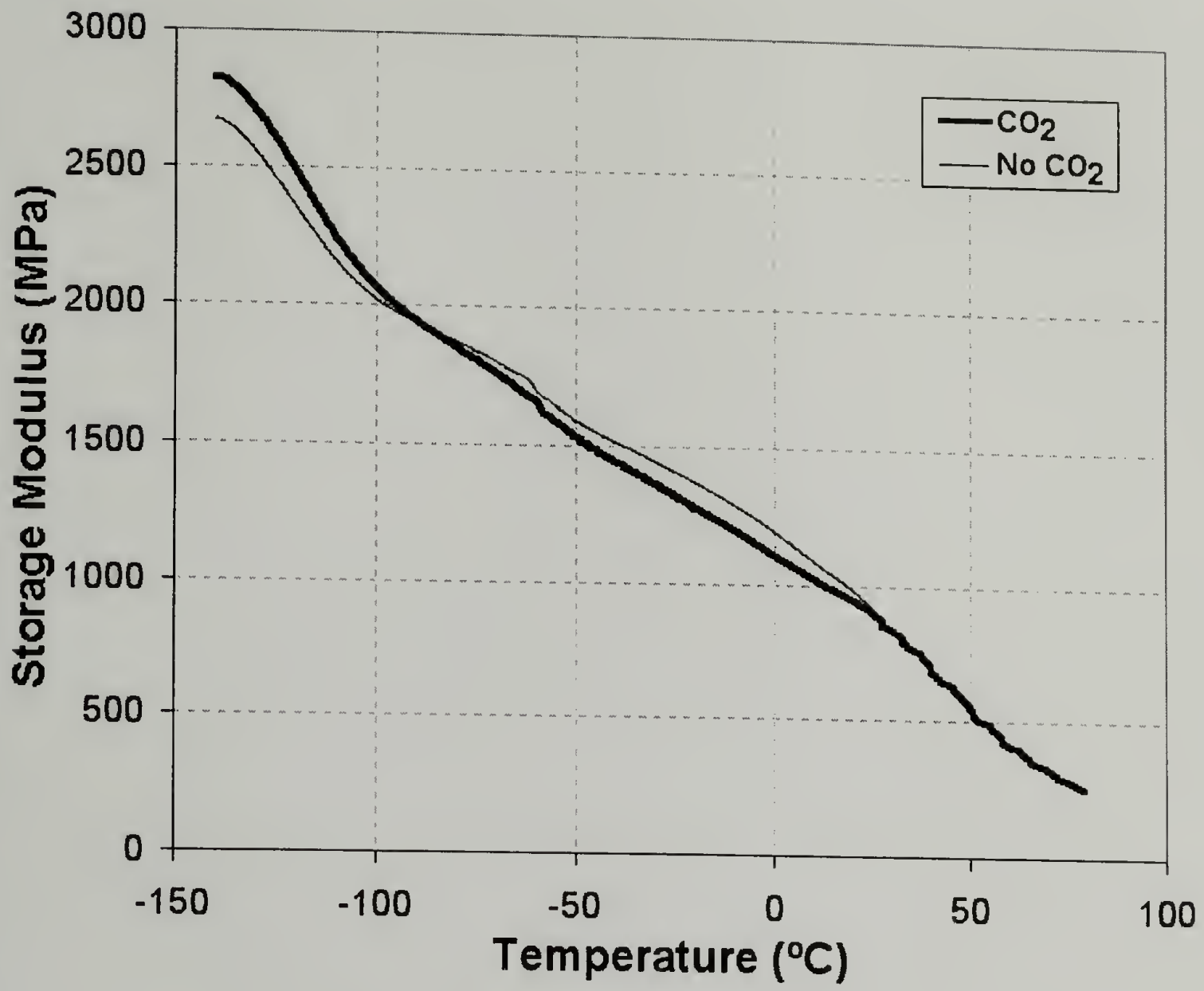

Figure 6.14. Storage Modulus of HDPE/PE-g-PEG blends produced by extrusion with and without $scCO_2$ using M15A clay. (Copolymer with 2% PEG).

Now, the effect of structure (intercalated or exfoliated) in the bulk properties is evident for the case of HDPE/PE-g-PEG blends prepared by extrusion with and without CO_2. However, as suggested before, in systems where the degree of intercalation is not as high and the clay dispersion is not as homogeneous as in these cases, the effect of structure in the final properties is not evident. In fact, as mentioned earlier, better properties are observed in traditional composites prepared with MNa+ clay than in intercalated systems prepared with the modified M15A clay.

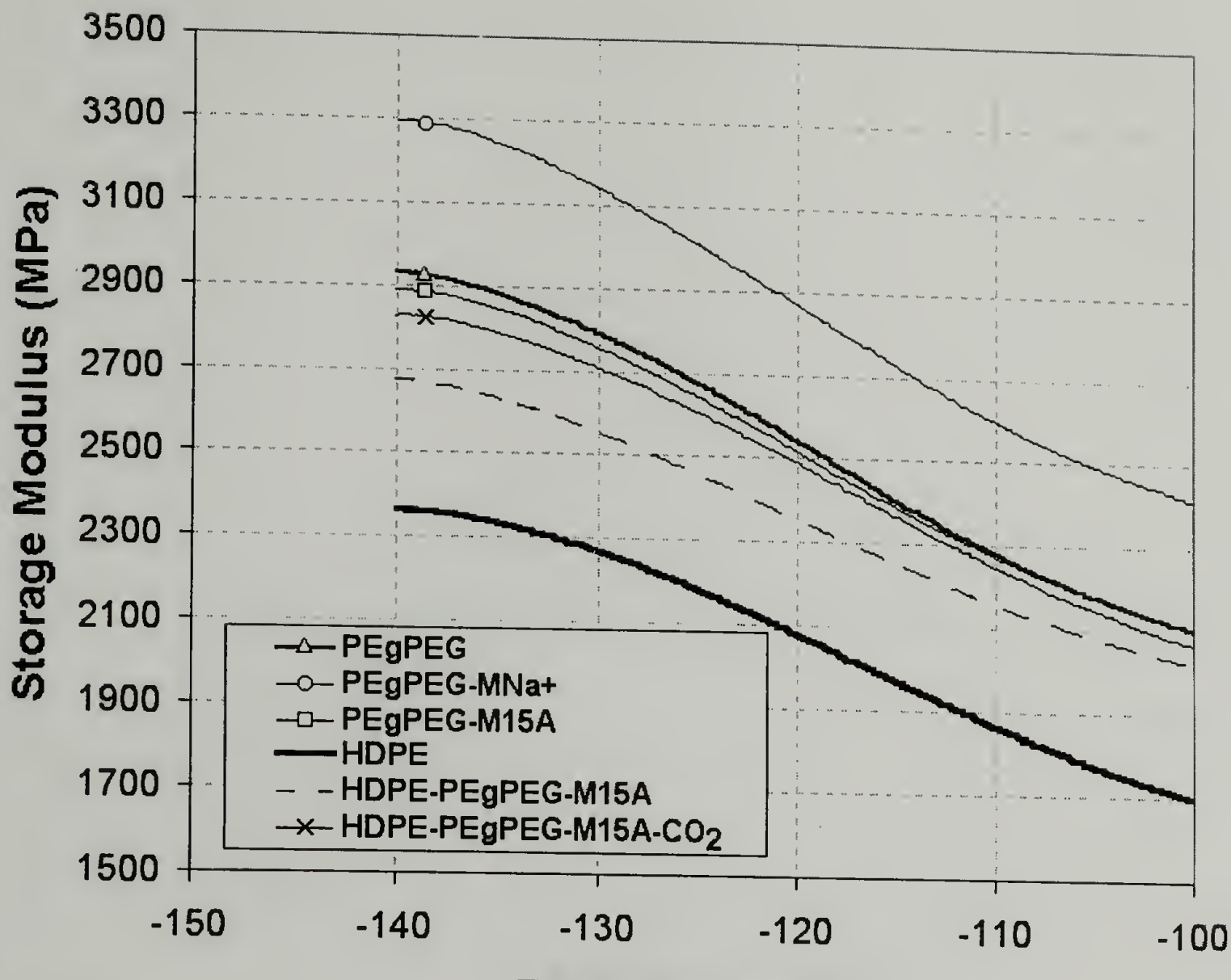

Figure 6.15. Storage Modulus at low temperatures of polyethylene-based systems produced by different routes using M15A clay. (Copolymer with 2% PEG).

This effect is clearly depicted in figure 6.15, where the storage moduli of various polyethylene-based systems are compared. It is evident that the well-known favorable contribution to the properties, brought about by the observed intercalated structure, is somehow balanced by another factor that has a detrimental effect in the modulus. Since this effect is present only in systems prepared with the modified M15A clay, it is believed that it might be related to the intrinsic physical characteristics of this system.

As mentioned in Chapter 5, the modified clay (M15A) is a surface-modified montmorillonite produced by a cation exchange reaction wherein sodium from natural montmorillonite (MNa+) is replaced by a long alkylammonium salt. The intrinsic

properties of this modifier dictate the interaction of this system with a certain polymer. One of the major concerns about using modified clay systems in typical processing techniques is their thermal stability and specific inorganic-organic content.

In order to understand further the contributions of these factors to our experimental observations, samples containing both types of clay are prepared and their thermal behavior is compared using Thermogravimetrical Analysis (TGA).

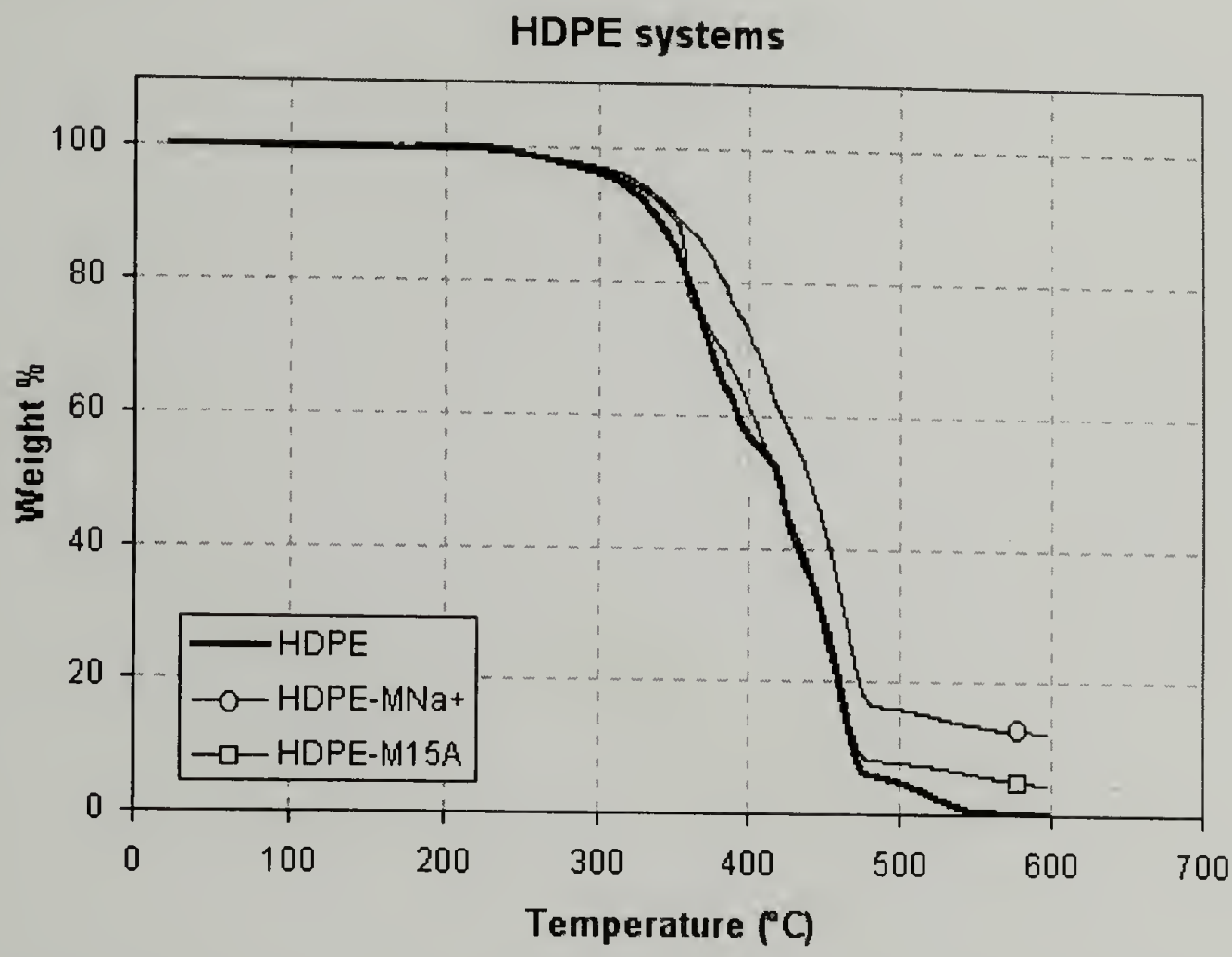

Figure 6.16. TGA results of HDPE systems produced by melt-pressing with different types of clay.

Figure 6.16 shows the TGA trace of HDPE samples prepared by melt-pressing containing approximately 10% wt. of clay. The behavior for pure HDPE is also shown for comparison. As suggested in this figure, regardless of the presence of clay or type of clay employed, the materials start to decompose when a temperature of 250 ˚C is reached. This decomposition process is dramatically enhanced at high temperatures and the polymer is completely consumed before the end of the test.

However, it is important to point out that the char yield is dramatically different in systems prepared with different clays. In the HDPE-MNa+ sample, 12.45% of the initial sample mass is recovered as char yield after the test is completed. This mass percentage relates to the amount of clay used to prepare the sample, or in other words, to its inorganic content. The concentration of inorganic material in this case is very close to the expected clay concentration. In contrast, in the HDPE-M15A sample the char yield is significantly lower. Only 4.57 % of the initial sample mass is recovered at the end of the test, suggesting that the inorganic content of this sample is much smaller. In fact, the concentration of inorganic material in this case is almost half of the expected clay concentration, suggesting that the alkylammonium salt modifier represents 50% of the total mass of the M15A clay system.

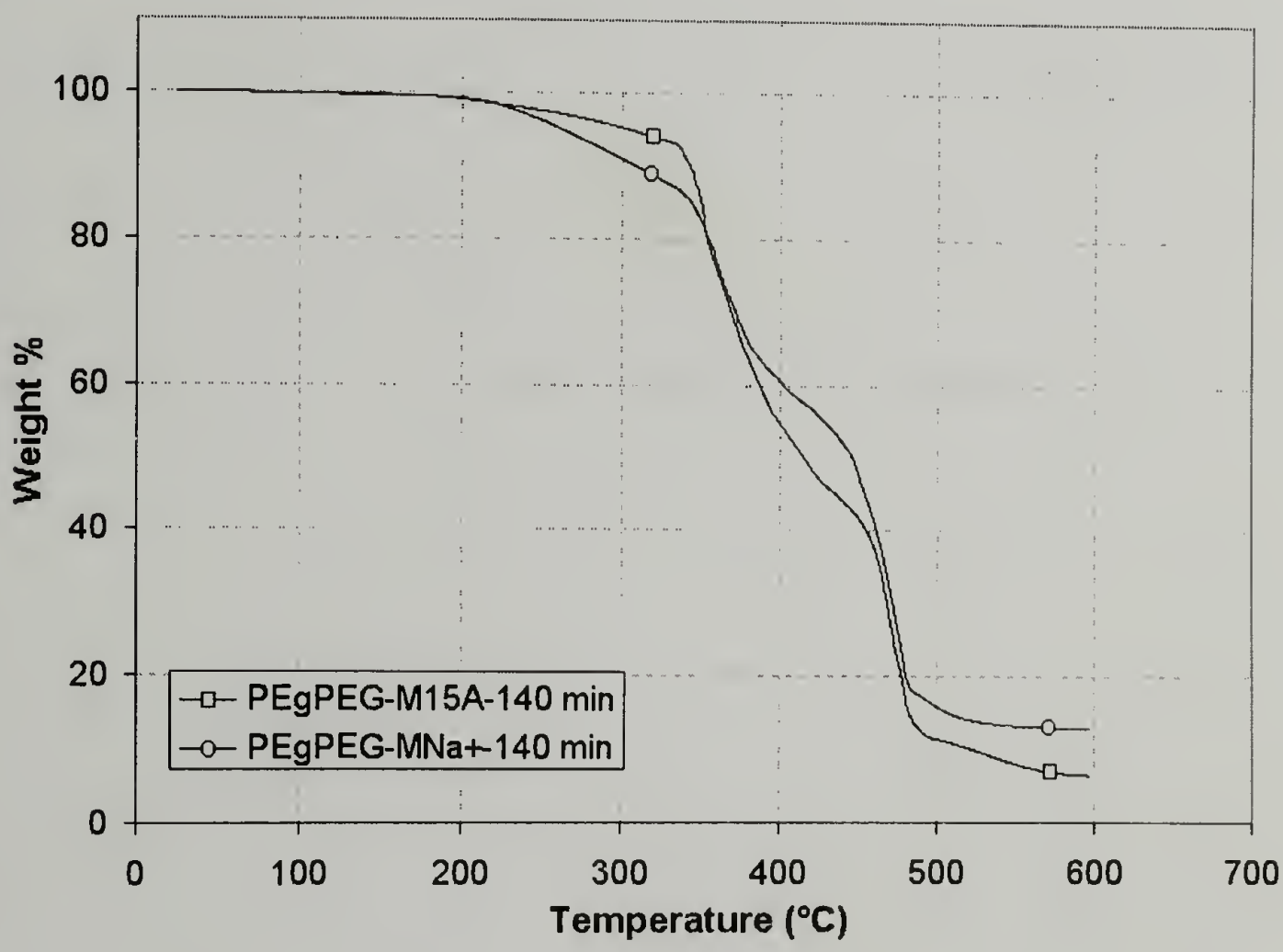

Figure 6.17. TGA results of PE-g-PEG systems produced by melt-pressing with different types of clay.

The same behavior is observed in PE-g-PEG systems as described in figure 6.17. These samples are also prepared by melt-pressing using approximately 10% wt. of clay. Again, regardless of the presence of clay or type of clay employed, decomposition is evident above 200 ˚C and the polymer is completely consumed at high temperatures. As in the case of HDPE samples, the char yield is dramatically different between these two systems. The PE-g-PEG/MNa+ sample shows a 12.96 % char yield after the test is completed, which again relates to the amount of clay used initially to prepare the sample. In contrast, the PE-g-PEG/M15A sample has a significantly lower char yield (6.45 %), suggesting again that for this clay system the inorganic content of this sample is only around 50% of the total mass of the clay.

Evidently, the stability of the modifier in M15A clay is reduced and most likely, even lower than that observed in high molecular weight polymers. After decomposition, the affinity and molecular similarity to conventional hydrocarbons of these modifiers, may promote them to act as plasticizers to the polymer, thus reducing in a significant way its bulk properties. This effect will act opposite to the expected improvement in properties due to the intercalated structure. As a consequence, the final properties of the structured system will be very similar to those observed originally in the polymer.

As compared to the unmodified clay system (MNa+), the reduced inorganic content along with the low thermal stability of the modifiers introduced in the modified clay (M15A) at typical processing temperatures, might be related to the observed lack of improvements in these systems. It is believed that this effect prevents the intercalated structure, observed for example in the PE-g-PEG/M15A sample, from enhancing its bulk

properties, and as a consequence, the melt-intercalation process does not provide a property-enhancement route to this system.

6.3.2. Polymer nanocomposites prepared by the addition of polyamines with controlled amine density

Herrera-Alonso and McCarthy[68] have reported the possibility of developing specific synthetic routes to produce surfaces with varying amine density, based on the chemical reduction of polyamides. The general idea of this type of chemistry is presented in figure 6.18.

Figure 6.18. Chemistry used to produce surfaces with varying amine densities.[68]

Recently, they have analyzed the possibility of using this chemistry for the reduction of commercially relevant nylon systems from the bulk, showing promising results for a variety of systems including Nylon 6/6, Nylon 6/9 and Nylon 4/6. The resulting material is a polyamine with different methylene/amine ratios, where the chemical structure is dictated by the parent nylon employed in the reduction, as shown in figure 6.19.

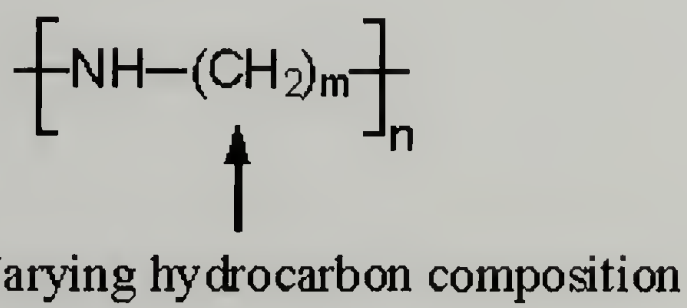

Figure 6.19. General chemical structure of polyamines used in this study.

The specific details of this reaction are shown in figure 6.20. As suggested, the reduction of the corresponding nylon system is done in a BH_3-THF solution, and in general, it involves the creation of a borane-amine complex that can be dissociated in both acidic and basic conditions. The relevance of these two possible synthetic routes is that the final properties of the resulting polyamine are dictated by the reduction conditions.

If an acidic medium is chosen and hydrochloric acid (HCl) is introduced to dissociate the borane-amine complex, the resulting polymer is effectively charged, creating a polyelectrolyte with controlled charge density, dictated by the structure of the parent nylon. Due to charge interactions (repulsions), the ability of this polyelectrolyte to crystallize is restricted and a completely amorphous system is obtained.

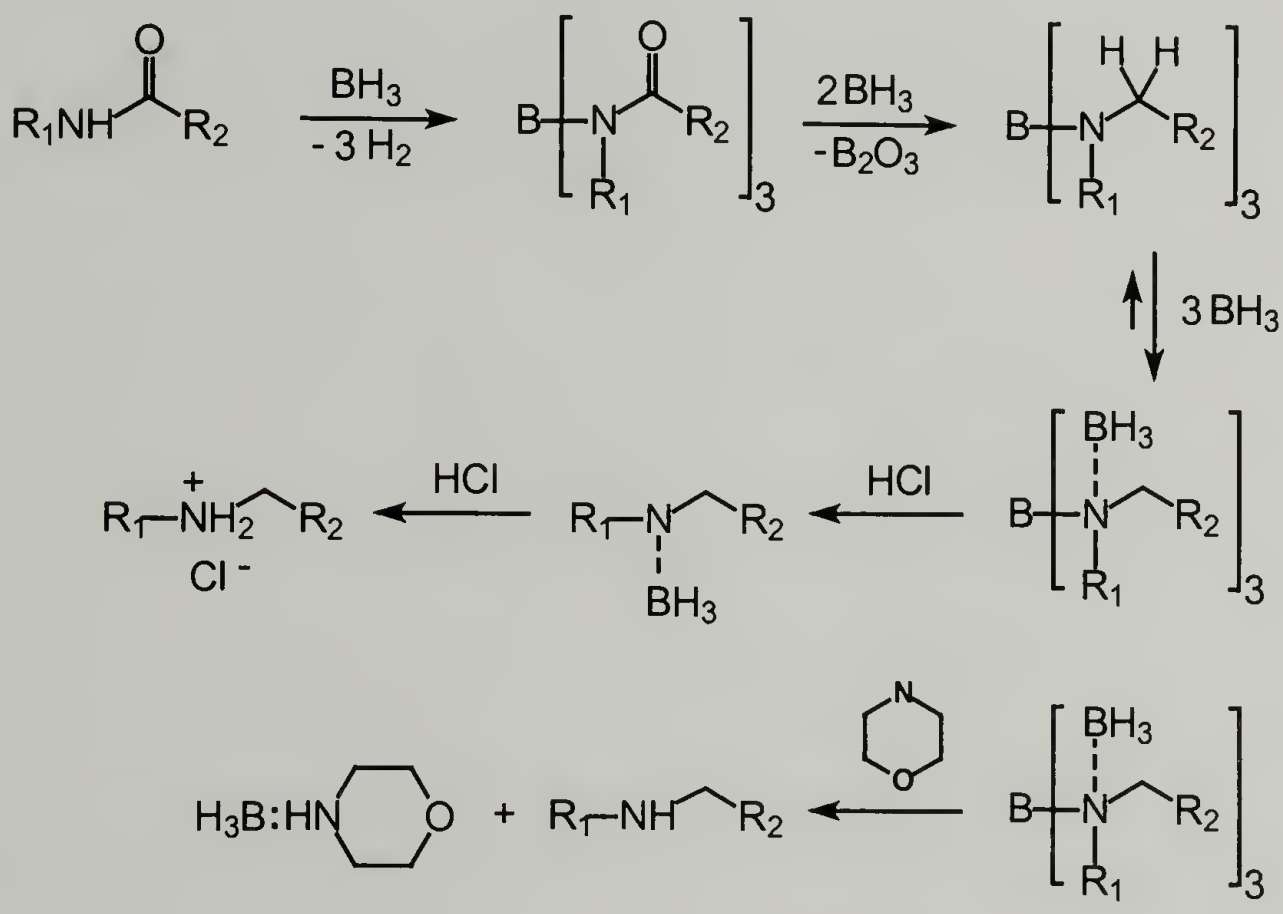

Figure 6.20. Synthesis of polyamines used in this study as compatibilizers to promote intercalation of polymer in clay systems.[68]

In contrast, if a basic medium is selected, morpholine is used to reduce the borane-amine complex, resulting in a polyamine, with a specific distribution of amine groups through the backbone that can be controlled by the original structure of the nylon employed. In this case, the polyamine can effectively crystallize and, once again, the overall crystallinity of these systems is dictated by the properties of the original polyamide.

A graphical description of the resulting polyamines using both reduction methods is presented in figure 6.21. As described before, the structure and physical properties of these systems make them very good candidates to be used as compatibilizers that could enhance the interactions between a hydrophobic polymer and a hydrophilic clay system. In this regard, it is believed that their structural similarity to conventional polyolefins and their enhanced hydrophilicity obtained after the reduction reaction enable them to interact in a very efficient way with commercial polymers and typical clay systems.

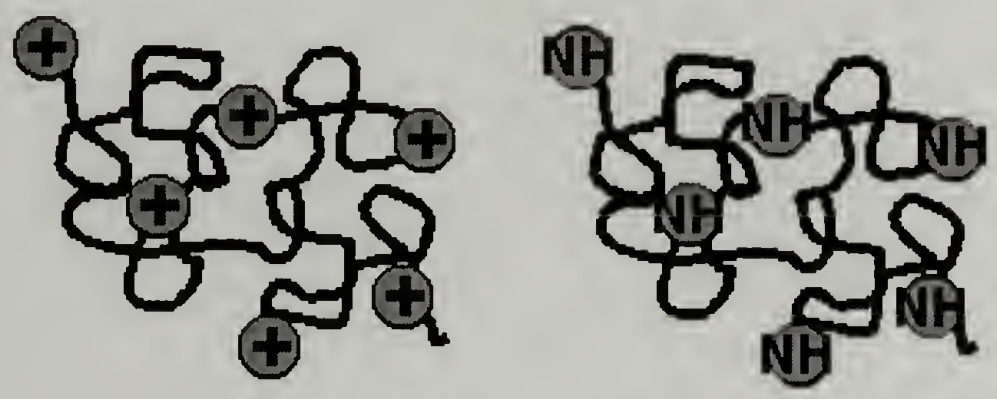

Figure 6.21. Graphical representation of polyamines obtained in acidic and basic media.

In this section, the possibility of using polyamine systems produced after reduction of commercially available nylon systems to enhance the intercalation process of a hydrophobic polymer into hydrophilic clay systems is analyzed. Preliminary results in this regard are presented for the case of polyolefins using M15A clay, and in general, this

section can be seen as an initial effort to the use of these materials to access well-defined nanostructured systems.

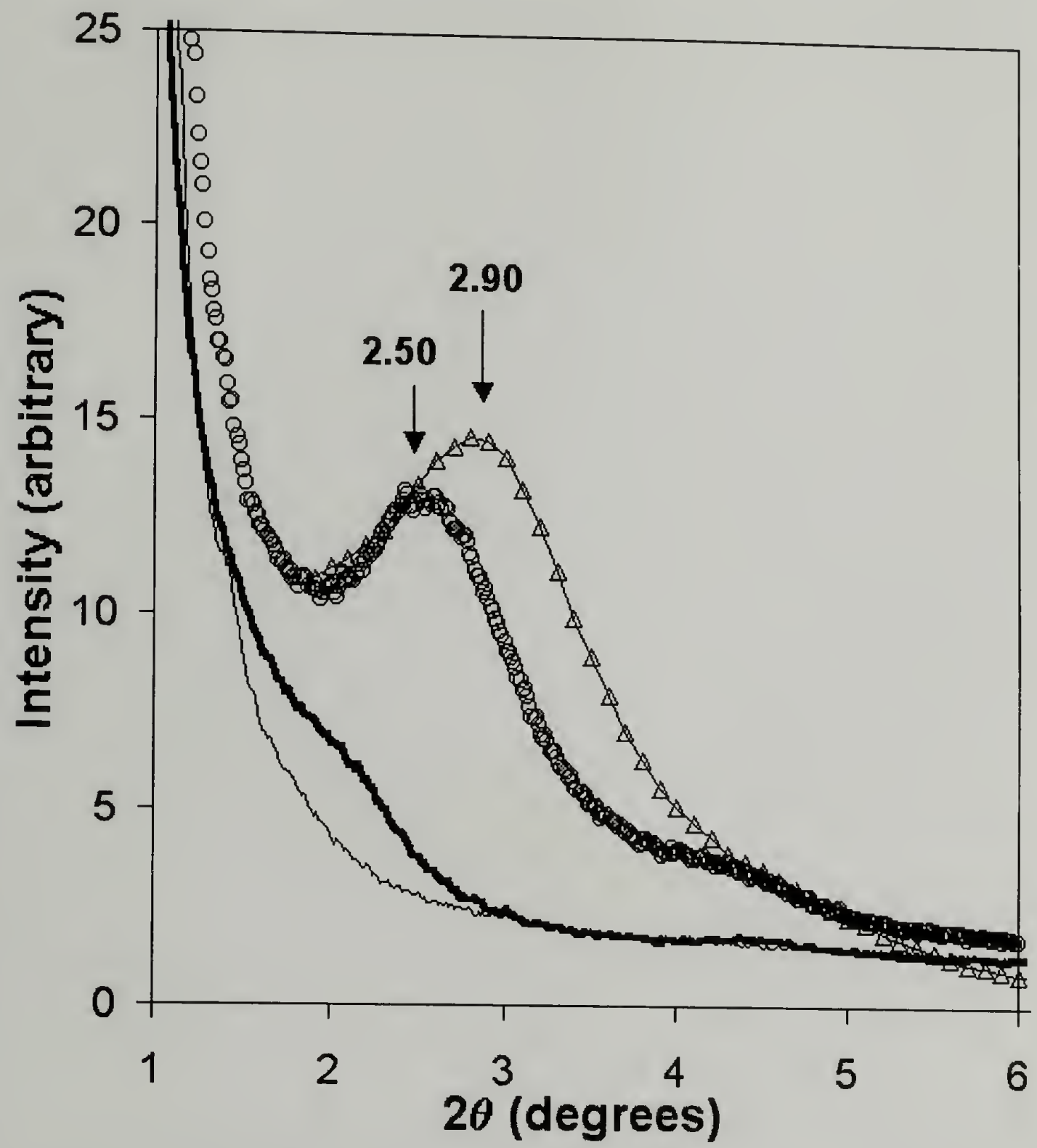

Figure 6.22. WAXS results of HDPE-M15A clay systems processed in the presence of polyamines created after reduction of nylon 6/6. HDPE with 5% polyamine produced by melt-pressing (—), HDPE-M15A clay (5% clay) with 5% polyamine produced by melt-pressing (o), Pure M15A clay (Δ), and HDPE-M15A clay (5% clay) with 5% polyamine extruded in CO_2 (▬).

Using different processing routes, a variety of HDPE-M15A samples are prepared in the presence of polyamines. In this particular case, the material obtained after reduction of Nylon 6/6 is chosen as the compatibilizer to enhance the interaction between HDPE

and M15A clay. Apparently the inherent properties of this polyamine reduce the energetic barrier associated for the intercalation of polymer into the M15A clay, as suggested by the structure of these systems presented in figure 6.22, where the scattering patterns of HDPE- M15A systems prepared using different processing routes are shown. As presented in this figure, it is evident that melt intercalation is significantly enhanced when the polyamine from reduced Nylon 6/6 is introduced as compatibilizer. As suggested in table 6.13, the clay d-spacing is considerably increased even in melt-pressed samples (16%), and this change is related to the presence of the polyamine that has inherent compatibility with the clay, along with structural similarity to the polyethylene backbone, enhancing in a significant manner the polymer-clay interactions.

Polymer	Process	Clay	% wt. clay	2θ (deg)	d-spacing (Å)
HDPE-reduced Nylon 6/6	Melt Press	-	0	-	-
HDPE	Melt Press	M15A	5	2.90	30.46
HDPE-reduced Nylon 6/6	Melt Press	M15A	5	2.50	35.29
HDPE-reduced Nylon 6/6	$ScCO_2$-extrusion	M15A	5	1.37	64.40

Table 6.13 WAXS results of HDPE-M15A clay systems produced by different routes using the polyamine created after reduction of nylon 6/6 as compatibilizer.

However, as also shown in this table, the introduction of $scCO_2$ appears to enhance the intercalation process, as in other polymer systems, and the material obtained by $scCO_2$-extrusion shows a very high degree of intercalation. The clay d-spacing changes in a very pronounced manner and as shown in figure 6.22, the reflection at low angles is not completely evident, displaying only a small shoulder that illustrates the existence of certain order within individual clay platelets, even though the dispersion of the clay through the sample is high. After analysis of this shoulder a d-spacing of 64.4Å can be

assigned. It is difficult to describe the structure of this system using traditional intercalated or exfoliated structures. A complex mixture of these two morphologies characterizes this system where an extremely large degree of intercalation that promotes the pronounced change in the d-spacing (table 6.13) is combined with individual clay platelets dispersed through the polymer matrix (partial exfoliation).

6.4 Conclusions

Polymer nanocomposites of commercially relevant systems can be produced via the specific routes presented in this study. As described in Chapter 5, $scCO_2$-assisted polymer processing can be used as an effective route to produce polymer nanocomposites.[76-78] Experimental results suggest that $scCO_2$ enhances the clay dispersion and polymer intercalation into clay nanoparticles, even when favorable interactions between the polymer and the clay are not present, as in the case of purely hydrophobic polymers. However, as described in this chapter, introducing chemically designed compatibilizers, promotes significant improvements in the degree of intercalation and exfoliation can be achieved. Results suggest that the intercalation/exfoliation process is considerably enhanced by $scCO_2$, showing significant increases in the clays d-spacings (40-100% increase) and in some cases controlling the rate at which the intercalation process takes place.

Amphiphilic copolymers of polyethylene and poly(ethylene glycol), PE-g-PEG can be successfully employed to enhance the interaction between highly hydrophobic systems and commercially available clay systems. In addition, chemical modification can be used to prepare specifically designed polyamines based on a variety of nylon systems that can

be used to enhance intercalation. This method provides specifie eontrol of the polymer-clay interactions and can be used as a direct route to intercalated nanoeomposites with well-defined structure.

These results suggest the possibility of using $scCO_2$ to aecess novel materials using systems that have been traditionally discarded. The routes presented in this study could be optimized to promote improved physieal and material properties in eomposite materials.

CHAPTER 7

SUMMARY

Supercritical carbon dioxide ($scCO_2$) has been widely studied as an environmentally friendly alternative to organic solvents in many applications. In this thesis specific routes for both melt and solid-state processing of polymers in $scCO_2$-mediated environments are presented. Throughout this thesis the influence of $scCO_2$ on the final properties of a polymer has been analyzed and novel processing routes using $scCO_2$ that could allow access to well-defined structures and novel materials have been designed, including a novel processing-route for high melt viscosity polymers.

As mentioned in Chapter 2, most of the fiber-drawing studies of semicrystalline polymers in $scCO_2$ have focused on permeable conditions, where the plasticization of $scCO_2$ dominates the interaction and the effect of the hydrostatic pressure to the state of deformation is negligible.[1-3] In Chapter 2, the interactions of $scCO_2$ with polymers in the solid state under non-permeable conditions has been analyzed through the drawing behavior of highly crystalline, highly oriented, polymorphic fibers of UHMWPE within this environment. The high-pressure medium of $scCO_2$ appears to stabilize the crystal structure of the fiber, which in this particular case is the major component, allowing crystals to grow without constraints through a possible crystal-crystal transformation to the hexagonal phase, increasing the processing temperature to 110°C. As a consequence, $scCO_2$-treated samples display a constant response compared to air-drawn samples, where significant temperature dependence is observed in their drawing and thermal behavior.

In addition, the interactions of $scCO_2$ with polymers in the melt have been analyzed in the subsequent sections. Chapter 3 describes the design of a modified processing system that allows to process polymers in $scCO_2$. The system includes a single screw extruder that has been modified to allow for high pressures created by the injection of CO_2. The new design includes a modified feed section that allows a given mass of polymer to interact with CO_2 prior and during extrusion. The foaming process of polyethylene in $scCO_2$ using this system is described in detail in Chapter 3, where a specific strategy to control the extrudate morphology and processability of a polymer is presented.

In Chapter 4, $scCO_2$-assisted polymer processing is introduced as a novel processing-route to high melt viscosity polymers, including fluoropolymers and high molecular weight polyolefins. Results suggest that this alternative design provides a new and easy route to melt process high melt viscosity polymers of commercial importance such as PTFE, FEP and s-PS. The increased processability of these systems in CO_2 is related to the effect that $scCO_2$ has on the melting behavior of semicrystalline polymers, along with its large plasticizing properties. that have been quantified through a depression in the glass transition temperature according to the Chow Model.

The feasibility of preparing polymer-clay nanocomposites by $scCO_2$-assisted polymer processing by a variety of approaches is described in Chapters 5 and 6. These methods include the use of polymer systems with different degrees of hydrophilicity, as well as the introduction of chemically-designed hydrophilic polymers or compatibilizers that enhance the interaction between a polymer and given clay system.

The results presented in these two chapters help to understand the effect of $scCO_2$ on the melt intercalation process as well as on the final structure and morphology of a polymer-clay nanocomposite. Polymer nanocomposites are successfully produced in the presence of $scCO_2$ even when favorable interactions between the polymer and the clay are not present, as described in Chapter 5. Experimental results show significant increases in the clay d-spacing for $scCO_2$-treated samples regardless of the nature of the polymer, showing significant amounts of intercalation even in purely hydrophobic polymers.

In Chapter 6, polymer nanocomposites of commercially relevant systems are prepared via the combination of $scCO_2$-assisted polymer processing and the addition of chemically-designed polymeric systems that enhance the interaction between the polymer and clay, acting as compatibilizers for melt intercalation. As suggested here, this method can be used as an effective route to produce polymer nanocomposites, with specific control over the degree of intercalation and in some cases allowing access to completely exfoliated structures.

BIBLIOGRAPHY

1. Hobbs, T.; Lesser, A.J. *J. Polym. Sci. Part B: Polym. Phys.* **1999**, *37*, 1881-1891.

2. Hobbs, T.; Lesser, A.J. *Polymer* **2000**, *41*, 6223-6230.

3. Hobbs, T.; Lesser, A.J. *Polym. Eng. Sci.* **2001**, *41*, 2, 135-144.

4. Brennecke, J.F. *Nature* **1997**, *389*, 333-334.

5. Blanchard, L.A.; Hancu, D.; Beckman, E.J.; Brennecke, J.F. *Nature* **1999**, *399*, 28-29.

6. Sarbu, T.; Styranec, T.; Beckman, E.J. *Nature* 2000, *405*, 165-168.

7. Leitner, W. *Nature* **2000**, *405*, 129-130.

8. Adam, D. *Nature* **2000**, *407*, 938-940.

9. Shieh, Y.; Su, J.; Manivannan, G.; Lee, P.H.C.; Sawan, S.P.; Spall, W.D. *J. Appl. Polym. Sci.* **1996**, *59*, 695-705.

10. Shieh, Y.; Su, J.; Manivannan, G.; Lee, P.H.C.; Sawan, S.P.; Spall, W.D. *J. Appl. Polym. Sci.* **1996**, *59*, 707-717.

11. Cooper, A.I.; Londono, J.D.; Wignall, G.; McClain, J.B.; Samulski, E.T.; Lin, J.S.; Dobrynin, A.; Rubinstein, M.; Burke, A.L.C.; Fréchet, J. M.; DeSimone, J.M. *Nature* **1997**. *389*, 368-371.

12. Zachariades, A.E.; Porter, R.S. *J. Appl. Polym. Sci.* **1979**, *24*, 1371-1382.

13. Beckman, E.J.; Porter, R.S. *J. Polym. Sci. Part B: Polym. Phys.* **1987**, *25*, 1511-1517.

14. Takayanagi, M.; Imada, K.; Nagai, A.; Tatsumi, T.; Matsuo, T. *J. Polym. Sci. Part C* 1967, *16*, 867-876.

15. Rastogi, S.; Kurelec, L.; Lemstra, P.J. *Macromolecules* **1998**, *31*, 5022-5031.

16. Kurelec, L.; Rastogi, S.; Meier, R.J.; Lemstra, P.J. *Macromolecules* **2000**, *33*, 5593-5601.

17. Tashiro, K.; Sasaki, S.; Kobayashi, M. *Macromolecules* **1996**, *29*, 7460-7469.

18. Kuwabara, K.; Horii, F. *Macromolecules* **1999**, *32*, 5600-5605.

19. Porter, R.S.; Wang, L. *J.Macromol. Sci.- Rev. Macromol. Chem. Phys.* **1995**, *C35(1)*, 63-115.

20. Kavesh, S.; Prevorsek, D.C. *Int. J. Polym. Mater.* **1995**, *30*, 15-56.

21. Nakae, M.; Uehara, H.; Kanamoto, T.; Ohara, T. Porter, R.S. *J. Polym. Sci. Polym. Phys.* **1999**, *37*, 1921-1930.

22. Lee, D.; Chen, W.; Yeh, M.; Chen, T. *Polym. Eng. Sci.* **1995**, *35*, 19.

23. Peacock, A. J. *Handbook of Polyethylene. Structures, Properties and Applications* Marcel Dekker, Inc., **2000**.

24. Garcia-Leiner, M.; Lesser, A.J. *J. Polym. Sci.: Part B: Polym. Phys.* **2003**, *42*, 12, 1375-1383.

25. Suh, N.P. "Microcellular plastics", in Stevenson J.F. *Innovation Polym. Process.: Molding*, Hanser Munich, Germany, **1996**, 93-149.

26. Baldwin, D.F.; Park, C.B.; Suh, N.P. *Polym. Eng. Sci.* **1996**, *36*, 10, 1425-1435.

27. Lee, S.T. *J. Cell. Plas.* **2001**, *37*, 221-230.

28. Park, C.B.; Baldwin, D.F.; Suh, N.P. *Polym. Eng. Sci.* **1995**, *35*, 5, 432-440.

29. Colton, J.S.; Suh, N.P. *Polym. Eng. Sci.* **1987**, *27*, 7, 500-503.

30. Lee, M.; Tzoganakis, C.; Park, C.B. *Polym. Eng. Sci.* **1998**, *38*, 7, 1112-1120.

31. Park, C.B.; Cheung, L.K. *Polym. Eng. Sci.* **1997**, *37*, 1, 1-10.

32. Colton, J.S.; Suh, N.P. *Polym. Eng. Sci.* **1987**, *27*, 7, 485-492.

33. Han, C.D.; Villamizar, C.A. *Polym. Eng. Sci.* **1978**, *18*, 687.

34. Han, C.D.; Ma, C.Y. *J. Appl Polym. Sci.* **1983**, *28*, 2961.

35. Yang, H.H.; Han, C.D.; Ma, C.Y. *J. Appl. Polym. Sci.* **1985**, *30*, 3297.

36. Lee, C.H.; Lee, K. J.; Jeong, H.G.; Kim, S.W. *Adv. Polym. Tech.* **2000**, *19*, 2, 97-112.

37. Chow, T.S. *Macromolecules* **1980**, *13*, 2, 362-364.

38. Royer, J.R.; DeSimone, J.M.; Kahn, S.A. *J. Polym. Sci. Part B: Polym. Phys.* **2001**, *39*, 3055-3066.

39. Tervoort, T.; Visjager, J.; Graf, B.; Smith, P. *Macromolecules* **2000**, *33*, 17, 6460-6465.

40. Handa, Y.P.; Zhang, Z.; Wong, B. *Macromolecules* **1997**, *30*, 26, 8499-8504.

41. Handa, Y.P.; Zhang, Z. *Macromolecules* **1997**, *30*, 26, 8505-8507.

42. Drobny, J.G. *Technology of Fluoropolymers* CRC Press LLC, **2000**.

43. Rajagopalan, P.; McCarthy, T.J. *Macromolecules* **1998**, *31*, 15, 4791-4797.

44. Lau, S.F.; Wesson, J.P.; Wunderlich, B. *Macromolecules* **1984**, *17*, 5, 1102-1104.

45. Lau, S.F.; Suzuki, H.; Wunderlich, B. *J. Polym. Sci. : Polym. Phys. Ed.* **1984**, *22*, 379-405.

46. Arora, K.A.; Lesser, A.J.; McCarthy, T.J. *Macromolecules* **1999**, *32*, 8, 2562-2568.

47. Wunderlich, B. *J. Phys. Chem.* **1960**, *64*, 1052-1056.

48. Gaur, U.; Wunderlich, B. *Polymer Preprints* **1979**, *20*, 429-434.

49. Pasztor, A.J.; Landes, B.J.; Karjala, P.J. *Thermochimica Acta* **1991**, *177*, 187-195.

50. Arora, K.A.; Lesser, A.J.; McCarthy, T.J. *Macromolecules* **1998**, *31*, 14, 4614-4620.

51. Garcia-Leiner, M.; Lesser, A.J., *J. Appl. Polym. Sci.* **2004,** 93, 4,1501-1511.

52. Pinnavaia, T. J.; Lan, T. *Chem. Mat.* **1994**, *6*, 2216-2219.

53. Giannelis, E. P.; Messersmith, P. B. *Chem. Mat.* **1994**, *6*, 1719-1725.

54. Usuki, A.; Kojima, Y.; Kawasumi, M.; Okada, A.; Fukushima, Y.; Kurauchi, T.; Kamigaito, O. *J. Mater. Res.* **1993**, *8*, 1185-1189.

55. Usuki, A.; Kojima, Y.; Kawasumi, M.; Okada, A.; Fukushima, Y.; Kurauchi, T.; Kamigaito, O. *J. Mater. Res.* **1993**, *8*, 1179-1184.

56. Yano, K.; Usuki, A.; Okada, A.; Kurauchi, T.; Kamigaito, O. *J. Polym. Sci. Pol. Chem.* **1993**, *31*, 2493-2498.

57. Vaia, R. A.; Jandt, K. D.; Kramer, E. J.; Giannelis, E. P. *Macromolecules* **1995**, *28*, 24, 8080-8085.

58. Pinnavaia, T. J.; Wang, Z. *Chem. Mat.* **1998**, *10*, 12, 3769.

59. Wei, K. H.; Chen, T. K.; Tien, Y. I. *Polymer* **2000**, *41*, 1345-1353.

60. Usuki, A.; Kawasumi, M.; Hasegawa, N.; Kato, M.; Okada, A. *Macromolecules* **1997**, *30*, 6333-6338.

61. Bergman, J. S.; Chen, H.; Giannelis, E. P.; Thomas, M. G.; Coates, G. W. *Chem. Commun.* **1999**, *21*, 2179-2180.

62. Zerda, A.S.; Lesser, A.J. *J. Polym. Sci: Part B: Polym. Phys.* **2001**, *39*, 11, 1137-1146.

63. Bucknall, C. B.; Karpodinis, A.; Zhang, X. C. *J. Mater. Sci.* **1994**, *29*, 3377–3383.

64. Lagaly, G. *Apply Clay Sci* **1999**, *15*, 1-9.

65. Pinnavaia, T.J.; Beall, G.W. In *Polymer-clay Nanocomposites*, John Wiley & Sons, Ltd., **2000**.

66. Hu, X.; Lesser, A.J. *J. Polym. Sci. Part B: Polym. Phys.* **2003**, *41*, 2275-2289.

67. Breitenkamp, K; Simeone, J.; Jin, E; Emrick, T. *Macromolecules* **2002**, *35*, 25, 9249-9252.

68. Herrera-Alonso, M.; McCarthy, T.J. *Polymer Preprints* **2004**, *45*, 1, 990-991.

69. Brandrup, J.; Immergut, E. H.; Grulke, E.A. *Polymer Handbook*, **2003**, Fourth edition.

70. Klempner, D; Frisch, K.C. *Handbook of Polymeric Foams and Foam Technology*, **1991**, Hanser Verlag.

71. Colton, J.S.; Suh, N.P. *Polym. Eng. Sci.*, **1987**, 27, 7, 493-499.

72. Park, C.B.; Behravesh, A.H.; Venter, R.D. *Polym. Eng. Sci.*, **1998**, 38, 11, 1812-1823.

73. Garcia-Leiner M. and Lesser A.J., *ANTEC Proceedings. Society of Plastics Engineers*, San Francisco CA, **2002**.

74. Kuag, C.; Manke, C.W.; Gulari, E.; *J. Polym. Sci. Part B: Polym. Phys.*, **1998**, 37, 19, 2771-2781.

75. Gerhardt, L.J., Manke, C.W.; Gulari, E.; *J. Polym. Sci. Part B: Polym. Phys.*, **1997**, 35, 3, 523-534.

76. Garcia-Leiner, M.; Lesser, A.J. *Abstr. Pap. Am. Chem. S.*, 225, 55-PMSE, Part 2, 668-669, Mar. **2003**.

77. Garcia-Leiner, M.; Lesser, A.J. *Abstr. Pap. Am. Chem. S.*, 226, 389-PMSE, Part 2, 519-520, Sep. **2003**.

78. Garcia-Leiner, M.; Lesser, A.J. *Polymer Preprints* **2004**, 45, 1, 520-521.

79. Couchman, P.R.; Karasz, F.E. *Macromolecules* **1978**, 11, 1, 117-119.